# MOLECULAR RECOGNITION OF INHIBITORS, METAL IONS AND SUBSTRATES BY RIBONUCLEASE P

**by**

**Xin Liu**

**A dissertation submitted in partial fulfillment**
**of the requirements for the degree of**
**Doctor of Philosophy**
**(Chemistry)**
**in the University of Michigan**
**2013**

**Doctoral Committee:**

**Professor Carol A. Fierke, Chair**
**Professor David R. Engelke**
**Professor George A. Garcia**
**Professor Anna K. Mapp**
**Professor Nils G. Walter**

## DEDICATION

To Lei Shi (石磊)

Lei, you believe in me and listen to my wildest dreams. You bring out the best in me.

Thank you for your endless love, patience and support!

愛你的馨!

## ACKNOWLEDGEMENTS

This work would not be possible without support from many mentors, friends and family members. First of all, I want to thank my advisor Professor Carol Fierke for her great guidance and enormous patience for the past few years. Without her encouragement and critical suggestions, I would have not been able to learn such a great deal of experimental and analytical methods and to finish this dissertation. Carol has set a role model for me as an extraordinary scientist and inspiring mentor that I hope to learn from in my future careers. I would also like to thank my committee members who have been patient and helped me in many different ways. Prof. David Engelke helped me to think and communicate my research more clearly during the monthly RNase P meetings. Prof. Ann Mapp allowed me to use the TECAN instruments in her laboratory and wrote letters for supporting my various fellowship applications. I have learned about many different research projects when attending the Midwest enzyme mechanism conference organized by Prof. George Garcia. I have also used the HPLC instrument and received help from many members in Prof. Nils Walter's laboratory (Matt Marek, Mario Blanco, Visha Krishnan and Sethu Pitchaiya).

I want to acknowledge all past and current members of the Fierke lab for being such wonderful and supportive colleagues. Dr. Daina Zeng showed me the basic experimental procedures for handling RNA samples and measuring RNase P

activity. Dr. John Hsieh has been answering all my questions about RNase P over the years. Dr. Wan Lim is a great friend and provided many insightful discussions. Dr. Elaina Zverina has been a great friend since my first day of class in graduate school at Michigan and offered me numerous help in adjusting to a foreign country and gave me many excellent suggestions for my experiments. Yu Chen is a colleague, friend but also a mentor who inspired me in improving efficiency and communications in my research. I want to thank Andrea Stoddard for providing her expertise in molecular biology, gracious support and encouragement to me over the years. I also thank Elia Wright for offering me experimental help as well as work-life balance strategies. Thanks also go to Michael Howard who taught me valuable tricks in protein purification and has been a great source of inspiration. I would like to thank Noah Wolfson for his support and discussions about research, science and life. I want to acknowledge all members of the RNase P subgroup for insightful discussions during the monthly meetings (Prof. Carol Fierke, Prof. David Engelke, Dr. John Hsieh, Dr. Nathan Zahler, Dr. Kristin Koutmos, Dr. Scott Walker, Dr. Michael Marvin, Dr. Wan Lim, Yu Chen, Micheal Howard, and Bradley Klemm). I also thank Dr. Manoj Cheriyan, Dr. James Hougland and Dr. Terry Watt for their help in my early years in the lab. Special thanks go to Paul Lin and Justin Liedel whom are the first two undergraduate students I have worked with. They have done great experiments and inspired me in many ways.

The work presented in each of my dissertation chapters was conducted not only by me, but also by many collaborators. I want to also list my acknowledgement to my collaborators and source of funding. For Chapter 2, I thank Dr. Lyra Chang,

Professor Jason Gestwicki, Professor Anna Mapp, Dr. Elaina Zverina, Dr. John Hsieh, Dr. Daina Zeng and Yu Chen for help with the development of this assay. I want to thank Dr. Jonas Hojfeldt, Dr. Chinmay Majmudar and Dr. Ningkun Wang (Mapp lab) for sharing their experience with fluorescence polarization and high-throughput screening techniques. I also acknowledge the help of Martha Larsen, Steven Swaney and Paul Kirchhoff at the Center for Chemical Genetics at University of Michigan with the compound library screen and data mining. I want to thank two internal grants that partially made the high-throughput screening project possible: the Rackham Graduate Student Research Grant and a Pilot Screening Grant from the Life Science Institute at University of Michigan. For Chapter 3, I want to thank Yu Chen, Dr. Katja Petzold and Prof. Hashim Al-Hashimi for their insightful discussions on the dynamics and structure studies of P4 helix. For Chapter 4, I want to specially thank Paul Lin for performing molecular cloning experiments for subcloning human mt-pre-tRNA genes and for his general help in preparing cell cultures, growth media and plates in the laboratory. I would like to thank Andrea Stoddard and Elia Wright for their help in growing HEK293 cells. The initial subcloning, purification and activity measurements of each human mtRNase P proteins were accomplished by Dr. Wan Lim and I also thank her for sharing regents and useful ideas during discussions. I would like to thank Michael Howard for help with protein purifications. Dr. Elaina Zverina provided valuable suggestions for purification of MRPP3 and experimental assistance in purification of MRPP1·MRPP2 complex. Thanks also go to Dr. Lubomir Dostal who performed ICP-MS experiments. I want to thank Yueyang Zhong (Ruotolo lab) for her passion and expertise in the IM-MS experiments. I would also

like to thank Department of Chemistry for a Research Excellence Award, which funded me for one winter semester when a large part of this work was undertaken. Special thanks go to who have critically read my thesis chapters (Prof. Carol Fierke, Yu Chen, Carol Ann Pitcairn, Elia Wright, Nancy Wu, Andrea Stoddard, Byung Chul Kim and Michael Howard).

Last but not least, millions of thanks go to my dear friends and families whom I have not yet mentioned above. I must thank Dr. Tracy Xiao Liu for bringing happiness in my life and for being understanding and caring to me all these years. Dr. Lyra Chang is my role model as a scientist and a dear friend whom I can trust even without much talking between us. Dr. Wenjing Chen taught me optimism and resilience. Dr. Jing Chen, Dr. Chenxi Shen, Dr. Penny Bo Peng and Dr. Liuling Gong also took care of me during hard times and taught me accountability. Dr. Yipei Wang showed me importance of efficiency in work and in life. I also want to thank Dr. Boyangzi Li for her encouragement and inspiration for pursuing life's dream courageously. I also thank Guangming Lang for inspiring me with wisdom in Buddhism. I want to express my utmost gratitude to my parents, who raised me up with unconditional love and support. Thanks go to my parents-in-laws who also gave me endless love. Finally, I thank my husband Lei Shi. I could not get to this point without his love, support and help.

Thank you all!

## TABLE OF CONTENTS

## LIST OF FIGURES

## LIST OF TABLES

## ABSTRACT

Ribonuclease P (RNase P) is a divalent metal ion-dependent endonuclease that catalyzes cleavage of the 5’ leader of precursor transfer RNA (pre-tRNA), an essential tRNA processing step in all domains of life. Bacterial RNase P is a potential antibacterial target because it is essential for cell survival and varies in composition from its eukaryotic counterparts. Bacterial RNase P contains a catalytic RNA (P RNA) with one protein subunit while eukaryotic nuclear RNase P has multiple protein subunits with a catalytic RNA core and the human mitochondrial RNase P (mtRNase P) consists solely of protein subunits.

In this dissertation research, first a novel fluorescence polarization (FP) assay was developed to facilitate rapid and real-time measurements of RNase P activity. This new FP assay was optimized for high-throughput screening to search for new inhibitors of bacterial RNase P in small molecule (2,880 compounds) and natural product extracts (22,720 samples) libraries. A new RNase P inhibitor was identified from the screen. Second, to test the biochemical role and metal ion binding function of a carbonyl oxygen (oxygen-4, O4) in the universally conserved bulged uridine (U51) of P RNA, RNase P with single atom modifications of 4-thiouridine, 4-deoxyuridine, 3-methyluridine and an abasic site were prepared and analyzed. Binding data demonstrate that the O4 of U51 enhances pre-tRNA affinity in a divalent metal-ion dependent fashion. In addition, kinetic data suggest that U51

enhances pre-tRNA cleavage by interacting with a magnesium ion stabilizing an active enzyme-substrate conformation. Third, a library of human mitochondiral pre-tRNAs and high purity human mtRNase P was prepared for studying the substrate specificity of human mtRNase P. Single-turnover cleavage data demonstrate that the MRPP3 subunit of human mtRNase P is catalytically active alone *in vitro* and that the MRPP1·MRPP2 subcomplex increases the cleavage rate and cleavage site fidelity. Overall, the work presented in this dissertation has provided a new real-time and high-throughput methodology to assay RNase P activity *in vitro*, enhanced our understanding of how bacterial RNase P recognizes inhibitors and metal ions, and laid the foundation for elucidating substrate recognition by the newly identified protein-only human mtRNase P.

# CHAPTER 1

# INTRODUCTION: MOLECULAR RECOGNITION BY RNASE P[1]

## 1.1 Introduction

Transfer RNA (tRNA) is a central adapter molecule during ribosome-dependent protein synthesis [1]. Biosynthesis of mature functional tRNA requires extensive processing steps, such as the removal of 5' and 3' end sequences from polycistronic precursor transcript, 3' CCA addition, splicing, editing, and base modifications [1] (Figure 1-1). The early steps for processing immature precursor tRNA (pre-tRNA) include the removal of extraneous sequences at the 5' and 3' termini by ribonucleases [2]. The 5' end maturation of tRNA is catalyzed by ribonuclease P (RNase P), a divalent metal ion-dependent endonuclease responsible for cleavage of the 5' end leader from pre-tRNA [3-6]. In all three domains of life, RNase P catalyzes endonucleolytic hydrolysis of the phosphodiester bond between the N(-1) and N(1) bases, generating a 5' monophosphate group (5' p) and a 3' hydroxyl group (3' OH) in tRNA body and 5' leader products, respectively (Figure 1-2) [4, 5, 7]. RNase P also processes various non-tRNA substrates in cells [8] and is implicated in regulating mRNA degradation and gene expression [9, 10].

[1] Contents in Chapter 1 are in preparation for an invited review article entitled "Molecular recognition by RNase P: an essential and diverse enzyme in tRNA processing" by Xin Liu and Carol A. Fierke.

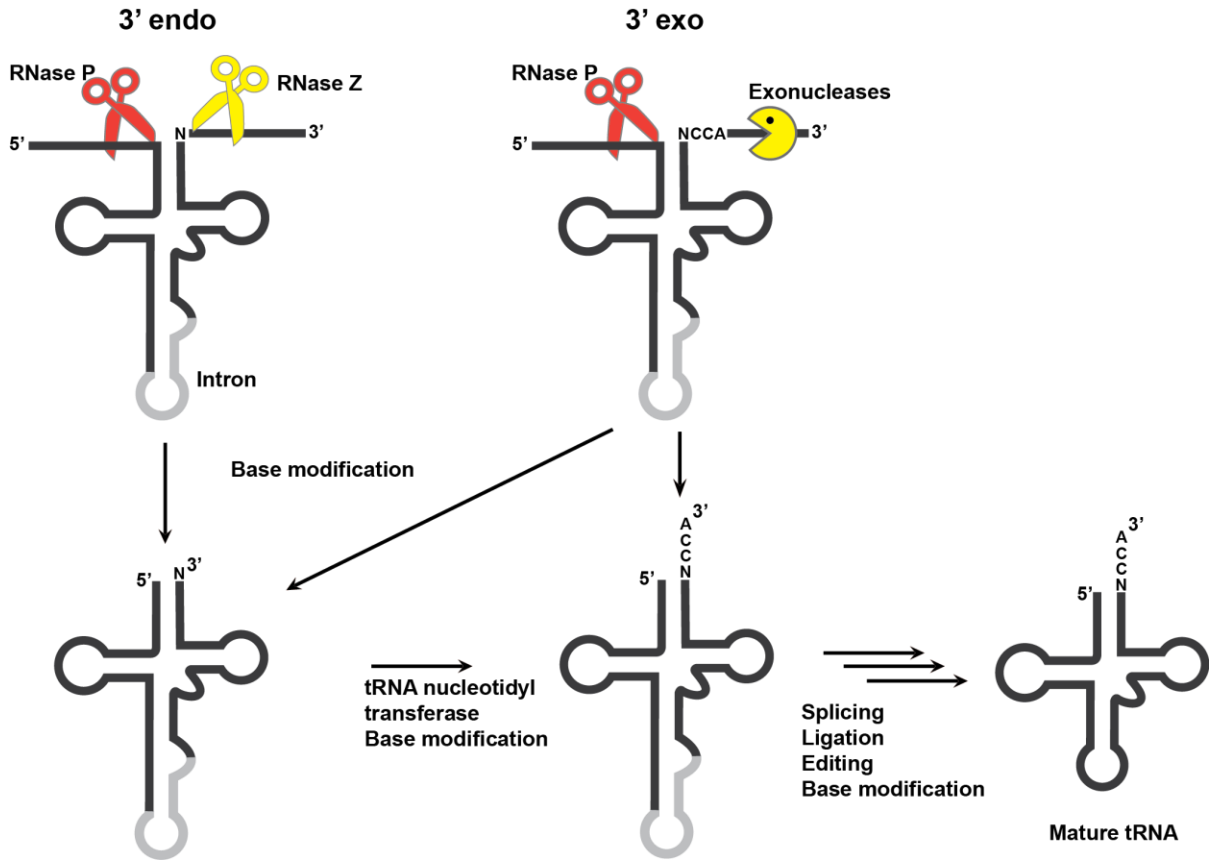


**Figure 1-1:** A simplified tRNA maturation pathway. RNase P is ubiquitously responsible for catalyzing the 5' end maturation of tRNA. 3' end processing has two major pathways by either an endonuclease such as RNase Z (3' endo pathway) or by multiple exonucleases (3' exo pathway), which typically depends on whether the 3'CCA is encoded in the sequence [2]. N: the discriminator nucleotide. Some tRNAs are also transcribed with intron sequences (in gray).

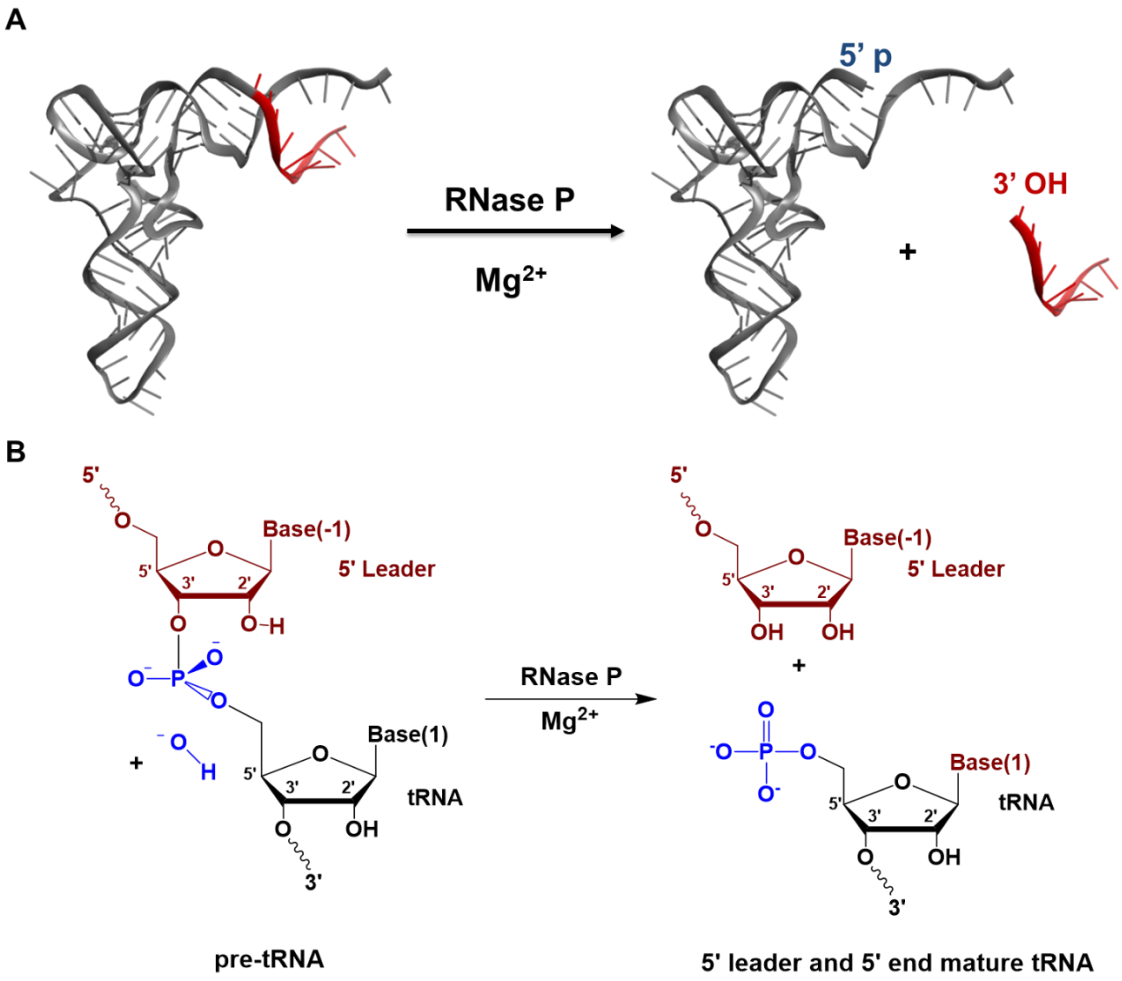


**Figure 1-2:** RNase P catalyzes 5' end maturation of tRNA. **(A)** Cartoon presentation of RNase P catalyzed hydrolysis of a phosphodiester bond in a pre-tRNA to generating tRNA with a mature 5' end and a 5' leader [7]. **(B)** RNase P is a divalent metal ion-dependent endonuclease that catalyzes the hydrolysis of a specific phosphodiester bond and generates a 5' monophosphate in the tRNA product.

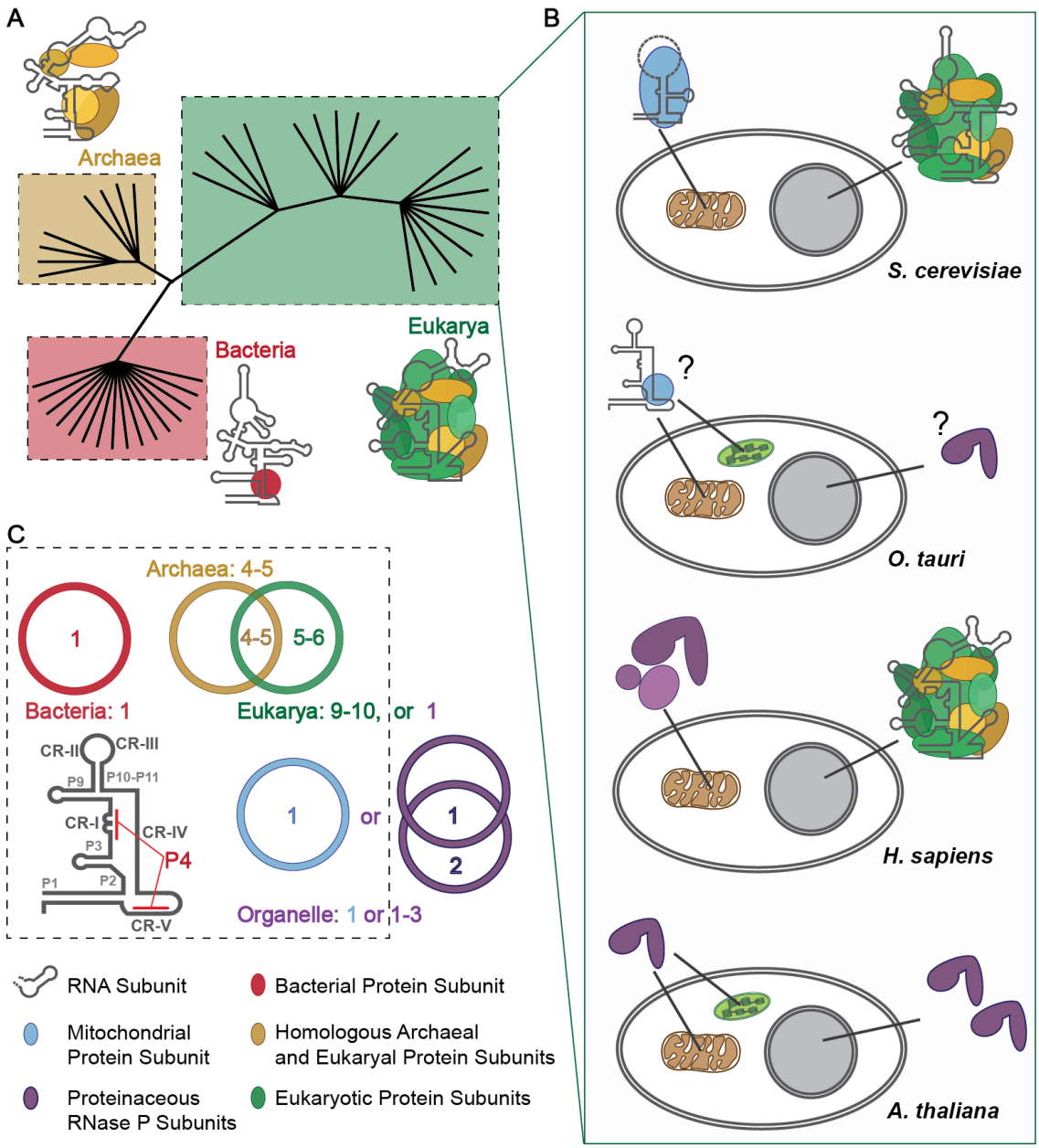


**Figure 1-3:** Evolution of RNase P enzymes. **(A)** RNase P is conserved in all three kingdoms of life. Ribonucleoprotein (RNP) RNase P consists of one RNA and variable numbers of protein subunits [2, 11]. **(B)** Eukaryal RNase P evolved from ribonucleoprotein complexes to protein-only isoforms [12]. **(C)** Venn diagrams illustrating the composition and homology among RNase P proteins and a cartoon drawing of a minimum consensus secondary structure highlights the position of the helix P4 and the conserved regions CR-I to CR-V [8, 13].

In most organisms, RNase P is a ribonucleoprotein (RNP) complex consisting of a single catalytic RNA subunit (P RNA) and variable numbers of protein subunits (1 in Bacteria, 4-5 in Archaea and 9-10 in Eukarya nuclei) [14-19] (Figure 1-3). In recent studies, examples of exclusively protein-based RNase P have been identified in eukaryal organisms, such as human mitochondria [20] and plants [21, 22]. These findings present RNase P as an excellent model system to compare RNA- and protein-based catalysis [23, 24]. Similar to the ribosome, another indispensable RNP and RNA-based catalyst, bacterial RNase P is also essential for bacterial cell survival and considered as a potential antibacterial drug target [25].

Over the past four decades, much progress has been made in understanding the composition, structure and function of RNP RNase P (see reviews by [4, 6, 13, 19, 26, 27]) which has led to the use of RNase P as a tool for regulating gene expression in cells [28]. However, we still lack a comprehensive understanding on a molecular basis of how RNase P RNA synergistically interacts with protein subunits and essential metal ions to recognize substrates and perform catalysis [6, 19]. Furthermore, specific and potent inhibitors for bacterial RNase P remain to be discovered as potential novel anti-infection agents [29, 30]. In addition, newly identified protein-only RNase P awaits systematic characterization [20-22, 31]. Here I describe the current picture of the evolutionary spread and diverse scaffolds of RNase P enzymes with a focus on bacterial and human mitochondrial RNase P. I also discuss recent advances in elucidating the kinetic mechanism and identification of important metal ions in RNase P, and compare the substrate specificity of RNP

and protein-based RNase Ps. Lastly, I will conclude with a summary of the objectives of this dissertation research.

## 1.2 RNase P Enzymes: Essential yet Diverse

RNase P is conserved in all organisms examed, with one exception in a small host-dependent archaeon, *Nanoachaeum equitans,* in which leader-less tRNAs are transcribed [32, 33]. The 5' end processing of tRNA catalyzed by RNase P is indispensable in all free-living organisms [2]. RNase P also processes various non-tRNA substrates *in vivo* (see summaries in [8, 34]). Most RNP RNase Ps have a single RNA subunit that folds into similar types of secondary structure, but share relatively low sequence homology [4, 6, 35]. The number of RNase P protein subunits has increased substantially from 1 in Bacteria, 4-5 in Archaea and 9-10 in Eukarya to the complete depletion of the RNA subunit in land plants. This makes RNase P one of the most diverse and essential enzymes characterized to date [12, 24] (Figure 1-3).

### 1.2.1 Ribonucleoprotein (RNP) RNase P

#### 1.2.1.1 RNase P RNA[2]

The first RNase P holoenzyme was identified in *E. coli* from two essential genes: *rnp*A, which encodes the protein subunit (~120 amino acids), and *rnp*B, which encodes the RNase P RNA (~400 nucleotides) [36-40]. Bacterial RNase P RNA is a true enzyme *in vitro* that catalyzes multiple turnover reactions under high

[2] Much of RNase P RNA sequence and secondary structure data were compiled in The "RNase P Database" (http://www.mbio.ncsu.edu/rnasep/seqs&structures.html) by James W. Brown at North Carolina State University.

ionic strength conditions [41-44]. RNase P RNA may therefore be considered a relic of the “RNA world” [6].

Phylogenetic analysis classified RNase P RNA (P RNA) into two major types of secondary structures [13, 35, 45, 46] (Figure 1-5), the type-A (for ancestral type) presents in most bacteria, and the type-B (for *Bacillus* type) found only in low-GC Gram-positive bacteria [47, 48]. In addition, type-C P RNA related to type-B but lacking P13 and P14 stems has been found in a member of green non-sulfur bacteria [47, 48].

A consensus sequence of bacterial P RNA contains five Conserved Regions (CR-I to CR-V) (Figure 1-3) that contain 13 universally conserved nucleotides in all P RNAs and 50 other nucleotides that are highly conserved in bacteria [49-51]. This minimum P RNA has catalytic activity *in vitro* [50]. RNase P RNA has two independent folding domains: the specificity-domain (S-domain), which contains CR-II and III, and the catalytic-domain (C-domain), which contains CR-I, IV and V (Figure 1-4) [52, 53]. Functions of these two domains in bacterial P RNA have been investigated using numerous biochemical studies such as footprinting, cross-linking, affinity cleavage, nucleotide analog interference mapping and structural studies [54-62]. The C-domain alone is catalytically active and in the presence of the protein subunit catalyzes cleavage of pre-tRNA that is 100- to 500-fold more slowely than intact P RNA, indicating that the C-domain contains the catalytic site [63-65]. However, the C-domain·protein complex binds pre-tRNA substrate at least 100-fold weaker than the intact holoenzyme [64]. The S-domain increases substrate binding affinity and specificity by interacting with the D- and TψC-domains of tRNA [57-59].

Type-A P RNAs in Archaea generally lack P8 and P13/14 stems. Less complex P RNA structures are found in archaea *Methanococcus* and *Archaeoglobus fulgidus*, (type-M, lacking P8, P16, P6 pseudoknot and the CCA recognition loop in P15) [66] and *Thermoproteaceae* (type-T, lacking most of the S-domain) [67]. Bioinformatic analysis of P RNA structure and sequence suggest that archaeal P RNA evolved from an early segregated lineage [68].

The eukaryal P RNAs (nuclear and organellar) surveyed to date have diverse secondary structures [35, 51]. The P13, P14 and L15 structural elements are missing in eukaryal nuclear P RNA [69]. In organelles, secondary structures of *Reclinomonas americana* (a small protozoan) mitochondrial and *Porphyra purpurea* (a non-green algae) chloroplast P RNA are similar to their bacterial ancestors [35]. However, *S. cerevisiae* mitochondrial P RNA only requires a considerably reduced sequence containing CR-I, CR-IV and CR-V (Figure 1-3) and one large protein subunit, RPM2, which shares no sequence homology with any known RNP proteins [70-72]. Certain archaeal and eukaryal P RNAs are capable of catalyzing the cleavage of their respective substrates under single-turnover conditions and extreme ionic strength and $MgCl_2$ concentrations with a slower cleavage rate than their bacterial counterparts [73, 74].

#### 1.2.1.2 Bacterial RNase P

Bacterial RNase P is the simplest (one RNA and one protein) and most extensively characterized RNP holoenzyme. Bacterial P RNA alone efficiently catalyzes cleavage of the 5’ leader from pre-tRNA under high ionic strength and divalent metal ion conditions *in vitro* [41], while the protein subunit is also essential *in*

*vivo* [75]. RNase P protein is suggested to affect the folding of P RNA moderately [76] and decrease the concentration of monovalent and divalent cations required for catalysis [77, 78]. It enhances reactivity under physiological conditions and directly contacts the pre-tRNA 5' leader to increase substrate affinity [76, 79-82]. In solution, bacterial RNase P holoenzyme forms a dimer in the absence of substrate [83, 84].

Crystal structures of S-domains and/or full length type-A and type B P RNA are available for *Thermotoga maritima* (type-A, PDB IDs: 1U9S [85] and 2A2E [86]), *Bacillus subtilis* (type-B, PDB ID: 1NBS [87]) and *Bacillus stearothermophilus* (type-B, PDB IDs: 2A64 [88]) (Figure 1-4). A crystal structure of *T. maritima* RNase P holoenzyme in complex with a yeast $tRNA^{Phe}$ and soaked with 5' leader has also been solved recently, providing many molecular details about the holoenzyme (PDB IDs: 3Q1R and 3Q1Q [89]) (Figure 1-4 and Figure 1-5). In this ternary complex, CR-II and CRIII regions in the S-domain form base stacking contacts with the D- and TψC-loop of tRNA. CR-I, CR-IV and CR-V regions in the C-domain adopt a non-helical module that forms an A-minor interaction with the acceptor-stem of tRNA, base pairs with 3' RCCA motif of tRNA, binds to the protein subunit, and contains the putative active site near helix P4 (Figure 1-4 and Figure 1-5) [89]. Catalytic metal ions are proposed near helix P4 and the 5' end of tRNA (Figure 1-5) [89]. The overall structure of this ternary complex agrees well with models built using free P RNA structures and/or solution probing and photoaffinity cross-linking data [76, 86, 90]. However, these models vary in positioning of the putative active site [76, 86, 90]. Higher resolution structures of RNase P ternary complex are still needed for refining the details of the active site and positioning the metal ions bound to RNase P.

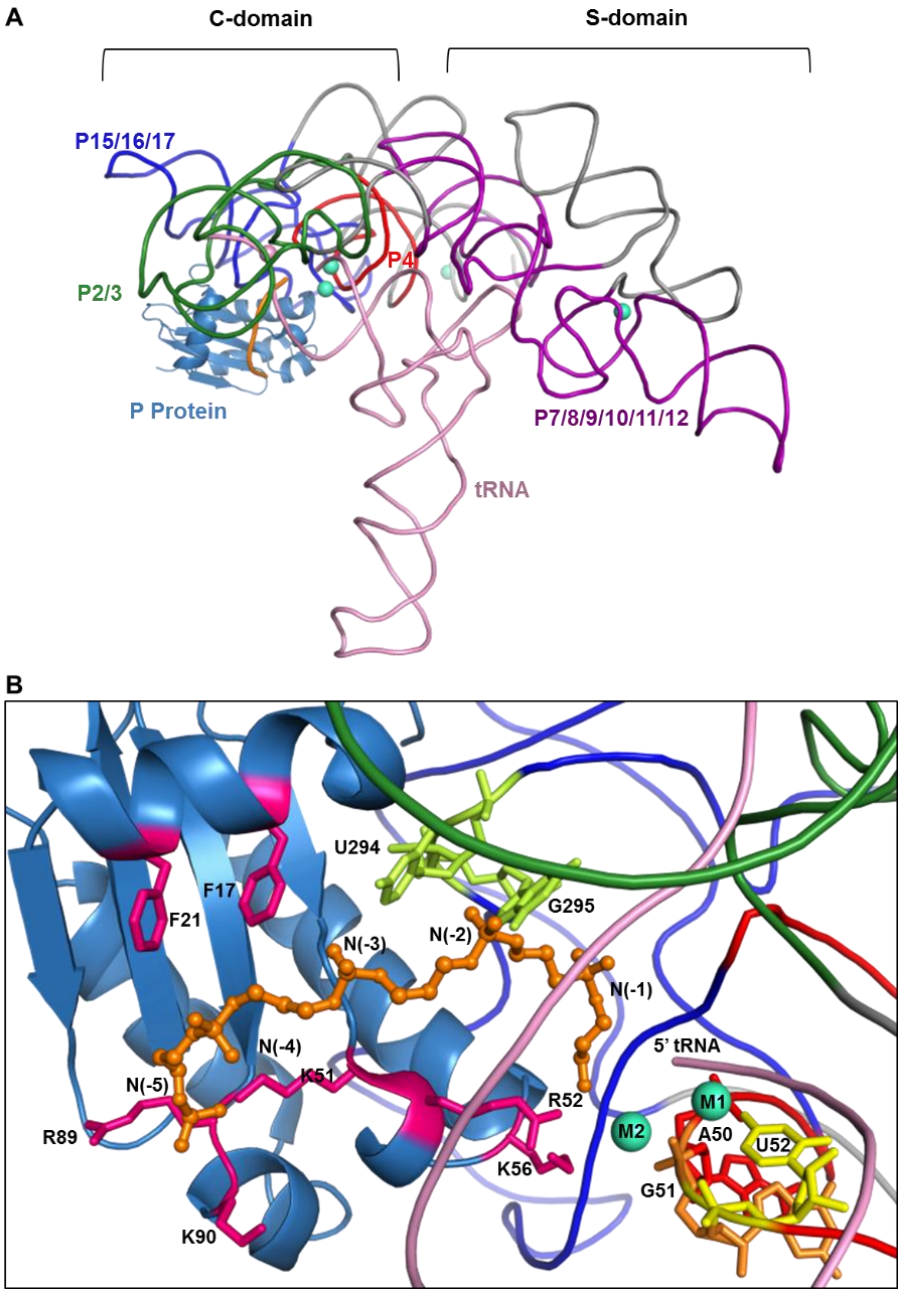


**Figure 1-4:** Crystal structure of *T. maritima* RNase P ternary complex. **(A)** A cartoon representation of *T. maritima* RNase P holoenzyme in complex with tRNA and a 5-nt leader (4.2 Å resolution, PDB code: 3Q1R [89]). The helix P4 is red, tRNA is pink, P protein is blue helices P2/3 are green, P15/16/17 are dark blue and P7-P12 are purple. Metal ions near the active site of P RNA are cyan spheres and a metal ion with 3' CCA of tRNA is a pink sphere. **(B)** An expanded view displaying the two metal ions (M1, M2, cyan spheres) near the P4 helix (U52 is yellow, G51 is orange and A50 is red) as well as the 5' leader interacting with the P protein and U294 and G295 (light green) in J18/2 of P RNA [89]. U294, G295, U52, G51 and A50 correspond to A318, G319, U51, G50 and A49 in *B. subtilis* P RNA. F17, F21, K51, R52, K56, R89 and K90 correspond to F16, F20, K52, K53, N56, R85 and K86 in *B. subtilis* P protein.

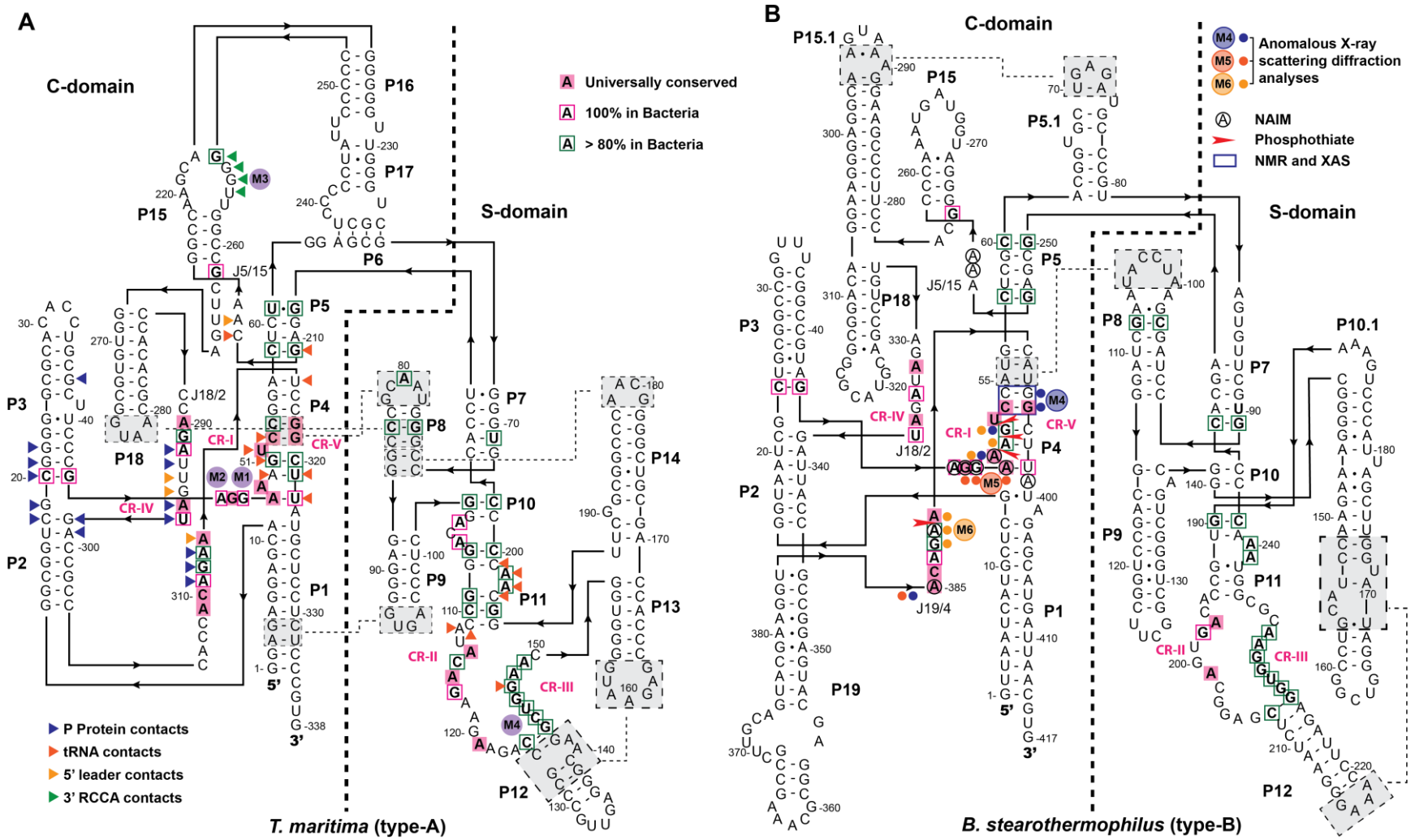
A
C-domain
S-domain
P15
P16
P17
P6
P5
P4
P3
P2
P1
P18
P7
P8
P9
P10
P11
P12
P13
P14
J5/15
J18/2
CR-I
CR-II
CR-III
CR-IV
CR-V
M1
M2
M3
M4
5'
3'
A Universally conserved
A 100% in Bacteria
A > 80% in Bacteria
P Protein contacts
tRNA contacts
5' leader contacts
3' RCCA contacts
T. maritima (type-A)
B
C-domain
S-domain
P15.1
P15
P5.1
P5
P18
P3
P2
P1
P19
P8
P7
P10.1
P10
P9
P11
P12
J5/15
J18/2
J19/4
CR-I
CR-II
CR-III
CR-IV
CR-V
M4
M5
M6
5'
3'
Anomalous X-ray scattering diffraction analyses
NAIM
Phosphothiate
NMR and XAS
B. stearothermophilus (type-B)

**Figure 1-5:** Bacterial P RNA secondary structure and molecular interactions. Tertiary interactions are shown in connected gray box (dashed lines). **(A)** Secondary structure adopted from *T. maritima* RNase P ternary complex [89]. Color-coded arrowheads indicate interaction sites in P RNA with P protein (blue), tRNA (red), 5' leader (orange) and 3'RCCA motif (green). The boxed nucleotides are conserved: universally conserved are in solid pink block, 100% conserved in bacterial are in pink box and >80% conserved in bacterial are in green box **(B)** Secondary structure adapted from *B. stearothermophilus* crystal structure (PDB IDs: 2A64 [88]). Metal ion binding sites from studies of *E. coli* (phosphorothioate modifications), *B. stearothermophilus* (anomalous X-ray scattering analysis of heavy metal soak), *and B. subtilis* (phosphothioate and NMR and XAS) RNase P are indicated [91-96].

Structures of bacterial RNase P proteins (~14 kDa) from *Bacillus subtilis* (PDB ID: 1A6F [33]), *Staphylococcus aureus* (type-B RNase P, NMR structure, PDB ID: 1D6T[97]), and *T. maritima* (PDB ID: 1NZ0 [98]) have also been determined individually [81, 97, 98]. These proteins share low sequence homology but adopt a similar structure which comprises of a central cleft formed by one α-helix and four β-sheets, a negatively charged loop and a left-handed βαβ cross-over connection that contains the most conserved region, termed RNR motif (RNRXKRXXR). Biochemical data suggest that the RNR motif interacts with both pre-tRNA and P RNA and stabilizes a conformational change that occur during the *B. subtilis* RNase P catalytic cycle [99]. The protein subunits of *E. coli* (type-A) and *B. subtilis* (type-B) RNase P are interchangeable *in vivo* [100], although the P RNA affinity is altered [101]. The *rnp*A gene encoding P protein in *B. subtilis* [102] and *E. coli* [103] can also be replaced by *rnp*A gene from other bacterial species *in vivo*, but the growth rate is slower [103]. On the other hand, archaeal and eukaryotic protein subunits Rpp21 and Rpp29 cannot rescue the rnpA gene deletion, which is consistent with these proteins being evolutionally disparate from bacterial RNase P proteins [15, 18, 102].

#### 1.2.1.3 Archaeal and Eukaryal RNP RNase P

RNP RNase P in Archaea and Eukarya has increased complexity in protein subunits (Figure 1-3). Archaeal RNase P contains at least four protein subunits, Rpp21, Rpp29, Rpp30 and Pop5 (by nomenclature of human RNase P protein subunits), which share sequence homology with yeast and human RNase P proteins [10]. An additional protein L7Ae, a ribosomal protein and homolog of human RNase P protein Rpp38, co-purifies with RNase P activity in *Methanococcus maripaludis (Mma)* and increases the catalytic efficiency ($k_{cat}/K_M$) of pre-tRNA cleavage by 360-fold [104].

Low-level single-turnover activity is detected from type-A archaeal RNase P RNA alone from certain species such as methanobacteria, thermococci and halobacteria under high ionic strength and $Mg^{2+}$ concentration conditions [73]. The poor catalytic activity of archaea P RNA is suggested to result from low substrate affinity ($K_M$ > 40 μM) [73]. The weak substrate affinity may due to loss of certain secondary structural elements (P18, P13/14) that form long-range tetraloop interactions and juxtapose the S- and C-domain observed in bacterial P RNA [8]. The bulges in P10/11 of bacterial S-domain that are proposed in substrate recognition are also missing in archaeal and eukaryal P RNAs. This lack of tertiary structure stabilization by P18 and P13/14 may be compensated by protein subunits that bind to and stabilize P RNA structure [105]. Footprinting data using recombinant proteins suggest that the protein pairs, Rpp21-Rpp29 and Pop5-Rpp30, contact the S-domain and C-domian of *Pyrococcus furiosus* P RNA, respectively [106, 107]. In accordance with this P RNA binding location, Rpp21-Rpp29 proteins enhance

substrate affinity and Pop5-Rpp30 increases the rate of cleavage [108, 109]. These proteins also play a role in cleavage site-selection in small model substrates [110]. Three-dimensional structures of some archaeal proteins have been determined: Rpp30 (PDB ID: 1V77 [111]), Pop5 (PDB ID: 2AV5 [112]), Rpp29 (PDB IDs: 1PC0 [113], 1OQK [114], 1V76 [115], and 1TS9 [116]), Rpp21 (PDB IDs: 1X0T [117] and 2K3R [118]) and Rpp38 (PDB ID: 2CZW [119]). In the future, structures of archaeal RNase P holoenzyme and/or ternary complex will provide great insights into the molecular recognition and catalytic mechanism of this multi-unit enzyme, in comparison with the bacterial enzyme [19].

Eukaryal nuclear RNP RNase P contains one RNA and nine to ten proteins (4-5 are archaeal homologs) and shares at least eight protein subunits with its sibling, RNase MRP (mitochondrial RNA processing ribonuclease) [120-125]. RNase MRP is mainly localized in the nucleus [126, 127] and processes precursor ribosomal RNA (pre-rRNA) [128-130]. Human RNase MRP has been implicated in diseases [131, 132]. Compared to their bacterial and archaeal counterparts, eukaryal RNase P enzymes are not as well characterized structurally and biochemically. A crystal structure of two yeast RNase P/MRP proteins, Pop6 and Pop7, in complex with the P3 domain of P RNA has been determined [133]. The P3 domain in eukaryal P RNA typically contains a distinct large internal loop not present in bacterial and archaeal P RNAs [35] (Figure 1-3). Two-hybrid analysis and UV-crosslinking studies have partially revealed the structural organization of the yeast RNase P holoenzyme [134, 135]. A recent low resolution modular architecture defined by electron microscopy studies suggests that the overall modular structures of yeast nuclear RNase P and

RNase MRP are different, which may explain their different substrate specificity [136].

### 1.2.2 RNase P without RNA

An RNase P enzyme lacking an RNA subunit has long been proposed in plants and human mitochondria from the different density, insensitivity to nuclease treatment and reactivity with *pro-R*p phosphorothioate modified pre-tRNA substrate [137-140]. Furthermore, RNase P RNA genes have not been identified in most land plants, and some algae and protists groups [12, 124], indicating either the absence of this gene or a sequence that diverges greatly. RNase P activity independent of an RNA subunit was first demonstrated in human mitochondrial RNase P from a complex of three recombinant proteins, MRPP1 (TRMT10C), MRPP2 (SDR5C1) and MRPP3 (or "proteinaceous RNase P, PRORP) [141]. Subsequently, a single protein that has RNase P activity has been identified and characterized from *Arabidopsis thaliana* (PRORP1 in mitochondria and chloroplast, PRORP2 and 3 in nucleus) [142, 143] and *Trypanosoma brucei* (PRORP1 in nucleus and PRORP2 in mitochondria) [31]. PRORP, MRPP1 and MRPP2 proteins do not show significant sequence homology to any previously identified RNase P protein components. Remarkably, *T. brucei* PRORP1 is able to substitute the large multi-subunit yeast nuclear RNase P *in vivo* albeit with a slower growth rate [31]. In small green algae, *Ostreococcus tauri*, mitochondrial and chloroplast genomes each encode a distinct RNase P RNA gene, and the nuclear genome encodes a bacterial P protein-like protein and a PRORP analog, but cellular locations and *in vitro* functions of these components have not been demonstrated [144]. These findings and sequence homology from a

wide range of eukaryal branches suggest that PRORP may have originated from the root of the eukaryal tree [31].

The crystal structure of *A. thaliana* PRORP1 revealed three distinct domains in this protein-only RNase P [23] (Figure 1-6). The C-terminal metallonuclease domain is linked to the N-terminal pentatricopeptide repeat domain (PPR) domain by a structural-zinc domain. The metallonuclease domain is structurally homologous to the Nedd4-BP1, YacP nucleases (NYN) which has structural homology to FLAP nucleases [145]. PRORP1 cleavage activity is also dependent on divalent metal ions such as $Mg^{2+}$ and $Mn^{2+}$ [23, 146]. The metal-bound structure of PRORP1 reveals an active site with conserved aspartate residues that can bind two manganese ions [23]. Therefore, a two metal ion, general acid/base mechanism is proposed [23] (Figure 1-8). The PPR domain has multiple helical repeats that enhance pre-tRNA affinity and is important for cleavage activity [23]. PPR domains are also found in a large number of RNA-binding proteins involved in mitochondrial and chloroplast gene expression [147-150].

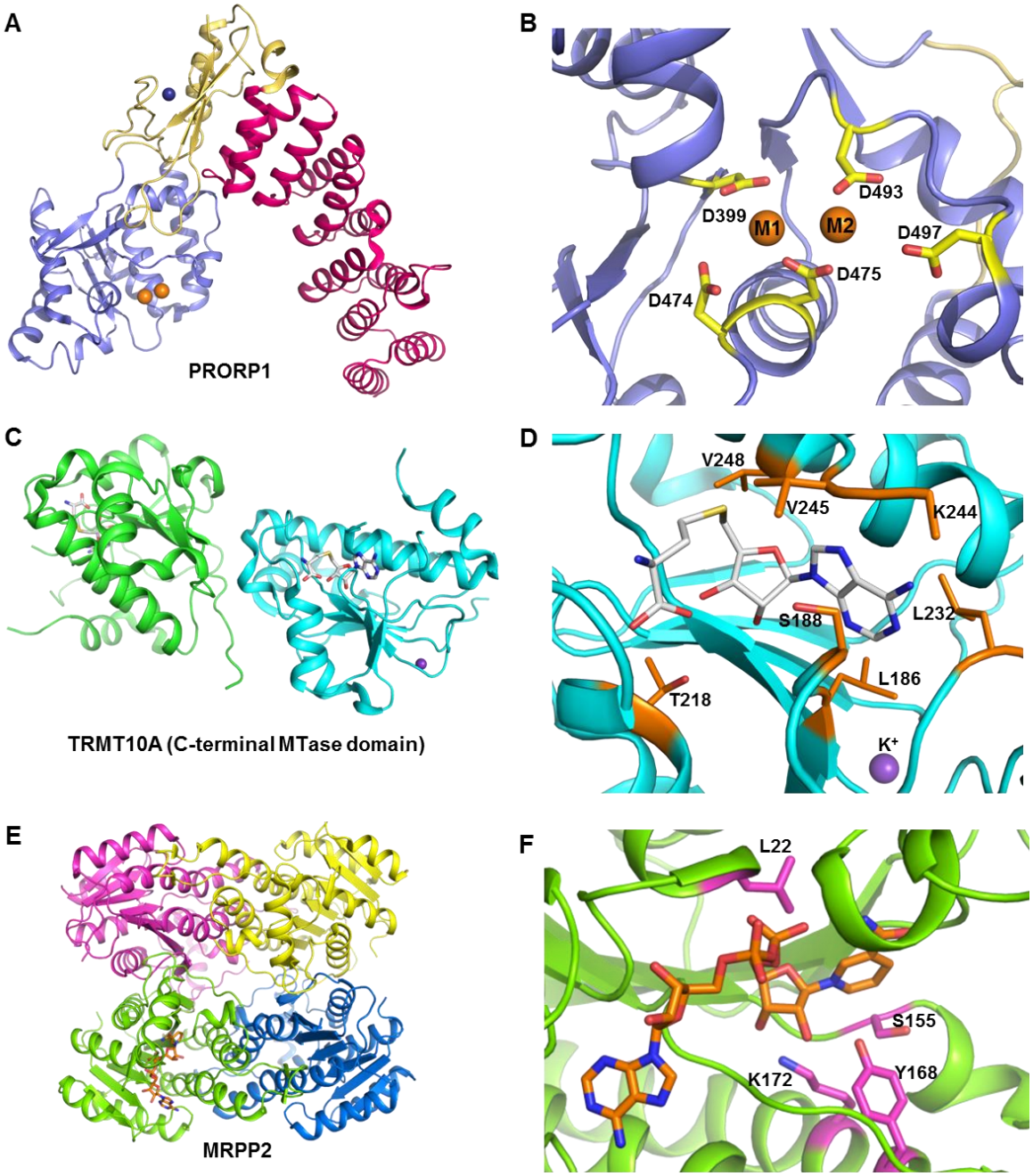


**Figure 1-6:** Crystal structures of protein-only RNase P proteins and/or analogs. **(A)** *A. thaliana* PRORP1 structure with two $Mn^{2+}$ ions (PDB ID: 4G24 [23]) showing the metallonuclease (blue, $Mn^{2+}$ in orange sphere), Zinc-domain (yellow, $Zn^{2+}$ as blue sphere) and PPR-domain (dark pink). **(B)** A close-up of $Mn^{2+}$-bound PRORP1 active site. **(C)** Crystal structure of C-terminal methyltransferase domain (MTase domain, PDB ID: 4FMW) of human TRMT10A, a homolog of MRPP1, showing a homodimer with bound *S*-adenosyl-L-homocysteine (SAH, gray molecule) and $K^+$ ion (purple sphere). **(D)** Close-up of the SAH binding site in TRMT10A. **(E)** Crystal structure of MRPP2 (PDB ID: 1U7T [151]) with a bound NAD molecule (orange). **(F)** Close-up the NAD binding site in MRPP2.

MRRP3 (PRORP), which shares 29% amino acid sequence similarity with *A. thaliana* PRORP1, is the metallonuclease subunit in human mitochondrial RNase P (mtRNase P). However, MRPP3 requires two other proteins, a tRNA methyltransferase (MRPP1) and a short-chain fatty acid dehydrogenase (MRPP2) to cleave mitochondrial pre-tRNA substrates [141]. All three human MRPP proteins are encoded in the nucleus and imported into the mitochondria [141]. MRPP1 (TRMT10C) belongs to the TM10 family of *S*-adenosyl-methionine (SAM) dependent tRNA $m^1$Guanosine methyltransferases [152, 153]. MRPP2 activates MRPP1 in catalyzing the $N^1$ methylation of both guanosine and adenosine at position 9 ($m^1$R9) in mt-tRNA [152]. A crystal structure of the MTase domain (C-terminal) of human TMRT10A (or TM10A), a MRPP1 analog, has been solved (Figure 1-6D, PDB ID: 4FMW [154]). The C-terminal region of MRPP1 likely adopts a similar MTase fold based on sequence homology [153]. MRPP2 (SDR5C1) is a $NAD^+$-dependent dehydrogenase that catalyzes β-oxidation of various short-chain steroid and fatty acid substrates [155, 156]. MRPP2 forms a homotetramer in solution and in crystal structures (PDB ID: 1U7Z [151], Figure 1-6F). Upon binding to β-amyloid (Aβ), MRPP2 has a deformed NAD binding site, which may provide a link to Alzheimer's disease (PDB ID 1SO8 [157]). Additional structural and biochemical studies are needed to elucidate the molecular details of the roles of each mtRNase P subunits in catalysis and substrate recognition.

In HeLa cells, a knockdown of each mtRNase P subunits by siRNA causes accumulation of mitochondrial precursor RNAs and subsequence defects in protein synthesis [141, 158]. MRPP1 and MRPP3 knockdown also affect processing of long

noncoding RNAs transcribed from the light strand of mtDNA [159]. Interestingly, MRPP1 and 2 localize to nascent RNA transcripts and co-localize with a newly identified mitochondrial RNA-binding protein, the G-rich sequence factor 1 (GRSF1), to form the so-called “mitochondrial RNA granules” [160]. According to the “punctuation mechanism” for human mitochondrial genome, mt-tRNA processing by mtRNase P is an important first step in mitochondrial mRNA biogenesis [161-163]. Our understanding of the cellular location, biological function and structure of human mtRNase P has just begun.

### 1.2.3 RNase P as a Drug Target

Bacterial RNase P is one of two known RNA-based catalysts that behave as classic enzymes, catalyzing multiple turnovers and remaining unchanged following catalysis [164]. The other example is the ribosome, a large ribonucleoprotein complex of which the ribosomal RNA is both catalytic and the prime target of numerous antibiotics, including aminoglycosides and macrolides [165]. As an essential RNA-based enzyme, bacterial RNase P fulfills several criteria as a novel broad-spectrum antimicrobial drug target [25, 166-168]. RNase P is essential for bacterial cell viability so the disruption of its function by inhibitors will affect bacterial cell growth [75, 169, 170]. Furthermore, the conserved structural features in the bacterial form of this enzyme suggest the possibility of developing compounds that inhibit a broad range of bacterial RNase Ps [25]. Additionally, substantial differences in composition between the bacterial and eukaryal RNase P indicate that it should be possible to achieve selectivity between the pathogen and the host enzymes to

limit toxicity [3, 171, 172]. However, clinically useful inhibitors targeting RNase P have not been reported (for a comprehensive discussion see [30]).

A few bacterial RNase P inhibitors, including small synthetic molecules and known antibiotics, have been reported (Figure 1-7). Several synthetic compounds such as bis-benzimidazoles ($IC_{50}$ = 5 – 21 μM) [173-175], porphines and porphyrins ($K_i$ = 1 – 4 μM) [175] inhibit *E. coli* RNase P by binding to the pre-tRNA substrates. Recently, a small molecule (RNP A1000, Figure 1-6C) has been suggested to interact with the protein component of *Staphylococcus aureus* RNase P and alter cellular mRNA turnover and pathogenesis [176]. This compound has not yet been studied against RNase P holoenzyme activity.

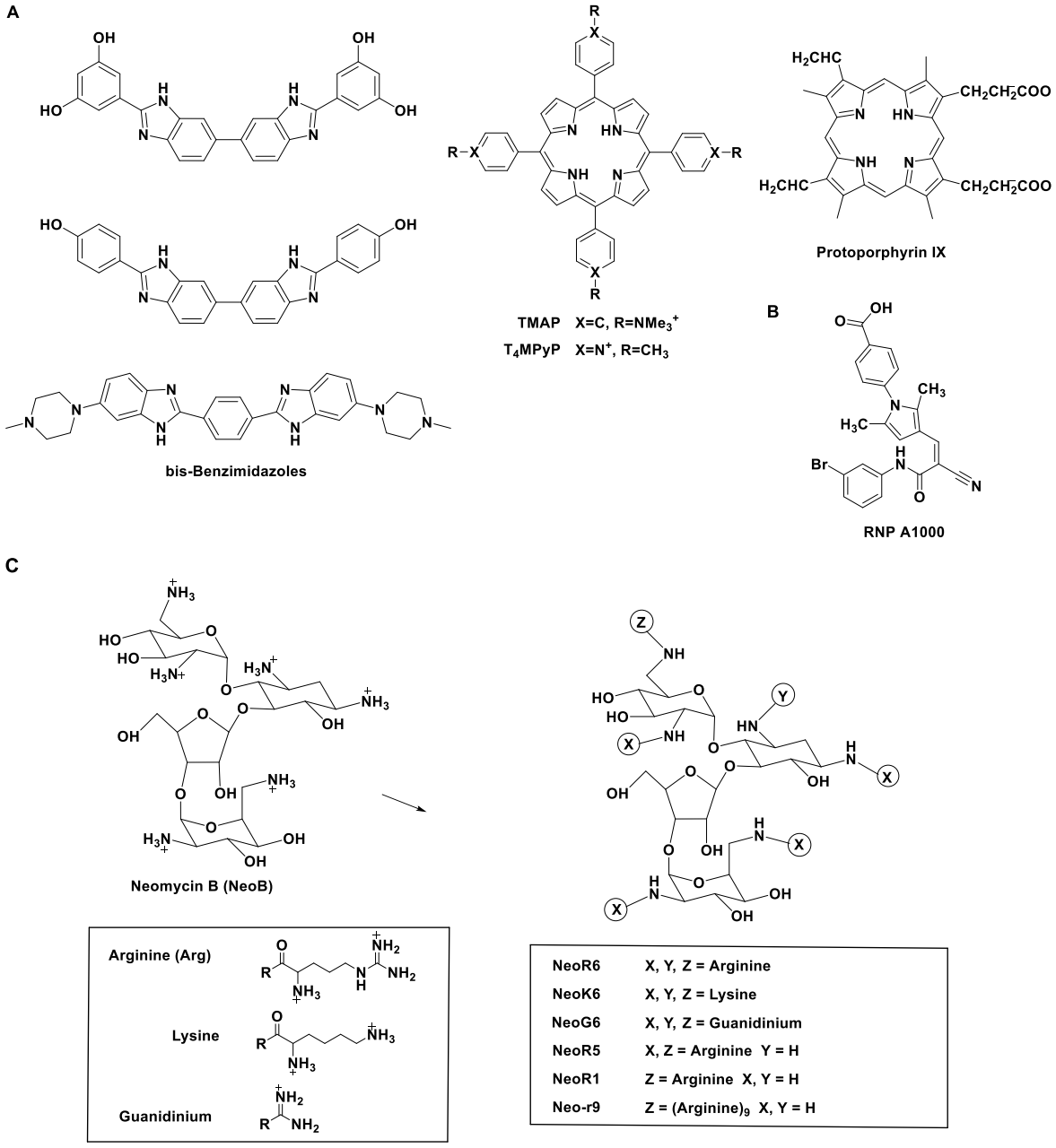


**Figure 1-7:** Bacterial RNase P inhibitors. (A) Synthetic compounds that inhibit *E. coli* RNase P by binding to pre-tRNA substrate [173-175]. (B) A small molecule inhibitor suggested to affect the protein subunit of S. aureus RNase P [176]. (C) Neomycin B and neomycin B-amino acid conjugates that inhibit *E. coli* RNase P [177-179].

Aminoglycosides (mainly neomycin B and kanamycin B) and neomycin B-amino acid conjugates, inhibit *E. coli* RNase P with $IC_{50}$ values from 0.1 to 6 μM (Figure 1-7) [177-179]. A neomycin B·hexa-arginine conjugate (NeoR6) has an $IC_{50}$

of about 125 nM for *E. coli* RNase P [178]. Inhibition of *E. coli* RNase P by aminoglycosides is competitive with $Mg^{2+}$ and decreases at high pH [177, 178]. Neomycin B also suppresses $Pb^{2+}$-induced cleavage by P RNA [177]. Thus, aminoglycosides are proposed to inhibit RNase P by displacing $Mg^{2+}$ ions bound to P RNA [177, 180]. Possible interaction of NeoR6 with metal ions near L15 region of bacterial P RNA has been proposed based on the loss of inhibition against an archaeal type-M RNase P that lacks L15 loop [179]. However, mutations and deletions in the proposed metal binding site in the L15 loop in *E. coli* P RNA do not significantly affect inhibition by NeoR6 conjugates [179], leaving the mode of inhibition unclear. Computational calculations suggest that the NeoR6 conjugates could compete with both pre-tRNA and P protein on binding to P4 and P15 helices and displace $Mg^{2+}$ ions near the P4 helix and the P15 loop [181], but biochemical studies directly testing these hypothesis have not been reported to date.

Discovery of more potent and specific inhibitors and analysis of the mechanism of inhibition will allow the evaluation of feasibility of targeting RNase P for novel antimicrobial agents [25]. In addition, the development of compounds that can specifically bind to the RNase P RNA and/or protein subunits will serve as useful chemical biology tools for probing structure and function of this essential enzyme. Traditional radiochemical assays for RNase P are discontinuous, labor-intensive and less suitable for a high-throughput screening format. Therefore, I have developed a real-time fluorescence polarization assay to facilitate measurement of the cleavage activity of *B. subtilis* RNase P and performed high-throughput screens to search for new inhibitors, which is reported in Chapter 2.

## 1.3 Catalytic Mechanism

### 1.3.1 Catalysis and Role of Divalent Metal Ions

RNase P catalytic activity is absolutely dependent on divalent metal ions [41, 44]. RNase P catalyzed pre-tRNA cleavage is activated by $Mg^{2+}$, $Ca^{2+}$, $Mn^{2+}$ and $Zn^{2+}$ *in vitro* [182-184], and likely utilizes $Mg^{2+}$ as a cofactor *in vivo* [42-44]. A large number of $Mg^{2+}$ ions (>150) associate with RNase P RNA [42-44, 185] and at least three specific $Mg^{2+}$ ions are involved in catalysis as suggested by Hill analysis [44, 186]. The interaction of these metal ions with RNase P can be through inner-sphere or outer-sphere contacts. An inner-sphere metal ion directly coordinates a functional group in the P RNA while the interaction with an outer-sphere metal ion is water-mediated [187]. Specific $Mg^{2+}$ ions could be catalytic or co-catalytic metal ions that coordinate functional groups in P RNA and/or pre-tRNA substrate to enhance substrate affinity, stabilize conformational change, activate the nucleophile and stabilize the transition state [188].

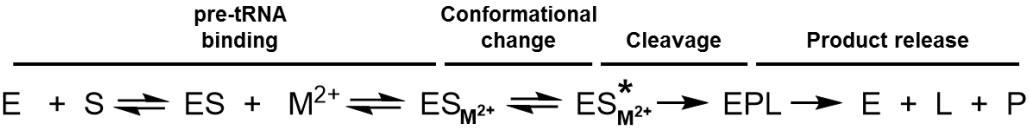


**Scheme 1-1:** A minimum kinetic mechanism for B. subtilis RNase P. This kinetic mechanism shows pre-tRNA substrate (S) association to RNase P (E), a metal ion stabilized conformational change (ES to ES*), cleavage and product release (L: 5' leader, and P: tRNA) [189, 190].

Our lab has developed a minimum kinetic mechanism for the *B. subtilis* holoenzyme using transient kinetic methods, which suggests that at least two classes of inner-sphere metal ions are required to achieve catalysis by *B. subtilis* RNase P (Scheme 1-1) [189, 190]. To investigate the role of inner-sphere metal ions

in RNase P, the RNase P-pre-tRNA complex (ES) can be formed in cobalt hexamine (Cohex, $Co(NH_3)_6^{3+}$), a $Mg(H_2O)_6^{2+}$ mimic. Cobalt hexamine does not catalyze phosphodiester cleavage so divalent metal ions can be mixed with $ES_{Cohex}$ to activate active ES* conformation and/or catalysis. Under these conditions, at least one high affinity metal ion ($K_{1/2,\,Mg^{2+}}^{\Delta cmf}$ ~ 60 μM) stabilizes a conformational change that occurs after pre-tRNA binding to RNase P (ES to ES*) and that increases substrate affinity [191, 192]. Another class of lower affinity metal ion ($K_{1/2,\,Mg^{2+}}^{cleavage}$ ~ 20 mM) activates cleavage. The conformational change step is coupled to the interaction between the P protein and the 5' leader of pre-tRNA and is rate-limiting for cleavage at high pH. Single molecule fluorescence resonance energy transfer (smFRET) experiments also show that in $Co(NH_3)_6^{3+}$ the majority of the RNase P-pre-tRNA complex is in the ES conformation (80-90%). Addition of calcium ions increases the population of ES*, indicating that the metal ions stabilize the active ES* conformation (Koutmou, Walter and Fierke, manuscript in preparation). However, the binding sites for these functionally important $Mg^{2+}$ ions in pre-tRNA and/or bacterial RNase P holoenzyme remain unclear.

The newly identified protein-only RNase P enzymes provide a model system to compare catalytic strategies used by ancient (RNA) and modern (protein) enzymes. It was speculated that protein enzymes evolved to increase catalytic efficiency [193, 194]. However, the efficiencies of pre-tRNA cleavage catalyzed by *A. thaliana* PRORP1, 2 and 3 are substantially slower ($k_{cat}/K_M$ ~1 x$10^5$ $M^{-1}s^{-1}$ at 37˚C) [22, 24, 195, 196] than the bacterial RNase P holoenzyme (~4 x$10^6$ $M^{-1}s^{-1}$) [164] and the yeast nuclear RNase P holoenzyme which reacts near the diffusion control limit (~1

x $10^8$ $M^{-1}s^{-1}$) at 37˚C [197]. P RNA is proposed to use a metal-bound hydroxide as the catalytic nucleophile and one or more metal ions for transition state stabilization [198], while PRORP1 may adopt a two-metal-ion general acid/base mechanism, as proposed from the recent crystal structure studies [23] (Figure 1-8). In addition, the *pro-R*p non-bridging oxygen at the scissile bond is proposed to coordinate an inner-sphere metal ion for bacterial RNase P [199-202], while the phosphorothioate substitution experiments suggest that a metal ion in PRORP1 interacts with *pro-S*p oxygen at the cleavage site of pre-tRNA [23, 137, 203] (Figure 1-8). Catalytic parameters and mechanism of human mtRNase P complex have yet to be established.

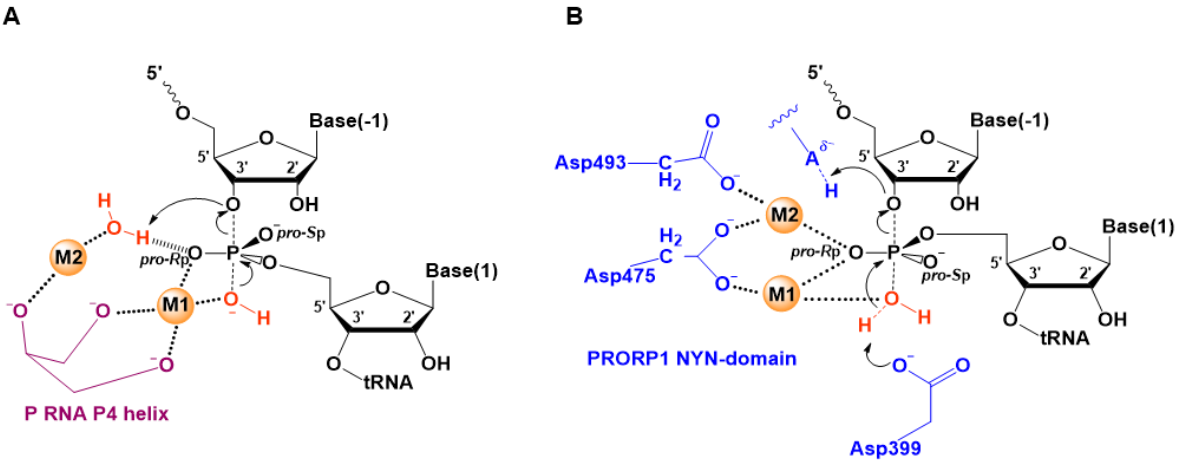


**Figure 1-8:** Comparison of proposed catalytic mechanisms for RNP and protein-only RNase P. **(A)** Model proposed from the crystal structure of *T. maritima* RNase P complex [89]. A magnesium-bound hydroxide is the nucleophile for RNA-based RNase P catalysis [204]. **(B)** A two-metal-ion general acid/base model is proposed as the mechanism for PRORP1 [23].

### 1.3.2 Identification of Metal Binding Sites in RNP RNase P

Identification of specific metal ion binding sites in RNase P RNA is complicated by the large number of nonspecific structural metal ions and the difficulties in capturing metal ions that mimic $Mg^{2+}$ in the current low-resolution crystallographic

studies [188]. Several specific metal ion ligands important for cleavage activity have been implicated by studies using atomic mutagenesis and functional group substitutions in both pre-tRNA and RNase P RNA (Figure 1-5 and Figure 1-9). Phosphorothioate substitution of the *pro-R*p nonbridging oxygen in the scissile phosphodiester bond decreases cleavage rate of P RNA by $10^3$- to $10^4$-fold which can be partially rescued by addition of thiophilic metal ions ($Mn^{2+}$ and $Cd^{2+}$) suggesting an inner-sphere coordination of a metal ion with this oxygen [199-202, 205]. Sulfur substitution of the *pro-S*p oxygen and the 3' bridging oxygen at the cleavage site lead to a slow miscleavage at -1 position catalyzed by P RNA, which suggests possible roles of these oxygen atoms in catalysis [206]. In the N(-1) nucleotide, 2'-deoxy substitution for the 2'-OH group decreases reaction rate 200- to 3000-fold and decreases $Mg^{2+}$ affinity by $10^4$-fold (cooperativity from 3 to 2) for P RNA. In addition, 2'-$NH_2$ substitution at 2' position leads to miscleavage at low pH and $10^3$-fold lower cleavage rate at high pH [205]. The reduced activity by 2'-$NH_2$ and 2'-H modifications can be increased by about 100-fold by $Mn^{2+}$ ions [205]. Therefore, this 2'-OH group is suggested to interact with a metal ion though a water molecule [207]

In P RNA, helix P4 is the most highly conserved region, harboring 6 of the 13 universally conserved nucleotides [6] (Figure 1-5 and Figure 1-9). Nucleotide analog interference mapping (NAIM) results suggest that the P1-P4 multihelix junction coordinates one or more $Mg^{2+}$ ions important for activity of *E. coli* RNase P [91] (Figure 1-55B). In *E. coli* and *B. subtilis* RNase P P RNA, phosphorothioate modification of the non-bridging oxygen atoms in the backbone phosphodiester

bonds of A49 and G50 (*B. subtilis* numbering corresponding to A67 and G68 in *E. coli*) reduce the single-turnover cleavage rate by 100- to $10^4$-fold without affecting global structure and substrate affinity [92, 93, 185]. Some of these sulfur substitutions can be rescued by $Mn^{2+}$ and/or $Cd^{2+}$, suggesting inner-sphere coordination with metal ions is important for catalysis. When $Mn^{2+}$ is used to rescue the catalytic activity of *E. coli* P RNA with *pro-R*p and *pro-S*p sulfur substitutions in A49, two different affinities of $Mn^{2+}$ ions are observed, suggesting two distinct metal ions bind to the nonbridging oxygens [92, 93]. An N7-deaza-2'deoxyadenosine substitution of either A48 or A47 in combination with the *pro-S*p sulfur substitution of A49 in *E. coli* P RNA further decrease cleavage rate but the N7-deaza modification alone in A48 or A47 does not affect catalytic activity [185].

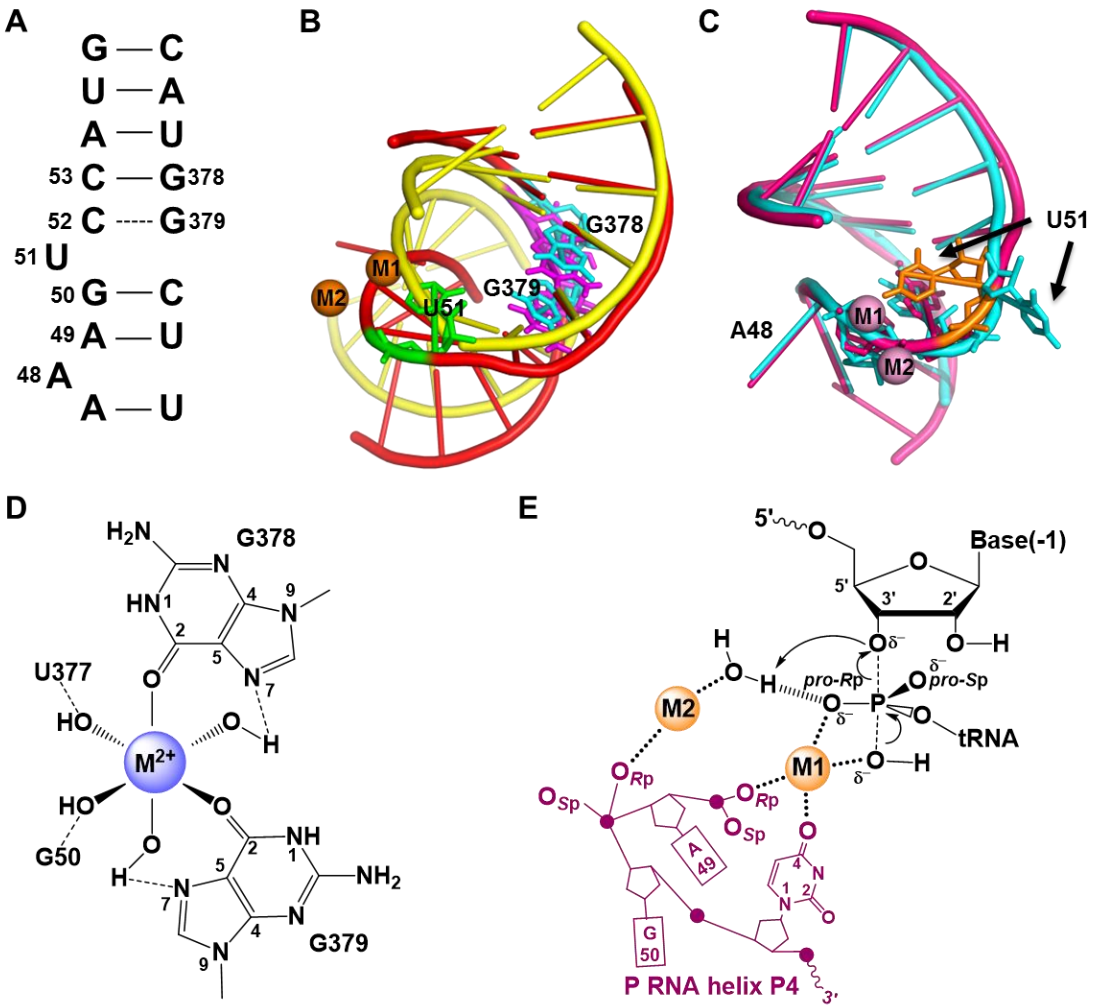


**Figure 1-9:** Models for inner-sphere metal ion binding sites in the helix P4 of baterial P RNA. **(A)** Sequence of *B. subtilis* RNase P helix P4. **(B)** Overlay of the NMR model of *B. subtilis* P4 helix [95] (yellow, and G378, G379 in cyan) with the *T. maritima* RNase P ternary structure [89] (red and orange spheres showing metal ions and G378, G379 in magenta, U51 is in green). **(C)** Overlay of helix P4 structure in *T. maritime* RNase P ternary complex [89] (dark pink with U51 colored in orange and metal ions are pink spheres) and *B. stearothermophilus* P RNA [88]. **(D)** Metal coordination in the NMR model [95]. **(E)** Transition state model proposed from *T. maritima* RNase P ternary complex crystal structure [89].

X-ray absorption and NMR spectroscopic studies on a P4 helix stem-loop mimic propose a model in which nucleobases corresponding to G378 and G379 coordinate an inner-sphere $Mg^{2+}$ ion (Figure 1-9) [94, 95]. Anomalous X-ray scattering analyses of *B. stearothermophilus* C-domain crystals (3.5 Å resolution)

soaked in heavy metal ions (such as $Os^{3+}$, $Pb^{2+}$, $Sm^{3+}$, $Gd^{3+}$, or $Yb^{3+}$) also indicate a number of possible metal ion binding sites near helix P4 (M4, M5, M6 in Figure 1-5B) [96]. In the recent *T. maritima* RNase P•tRNA ternary complex, two metal ions ($Sm^{3+}$, and $Eu^{3+}$ soak, 4.2 Å resolution) are observed adjacent to the backbone phosphate of A49 and G50 and the carbonyl oxygen at position 4 (O4) in the base of U51 [89] (M1, M2 in Figure 1-9C). This observation is in accordance with previous phosphorothioate substitution data that the pro-*R*p oxygen at A49 and G50 backbone phosphodiester bonds directly coordinates a metal ion important for catalysis. However, there is little biochemical evidence of the proposed inner-sphere coordination of the M1 metal with O4 in U51, a universally conserved nucleotide that is often identified as a bulge by solution probing [208] and in free P RNA structures [86, 88] (Figure 1-9). In contrast, in the *T. maritima* RNase P ternary complex crystal structure, this U is flipped to an inward position [89] (Figure 1-9C).

In *E. coli* P RNA, site-directed mutations that delete or reposition the bulged uridine in helix P4 decrease cleavage of normal substrate by up to 70-fold (U to C), and decrease the substrate affinity of P RNA by 50- and 100-fold (U to G and double U bulge, respectively) [209]. $Tb^{3+}$-catalyzed cleavage of P RNA suggest that none of these mutations affect the global folding of P RNA [209]. The 4-thiouridine modification of this nucleotide cross-links to the +5 nucleotide in the acceptor-stem of pre-tRNA substrate [210], which might suggest that this uridine is not located next to the cleavage site in an active conformation. Mutation of this uridine in the *T. maritima* RNase P to cytosine affects the catalytic efficiency ($k_{cat}/K_M$) of holoenzyme by 10-fold. But the U52C/R89A and U52C/F17A double mutants (Figure 1-4B) lead

to 200- to 1700-fold decrease in activity ($k_{cat}/K_M$) [211]. These biochemical studies suggest that the positioning and identity of this uridine play an important role in RNase P catalysis but did not provide direct evidence for an inner-sphere interaction with a catalytic metal ion. Therefore, in Chapter 3, I applied nucleotide analog substitutions in combination with transient kinetics to directly probe the divalent metal ion binding and biochemical functions of this universally conserved uridine in *B. subtilis* RNase P.

### 1.4 Substrate Recognition

RNase P is a versatile enzyme that can catalyze the cleavage of various substrates *in vivo* and *in vitro* (see summaries in [34, 212]). Bacterial RNase P can process pre-4.5S RNA [213], pre-tmRNA [214], mRNAs [215-217], and riboswitches [218, 219]. The catalytic efficiency ($k_{cat}/K_M$) for certain non-tRNA substrates, such as pre-4.5S RNA, is comparable to that of pre-tRNA but with a higher $K_M$. Eukaryal RNP RNase P cleaves unstructured RNAs [220] and non-coding RNAs [221, 222] in a manner that is independent of structure or sequence. These broad substrate pools highlight the importance of RNase P function in cells. The primary and most studied RNase P substrate is pre-tRNA. Therefore I will focus the following discussion on substrate recognition of pre-tRNA substrates and pre-tRNA-derived model substrates.

#### 1.4.1 Structural Features of tRNA

Most tRNAs from all kingdoms have a consensus “canonical” cloverleaf secondary structure (Figure 1-10), except for many metazoan mitochondrial tRNAs

which deviate from the canonical tRNA in primary sequence, secondary structure and likely tertiary structure [223]. Mammalian tRNA can be divided into four different groups [110]. One type is similar to canonical tRNA where the majority of nucleotides in the D-loop and TψC-loop engaged in tertiary interactions (Figure 1-10) are conserved, such as human mt-tRNA$^{Leu(UUR)}$ (Figure 1-12L). The majority of mammalian mt-tRNAs have lost the conserved tertiary interactions between the D- and TψC-loop, such as in human mt-tRNA$^{Tyr}$ (Figure 1-12M). In an extreme case, mammalian mt-tRNA$^{Ser(AGY)}$ lacks the entire D- or T-domain (Figure 1-12N). These "bizarre" tRNAs raise the question whether the human mtRNase P proteins are evolved to specifically recognize these substrates [224].

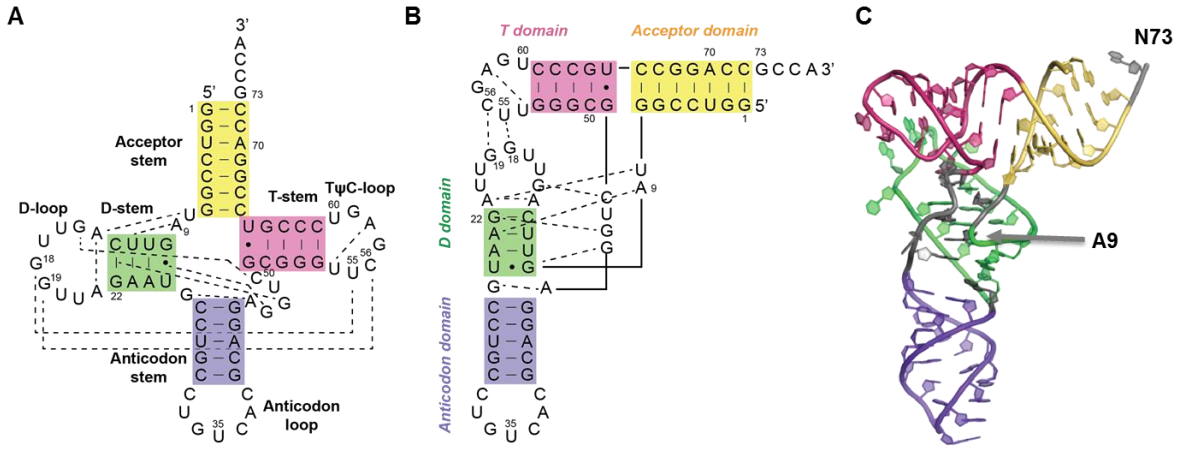


**Figure 1-10:** Secondary and tertiary structures of canonical tRNA. **(A)** and **(B)** Secondary structure of *B. subtilis* tRNA$^{Asp}$. **(C)** A crystal structure of an unmodified *E. coli* tRNA$^{Phe}$ (PDB ID: 3L0U, [225])

### 1.4.2 Sequence-specific Interactions by Bacterial RNase P

Both P protein and P RNA contribute to the recognition of pre-tRNA substrates (Figure 1-5 and Figure 1-11). RNase P holoenzyme has a higher binding affinity for

pre-tRNA relative to tRNA [164]. The affinity and cleavage rate of pre-tRNA by holoenzyme also depends on the leader length from 2- to 5-nt [79, 226]. This trend is not observed in P RNA alone [79, 226], suggesting that the bacterial P protein enhances the substrate affinity and cleavage activity of RNase P by interacting with the 5' leader. This interaction with 5' leader also results in uniformed binding affinity of various pre-tRNA substrates by combining low affinity tRNA body with high affinity leader sequences [227]. Cross-linking and fluorescence resonance energy transfer (FRET) experiments first demonstrated a direct interaction between the 5' leader and P protein [80, 226]. The observed leader position in the *T. maritima* RNase P complex structure is consistent with these biochemical data [89].

Sequence-specific interactions between bacterial RNase P have been identified in both 5' sequence flanking the tRNA genes and the 3' RCCA motif [61, 62, 228, 229], Figure 1-10). These interactions enhance pre-tRNA affinity and cleavage. The 3' RCCA motif of tRNA forms Watson-Crick base pairs with a UGG sequence in the P15 loop (L15) [230]. The 3' RCCA interaction motif is missing in archaeal type-M P RNA and eukaryal P RNA, consistent with the lack of encoded 3' CCA motif in pre-tRNA genes in these organisms [2].

In the 5' leader, biochemical studies identified a sequence preference for uracil at position N(-1) in pre-tRNA in both *E. coli* and *B. subtilis* and suggest a base pairing interaction between this nucleotide and an adenine in J5/15 of P RNA [62, 231]. Statistical analyses of the sequences of pre-tRNA genes for these species also reveal an enrichment of U at this position [232]. For *B. subtilis* RNase P, mutations at the N(-2) position also modulate substrate affinity and adenine is preferred at this

position forming a trans-Waston-Crick-sugar-edge interaction with G319 in *B. subtilis* P RNA (Lim, Chen and Fierke, unpublished data) [233]. This A preference is consistent with a statistically significant enhancement of A content at the N(-2) position in *B. subtilis* pre-tRNA genes [232]. A nucleotide preference of adenine at the N(-4) position is suggested from a combination of hydrogen bonding and steric interactions with F20 and Y34 residues in *B. subtilis* P protein [232]. In *B. subtilis* this sequence selectivity is magnified at physiologically relevant divalent metal ion concentrations (~1-3 mM). The base identity at the N(-3) position of *B. subtilis* pre-tRNA also affects pre-tRNA affinity and is proposed to be located near P RNA/P protein interface and interact with both subunits [233]. These proposal of N(-1) to N(-4) interactions are consistent with the leader position observed in the crystal structure of *T. maritima* RNase P ternary complex [89] (Figure 1-4). These sequence preferences are also interdependent, varying as the identity of the neighboring base changes [232, 233].

Bioinformatic analyses on pre-tRNA genes from 161 bacterial species suggest that 91% of these species have statistically significant enrichments in the 5' leader region [232]. Nucleotides N(-1) to N(-4) have the highest enrichment with an increasing number of species showing preferences as the position is closer to the RNase P cleavage site. These genomic data also suggest different patterns of nucleotide enrichments for different bacterial species [232]. These results together suggest that sequence-specific recognition between RNase P and pre-tRNA 5' leaders are widespread but diverse among bacterial species.

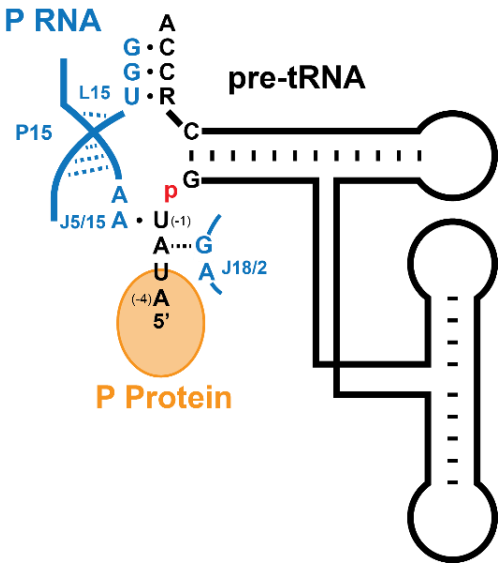


**Figure 1-11:** Sequence specific interactions between 5' and 3' sequences of pre-tRNA and bacterial RNase P. The 3' RCCA base pairs with UGG motif in the L15 loop. U(-1) contacts A256 (B. subtilis numbering, A213 in T. maritima). A(-2) interacts with G318 in B. subtilis (U294 in T. maritima).

### 1.4.3 Substrate Specificity

Identification of minimum substrate elements has also provided clues into mechanism of substrate recognition. In general, the anticodon-stem-loop domain is not needed for recognition by RNase P [234], consistent with the exposure of the anti-codon domain observed in the ternary crystal structure [89]. The first model substrate of bacterial RNase P contains the 5' leader sequence, 3' RCCA, acceptor -stem and T-stem-loop of *E. coli* pre-tRNA$^{Phe}$ [234]. A similar stem-loop model substrate and even a 3-bp-stem-tetraloop substrate derived from *E. coli* pre-tRNA$^{Tyr}$ suppressor (pre-tRNA$^{Tyr}_{su3+}$, or pSu3) can be accurately processed by P RNA with decreased catalytic efficiency (Figure 1-12A) [235]. The 5' leader, 3' RCCA and acceptor-T-stem-loop therefore are proposed as three important substrate recognition elements [5, 236]. But a D-armless mt-pre-tRNA$^{Ser(AGY)}$ (Figure 1-12N) is cleavable by *E. coli* P RNA with a 10-fold slower rate compare with D-domain

deleted *T. thermophillus* pre-tRNA$^{Gly}$ substrates (Figure 1-12H) [237], which may indicate that mitochondrial substrate is not ideal for bacterial RNase P.

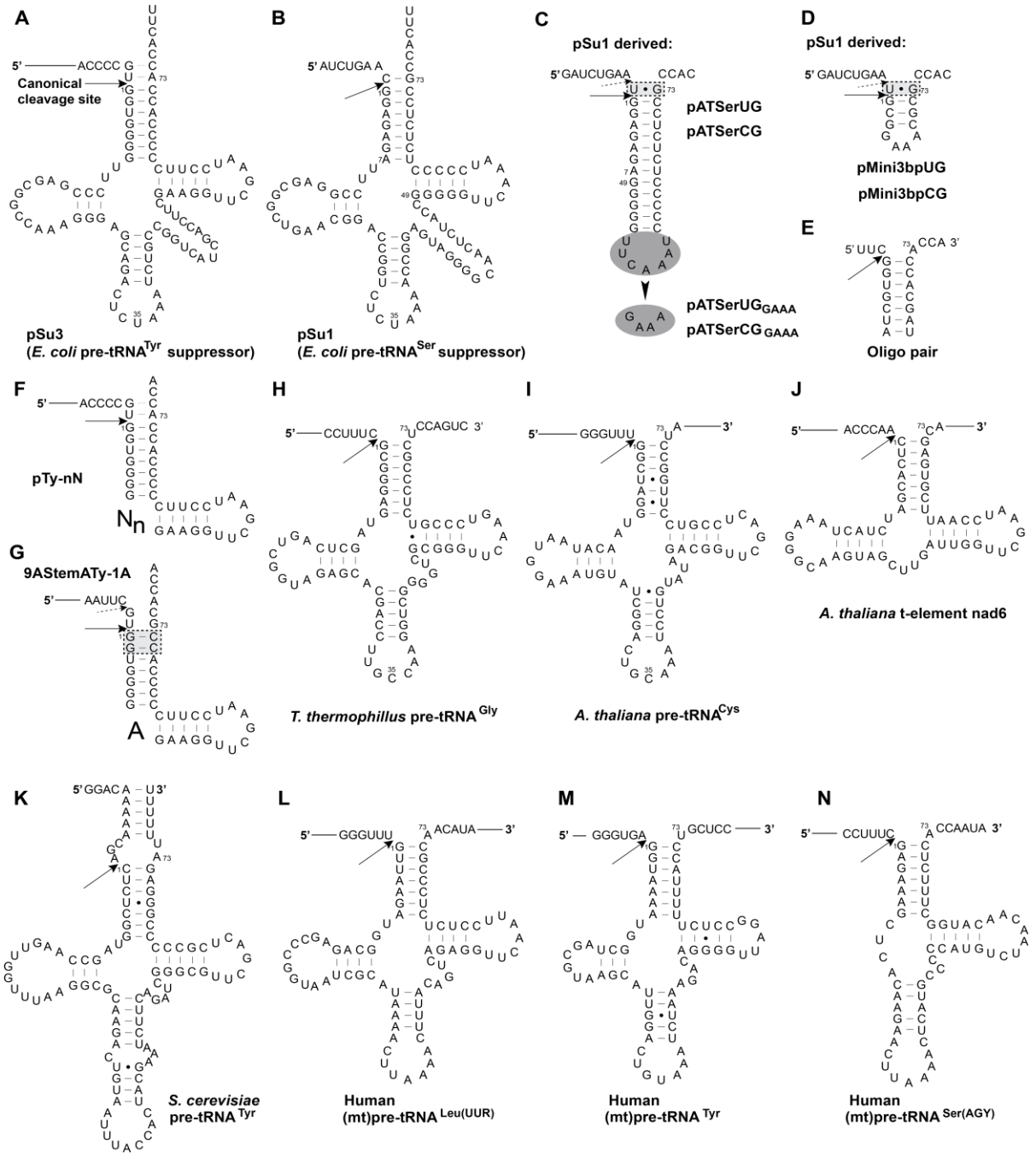


**Figure 1-12:** Secondary structure of pre-tRNA and pre-tRNA-related model substrates for RNase P. The solid arrow indicates canonical RNase P cleavage site and dashed arrow indicate miscleavage sites.

In archaeal RNase P, the protein subunits and divalent metal ions affect both cleavage fidelity and efficiency [110, 238]. For *Py*rococcus *furiosus* (*Pfu*) P RNA, either in complex with four proteins (Rpp21·Rpp29 and Pop5·Rpp30) or additions of high $Mg^{2+}$ reduce miscleavage of pATSerCG$_{GAAA}$ and pMini3bpCG model substrates [110] derived from *E. coli* pre-tRNA$^{Ser}$ suppressor [239] (Figure 1-12B to D). However, a pMini3bpUG substrate (wobble base pair at N(-1) to N73) is not detectably cleaved by *Pfu* P RNA complexed only with Rpp21·Rpp29 while the pATSerUG$_{GAAA}$ and pMini3bpUG model substrates can be cleaved by *Pfu* P RNA alone [110]. But deletion or elongation of the D-domain of a cyanobacterial pre-tRNA$^{Gln}$ substrate lead to a considerable amount of miscleavage at -1 position by *E. coli* RNase P holoenzyme [238], indicating that D-TψC-loop interaction in pre-tRNA is also an important factor for bacterial RNase P to recognize non-cognate substrates.

For human nuclear RNase P, a linker sequence of at least one nucleotide between the acceptor-stem and TψC-stem in model substrate is needed for catalytic activity [240] (Figure 1-12F). Substrate lacking the anticodon domain and most of the V-loop is not cleaved by human nRNase P, indicating that this enzyme likely recognizes a different tertiary structure features of tRNA [240]. In addition, insertions of extra base pairs (2-bp) in either the acceptor-stem (Figure 1-12G) or the T-stem in the model substrate resulted in a miscleavage at -2 position by human nuclear RNase P but did not affect the fidelity of cleavage by *E. coli* P RNA [240]. These data led to a hypothesis that eukaryal RNase P likely uses a more strict “measuring mechanism” to recognize the cleavage site [2]. In addition, a short A-U duplex region

between 5’ leader and 3’ trailer sequences of eukaryal nuclear pre-tRNA may also affect processing rate by RNase P [60, 197] (Figure 1-12K).

Because most plant tRNAs are canonical [241, 242], it is not unexpected that *A. thaliana* PRORPs can cleave a bacterial substrate (*T*. *thermophillus* pre-tRNA$^{Gly}$) [203]. Notably, *A. thaliana* PRORP2 is only able to cleave this bacterial substrate at 28 ˚C instead of 37 ˚C [203], which may suggest that dynamics of either pre-tRNA or PRORP1 are important for recognition. *A. thaliana* PRORP1 can also catalyze cleavage of a t-element substrate (Figure 1-12J) [142]. For *A. thaliana* PRORP1, conserved nucleotides in D- and TψC-loop (G18, G19, C56, and C57) are protected by PRORP1 in footprinting studies, leading to the hypothesis that the PPR-domain in the enzyme contacts this region [146]. Deletion of D- and anticodon- domains or mutation of the conserved G18 nucleotide in the *A. thaliana* pre-tRNA$^{Cys}$ (Figure 1-12I) abolishes PRORP1 catalyzed cleavage under multiple-turnover conditions [146]. However, deletion or elongation of the D-stem in the cyanobacterial pre-tRNA$^{Gln}$ substrate does not affect cleavage by *A. thaliana* RNase P extracts under single turnover conditions [238]. These data argue that the D-stem-loop contribution for PRORP catalyzed reaction is substrate-dependent.

Although plant PRORPs function as a single protein, human mtRNase P require two additional proteins (MRPP1 and 2) that may assist MRPP3 in recognizing non-canonical mt-tRNAs. Canonical tRNA species are generally cleavable by most RNase P holoenzymes except for partially purified human mtRNase P [243]. MRPP1·MRPP2 subcomplex catalyzes $N^1$ methylation of both G9 and A9 such as in mt-tRNA$^{Ile}$ and mt-tRNA$^{Lys}$ [152]. The methylation site by MRPP1

(R9) is normally buried in the tRNA structure making reverse-Hoogsten triple-base interactions with the N12-N23 base pair (Figure 1-10) [244-246]. $N^1$ methylation of A9 in mt-tRNA$^{Lys}$ has been demonstrated to switch the primary transcript from an extended hairpin to a canonical cloverleaf structure by solution structure probing and single molecule FRET experiments [247-249]. Recognition of R9 by MRPP1 may provoke a conformational change in mt-tRNA and facilitate cleavage by MRPP3 [250]. However, experimental data suggest that the methyltransferase activity is not essential for activation of MRPP3 cleavage [152]. In addition, human mt-tRNA is a hot spot for pathogenic point mutations [251, 252], but the effects of these mutations on mt-pre-tRNA processing has not been studied with recombinant human mtRNase P proteins.

Clearly, cleavage activity and recognition mechanism vary for the different classes of RNase P enzymes and may also depend on substrate identities and experimental conditions. Dissecting the mechanism of substrate recognition by different RNase P enzymes is important for designing inhibitors that specifically target RNase P in pathogens while leaving human isoforms intact. In the future, further mechanistic studies of highly purified eukaryal RNase P enzymes are still needed. Molecular details of substrate recognition by the protein-only human mtRNase P remain underexplored. Therefore, in Chapter 4, I investigate catalytic activity and substrate recognition by human mtRNase P.

## 1.5 Conclusion

In summary, recent structure and function studies of RNP RNase P have revealed new insights into the molecular basis of the interactions of the P RNA subunit interacts with protein subunits, metal ions and substrates. The structure of the bacterial RNase P holoenzyme-tRNA complex enabled a direct view of the architecture of the enzyme. In addition, the discoveries of protein-only RNase P further increased the compositional diversity of this essential enzyme and provided a new direction to investigate the evolution of RNase P. Additional high-resolution structures of all forms of RNase P and continuing structure and function studies will provide a fundamental understanding of this essential enzyme, which may ultimately assist in designing therapeutics to either target or utilize RNase P for human health.

## 1.6 Objectives of this Research

The overall objective of this thesis research is to advance our understanding of the function of RNase P, an essential divalent metal ion-dependent endonuclease and a potential drug target. Specific RNase P inhibitors have not been identified to date. Therefore, Chapter 2 describes the development of a novel real-time fluorescence polarization assay that is capable of measuring both single- and multiple-turnover cleavage activity of *B. subtilis* RNase P and ligand binding to tRNA. This assay is further optimized for high-throughput screening and a new *B. subtilis* RNase P inhibitor is identified.

In Chapter 3, I utilized the FP assay and a combination of nucleotide substitutions to probe metal binding properties of the conserved uridine in the P4

helix of P RNA and the data suggest that this universally conserved nucleotide forms an outer-sphere metal contact and is important for a conformational change step in *B. subtilis* RNase P catalysis. This is the first P RNA site identified that significantly alters the conformational change that limits the cleavage rate of RNase P.

In Chapter 4, I purified all of the three protein subunits of human mtRNase P and cloned a library of human mitochondrial pre-tRNA genes to start investigating substrate recognition by this new member of the RNase P family. Single-turnover cleavage data revealed that, unlike previously published results [141, 152], the MRPP3 subunit by itself is catalytically active. However, the MRPP1·MRPP2 subunits enhance both cleavage rate and fidelity of mitochondrial pre-tRNA substrate. Last, Chapter 5 discusses future directions that can apply the methodology and framework described in this work to further investigate the molecular basis of RNase P function.

## 1.7 References


1. Phizicky, E.M. and A.K. Hopper, *tRNA biology charges to the front.* Genes Dev, 2010. **24**(17): p. 1832-60.
2. Hartmann, R., et al., *The making of tRNAs and more - RNase P and tRNase Z.* Progress in molecular biology and translational science, 2009. **85**: p. 319-368.
3. Frank, D.N. and N.R. Pace, *Ribonuclease P: unity and diversity in a tRNA processing ribozyme.* Annu Rev Biochem, 1998. **67**: p. 153-80.
4. Kazantsev, A.V. and N.R. Pace, *Bacterial RNase P: a new view of an ancient enzyme.* Nat Rev Microbiol, 2006. **4**(10): p. 729-40.
5. Kirsebom, L.A., *RNase P RNA mediated cleavage: substrate recognition and catalysis.* Biochimie, 2007. **89**(10): p. 1183-94.
6. Walker, S.C. and D.R. Engelke, *Ribonuclease P: the evolution of an ancient RNA enzyme.* Crit Rev Biochem Mol Biol, 2006. **41**(2): p. 77-102.
7. Smith, J.K., J. Hsieh, and C.A. Fierke, *Importance of RNA-protein interactions in bacterial ribonuclease P structure and catalysis.* Biopolymers, 2007. **87**(5-6): p. 329-38.
8. Hernandez-Cid, A., et al., *Ribonucleases P/MRP and the expanding ribonucleoprotein world.* IUBMB Life, 2012. **64**(6): p. 521-8.
9. Jarrous, N. and R. Reiner, *Human RNase P: a tRNA-processing enzyme and transcription factor.* Nucleic Acids Res, 2007. **35**(11): p. 3519-24.
10. Jarrous, N. and V. Gopalan, *Archaeal/eukaryal RNase P: subunits, functions and RNA diversification.* Nucleic Acids Res, 2010. **38**(22): p. 7885-94.
11. Walker, S.C. and D.R. Engelke, *A protein-only RNase P in human mitochondria.* Cell, 2008. **135**(3): p. 412-4.
12. Goldfarb, K.C., S. Borah, and T.R. Cech, *RNase P branches out from RNP to protein: organelle-triggered diversification?* Genes Dev, 2012. **26**(10): p. 1005-9.
13. Evans, D., S.M. Marquez, and N.R. Pace, *RNase P: interface of the RNA and protein worlds.* Trends Biochem Sci, 2006. **31**(6): p. 333-41.
14. Hsieh, J., A. Andrews, and C. Fierke, *Roles of protein subunits in RNA-protein complexes: lessons from ribonuclease P.* Biopolymers, 2004. **73**(1): p. 79-89.
15. Walker, S. and D. Engelke, *Ribonuclease P: the evolution of an ancient RNA enzyme.* Critical reviews in biochemistry and molecular biology, 2006. **41**(2): p. 77-102.
16. Smith, J., J. Hsieh, and C. Fierke, *Importance of RNA-protein interactions in bacterial ribonuclease P structure and catalysis.* Biopolymers, 2007. **87**(5-6): p. 329-338.
17. Lai, L.B., et al., *Unexpected diversity of RNase P, an ancient tRNA processing enzyme: challenges and prospects.* Febs Letters, 2010. **584**(2): p. 287-296.
18. Hartmann, E. and R.K. Hartmann, *The enigma of ribonuclease P evolution.* Trends Genet, 2003. **19**(10): p. 561-9.
19. Esakova, O. and A.S. Krasilnikov, *Of proteins and RNA: the RNase P/MRP family.* RNA, 2010. **16**(9): p. 1725-47.
20. Holzmann, J., et al., *RNase P without RNA: identification and functional reconstitution of the human mitochondrial tRNA processing enzyme.* Cell, 2008. **135**(3): p. 462-474.
21. Gobert, A., et al., *A single Arabidopsis organellar protein has RNase P activity.* Nature structural & molecular biology, 2010. **17**(6): p. 740-744.
22. Gutmann, B., A. Gobert, and P. Giegé, *PRORP proteins support RNase P activity in both organelles and the nucleus in Arabidopsis.* Genes & development, 2012. **26**(10): p. 1022-1027.
23. Howard, M.J., et al., *Mitochondrial ribonuclease P structure provides insight into the evolution of catalytic strategies for precursor-tRNA 5' processing.* Proc Natl Acad Sci U S A, 2012. **109**(40): p. 16149-54.
24. Howard, M.J., et al., *RNase P enzymes: Divergent scaffolds for a conserved biological reaction.* RNA Biol, 2013. **10**(6).
25. Eder, P.S., et al., *Bacterial RNase P as a potential target for novel anti-infectives.* Curr Opin Investig Drugs, 2003. **4**(8): p. 937-43.

26. McClain, W.H., L.B. Lai, and V. Gopalan, *Trials, travails and triumphs: an account of RNA catalysis in RNase P.* J Mol Biol, 2010. **397**(3): p. 627-46.
27. Lai, L.B., et al., *Unexpected diversity of RNase P, an ancient tRNA processing enzyme: challenges and prospects.* FEBS Lett, 2010. **584**(2): p. 287-96.
28. Liu, F., *Ribonuclease P as a Tool*, in *Ribonuclease P*, F. Liu and S. Altman, Editors. 2010, Springer New York. p. 257-275.
29. Payne, D.J., et al., *Drugs for bad bugs: confronting the challenges of antibacterial discovery.* Nat Rev Drug Discov, 2007. **6**(1): p. 29-40.
30. Willkomm, D., et al., *RNase P as a Drug Target*, in *Ribonuclease P*, F. Liu and S. Altman, Editors. 2010, Springer New York. p. 235-256.
31. Taschner, A., et al., *Nuclear RNase P of Trypanosoma brucei: a single protein in place of the multicomponent RNA-protein complex.* Cell Rep, 2012. **2**(1): p. 19-25.
32. Randau, L., I. Schröder, and D. Söll, *Life without RNase P.* Nature, 2008. **453**(7191): p. 120-123.
33. Randau, L., *RNA processing in the minimal organism Nanoarchaeum equitans.* Genome biology, 2012. **13**(7).
34. Marvin, M.C. and D.R. Engelke, *Broadening the mission of an RNA enzyme.* J Cell Biochem, 2009. **108**(6): p. 1244-51.
35. Ellis, J.C. and J.W. Brown, *The RNase P family.* RNA Biol, 2009. **6**(4): p. 362-9.
36. Schedl, P. and P. Primakoff, *Mutants of Escherichia coli thermosensitive for the synthesis of transfer RNA.* Proc Natl Acad Sci U S A, 1973. **70**(7): p. 2091-5.
37. Ikemura, T., et al., *Precursor molecules of Escherichia coli transfer RNAs accumulated in a temperature-sensitive mutant.* J Mol Biol, 1975. **96**(1): p. 69-86.
38. Kole, R. and S. Altman, *Reconstitution of RNase P activity from inactive RNA and protein.* Proc Natl Acad Sci U S A, 1979. **76**(8): p. 3795-9.
39. Kole, R., et al., *E. coli RNAase P has a required RNA component.* Cell, 1980. **19**(4): p. 881-7.
40. Hansen, F.G., E.B. Hansen, and T. Atlung, *Physical mapping and nucleotide sequence of the rnpA gene that encodes the protein component of ribonuclease P in Escherichia coli.* Gene, 1985. **38**(1-3): p. 85-93.
41. Guerrier-Takada, C., et al., *The RNA moiety of ribonuclease P is the catalytic subunit of the enzyme.* Cell, 1983. **35**(3 Pt 2): p. 849-857.
42. Smith, D. and N.R. Pace, *Multiple magnesium ions in the ribonuclease P reaction mechanism.* Biochemistry, 1993. **32**(20): p. 5273-81.
43. Perreault, J.P. and S. Altman, *Pathway of activation by magnesium ions of substrates for the catalytic subunit of RNase P from Escherichia coli.* J Mol Biol, 1993. **230**(3): p. 750-6.
44. Beebe, J.A., J.C. Kurz, and C.A. Fierke, *Magnesium ions are required by Bacillus subtilis ribonuclease P RNA for both binding and cleaving precursor tRNA$^{Asp}$.* Biochemistry, 1996. **35**(32): p. 10493-505.
45. Brown, J.W., *The Ribonuclease P Database.* Nucleic Acids Res, 1999. **27**(1): p. 314.
46. Brown, J.W., et al., *Phylogenetic analysis and evolution of RNase P RNA in proteobacteria.* J Bacteriol, 1991. **173**(12): p. 3855-63.
47. Haas, E.S. and J.W. Brown, *Evolutionary variation in bacterial RNase P RNAs.* Nucleic Acids Res, 1998. **26**(18): p. 4093-9.
48. Haas, E.S., et al., *Structure and evolution of ribonuclease P RNA in Gram-positive bacteria.* Nucleic Acids Res, 1996. **24**(23): p. 4775-82.
49. Pace, N.R. and J.W. Brown, *Evolutionary perspective on the structure and function of ribonuclease P, a ribozyme.* J Bacteriol, 1995. **177**(8): p. 1919-28.
50. Siegel, R.W., et al., *Mycoplasma fermentans simplifies our view of the catalytic core of ribonuclease P RNA.* RNA, 1996. **2**(5): p. 452-62.
51. Marquez, S.M., et al., *Structural implications of novel diversity in eucaryal RNase P RNA.* RNA, 2005. **11**(5): p. 739-51.
52. Loria, A. and T. Pan, *Domain structure of the ribozyme from eubacterial ribonuclease P.* RNA, 1996. **2**(6): p. 551-63.
53. Pan, T. and M. Jakacka, *Multiple substrate binding sites in the ribozyme from Bacillus subtilis RNase P.* EMBO J, 1996. **15**(9): p. 2249-55.

54. Chen, J.L., et al., *Comparative photocross-linking analysis of the tertiary structures of Escherichia coli and Bacillus subtilis RNase P RNAs.* EMBO J, 1998. **17**(5): p. 1515-25.
55. Christian, E.L., D.S. McPheeters, and M.E. Harris, *Identification of individual nucleotides in the bacterial ribonuclease P ribozyme adjacent to the pre-tRNA cleavage site by short-range photo-cross-linking.* Biochemistry, 1998. **37**(50): p. 17618-28.
56. Niranjanakumari, S., et al., *Probing the architecture of the B. subtilis RNase P holoenzyme active site by cross-linking and affinity cleavage.* RNA, 2007. **13**(4): p. 521-35.
57. Harris, M.E., et al., *Use of photoaffinity crosslinking and molecular modeling to analyze the global architecture of ribonuclease P RNA.* EMBO J, 1994. **13**(17): p. 3953-63.
58. Pan, T., A. Loria, and K. Zhong, *Probing of tertiary interactions in RNA: 2'-hydroxyl-base contacts between the RNase P RNA and pre-tRNA.* Proc Natl Acad Sci U S A, 1995. **92**(26): p. 12510-4.
59. Westhof, E. and S. Altman, *Three-dimensional working model of M1 RNA, the catalytic RNA subunit of ribonuclease P from Escherichia coli.* Proc Natl Acad Sci U S A, 1994. **91**(11): p. 5133-7.
60. Ziehler, W.A., et al., *Effects of 5' leader and 3' trailer structures on pre-tRNA processing by nuclear RNase P.* Biochemistry, 2000. **39**(32): p. 9909-16.
61. Christian, E.L., et al., *Analysis of substrate recognition by the ribonucleoprotein endonuclease RNase P.* Methods, 2002. **28**(3): p. 307-22.
62. Zahler, N.H., E.L. Christian, and M.E. Harris, *Recognition of the 5' leader of pre-tRNA substrates by the active site of ribonuclease P.* RNA, 2003. **9**(6): p. 734-45.
63. Green, C.J., R. Rivera-Leon, and B.S. Vold, *The catalytic core of RNase P.* Nucleic Acids Res, 1996. **24**(8): p. 1497-503.
64. Loria, A. and T. Pan, *Modular construction for function of a ribonucleoprotein enzyme: the catalytic domain of Bacillus subtilis RNase P complexed with B. subtilis RNase P protein.* Nucleic Acids Res, 2001. **29**(9): p. 1892-7.
65. Wu, S., et al., *Cleavage mediated by the catalytic domain of bacterial RNase P RNA.* J Mol Biol, 2012. **422**(2): p. 204-14.
66. Harris, J.K., et al., *New insight into RNase P RNA structure from comparative analysis of the archaeal RNA.* RNA, 2001. **7**(2): p. 220-32.
67. Lai, L.B., et al., *Discovery of a minimal form of RNase P in Pyrobaculum.* Proc Natl Acad Sci U S A, 2010. **107**(52): p. 22493-8.
68. Sun, F.J. and G. Caetano-Anolles, *The ancient history of the structure of ribonuclease P and the early origins of Archaea.* BMC Bioinformatics, 2010. **11**: p. 153.
69. Frank, D.N., et al., *Phylogenetic-comparative analysis of the eukaryal ribonuclease P RNA.* RNA, 2000. **6**(12): p. 1895-904.
70. Morales, M.J., et al., *Characterization of yeast mitochondrial RNase P: an intact RNA subunit is not essential for activity in vitro.* Nucleic Acids Res, 1989. **17**(17): p. 6865-81.
71. Morales, M.J., et al., *A 105-kDa protein is required for yeast mitochondrial RNase P activity.* Proc Natl Acad Sci U S A, 1992. **89**(20): p. 9875-9.
72. Seif, E.R., et al., *Mitochondrial RNase P RNAs in ascomycete fungi: lineage-specific variations in RNA secondary structure.* RNA, 2003. **9**(9): p. 1073-83.
73. Pannucci, J.A., et al., *RNase P RNAs from some Archaea are catalytically active.* Proc Natl Acad Sci U S A, 1999. **96**(14): p. 7803-8.
74. Kikovska, E., S.G. Svard, and L.A. Kirsebom, *Eukaryotic RNase P RNA mediates cleavage in the absence of protein.* Proc Natl Acad Sci U S A, 2007. **104**(7): p. 2062-7.
75. Gossringer, M., R. Kretschmer-Kazemi Far, and R.K. Hartmann, *Analysis of RNase P protein (rnpA) expression in Bacillus subtilis utilizing strains with suppressible rnpA expression.* J Bacteriol, 2006. **188**(19): p. 6816-23.
76. Buck, A.H., et al., *Protein activation of a ribozyme: the role of bacterial RNase P protein.* EMBO J, 2005. **24**(19): p. 3360-8.
77. Kurz, J.C. and C.A. Fierke, *The affinity of magnesium binding sites in the Bacillus subtilis RNase P·pre-tRNA complex is enhanced by the protein subunit.* Biochemistry, 2002. **41**(30): p. 9545-58.
78. Sun, L. and M.E. Harris, *Evidence that binding of C5 protein to P RNA enhances ribozyme catalysis by influencing active site metal ion affinity.* RNA, 2007. **13**(9): p. 1505-15.

79. Crary, S.M., S. Niranjanakumari, and C.A. Fierke, *The protein component of Bacillus subtilis ribonuclease P increases catalytic efficiency by enhancing interactions with the 5' leader sequence of pre-tRNAAsp.* Biochemistry, 1998. **37**(26): p. 9409-16.
80. Niranjanakumari, S., et al., *Protein component of the ribozyme ribonuclease P alters substrate recognition by directly contacting precursor tRNA.* Proc Natl Acad Sci U S A, 1998. **95**(26): p. 15212-7.
81. Stams, T., et al., *Ribonuclease P protein structure: evolutionary origins in the translational apparatus.* Science, 1998. **280**(5364): p. 752-5.
82. Tsai, H.Y., et al., *Molecular modeling of the three-dimensional structure of the bacterial RNase P holoenzyme.* J Mol Biol, 2003. **325**(4): p. 661-75.
83. Fang, X.W., et al., *The Bacillus subtilis RNase P holoenzyme contains two RNase P RNA and two RNase P protein subunits.* RNA, 2001. **7**(2): p. 233-41.
84. Barrera, A., et al., *Dimeric and monomeric Bacillus subtilis RNase P holoenzyme in the absence and presence of pre-tRNA substrates.* Biochemistry, 2002. **41**(43): p. 12986-94.
85. Krasilnikov, A.S., et al., *Basis for structural diversity in homologous RNAs.* Science, 2004. **306**(5693): p. 104-7.
86. Torres-Larios, A., et al., *Crystal structure of the RNA component of bacterial ribonuclease P.* Nature, 2005. **437**(7058): p. 584-7.
87. Krasilnikov, A.S., et al., *Crystal structure of the specificity domain of ribonuclease P.* Nature, 2003. **421**(6924): p. 760-4.
88. Kazantsev, A.V., et al., *Crystal structure of a bacterial ribonuclease P RNA.* Proceedings of the National Academy of Sciences of the United States of America, 2005. **102**(38): p. 13392-13397.
89. Reiter, N.J., et al., *Structure of a bacterial ribonuclease P holoenzyme in complex with tRNA.* Nature, 2010. **468**(7325): p. 784-9.
90. Torres-Larios, A., et al., *Structure of ribonuclease P--a universal ribozyme.* Curr Opin Struct Biol, 2006. **16**(3): p. 327-35.
91. Kaye, N.M., E.L. Christian, and M.E. Harris, *NAIM and site-specific functional group modification analysis of RNase P RNA: magnesium dependent structure within the conserved P1-P4 multihelix junction contributes to catalysis.* Biochemistry, 2002. **41**(14): p. 4533-45.
92. Christian, E.L., N.M. Kaye, and M.E. Harris, *Helix P4 is a divalent metal ion binding site in the conserved core of the ribonuclease P ribozyme.* RNA, 2000. **6**(4): p. 511-519.
93. Crary, S.M., J.C. Kurz, and C.A. Fierke, *Specific phosphorothioate substitutions probe the active site of Bacillus subtilis ribonuclease P.* RNA, 2002. **8**(7): p. 933-47.
94. Getz, M.M., et al., *Structural plasticity and Mg2+ binding properties of RNase P P4 from combined analysis of NMR residual dipolar couplings and motionally decoupled spin relaxation.* RNA, 2007. **13**(2): p. 251-66.
95. Koutmou, K.S., et al., *NMR and XAS reveal an inner-sphere metal binding site in the P4 helix of the metallo-ribozyme ribonuclease P.* Proc Natl Acad Sci U S A, 2010. **107**(6): p. 2479-84.
96. Kazantsev, A.V., A.A. Krivenko, and N.R. Pace, *Mapping metal-binding sites in the catalytic domain of bacterial RNase P RNA.* RNA, 2009. **15**(2): p. 266-276.
97. Spitzfaden, C., et al., *The structure of ribonuclease P protein from Staphylococcus aureus reveals a unique binding site for single-stranded RNA.* J Mol Biol, 2000. **295**(1): p. 105-15.
98. Kazantsev, A.V., et al., *High-resolution structure of RNase P protein from Thermotoga maritima.* Proc Natl Acad Sci U S A, 2003. **100**(13): p. 7497-502.
99. Koutmou, K.S., J.J. Day-Storms, and C.A. Fierke, *The RNR motif of B. subtilis RNase P protein interacts with both PRNA and pre-tRNA to stabilize an active conformer.* RNA, 2011. **17**(7): p. 1225-35.
100. Wegscheid, B., C. Condon, and R.K. Hartmann, *Type A and B RNase P RNAs are interchangeable in vivo despite substantial biophysical differences.* EMBO Rep, 2006. **7**(4): p. 411-7.
101. Day-Storms, J.J., S. Niranjanakumari, and C.A. Fierke, *Ionic interactions between PRNA and P protein in Bacillus subtilis RNase P characterized using a magnetocapture-based assay.* RNA, 2004. **10**(10): p. 1595-608.
102. Gosringer, M. and R.K. Hartmann, *Function of heterologous and truncated RNase P proteins in Bacillus subtilis.* Mol Microbiol, 2007. **66**(3): p. 801-13.

103. Turrini, P.C., J.L. Loveland, and R.L. Dorit, *By any other name: heterologous replacement of the Escherichia coli RNase P protein subunit has in vivo fitness consequences.* PLoS One, 2012. **7**(3): p. e32456.
104. Cho, I.M., et al., *Ribosomal protein L7Ae is a subunit of archaeal RNase P.* Proc Natl Acad Sci U S A, 2010. **107**(33): p. 14573-8.
105. Chen, W.Y., et al., *Cooperative RNP assembly: complementary rescue of structural defects by protein and RNA subunits of archaeal RNase P.* J Mol Biol, 2011. **411**(2): p. 368-83.
106. Tsai, H.Y., et al., *Functional reconstitution and characterization of Pyrococcus furiosus RNase P.* Proc Natl Acad Sci U S A, 2006. **103**(44): p. 16147-52.
107. Xu, Y., et al., *Solution structure of an archaeal RNase P binary protein complex: formation of the 30-kDa complex between Pyrococcus furiosus RPP21 and RPP29 is accompanied by coupled protein folding and highlights critical features for protein-protein and protein-RNA interactions.* J Mol Biol, 2009. **393**(5): p. 1043-55.
108. Pulukkunat, D.K. and V. Gopalan, *Studies on Methanocaldococcus jannaschii RNase P reveal insights into the roles of RNA and protein cofactors in RNase P catalysis.* Nucleic Acids Res, 2008. **36**(12): p. 4172-80.
109. Chen, W.Y., et al., *Dissecting functional cooperation among protein subunits in archaeal RNase P, a catalytic ribonucleoprotein complex.* Nucleic Acids Res, 2010. **38**(22): p. 8316-27.
110. Sinapah, S., et al., *Cleavage of model substrates by archaeal RNase P: role of protein cofactors in cleavage-site selection.* Nucleic Acids Res, 2011. **39**(3): p. 1105-16.
111. Takagi, H., et al., *Crystal structure of the ribonuclease P protein Ph1877p from hyperthermophilic archaeon Pyrococcus horikoshii OT3.* Biochem Biophys Res Commun, 2004. **319**(3): p. 787-94.
112. Wilson, R.C., et al., *Structure of Pfu Pop5, an archaeal RNase P protein.* Proc Natl Acad Sci U S A, 2006. **103**(4): p. 873-8.
113. Sidote, D.J. and D.W. Hoffman, *NMR structure of an archaeal homologue of ribonuclease P protein Rpp29.* Biochemistry, 2003. **42**(46): p. 13541-50.
114. Boomershine, W.P., et al., *Structure of Mth11/Mth Rpp29, an essential protein subunit of archaeal and eukaryotic RNase P.* Proc Natl Acad Sci U S A, 2003. **100**(26): p. 15398-403.
115. Numata, T., et al., *Crystal structure of archaeal ribonuclease P protein Ph1771p from Pyrococcus horikoshii OT3: an archaeal homolog of eukaryotic ribonuclease P protein Rpp29.* RNA, 2004. **10**(9): p. 1423-32.
116. Sidote, D.J., J. Heideker, and D.W. Hoffman, *Crystal structure of archaeal ribonuclease P protein aRpp29 from Archaeoglobus fulgidus.* Biochemistry, 2004. **43**(44): p. 14128-38.
117. Kakuta, Y., et al., *Crystal structure of a ribonuclease P protein Ph1601p from Pyrococcus horikoshii OT3: an archaeal homologue of human nuclear ribonuclease P protein Rpp21.* Biochemistry, 2005. **44**(36): p. 12086-93.
118. Amero, C.D., et al., *Solution structure of Pyrococcus furiosus RPP21, a component of the archaeal RNase P holoenzyme, and interactions with its RPP29 protein partner.* Biochemistry, 2008. **47**(45): p. 11704-10.
119. Fukuhara, H., et al., *A fifth protein subunit Ph1496p elevates the optimum temperature for the ribonuclease P activity from Pyrococcus horikoshii OT3.* Biochem Biophys Res Commun, 2006. **343**(3): p. 956-64.
120. Marvin, M.C., et al., *Binding and cleavage of unstructured RNA by nuclear RNase P.* RNA, 2011. **17**(8): p. 1429-40.
121. Chamberlain, J.R., et al., *Purification and characterization of the nuclear RNase P holoenzyme complex reveals extensive subunit overlap with RNase MRP.* Genes Dev, 1998. **12**(11): p. 1678-90.
122. Salinas, K., et al., *Characterization and purification of Saccharomyces cerevisiae RNase MRP reveals a new unique protein component.* J Biol Chem, 2005. **280**(12): p. 11352-60.
123. Schmitt, M.E. and D.A. Clayton, *Characterization of a unique protein component of yeast RNase MRP: an RNA-binding protein with a zinc-cluster domain.* Genes Dev, 1994. **8**(21): p. 2617-28.

124. Piccinelli, P., M.A. Rosenblad, and T. Samuelsson, *Identification and analysis of ribonuclease P and MRP RNA in a broad range of eukaryotes.* Nucleic Acids Res, 2005. **33**(14): p. 4485-95.
125. Welting, T.J., et al., *Differential association of protein subunits with the human RNase MRP and RNase P complexes.* RNA, 2006. **12**(7): p. 1373-82.
126. Kiss, T. and W. Filipowicz, *Evidence against a mitochondrial location of the 7-2/MRP RNA in mammalian cells.* Cell, 1992. **70**(1): p. 11-6.
127. Jacobson, M.R., et al., *Dynamic localization of RNase MRP RNA in the nucleolus observed by fluorescent RNA cytochemistry in living cells.* J Cell Biol, 1995. **131**(6 Pt 2): p. 1649-58.
128. Schmitt, M.E. and D.A. Clayton, *Nuclear RNase MRP is required for correct processing of pre-5.8S rRNA in Saccharomyces cerevisiae.* Mol Cell Biol, 1993. **13**(12): p. 7935-41.
129. Lygerou, Z., et al., *Accurate processing of a eukaryotic precursor ribosomal RNA by ribonuclease MRP in vitro.* Science, 1996. **272**(5259): p. 268-70.
130. Lindahl, L., et al., *RNase MRP is required for entry of 35S precursor rRNA into the canonical processing pathway.* RNA, 2009. **15**(7): p. 1407-16.
131. Clayton, D.A., *A big development for a small RNA.* Nature, 2001. **410**(6824): p. 29, 31.
132. Mattijssen, S., T.J. Welting, and G.J. Pruijn, *RNase MRP and disease.* Wiley Interdiscip Rev RNA, 2010. **1**(1): p. 102-16.
133. Perederina, A., et al., *Eukaryotic ribonucleases P/MRP: the crystal structure of the P3 domain.* EMBO J, 2010. **29**(4): p. 761-9.
134. Houser-Scott, F., et al., *Interactions among the protein and RNA subunits of Saccharomyces cerevisiae nuclear RNase P.* Proc Natl Acad Sci U S A, 2002. **99**(5): p. 2684-9.
135. Khanova, E., et al., *Structural organizations of yeast RNase P and RNase MRP holoenzymes as revealed by UV-crosslinking studies of RNA-protein interactions.* RNA, 2012. **18**(4): p. 720-8.
136. Hipp, K., et al., *Modular architecture of eukaryotic RNase P and RNase MRP revealed by electron microscopy.* Nucleic Acids Res, 2012. **40**(7): p. 3275-88.
137. Wang, M.J., N.W. Davis, and P. Gegenheimer, *Novel mechanisms for maturation of chloroplast transfer RNA precursors.* EMBO J, 1988. **7**(6): p. 1567-74.
138. Thomas, B.C., et al., *Spinach chloroplast RNase P: a putative protein enzyme.* Nucleic Acids Symp Ser, 1995(33): p. 95-8.
139. Rossmanith, W. and R.M. Karwan, *Characterization of human mitochondrial RNase P: novel aspects in tRNA processing.* Biochem Biophys Res Commun, 1998. **247**(2): p. 234-41.
140. Salavati, R., A.K. Panigrahi, and K.D. Stuart, *Mitochondrial ribonuclease P activity of Trypanosoma brucei.* Mol Biochem Parasitol, 2001. **115**(1): p. 109-17.
141. Holzmann, J., et al., *RNase P without RNA: identification and functional reconstitution of the human mitochondrial tRNA processing enzyme.* Cell, 2008. **135**(3): p. 462-74.
142. Gobert, A., et al., *A single Arabidopsis organellar protein has RNase P activity.* Nat Struct Mol Biol, 2010. **17**(6): p. 740-4.
143. Gutmann, B., A. Gobert, and P. Giege, *PRORP proteins support RNase P activity in both organelles and the nucleus in Arabidopsis.* Genes Dev, 2012. **26**(10): p. 1022-7.
144. Lai, L., et al., *A functional RNase P protein subunit of bacterial origin in some eukaryotes.* Molecular genetics and genomics : MGG, 2011. **286**(5-6): p. 359-369.
145. Anantharaman, V. and L. Aravind, *The NYN domains: novel predicted RNAses with a PIN domain-like fold.* RNA biology, 2006. **3**(1): p. 18-27.
146. Gobert, A., et al., *Structural insights into protein-only RNase P complexed with tRNA.* Nat Commun, 2013. **4**: p. 1353.
147. Barkan, A., et al., *A combinatorial amino acid code for RNA recognition by pentatricopeptide repeat proteins.* PLoS genetics, 2012. **8**(8).
148. Karpenahalli, M.R., A.N. Lupas, and J. Soding, *TPRpred: a tool for prediction of TPR-, PPR- and SEL1-like repeats from protein sequences.* BMC Bioinformatics, 2007. **8**: p. 2.
149. Saha, D., A.M. Prasad, and R. Srinivasan, *Pentatricopeptide repeat proteins and their emerging roles in plants.* Plant Physiol Biochem, 2007. **45**(8): p. 521-34.
150. Lightowlers, R.N. and Z.M. Chrzanowska-Lightowlers, *PPR (pentatricopeptide repeat) proteins in mammals: important aids to mitochondrial gene expression.* Biochem J, 2008. **416**(1): p. e5-6.

151. Kissinger, C.R., et al., *Crystal structure of human ABAD/HSD10 with a bound inhibitor: implications for design of Alzheimer's disease therapeutics.* J Mol Biol, 2004. **342**(3): p. 943-52.
152. Vilardo, E., et al., *A subcomplex of human mitochondrial RNase P is a bifunctional methyltransferase--extensive moonlighting in mitochondrial tRNA biogenesis.* Nucleic Acids Res, 2012. **40**(22): p. 11583-93.
153. Jackman, J.E., et al., *Identification of the yeast gene encoding the tRNA m1G methyltransferase responsible for modification at position 9.* RNA, 2003. **9**(5): p. 574-85.
154. Zeng, H., Dong, A., Loppnau, P., Tempel, W., Bountra, C., Weigelt, J., Arrowsmith, C.H., Edwards, A.M., Wu, H., *Crystal structure of methyltransferase domain of human RNA (guanine-9-) methyltransferase domain containing protein 2*, 2012: New York Structural GenomiX Research Consortium (NYSGXRC).
155. Powell, A.J., et al., *Recognition of structurally diverse substrates by type II 3-hydroxyacyl-CoA dehydrogenase (HADH II)/amyloid-beta binding alcohol dehydrogenase (ABAD).* J Mol Biol, 2000. **303**(2): p. 311-27.
156. Lukacik, P., K.L. Kavanagh, and U. Oppermann, *Structure and function of human 17beta-hydroxysteroid dehydrogenases.* Mol Cell Endocrinol, 2006. **248**(1-2): p. 61-71.
157. Lustbader, J.W., et al., *ABAD directly links Abeta to mitochondrial toxicity in Alzheimer's disease.* Science, 2004. **304**(5669): p. 448-52.
158. Sanchez, M.I., et al., *RNA processing in human mitochondria.* Cell Cycle, 2011. **10**(17): p. 2904-16.
159. Rackham, O., et al., *Long noncoding RNAs are generated from the mitochondrial genome and regulated by nuclear-encoded proteins.* RNA, 2011. **17**(12): p. 2085-93.
160. Jourdain, A.A., et al., *GRSF1 regulates RNA processing in mitochondrial RNA granules.* Cell Metab, 2013. **17**(3): p. 399-410.
161. Montoya, J., G.L. Gaines, and G. Attardi, *The pattern of transcription of the human mitochondrial rRNA genes reveals two overlapping transcription units.* Cell, 1983. **34**(1): p. 151-9.
162. Ojala, D., J. Montoya, and G. Attardi, *tRNA punctuation model of RNA processing in human mitochondria.* Nature, 1981. **290**(5806): p. 470-4.
163. Ojala, D., et al., *The tRNA genes punctuate the reading of genetic information in human mitochondrial DNA.* Cell, 1980. **22**(2 Pt 2): p. 393-403.
164. Kurz, J.C., S. Niranjanakumari, and C.A. Fierke, *Protein component of Bacillus subtilis RNase P specifically enhances the affinity for precursor-tRNAAsp.* Biochemistry, 1998. **37**(8): p. 2393-400.
165. Poehlsgaard, J. and S. Douthwaite, *The bacterial ribosome as a target for antibiotics.* Nat Rev Microbiol, 2005. **3**(11): p. 870-81.
166. Harris, M.E. and E.L. Christian, *Recent insights into the structure and function of the ribonucleoprotein enzyme ribonuclease P.* Curr Opin Struct Biol, 2003. **13**(3): p. 325-33.
167. Willkomm, D.K., et al., *Evaluation of bacterial RNase P RNA as a drug target.* Chembiochem, 2003. **4**(10): p. 1041-8.
168. Tekos, A., et al., *RNase P: a promising molecular target for the development of new drugs.* Curr Med Chem, 2004. **11**(22): p. 2979-89.
169. Waugh, D.S. and N.R. Pace, *Complementation of an RNase P RNA (rnpB) gene deletion in Escherichia coli by homologous genes from distantly related eubacteria.* J Bacteriol, 1990. **172**(11): p. 6316-22.
170. Kobayashi, K., et al., *Essential Bacillus subtilis genes.* Proc Natl Acad Sci U S A, 2003. **100**(8): p. 4678-4683.
171. Jarrous, N., *Human ribonuclease P: subunits, function, and intranuclear localization.* RNA, 2002. **8**(1): p. 1-7.
172. Xiao, S., F. Houser-Scott, and D.R. Engelke, *Eukaryotic ribonuclease P: increased complexity to cope with the nuclear pre-tRNA pathway.* J Cell Physiol, 2001. **187**(1): p. 11-20.
173. Bichenkova, E.V., et al., *Strong, specific, reversible binding ligands for transfer RNA: Comparison by fluorescence and NMR spectroscopies with distamycin binding for a new structural class of ligand.* Nucleosides & Nucleotides, 1998. **17**(9-11): p. 1651-1665.

174. Hori, Y., et al., *Synthetic inhibitors of the processing of pretransfer RNA by the ribonuclease P ribozyme: enzyme inhibitors which act by binding to substrate.* Biochemistry, 2001. **40**(3): p. 603-8.
175. Hori, Y., et al., *Porphyrins and porphines bind strongly and specifically to tRNA, precursor tRNA and to M1 RNA and inhibit the ribonuclease P ribozyme reaction.* Biochim Biophys Acta, 2005. **1730**(1): p. 47-55.
176. Olson, P., et al., *Small molecule inhibitors of Staphylococcus aureus RnpA alter cellular mRNA turnover, exhibit antimicrobial activity, and attenuate pathogenesis.* PLoS pathogens, 2011. **7**(2).
177. Mikkelsen, N.E., et al., *Inhibition of RNase P RNA cleavage by aminoglycosides.* Proc Natl Acad Sci U S A, 1999. **96**(11): p. 6155-60.
178. Eubank, T.D., et al., *Inhibition of bacterial RNase P by aminoglycoside-arginine conjugates.* FEBS Lett, 2002. **511**(1-3): p. 107-12.
179. Kawamoto, S.A., et al., *Studies on the mechanism of inhibition of bacterial ribonuclease P by aminoglycoside derivatives.* Nucleic Acids Res, 2008. **36**(2): p. 697-704.
180. Eubank, T.D., et al., *Inhibition of bacterial RNase P by aminoglycoside-arginine conjugates.* FEBS Letters, 2002. **511**(1-3): p. 107-12.
181. Berchanski, A. and A. Lapidot, *Bacterial RNase P RNA is a drug target for aminoglycoside-arginine conjugates.* Bioconjug Chem, 2008. **19**(9): p. 1896-906.
182. Cuzic, S. and R.K. Hartmann, *Studies on Escherichia coli RNase P RNA with Zn2+ as the catalytic cofactor.* Nucleic Acids Res, 2005. **33**(8): p. 2464-74.
183. Brannvall, M. and L.A. Kirsebom, *Manganese ions induce miscleavage in the Escherichia coli RNase P RNA-catalyzed reaction.* J Mol Biol, 1999. **292**(1): p. 53-63.
184. Smith, D., et al., *Influence of metal ions on the ribonuclease P reaction. Distinguishing substrate binding from catalysis.* J Biol Chem, 1992. **267**(4): p. 2429-36.
185. Christian, E.L., N.M. Kaye, and M.E. Harris, *Evidence for a polynuclear metal ion binding site in the catalytic domain of ribonuclease P RNA.* EMBO J, 2002. **21**(9): p. 2253-62.
186. Kurz, J.C. and C.A. Fierke, *The affinity of magnesium binding sites in the Bacillus subtilis RNase P x pre-tRNA complex is enhanced by the protein subunit.* Biochemistry, 2002. **41**(30): p. 9545-58.
187. Misra, V.K. and D.E. Draper, *On the role of magnesium ions in RNA stability.* Biopolymers, 1998. **48**(2-3): p. 113-35.
188. Frederiksen, J.K. and J.A. Piccirilli, *Identification of catalytic metal ion ligands in ribozymes.* Methods, 2009. **49**(2): p. 148-66.
189. Hsieh, J., et al., *A divalent cation stabilizes the active conformation of the B. subtilis RNase P•pre-tRNA complex: a role for an inner-sphere metal ion in RNase P* submitted, 2010.
190. Hsieh, J. and C.A. Fierke, *Conformational change in B. subtilis RNase P-pre-tRNA Complex Enhances Substrate Affinity and Limits Cleavage Rate.* In press, 2009.
191. Hsieh, J. and C.A. Fierke, *Conformational change in the Bacillus subtilis RNase P holoenzyme--pre-tRNA complex enhances substrate affinity and limits cleavage rate.* RNA, 2009. **15**(8): p. 1565-77.
192. Hsieh, J., et al., *A divalent cation stabilizes the active conformation of the B. subtilis RNase P x pre-tRNA complex: a role for an inner-sphere metal ion in RNase P.* J Mol Biol, 2010. **400**(1): p. 38-51.
193. Narlikar, G. and D. Herschlag, *Mechanistic aspects of enzymatic catalysis: lessons from comparison of RNA and protein enzymes.* Annual review of biochemistry, 1997. **66**: p. 19-59.
194. Doudna, J. and J. Lorsch, *Ribozyme catalysis: not different, just worse.* Nature structural & molecular biology, 2005. **12**(5): p. 395-402.
195. Howard, M., et al., *Mitochondrial ribonuclease P structure provides insight into the evolution of catalytic strategies for precursor-tRNA 5' processing.* Proceedings of the National Academy of Sciences of the United States of America, 2012. **109**(40): p. 16149-16154.
196. Pavlova, L., et al., *tRNA Processing by Protein-Only versus RNA-Based RNase P: Kinetic Analysis Reveals Mechanistic Differences.* Chembiochem : a European journal of chemical biology, 2012. **13**(15): p. 2270-2276.
197. Hsieh, J., et al., *Pre-tRNA turnover catalyzed by the yeast nuclear RNase P holoenzyme is limited by product release.* RNA, 2009. **15**(2): p. 224-34.

198. Cassano, A., V. Anderson, and M. Harris, *Analysis of solvent nucleophile isotope effects: evidence for concerted mechanisms and nucleophilic activation by metal coordination in nonenzymatic and ribozyme-catalyzed phosphodiester hydrolysis.* Biochemistry, 2004. **43**(32): p. 10547-10559.
199. Warnecke, J.M., et al., *Ribonuclease P (RNase P) RNA is converted to a Cd(2+)-ribozyme by a single Rp-phosphorothioate modification in the precursor tRNA at the RNase P cleavage site.* Proc Natl Acad Sci U S A, 1996. **93**(17): p. 8924-8.
200. Li, X. and P. Gegenheimer, *Ribonuclease P Catalysis Requires Mg2+ Coordinated to the pro-RP Oxygen of the Scissile Bond†.* Biochemistry, 1997. **36**(9): p. 2425-2438.
201. Warnecke, J.M., et al., *Role of metal ions in the hydrolysis reaction catalyzed by RNase P RNA from Bacillus subtilis.* J Mol Biol, 1999. **290**(2): p. 433-45.
202. Pfeiffer, T., et al., *Effects of phosphorothioate modifications on precursor tRNA processing by eukaryotic RNase P enzymes.* J Mol Biol, 2000. **298**(4): p. 559-65.
203. Pavlova, L.V., et al., *tRNA processing by protein-only versus RNA-based RNase P: kinetic analysis reveals mechanistic differences.* Chembiochem, 2012. **13**(15): p. 2270-6.
204. Cassano, A.G., V.E. Anderson, and M.E. Harris, *Analysis of Solvent Nucleophile Isotope Effects: Evidence for Concerted Mechanisms and Nucleophilic Activation by Metal Coordination in Nonenzymatic and Ribozyme-Catalyzed Phosphodiester Hydrolysis†.* Biochemistry, 2004. **43**(32): p. 10547-10559.
205. Persson, T., S. Cuzic, and R.K. Hartmann, *Catalysis by RNase P RNA: unique features and unprecedented active site plasticity.* J Biol Chem, 2003. **278**(44): p. 43394-401.
206. Warnecke, J.M., et al., *Active site constraints in the hydrolysis reaction catalyzed by bacterial RNase P: analysis of precursor tRNAs with a single 3′-S-phosphorothiolate internucleotide linkage.* Nucleic Acids Research, 2000. **28**(3): p. 720-727.
207. Frederiksen, J.K., et al., *Metal-ion rescue revisited: biochemical detection of site-bound metal ions important for RNA folding.* RNA, 2012. **18**(6): p. 1123-41.
208. Kazantsev, A.V., et al., *Solution structure of RNase P RNA.* RNA, 2011. **17**(6): p. 1159-1171.
209. Kaye, N.M., et al., *Conservation of Helical Structure Contributes to Functional Metal Ion Interactions in the Catalytic Domain of Ribonuclease P RNA.* Journal of Molecular Biology, 2002. **324**(3): p. 429-442.
210. Christian, E.L., et al., *The P4 metal binding site in RNase P RNA affects active site metal affinity through substrate positioning.* RNA, 2006. **12**(8): p. 1463-1467.
211. Reiter, N.J., A.K. Osterman, and A. Mondragón, *The bacterial ribonuclease P holoenzyme requires specific, conserved residues for efficient catalysis and substrate positioning.* Nucleic Acids Research, 2012. **40**(20): p. 10384-10393.
212. Hernandez-Cid, A., et al., *Ribonucleases P/MRP and the expanding ribonucleoprotein world.* IUBMB Life, 2012. **64**(6): p. 521-528.
213. Peck-Miller, K.A. and S. Altman, *Kinetics of the processing of the precursor to 4.5 S RNA, a naturally occurring substrate for RNase P from Escherichia coli.* J Mol Biol, 1991. **221**(1): p. 1-5.
214. Komine, Y., et al., *A tRNA-like structure is present in 10Sa RNA, a small stable RNA from Escherichia coli.* Proc Natl Acad Sci U S A, 1994. **91**(20): p. 9223-7.
215. Alifano, P., et al., *Ribonuclease E provides substrates for ribonuclease P-dependent processing of a polycistronic mRNA.* Genes Dev, 1994. **8**(24): p. 3021-31.
216. Li, Y. and S. Altman, *A specific endoribonuclease, RNase P, affects gene expression of polycistronic operon mRNAs.* Proc Natl Acad Sci U S A, 2003. **100**(23): p. 13213-8.
217. Marvin, M.C., et al., *Accumulation of noncoding RNA due to an RNase P defect in Saccharomyces cerevisiae.* RNA, 2011. **17**(8): p. 1441-50.
218. Altman, S., et al., *RNase P cleaves transient structures in some riboswitches.* Proc Natl Acad Sci U S A, 2005. **102**(32): p. 11284-9.
219. Seif, E. and S. Altman, *RNase P cleaves the adenine riboswitch and stabilizes pbuE mRNA in Bacillus subtilis.* RNA (New York, N.Y.), 2008. **14**(6): p. 1237-1243.
220. Marvin, M., et al., *Binding and cleavage of unstructured RNA by nuclear RNase P.* RNA (New York, N.Y.), 2011. **17**(8): p. 1429-1440.
221. Yang, L. and S. Altman, *A noncoding RNA in Saccharomyces cerevisiae is an RNase P substrate.* RNA (New York, N.Y.), 2007. **13**(5): p. 682-690.

222. Marvin, M., et al., *Accumulation of noncoding RNA due to an RNase P defect in Saccharomyces cerevisiae.* RNA (New York, N.Y.), 2011. **17**(8): p. 1441-1450.
223. Suzuki, T., A. Nagao, and T. Suzuki, *Human mitochondrial tRNAs: biogenesis, function, structural aspects, and diseases.* Annu Rev Genet, 2011. **45**: p. 299-329.
224. Rossmanith, W., *Of P and Z: mitochondrial tRNA processing enzymes.* Biochim Biophys Acta, 2012. **1819**(9-10): p. 1017-26.
225. Byrne, R.T., et al., *The crystal structure of unmodified tRNAPhe from Escherichia coli.* Nucleic Acids Res, 2010. **38**(12): p. 4154-62.
226. Rueda, D., et al., *The 5' leader of precursor tRNAAsp bound to the Bacillus subtilis RNase P holoenzyme has an extended conformation.* Biochemistry, 2005. **44**(49): p. 16130-9.
227. Sun, L., et al., *Evidence that substrate-specific effects of C5 protein lead to uniformity in binding and catalysis by RNase P.* EMBO J, 2006. **25**(17): p. 3998-4007.
228. Tallsjo, A. and L.A. Kirsebom, *Product release is a rate-limiting step during cleavage by the catalytic RNA subunit of Escherichia coli RNase P.* Nucleic Acids Res, 1993. **21**(1): p. 51-7.
229. Oh, B.K. and N.R. Pace, *Interaction of the 3'-end of tRNA with ribonuclease P RNA.* Nucleic Acids Res, 1994. **22**(20): p. 4087-94.
230. Kirsebom, L.A. and S.G. Svard, *Base pairing between Escherichia coli RNase P RNA and its substrate.* EMBO J, 1994. **13**(20): p. 4870-6.
231. Zahler, N.H., et al., *The pre-tRNA nucleotide base and 2'-hydroxyl at N(-1) contribute to fidelity in tRNA processing by RNase P.* J Mol Biol, 2005. **345**(5): p. 969-85.
232. Koutmou, K.S., et al., *Protein-precursor tRNA contact leads to sequence-specific recognition of 5' leaders by bacterial ribonuclease P.* J Mol Biol, 2010. **396**(1): p. 195-208.
233. Lim, W.H., *Importance of substrate recognition and metal ions in the Ribonuclease P catalysis*, 2011, University of Michigan.
234. McClain, W.H., C. Guerrier-Takada, and S. Altman, *Model substrates for an RNA enzyme.* Science, 1987. **238**(4826): p. 527-30.
235. Kikovska, E., N.E. Mikkelsen, and L.A. Kirsebom, *The naturally trans-acting ribozyme RNase P RNA has leadzyme properties.* Nucleic Acids Res, 2005. **33**(21): p. 6920-30.
236. Kirsebom, L.A. and S. Trobro, *RNase P RNA-mediated cleavage.* IUBMB Life, 2009. **61**(3): p. 189-200.
237. Hardt, W.D., et al., *Role of the D arm and the anticodon arm in tRNA recognition by eubacterial and eukaryotic RNase P enzymes.* Biochemistry, 1993. **32**(48): p. 13046-53.
238. Chen, W.Y., et al., *Fidelity of tRNA 5'-maturation: a possible basis for the functional dependence of archaeal and eukaryal RNase P on multiple protein cofactors.* Nucleic Acids Res, 2012. **40**(10): p. 4666-80.
239. Brannvall, M., et al., *RNase P RNA structure and cleavage reflect the primary structure of tRNA genes.* J Mol Biol, 1998. **283**(4): p. 771-83.
240. Yuan, Y. and S. Altman, *Substrate recognition by human RNase P: identification of small, model substrates for the enzyme.* EMBO J, 1995. **14**(1): p. 159-68.
241. Marechal-Drouard, L., J.H. Weil, and A. Dietrich, *Transfer RNAs and Transfer RNA Genes in Plants.* Annual Review of Plant Physiology and Plant Molecular Biology, 1993. **44**(1): p. 13-32.
242. Cognat, V., et al., *PlantRNA, a database for tRNAs of photosynthetic eukaryotes.* Nucleic Acids Res, 2013. **41**(Database issue): p. D273-9.
243. Rossmanith, W., et al., *Human mitochondrial tRNA processing.* J Biol Chem, 1995. **270**(21): p. 12885-91.
244. Shi, H. and P.B. Moore, *The crystal structure of yeast phenylalanine tRNA at 1.93 A resolution: a classic structure revisited.* RNA, 2000. **6**(8): p. 1091-105.
245. Kim, S.H., et al., *Three-dimensional tertiary structure of yeast phenylalanine transfer RNA.* Science, 1974. **185**(4149): p. 435-40.
246. Giege, R., et al., *Structure of transfer RNAs: similarity and variability.* Wiley Interdiscip Rev RNA, 2012. **3**(1): p. 37-61.
247. Voigts-Hoffmann, F., et al., *A methyl group controls conformational equilibrium in human mitochondrial tRNA(Lys).* J Am Chem Soc, 2007. **129**(44): p. 13382-3.
248. Dammertz, K., et al., *Single-molecule FRET studies of counterion effects on the free energy landscape of human mitochondrial lysine tRNA.* Biochemistry, 2011. **50**(15): p. 3107-15.

249. Kobitski, A.Y., et al., *Single-molecule FRET reveals a cooperative effect of two methyl group modifications in the folding of human mitochondrial tRNA(Lys).* Chem Biol, 2011. **18**(7): p. 928-36.
250. Holzmann, J. and W. Rossmanith, *tRNA recognition, processing, and disease: hypotheses around an unorthodox type of RNase P in human mitochondria.* Mitochondrion, 2009. **9**(4): p. 284-8.
251. Taylor, R.W. and D.M. Turnbull, *Mitochondrial DNA mutations in human disease.* Nat Rev Genet, 2005. **6**(5): p. 389-402.
252. Schon, E.A., S. DiMauro, and M. Hirano, *Human mitochondrial DNA: roles of inherited and somatic mutations.* Nat Rev Genet, 2012. **13**(12): p. 878-90.

# CHAPTER 2

# DEVELOPMENT OF A FLUORESCENCE POLARIZATION ASSAY TO MEASURE ACTIVITY AND SCREEN FOR INHIBITORS OF *B. SUBTILIS* RNASE P[1]

## 2.1 Abstract

Ribonuclease P (RNase P) is an essential endonuclease that catalyzes the 5' end maturation of precursor-tRNA (pre-tRNA). Bacterial RNase P is an attractive potential antibacterial target because it is essential for cell survival and has a distinct subunit composition from its eukaryal counterparts. To accelerate both structure-function studies and discovery of inhibitors of RNase P, we developed a real-time fluorescence polarization (FP) assay to measure RNase P activity using pre-tRNA with fluorophore attached at the 5' end. This FP assay can also measure binding of small molecules to pre-tRNA. Inhibition of *B. subtilis* RNase P by neomycin B and kanamycin B was examined by the FP assay. These compounds bind to the pre-tRNA substrate with a $K_d$ value that is comparable to the $IC_{50}$ for inhibition of RNase P, suggesting that the mode of inhibition is binding to the substrate. To identify inhibitors that function by binding to RNase P, we optimized this FP assay for high-throughput screening (HTS) of both RNase P inhibition and pre-tRNA binding. Using

[1] Chapter 2 is adapted from the manuscript in preparation entitled "Fluorescence polarization to measure activity and screen for inhibitors of bacterial ribonuclease P" by Xin Liu, Yu Chen, and Carol A. Fierke.

the assay we screened compound libraries that contain over 25,000 samples and identified a new *in vitro* inhibitor of *B. subtilis* RNase P. The FP methodology and inhibitors identified in this work will further our understanding of how RNase P recognizes ligands and assist in designing antibacterial compounds that target RNase P in future.

## 2.2 Background

RNA exerts numerous important functions in living systems and has become a target for novel drug discovery [1-4]. In the pathway for generating mature functional transfer RNA (tRNA), ribonuclease P (RNase P) catalyzes cleavage of the 5' end from all precursor tRNAs (pre-tRNAs) [5-7]. Bacterial RNase P also catalyzes cleavage of various RNA substrates [8], such as pre-4.5S RNA [9], pre-tmRNA [10], mRNAs [11-13], and riboswitches [14, 15]. In most organisms, RNase P is a ribonucleoprotein consisting of a single catalytic RNA subunit (P RNA) and variable numbers of protein subunits depending on the organism (1 in Bacteria, ≥ 4 in Archaea and ≥ 9 in Eukarya nuclei) [16-19]. Recently, examples of solely protein-based RNase P have been identified or predicted in human mitochondria [20], the plant *Arabidopsis thaliana* [21, 22], and some algae and protists [23, 24]. Bacterial RNase P is a potential antibacterial drug target because of the essential role in RNA processing and the differential subunit composition from its eukaryal counterparts [25]. However, no specific bacterial RNase P inhibitors have been reported to date, despite screens of small molecule libraries for inhibitors [26],

Several reported inhibitors of *E. coli* RNase P are known ribosomal antibiotics, including puromycin ($IC_{50}$ ~ 3 mM) [27], aminoglycosides (e.g. neomycin B, $IC_{50}$ = 60 μM) [28], and neomycin B derivatives with arginine, lysine and guanidinium moieties ($IC_{50}$ values ranging from 0.1 to 6 μM) [29, 30]. The usefulness of these aminoglycoside derivatives *in vivo* may be limited due to their high positive charges that lead to promiscuous binding to nucleic acids. Aminoglycosides are also weak non-competitive inhibitors of eukaryal RNase P ($K_i$ = 143 μM for neomycin B to *Dictyostelium discoideum* RNase P). A series of synthetic compounds, such as bis-benzimidazoles ($IC_{50}$ = 5 – 21 μM) [31, 32], porphines and porphyrins ($K_i$ = 1 – 4 μM) [33] have also been identified as inhibitors of *E. coli* RNase P. However, the mode of inhibition of these compounds is mainly through binding to substrates and therefore they are not specific RNase P inhibitors [32, 33]. Spiramycin, a macrolide antibiotic, was reported to activate the steady state turnover catalyzed by *E. coli* RNase P holoenzyme and P RNA by 18- and 12- fold respectively [34]. Recently, a small molecule has been suggested to bind to the protein component of RNase P (*Rnp*A) from *Staphylococcus aureus* to alter mRNA turnover and pathogenesis [35]. Possibly this compound could inhibit bacterial RNase P by interfering with formation of P protein-P RNA complex but no biochemical studies has been reported on how it could modulate RNase P holoenzyme activity.

Rational design of inhibitions using an antisense approach and an *in silico* screening, has also been applied to RNase P. Antisense RNAs have been developed to target P RNA in the region of P11 and L15 for *E. coli* and P5.1 for *B. subtilis* RNase P ($IC_{50}$ = 2 nM – 1 μM) [36-39]. However, to enter bacterial cells and

target RNase P *in vivo*, the antisense nucleic acids have to be conjugated with invasive peptides [39]. To discover inhibitors that function by disrupting interactions between the pre-tRNA substrate and the P protein subunit, virtual screening was used to dock compounds from the ZINC database [40] to the central cleft of the *B. subtilis* P protein. The proposed hits await experimental evaluation [26]. To further evaluate bacterial RNase P as a viable drug target, more potent and specific inhibitors of bacterial RNase P need to be discovered and characterized.

Conventional methods for measuring RNase P activity and inhibition are mainly radiochemical [28]. Pre-tRNAs are labeled with $^{32}$P-labeled to monitor cleavage rate by following the reactions using denaturing polyacrylamide gel electrophoresis (PAGE) and quantification of the extent of cleavage by phosphorimaging. These radiochemical assays are discontinuous, labor-intensive and relatively low-throughput.

Fluorescence techniques provide an attractive non-radioactive approach to measure RNase P activity. Previously, substrate binding and transient kinetics of *B. subtilis* RNase P have been measured using a fluorescein-labeled pre-tRNA$^{Asp}$ or a Fl-pre-tRNA$^{Asp}$ paired with or without a tetramethylrodamine-labeled P protein to monitor a change in fluorescence intensity or fluorescence resonance energy transfer (FRET) [41-43]. In these single-turnover experiments, sensitivity and signal dynamic range are sufficient [42]. However, these approaches lack sensitivity for measuring steady-state kinetics where the substrate is in excess and the enzyme catalyzes multiple turnovers.

Here we describe a new fluorescence polarization (FP) assay for *B. subtilis* RNase P activity using a previously reported 5' fluorescein-labeled pre-tRNA$^{Asp}$ substrate (Fl-pre-tRNA [41], Scheme 2-1). This FP assay measures RNase P activity in a continuous format and is suitable to high-throughput screening of inhibitors. Using this FP assay, I measured inhibition of *B. subtilis* RNase P by previously reported *E. coli* RNase P inhibitors, neomycin B (NeoB) and kanamycin B (KanB). I measured the affinity of pre-tRNA for these inhibitors by FP assay, suggesting that inhibition of RNase P is at least partly due to binding to the substrate. The FP assay therefore also has a potential application of identifying compounds that interact with pre-tRNA. Finally, I used this assay to conduct a pilot high-throughput screen for RNase P inhibitors and identified a new *in vitro* inhibitor of *B. subtilis* RNase P. These results demonstrate that the FP assay facilitates both analysis of pre-tRNA processing catalyzed by RNase P and the screening for inhibitors of RNase P.

## 2.3 Results

### 2.3.1 Fluorescence Polarization to Measure Pre-tRNA Cleavage

To develop a non-radiochemical assay for measuring RNase P activity in real-time, and for identification of RNase P we developed a fluorescence polarization (FP) method because it is sensitive, ratio-metric, robust and easy to transition to a high-throughput mode [44]. In general, FP assays are based on the phenomenon that the degree of polarization of a fluorophore reflects the mobility of the fluorophore based on molecular mass ([45] and reference therein). To measure the cleavage activity of *B. subtilis* RNase P by FP, I choose to use the previously reported 5'

fluorescein labeled pre-tRNA$^{Asp}$ substrate with a 5-nucleotide leader (Fl-pre-tRNA [41], Scheme 2-1). In theory, when Fl-pre-tRNA is excited by polarized light, the emission light remains largely polarized (higher anisotropy) because the Fl-pre-tRNA macromolecule rotates substantially slower than the fluorescence lifetime of fluorescein. After RNase P catalyzed cleavage of the Fl-pre-tRNA, emitted light from the fluorescein-5-nucleotide leader (Fl-5-nt-leader) product is depolarized (lower anisotropy) Because the 5-nt leader rotates more rapidly than the 82-nt Fl-pre-tRNA substrate, the anisotropy of the Fl-pre-tRNA and the 5-nt leader product differ by 2 to 3-fold, providing a wide dynamic range for the cleavage assay (Figure 2-1). A time-dependent decrease in FP signal was observed upon mixing *B. subtilis* RNase P holoenzyme with the Fl-pre-tRNA substrate under both single- ([E]/[S]>10) and multiple-turnover ([S]/[E]>10) conditions (Figure 2-1). Similar FP reaction curves have also been observed for RNase P catalyzed cleavage of 5' fluorescein labeled pre-tRNA$^{Asp}$ with 2, 7, and 10-nucleotide leaders (data not shown). Fluorescence polarization/anisotropy measures the ratio of parallel and perpendicular light so the assay is ratio-metric and highly accurate (error < 5% even with just a 2-fold dynamic range) [45].

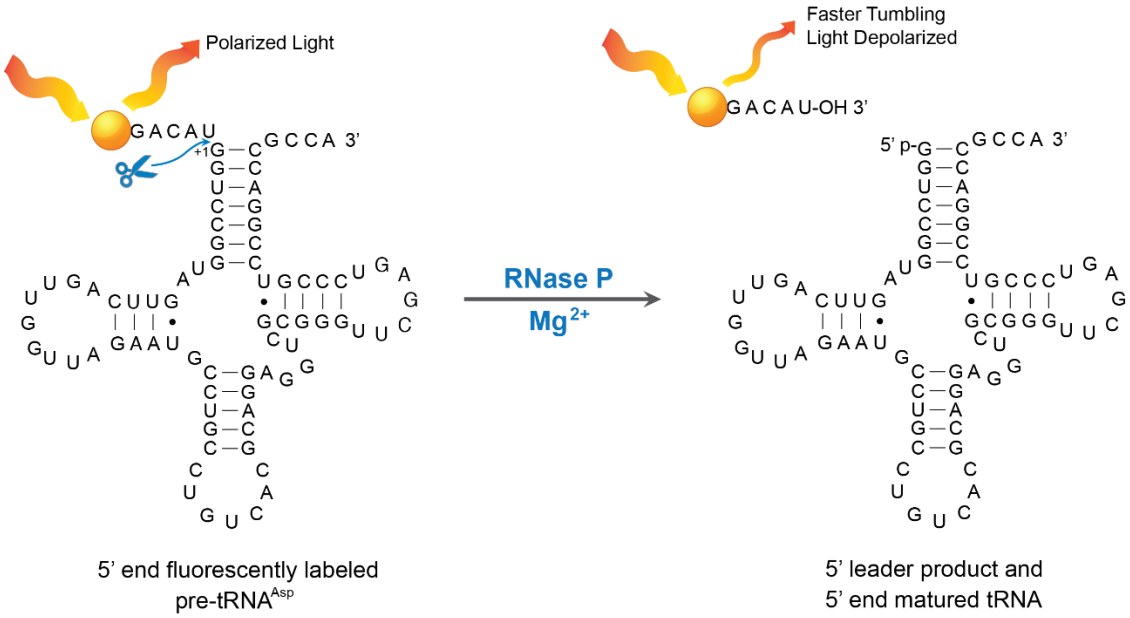


**Scheme 2-1:** A fluorescence polarization cleavage assay for RNase P. A fluorescein dye (orange dot) is attached to the 5' end of a *B. subtilis* pre-tRNA$^{Asp}$ with a 5-nt leader (Fl-pre-tRNA). When excited with polarized light, the Fl-pre-tRNA tumbles slower than the lifetime of the fluorophore so that the emitted light remains polarized. Upon cleavage of 5' end leader by RNase P, the Fl-5nt-leader strand rotates faster leading to enhanced depolarization of the emitted light.

To examine whether the FP change directly reflects cleavage catalyzed by RNase P, endpoint gel assays were carried out in parallel to compare the cleavage rate constants. These assay results demonstrated that the single-turnover cleavage rate constant and the multiple-turnover reaction velocity calculated from the FP assay are comparable to the values determined from the gel assay (Table 2-1). These data demonstrate that the real-time FP signal accurately measure the cleavage activity of RNase P under these conditions.

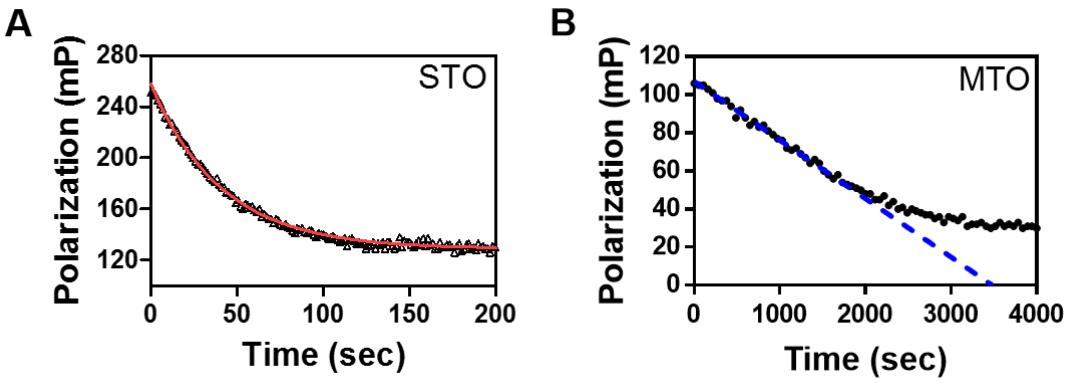


**Figure 2-1:** Fluorescence polarization measurements of pre-tRNA cleavage catalyzed by RNase P. **(A)** A single-turnover (STO) reaction time course measured in buffer A (50 mM Tris/Mes pH = 5.5, 10 mM $MgCl_2$, 200 mM KCl, 20 mM DTT); with 25 nM Fl-pre-tRNA and 500 nM *B. subtilis* RNase P holoenzyme at 37 ˚C. The solid line is a single exponential fit of the data with $k_{obs}$ = 0.024, when Equation 2-1 and 2-2 was used to adjust for total florescence change the $k_{obs}$ = 0.032 (see Materials and Methods). **(B)** A multiple-turnover (MTO) reaction measured in buffer C (50 mM Tris-HCl pH = 8, 10 mM $MgCl_2$, 100 mM KCl, 20 mM DTT) with 20 nM Fl-pre-tRNA and 1 nM *B. subtilis* RNase P holoenzyme and 4 nM P protein at 37 ˚C. Total fluorescence does not change for multiple turnover reactions compared to substrate alone controls. The steady-state cleavage velocity is measured from the initial rate (dashed blue line).

**Table 2-1:** Comparison of cleavage rates measured by different assays[2]

| Assay methods | Single turnover cleavage rate[a], $k_{obs}$ ($s^{-1}$) | Multiple turnover velocity[b], $v_0$ ($nM \cdot s^{-1}$) |
|---|---|---|
| FP real-time assay | 0.032 ± 0.001 | 2.2 ± 0.1 |
| Fluorescence gel assay | 0.033 ± 0.006 | — |
| $^{32}$P gel assay | — | 1.9 ± 0.1 |

[a] Measured in buffer A (50 mM Tris/Mes pH = 5.5, 10 mM $MgCl_2$, 200 mM KCl, 20 mM DTT) with 25 nM Fl-pre-tRNA, 500 nM holoenzyme at 37˚C;
[b] Measured in HTS buffer (50 mM Tris-HCl pH = 7.2, 10 mM $MgCl_2$, 100 mM KCl, 20 mM DTT, 12 mg/ml yeast $tRNA^{Mix}$, 10 mM spermidine, and 0.01% (v/v) NP-40) by 100nM Fl-pre-tRNA or $^{32}$P-prtRNA substrate, 0.15 nM holoenzyme and 1.5 nM of P protein at 25˚C.

Furthermore, the steady-state kinetic parameters calculated by the FP assay ($k_{cat}$ = 0.18 ± 0.01 s-1, $K_M$ = 101 ± 15 nM, $k_{cat}/K_M$ =1800 ± 200 $mM^{-1}s^{-1}$, Figure 2-2) are in the same range as previously reported for cleavage of pre-$tRNA^{Asp}$ with a 35-

[2] Data from the fluorescence gel assay were collected and analyzed by Yu Chen.

nt leader ([46], $k_{cat}$ = 0.83 $s^{-1}$, $K_M$ = 230 nM, $k_{cat}/K_M$ =3500 $mM^{-1}s^{-1}$). The modest decrease in activity is likely due to variation in assay conditions, such as the substitution of KCl for $NH_4Cl$ [46]. Under identical buffer conditions, the initial rate from the FP assay is in good agreement with that measured using the radioactive assay (Table 2-1).

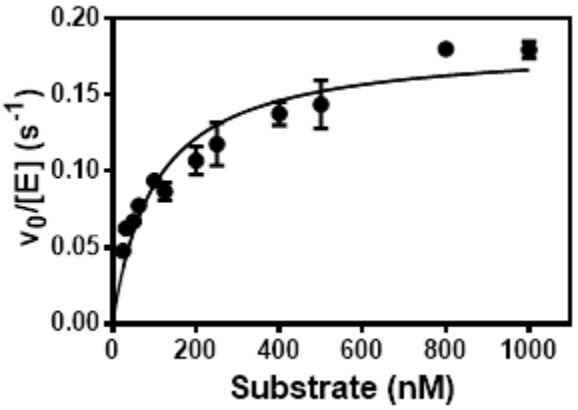


**Figure 2-2:** Steady-state kinetics measured by fluorescence polarization assay. Reaction condition is the same as described in Figure 2-1 with varying Fl-pre-tRNA concentrations. Results are in duplicates and error bars are showing standard deviations. Data were fit to Michaelis-Menten equation and $k_{cat}$ = 0.18 ± 0.01 s-1, $K_M$ = 101 ± 15 nM, $k_{cat}/K_M$ =1800 ± 200 $mM^{-1}s^{-1}$.

The term fluorescence polarization (FP) is closely related to fluorescence anisotropy (FA) that describes the same phenomenon ([45] and reference therein). Both FP and FA have been widely used in literature across biochemical applications to calculate percentage of reaction progress and ligand bound [47, 48]. Anisotropy has a simple linear additive relationship for calculating fraction of species in solution, while the additivity of polarization is not linear [49]. In the present study of RNase P, both FP and FA values were recorded and the rate constants calculated from these data are the same within error (< 3%). The FP measurements provide a larger dynamic range and therefore lead to better Z' factor in the high-throughput screens

(Equation 2-8). Therefore, data described in this chapter used FP values for analyzing RNase P activity and high-throughput screening.

The degree of fluorescence polarization is dependent on various factors that affect the mobility of the fluorophore, including molecular size, viscosity and temperature [45]. Polarization is a ratiometric measurement since it is defined as a function of the observed parallel and perpendicular fluorescence light intensity. Therefore, polarization of Fl-pre-tRNA is independent of concentration. However, the FP signal is dependent on the cation concentration and buffer composition. The FP of Fl-pre-tRNA increases with a hyperbolic dependence on the concentration of $Mg^{2+}$ or spermidine (Figure A-1, Appendix A). This cation dependence of FP suggests that the mobility of fluorescein in Fl-pre-tRNA decreases at high cation concentrations, likely reflecting a more stable pre-tRNA structure under these conditions.

### 2.3.2 Neomycin B and Kanamycin B Inhibit *B. subtilis* RNase P and Bind to Pre-tRNA Substrate

Next we applied the assay to measure inhibition of *B. subtilis* RNase P by aminoglycosides such as neomycin B (NeoB) and kanamycin B (KanB) that have been reported previously to inhibit *E. coli* RNase P[28]. Using the FP assay, we measured the dependence of *B. subtilis* RNase P activity on the concentration of NeoB and KanB under a $k_{cat}/K_M$ condition (Figure 2-3). Both compounds inhibit *B. subtilis* RNase P cleavage activity. NeoB is slightly more potent ($IC_{50}$= 23 μM) than KanB ($IC_{50}$= 52 μM). These $IC_{50}$ values are comparable to those measured inhibition of *E.* coli RNase P by these two compounds [28].

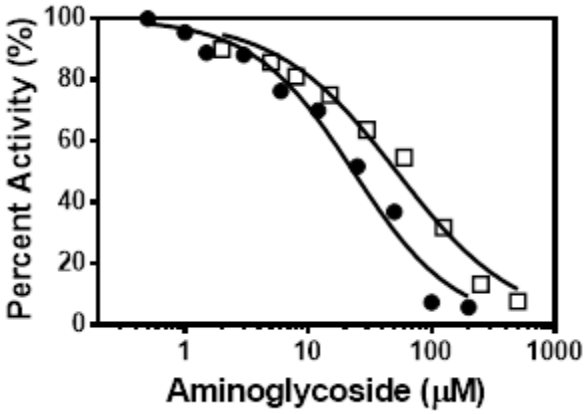


**Figure 2-3:** Neomycin B and kanamycin B inhibit B. subtilis RNase P. Dose-response curves of inhibition by neomycin B (●) and kanamycin B (□) were measured in buffer B (50 mM Tris-HCl pH = 7.2, 10 mM $MgCl_2$, 100 mM KCl, 20 mM DTT) with 20 nM Fl-pre-tRNA and 0.4 nM RNase P with 4 nM P protein at 37˚C. The concentrations for neomycin B and kanamycin B that inhibit activity by 50% ($IC_{50}$) are 23 ± 3 μM and 52 ± 6 μM, respectively.

Interestingly, titration of NeoB or KanB into the Fl-pre-tRNA alone led to an enhancement in FP (Figure 2-4), indicating that these compounds are binding to the Fl-pre-tRNA. The total fluorescence intensity remained constant (data not shown). The dissociation constants ($K_d$) were obtained from fitting Equation 2-5 to the FP titration curve (Figure 2-4 and Table 2-2). The $K_d$ of NeoB (90 μM) agrees well with published value for NeoB binding to a native yeast $tRNA^{Phe}$ ($K_d$= 90 μM) [50]. Unexpectedly, the FP of the fully bound complexes with NeoB and KanB varies (Figure 2-4). The significant change in FP upon binding of NeoB (M.W. = 614.6 g/mol) or KanB (483.3 g/mol) to Fl-pre-tRNA could not be explained by the modest increase of the molecular mass of the complex (Equations 2-6 and 2-7). Additionally, ΔFP of ~ 30 mP of the fully bound complex with NeoB compound compared to Kan B cannot be explained by the small different in mass (ΔM.W. = 131 g/mol). Dimerization of the Fl-pre-tRNA could be a possibility for the observed increase in polarization. It is also likely that differential stabilization of the tRNA structure by

NeoB compared to KanB [50] leads to an alteration in the mobility of the attached fluorescein in Fl-pre-tRNA. Furthermore, the affinity of NeoB ($K_d$ = 90 µM) and KanB ($K_d$ = 217 µM) are similar to the values of $IC_{50}$ for inhibition of RNase P ($IC_{50}$= 23 µM and = 52 µM, respectively), suggesting that the binding of these compounds to the pre-tRNA substrate could contribute to RNase P inhibition.

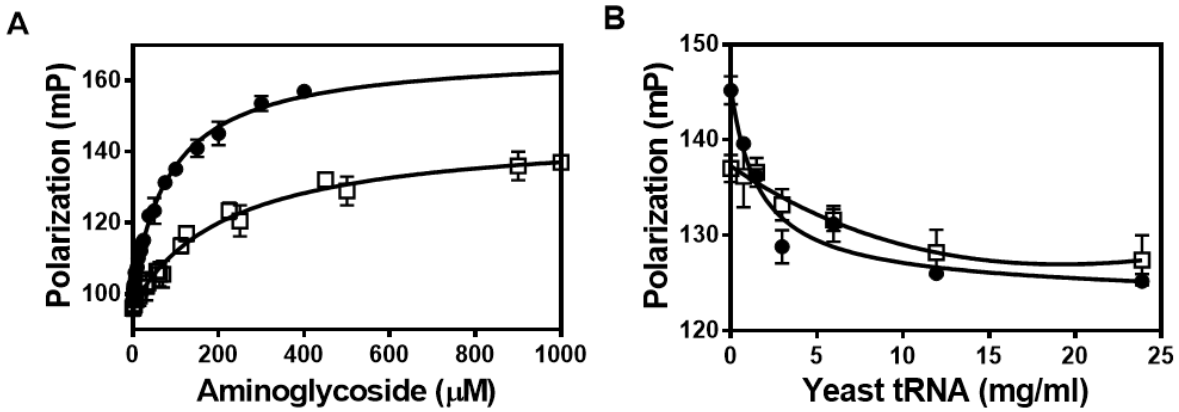


**Figure 2-4:** Neomycin B and kanamycin B bind to Fl-pre-tRNA**. (A)** Binding of NeoB (●) and KanB (□) to Fl-pre-tRNA measured by FP in Buffer B (50 mM Tris-HCl pH = 7.2, 10 mM $MgCl_2$, 100 mM KCl, 20 mM DTT), at 37˚C with 50 nM Fl-pre-tRNA. $K_d$ of neomycin B and kanamycin B to Fl-pre-tRNA are 90 ± 5 µM and 217 ± 20 µM, respectively. **(B)** Yeast $tRNA^{Mix}$ competes with Fl-pre-tRNA for binding neomycin B and kanamycin B with into either 200 µM NeoB (●) or 1 mM KanB (□) and varying concentrations of yeast $tRNA^{Mix}$. Error bars are showing standard deviations from five replicates.

Further studies support that NeoB and KanB bind to Fl-pre-tRNA and that the binding contributes to the mode of inhibition. Competition of yeast $tRNA^{Mix}$ with the Fl-pretRNA for binding NeoB or KanB was demonstrated by a decrease in FP (Figure 2-4). Yeast $tRNA^{Mix}$ increases the $K_{d,app}$ of NeoB and KanB to Fl-pre-tRNA by up to 3-fold (Table 2-2). Yeast $tRNA^{Mix}$ also increases the $IC_{50}$ of NeoB and KanB for inhibition of RNase P by 5-fold and > 40-fold, respectively (Table 2-2). Control experiments showed that yeast $tRNA^{Mix}$ does not affect the cleavage rate of RNase P suggesting that this tRNA does not compete with pre-tRNA binding for RNase P

(data not shown). Therefore, the decreased inhibition of NeoB and KanB in presence of yeast $tRNA^{Mix}$ is most likely due to a decreased fraction of inhibitor bound to Fl-pre-tRNA, consistent with the substrate binding playing a role in observed inhibition of RNase P by these compounds.

Spermidine is also competitive with NeoB inhibition of RNase P. In the presence of 100 mM KCl, 5-10 mM $Mg^{2+}$ and 10 mM spermidine, < 10% inhibition of enzyme activity or binding of Fl-pre-tRNA was observed at 1 mM of NeoB. This is consistent with previous studies indicating that inhibition of *E. coli* RNase P by aminoglycosides is demolished by high concentrations of $NH_4Cl$ (100 mM) and spermidine (10 mM) [28, 29]. Spermidine also increased the FP signal for Fl-pre-tRNA to a level comparable to saturating NeoB (400 µM). This result is consistent with the previously observed stabilization of native yeast $tRNA^{Phe}$ by spermidine [50]. In addition, the steady-state cleavage activity ($k_{cat}/K_M$ conditions) of *B. subtilis* RNase P increases with the spermidine concentration. At 10 mM sperimidine activity is enhanced by 2- and 6-fold for holoenzyme and P RNA, respectively (Figure A-2, Appendix A). This stimulation effect is comparable to the enhancement of cleavage activity on the M1 RNA by spermidine [51]. As observed with *E. coli* RNase P [28], high concentrations of $Mg^{2+}$ also decrease NeoB inhibition of *B. subtilis* RNase P (Figure A-3, Appendix A). To increase the selectivity of ligand binding to RNase P, yeast $tRNA^{Mix}$ and spermidine were included in the development of a high-throughput screening to reduce the hit rate and screen for more specific inhibitors.

**Table 2-2:** Yeast tRNA and spermidine decrease inhibition of *B. subtilis* RNase P by neomycin B and kanamycin B.

| | NeoB | | KanB | |
|---|---|---|---|---|
| Assay condition | $IC_{50}$ | $K_d$ | $IC_{50}$ | $K_d$ |
| Buffer B[a] | 23 ± 3 μM | 90 ± 5 μM | 52 ± 6 μM | 217 ± 20 μM |
| + 12 mg/ml Yeast tRNA[b] | > 100 μM[d] | 97 ± 23 μM | > 2 mM[d] | 540 ± 60 μM |
| + 10 mM Spermidine[c] | >> 1 mM[e] | >> 1 mM[e] | n.d.[f] | n.d.[f] |

[a] Measured in buffer B (50 mM Tris-HCl pH = 7.2, 10 mM $MgCl_2$, 100 mM KCl, 20 mM DTT) and with 20 nM Fl-pre-tRNA, 0.4 nM holoenzyme and 4 nM P protein at 37˚C.
[b and c] Same as [a] but with 50 nM Fl-pre-tRNA.
[d] Less than 50% of inhibition or percent bound is observed at this concentration measured.
[e] <10% inhibition or binding was observed at this this concentration measured.
[f] n.d. = not determined.

### 2.3.3 Comparison of Theoretical and Experimental FP of Fl-pre-tRNA

The observation that binding of NeoB and KanB to Fl-pre-tRNA altered the FP signal was unexpected because these compounds (0.4-0.6 Da) should not generate a noticeable change in FP upon binding to Fl-pre-tRNA (26 kDa) according to the Perrin equation [45]. The Perrin equation indicates that a large molecule will have a longer rotational correlation time (Equation 2-6) thus higher polarization (Equation 2-7). The rotational correlation time is usually calculated using the Stoke's equation (Equation 2-6) by adopting a rigid attachment model for of the fluorophore to spherical proteins. Using this equation, we calculated the theoretical FP value (Equation 2-6 and 2-7). The calculation for FP of Fl-5-nt-leader and the fully bound Fl-pre-tRNA·RNase P complex recapitulate the experimental values. However, the experimental FP reading for Fl-pre-tRNA is ~100 mP (marked by ★ in Figure 2-5)

which is much smaller than predicted theoretical value at ~190 mP. This discrepancy suggests that either the 5' end fluorescein molecule or the Fl-pre-tRNA complex is more dynamic than predicted by the model. In contrast, the FP reading of the fully bound NeoB·Fl-pre-tRNA complex (~160 mP, marked by ▼ in Figure 2-5) is close to the calculated value, consistent with previous observations that NeoB substantially stabilizes the secondary and tertiary structure of native yeast $tRNA^{Phe}$ [50].

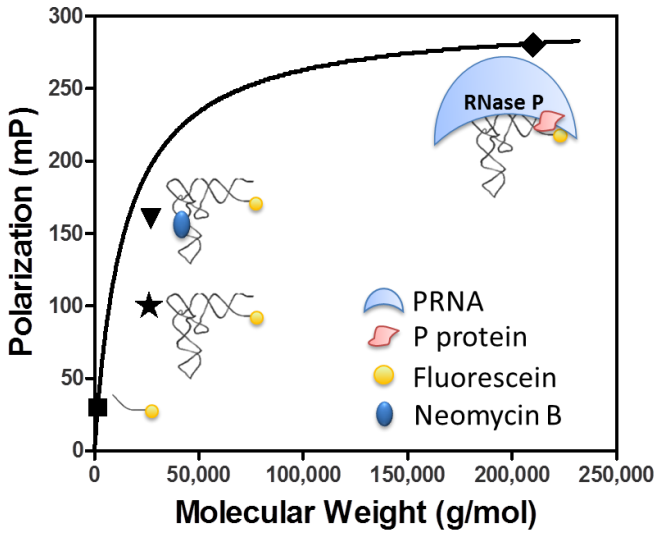


**Figure 2-5:** Comparison of theoretical calculation and experimental results on the polarization value of fluorescein labeled pre-tRNA in relation to molecular weight. The molecular weight of a pre-tRNAAsp with 5-nt leader is calculated from the sequence as shown in Figure 2-1. Solid line is the theoretical FP value generated by Equation 2-7. Solid symbols indicate experimental FP values measured in Buffer B (50 mM Tris-HCl pH = 7.2, 10 mM MgCl2, 100 mM KCl, 20 mM DTT) except for Fl-pre-tRNA·RNase P were measured in 10 mM CaCl2 and 200 mM KCl. Fl-5-nt-leader (■), Fl-pre-tRNA (★), Fl-pre-tRNA bound to NeoB (▼), Fl-pre-tRNA·RNase P (◆).

### 2.3.4 High-throughput Screen for Inhibitors of *B. subtilis* RNase P[3]

To optimize the FP assay for high-throughput screening (HTS), a matrix of experiments were carried out to choose the conditions for an RNase P-catalyzed

[3] The compound pinpointing and cherry-picking for the high-throughput screen were carried out by Steven Swaney from the Center for Chemical Genomics (CCG) at the University of Michigan. Xin Liu performed the HTS experiments. Paul Kirchhoff from the Vahlteich Medicinal Chemistry Core at University of Michigan performed statistical analysis of raw data and compound triage. Martha Larsen at CCG supervised data quality control.

cleavage end point assay in a 384-well microplate format (details in Appendix A). First, we tested sensitivity of *B. subtilis* RNase P activity to commonly used HTS reagents such as DMSO and detergent. The activity of *B. subtilis* RNase P decreased upon increasing concentrations of DMSO (Figure A-4B, Appendix A). About 80% activity remained when the enzyme is pre-incubated with 2% DMSO. Therefore, no more than 2% DMSO was included in the pre-incubation of samples with RNase P and the final DMSO concentration was maintained at 1% in all reactions. The non-ionic detergent NP-40 (0.01%) was added to enhance the performance of liquid handling and does not affect RNase P activity at concentrations from 0.01 to 0.1% (v/v) (Figure A-4C, Appendix A).

Second, the robustness of HTS assays, indicated by the Z' factor [52], was optimized by examining the methods to measure positive controls (maximum inhibition, or 0% activity). Quenching the RNase P catalyzed cleavage reaction by EDTA to chelate the $Mg^{2+}$ decreases the polarization value for Fl-pre-tRNA with little effect on the readings of the cleaved product (data not shown). This alteration in FP leads to a narrower dynamic range and a smaller Z' factor (Equation 2-8). Therefore, the reaction was quenched by a final concentration of 80 mM $CaCl_2$ because it both provides a larger dynamic range and slows the reaction dramatically, mimicking an inhibitor of RNase P (Figure 2-6).

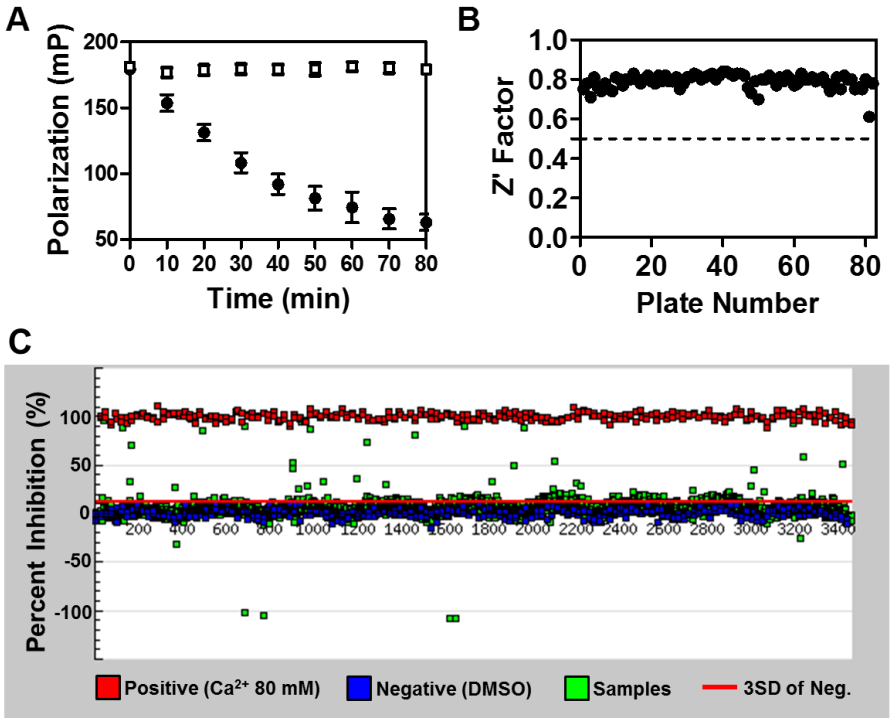


**Figure 2-6:** High-throughput FP assay is robust for screening inhibitors of *B. subtilis* RNase P. **(A)** Reaction progress curves measured by quenching the reaction with calcium ions at specified time points in HTS buffer (50 mM Tris-HCl pH = 7.2, 10 mM $MgCl_2$, 100 mM KCl, 20 mM DTT, 12 mg/ml yeast $tRNA^{Mix}$, 10 mM spermidine, and 0.01% (v/v) NP-40) with 1% DMSO, 20 nM FL-pre-tR5, and 0.15 nM RNase P holoenzyme with 1.5 nM P protein at 30˚C. The reactions contained either no inhibitor (1% DMSO blank, ●) as negative control or 80 mM $CaCl_2$ (□) as positive control for inhibition. Error bars are derived from 18-32 replicates in one 384-well plate. **(B)** The Z' factor values for the FP HTS assay across 384-well microplate. **(C)** A scatter plot of showing the percent inhibition by plate in the pilot screen of the 2880 compound library. Positive controls by 80 mM $CaCl_2$ are shown by red squares. Negative controls with 1% DMSO are blue. Compound samples are green. The red solid line indicates percent inhibition at three times of standard deviation of negative controls (3SD).

Using the established optimum conditions, a high-throughput screen of 2880 compounds and 22720 natural product extracts (NPEs) was carried out in 384-well microplates using the endpoint FP assay. The 2880 compound library, containing small molecules and natural products of known structure, is a pilot set for evaluating assay performance. In the NPE library, each sample is often a mixture of substances with unknown identity. The 82 plates in the primary screen has a Z' factor varying

from 0.6 to 0.8 (average Z' factor = 0.79, (Figure 2-6), demonstrating that the assay is suitable for high-throughput screens [52].

The primary screen results (n=1) were triaged (Figure 2-7) to select samples for further screens. First, active samples were defined by showing a percent inhibition that is higher than 3 standard deviations (3SD) of negative controls on each plate. Second, fluorescence intensity of perpendicular channel was analyzed to eliminate false positives that have a fluorescence intensity 3SD higher or lower than negative controls. Promiscuous compounds recorded in the MScreen database (Hit% ≥ 21% in all screens performed at CCG, University of Michigan) were also eliminated.

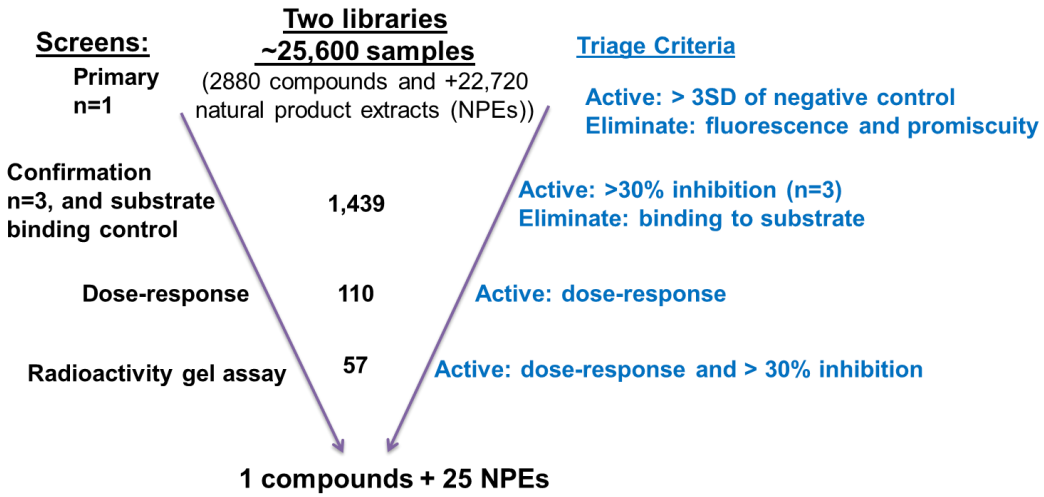


**Figure 2-7:** HTS screens and triage process for identification of inhibitors of *B. subtilis* RNase P.

From the total of ~25600 samples from the primary screen, 1439 were selected for a confirmation screen (n=3). A control screen was carried out by first incubating compounds with Fl-pre-tRNA to screen for compounds that bind to substrate.

Subsequently, RNase P enzyme was added to the plate for the end-point activity assay similar to procedures in the primary screen (30 ˚C and 35 min reaction time). From these two screens, 110 Samples showed repeatable inhibition (percent inhibition >30%) and no significant affinity to pre-tRNA (within 3SD of negative controls in the control screen). These 110 samples were further tested by a dose-response assay. 57 samples inhibit *B. subtilis* RNase P activity in a concentration-dependent fashion and therefore were further tested by an orthogonal radiochemical gel assay using the 5' end $^{32}$P labeled pre-tRNA substrate (data not shown). Only one compound (iriginol hexaacetate) was considered as a hit (>30% inhibition with two different concentrations) from the 2880-compound set after these series of screens. For the NPE library, we are following up on dissecting the top-25 hits in collaboration with Professor David Sherman's laboratory at the University of Michigan (Figure A-5, Appendix A).

### 2.3.5 A Natural Product Derivative Inhibits *B. subtilis* RNase P *in vitro*

From the 2880-compound set, iriginol hexaacetate (Ir6Ac, Figure 2-8) is the only compound that inhibits *B. subtilis* RNase P (percent inhibition > 30%) at 10 μM concentrations under the HTS buffer conditions (10 mM spermidine and 12 mg/mL yeast $tRNA^{Mix}$) (Figure 2-8). Ir6Ac is a derivative of irigenol, a member of the isoflavone natural products family. The $IC_{50}$ of Ir6Ac against *B. subtilis* RNase P in HTS buffer is 1.7 ± 0.1 μM, while previous reported aminoglycoside inhibitors such as neomycin B has a less than 10% inhibition at 1 mM concentrations under this condition. In addition, Ir6Ac likely does not bind to Fl-pre-tRNA substrate under this condition, as indicated by no observed increase in FP signal when Ir6Ac is titrated

into Fl-pre-tRNA substrate (data not shown). These data suggest that Ir6Ac is likely more specific and potent for inhibition of RNase P than previous reported inhibitors such as neomycin B.

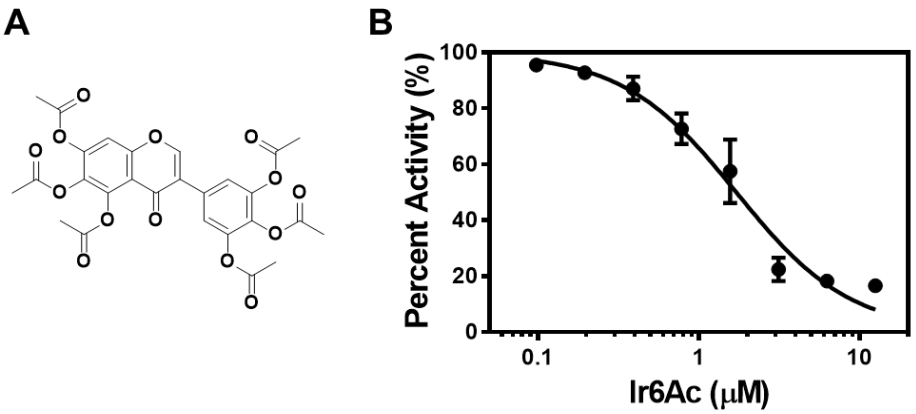


**Figure 2-8:** Iriginol hexaacetate inhibits *B. subtilis* RNase P catalyzed cleavage**. (A)** Chemical structure of iriginol hexaacetate (Ir6Ac). **(B)** Dose-response curve of inhibition by Ir6Ac of multiple-turnover cleavage activity catalyzed by RNase P to Ir6Ac measured by FP in HTS buffer (50 mM Tris-HCl pH = 7.2, 10 mM $MgCl_2$, 100 mM KCl, 20 mM DTT, 12 mg/ml yeast $tRNA^{Mix}$, 10 mM spermidine, and 0.01% (v/v) NP-40) with 20 nM Fl-pre-tRNA and 0.1 nM *B. subtilis* RNase P holoenzyme with 1 nM P protein. $IC_{50}$ is 1.7 ± 0.1 μM.

## 2.4 Discussion

### 2.4.1 Advantage of the Fluorescence Polarization Assay

To facilitate mechanistic studies and discovery of inhibitors of bacterial RNase P, we have developed a high-throughput FP assay that can measure both cleavage activity of RNase P in real-time and binding of small ligands to tRNA (Scheme 2-1). The FP assay is safer and cost-effective compared to the radioactivity-based assay and is ratiometric with great precision. The real-time cleavage assay by FP is validated by comparison with gel-based cleavage assays (Table 2-1). The FP assay is also suitable for high-throughput screening for inhibitors of RNase P (Figure 2-6) and for direct measurement of ligands binding to Fl-pre-tRNA (Figure 2-4). Because

the FP assay does not require separation of substrate and product and can be used as a real-time assay, the time needed to measure RNase P activity is much shorter. The 96-well or 384-well plate high-throughput assay format greatly enhances the ability to measure RNase P activity under multiple conditions and to identify inhibitors.

The FP assay reported here is also robust (Z' factor >0.5) and cost-effective for large scale high-throughput screens. Compared to other ratio-metric assays, such as fluorescence resonance energy transfer (FRET), FP is easier to use because it only requires one fluorescent probe and does not require 100% labeling efficiency. A yield of 60-90% fluorescein labeled pre-tRNA is routinely obtained from the *in vitro* transcription primed by guanosine 5'-monothiophosphate (GMPS) and subsequent labeling by 5-Iodoacetamido-fluorescein. Moreover, unlike the short half-life of $^{32}P$ in the radioactivity assays, Fl-pre-tRNA can be stored in ethanol at -80˚C for many months without significantly altering the activity or fluorescence signal. One limitation of using a fluorescein is the interference from fluorescent compounds [47]. Fluorescent dyes with a higher emission wavelength could further improve the performance of the FP HTS assay [47].

RNA molecules have gained growing attention as drug targets [53, 54]. Development of RNA-friendly methods for studying RNA function and inhibitor screening are in great demand [55]. Fluorescence polarization/fluorescence anisotropy (FP/FA) methods are increasingly used in studying biomolecule-ligand interactions, enzyme kinetics, and high-throughput screening [56]. Recently, FP/FA methods have been explored to study RNA dynamics [57], ribozyme self-cleavage

[58], peptidyl-tRNA hydrolysis [59], RNA binding to fluorescently-labeled compounds [60], and RNA-ligand affinity and specificity by competition [61]. The FP assay reported here provides a simple method to measure not only pre-tRNA processing but also pre-tRNA-ligand interactions. This new methodology will accelerate study of RNase P inhibition and facilitate evaluation of bacterial RNase P as an antimicrobial drug target [26].

### 2.4.2 NeoB and KanB Inhibit *B. subtilis* RNase P by Binding to Substrate

The mechanisms for inhibition of bacterial RNase P function are multifold. For example, inhibitors could disrupt P RNA·P protein association, chelate structurally and functionally important metal ions, alter P RNA conformation, and/or interfere with substrate recognition [26]. Highly positively charged compounds could function as potent RNA binders and inhibitors but may also be nonspecific. Previous biochemical and computational docking studies suggested three possible mechanisms for inhibition of RNase P by aminoglycosides and derivatives through interaction with P RNA [28, 30, 62, 63]: (1) competition with the P protein and/or pre-tRNA for binding to P RNA through P1-P4 helix junction and to J19/4 region (computational prediction); (2) competition with $Mg^{2+}$binding with $Mg^{2+}$ near the P15 loop (based on $Pb^{2+}$-induced cleavage data); and (3) competition with pre-tRNA binding to RNase P in P15 region (computational prediction). However, the hypotheses listed above have not been directly tested.

The affinity of NeoB and KanB to Fl-pre-tRNA is only 4-fold lower than the $IC_{50}$ (Table 2-2), suggesting the binding of substrate could contribute to inhibition. It was also known that NeoB binds to native yeast $tRNA^{Phe}$, as demonstrated by

fluorescence titration ($K_d$ = 90 μM), inhibition of $Pb^{2+}$-induced cleavage ($IC_{50}$ = 100 μM), UV-melt experiments [50] and X-ray crystallography [64]. NeoB also stabilizes $tRNA^{Phe}$ structure as indicated by an increase in the $T_m$ of the native $tRNA^{Phe}$ when bound to NeoB [50]. This increase in thermal stability provides a possible explanation for the observation that NeoB binding leads to a striking increase in the FP of Fl-pre-tRNA (Figure 2-4, ΔmP > 50 mP, $K_d$= 90 μM). The binding of Fl-pre-tRNA by NeoB measured by the FP assay is also consistent with a structural evidence of a NeoB bound yeast $tRNA^{Phe}$ complex [64]. In this 2.6 Å resolution co-crystal structure, NeoB displaces a magnesium binding site in the deep groove below the D-loop of the yeast $tRNA^{Phe}$. NeoB and KanB also bind to tRNA nonspecifically as demonstrated by the ability of yeast $tRNA^{Mx}$ to compete with the binding (Figure 2-4). In addition, when yeast $tRNA^{Mix}$ was used to compete with Fl-pre-tRNA in binding NeoB and KanB, the inhibition of *B. subtilis* RNase P was weakened by more than 5-fold (Table 2-2). Based on these results, we speculate that the NeoB-bound pre-tRNA has an altered conformation or mobility that inhibits RNase P. Another possibility for the observed increase in FP is that binding of NeoB and KanB may cause dimerization of the Fl-pre-tRNA, which could be further investigated by gel mobility shift and ultracentrifugation assays.

Spermidine is also competitive with NeoB inhibition. At high ionic strength (100 mM KCl), spermidine (10 mM) abolished inhibition of *B. subtilis* RNase P by NeoB and KanB (Table 2-2), consistent with lack of inhibition for *E. coli* RNase P under similar conditions [28]. Spermidine is a biogenic polyamine that is polycationic and interacts nucleic acids [65]. Spermidine stabilizes tRNA [66-69] and may potentially

compete with the binding of aminoglycoside to the Fl-pre-tRNA. However, spermidine decreases the concentration of $Mg^{2+}$ required to activate catalysis by *E. coli* P RNA [51], suggesting a stabilization effect on P RNA as well. Similarly, spermidine stimulates activity of *B. subtilis* RNase P holoenzyme (Figure A-2, Appendix A). Spermidine also protects certain sites in the P RNA from $Pb^{2+}$-induced cleavage [70]. Therefore, spermidine could interfere with NeoB inhibition through competition with binding to Fl-pre-tRNA and/or P RNA. Since the *in vivo* concentration of spermidine is high (~5 mM) in *E. coli* [71], inclusion of spermidine in the screen for RNase P inhibitors is necessary and may lead to identification of RNase P-specific inhibitors.

### 2.4.3 FP for Measuring Compound Binding to Pre-tRNA

Unexpectedly, binding of low molecular weight compounds, such as NeoB and KanB, to Fl-pre-tRNA can be observed by FP (Figure 2-4). Calculations by Perrin equation [45] suggest that binding a small molecule to tRNA should not generate a detectable change in FP signal (Equations 2-6 and 2-7, Figure 2-5). However, a more than 50 mP increase in FP was observed when NeoB binds to Fl-pre-tRNA (Figure 2-4). Furthermore, the experimental FP of Fl-pre-tRNA (~100 mP) deviated markedly from the theoretical calculation (~190 mP) (Figure 2-5). A low FP signals for 3' end fluorescein labeled $tRNA^{fmet}$ [72], and 5' end labeled peptidyl-tRNA have also been reported [59]. Two scenarios could explain the low FP values. First, the fluorescein substituent on the 5' end could rotate more freely and rapidly than the rest of the pre-tRNA molecule. Second, pre-tRNA could be more dynamic than a macromolecule of the same molecular weight and therefore rotate more rapidly in

the solution, sampling different conformations. This second hypothesis is highly likely as NeoB and KanB binding increased the FP of Fl-pre-tRNA markedly, which is in line with previous observations that these compounds interact with and stabilize $tRNA^{Phe}$ [50, 64]. Therefore, the relative low polarization state of free Fl-pre-tRNA, which likely reflects the highly dynamic nature of the tRNA, is an advantage because it is sensitive to binding of small ligands, such as aminoglycosides, at moderate divalent metal ion concentrations.

To develop specific inhibitors targeting RNase P enzyme, it is important to distinguish compounds that function by binding to pre-tRNA. The FP assay can measure small ligand binding to pre-tRNA if the interactions alter the solution structure (Figure 2-4). Previously, small ligands binding to native $tRNA^{Phe}$ were assayed from change in the intrinsic fluorescence of a modified Y base [50]. The FP assay reported here using end-labeled pre-tRNA provides a more general and convenient way of measuring ligand binding and stabilization using *in vitro* transcribed tRNA. Additionally, this assay does not rely on binding to a given site [54] but can identify ligands that bind to any site that alters the conformational mobility of tRNA. One limitation of this approach is that if a small molecule binds to without affecting the RNA structure, no increase of FP signal will occur. Nonetheless, compounds that stabilize RNA structure might be of interest for drug development for many RNA targets [2]. For example, tRNA stabilizing agents will be a valuable tool for studying the structure, function and biology of the vast number of pathogenic mutations in human mitochondrial tRNAs [73]. Identification of

compounds that bind tRNA will potentially be useful for analyzing selectivity of other RNA-targeting drugs [3].

### 2.4.4 FP Assay Has Robust Performance for High-throughput Screening

To screen for specific inhibitors against RNase P cleavage activity, yeast $tRNA^{Mix}$ and spermidine were added to the assay buffer to minimize nonspecific binding to pre-tRNA. As a result, aminoglycosides and previously reported substrate-binding inhibitors, such as bis-benzimidazoles [31, 32], porphines and porphyrins [33], were not identified as inhibitors in the screens. These conditions decreased hit rate from 2-5% to 0.1% and increased the possibility of identifying specific inhibitors. Furthermore, orthogonal radioactivity cleavage assays were performed to confirm the hits from FP screens. Inhibitors identified in HTS also need to be further investigated *in vivo*. According to a publication from GSK [74], a compound identified in a HTS effort targeting RNase P failed because later investigation discovered that the compound has a major off-target mode of action. Therefore, the antibacterial activity of the inhibitors need to be validated *in vivo*, such as determining the minimum inhibitory concentration (MIC) [75] and the response of MIC to down- or up-regulation of the RNase P target.

### 2.4.5 High-throughput Screening Identified a New Inhibitor of RNase P

From a pilot high-throughput screen, we identified a new *B. subtilis* RNase P inhibitor Ir6Ac (Figure 2-6). Ir6Ac is a semisynthetic compound derived from irigenol, a member of the isoflavone natural products family produced by higher plants such as *Leguminosae*. Most isoflavones, including genistein and daidzein, were

suggested to function as phytoestrogens and antioxidants [76]. However, the proposed anti-cancer effects of isoflavones on mortality and recurrence rates in breast cancer patients are still under debate [77, 78]. To date, no pharmacological functions of Ir6Ac have been reported although in the PubChem website lists 14 records marking Ir6Ac as an active hit in HTS results. Ir6Ac has a good potency ($IC_{50}$=1.7 μM) for inhibition of RNase P and does not bind the substrate based on FP measurements, suggesting that it may be a more specific RNase P inhibitor than previously reported compounds. Ir6Ac is unlikely to function *in vivo* because the acetate groups are readily hydrolyzed in cells. Further studies on the mode of inhibition by Ir6Ac, such as investigation of irreversibility of inhibition and competition with subsrate and $Mg^{2+}$ ions, will provide insights into molecular recognition of inhibitors by RNase P.

The crystal structures of P RNAs [79, 80] and *T. maritima* RNase P holoenzyme with bound tRNA product demonstrate that the substrate binding surface in P RNA is large and shallow [81] (Figure 1-4, Chapter 1). These structural features suggest that the active site of RNase P might be less ideal for small molecule inhibitors. Therefore, natural products and compounds with novel chemical scaffolds might be better starting points for discovering inhibitors of bacterial RNase P. To search for novel RNase P inhibitors, we are collaborating with Dr. Avi Raveh, Pamela Schulz, and Michael Schillaci-Schofield in Professor David Sherman's laboratory (University of Michigan) to further investigate the top hits from the NPE library. Ongoing and future works include regrowth of the microorganism for natural product extraction, fractionation of the extracts through the guidance of the FP assay

(Figure A-5, Appendix A) as well as bacterial growth assay, and structural characterization of active components by mass spectroscopy and NMR.

### 2.4.6 Conclusion

RNase P plays an essential role in tRNA biogenesis and is considered a novel antibacterial target [25]. However, RNase P assays relied mainly on radiochemical methods which limit the capacity for high-throughput screens to discover novel RNase P inhibitors. The FP assay developed in this study is the first non-radioactive method capable of measuring steady-state cleavage activity of bacterial RNase P in real-time as well as detecting small ligand binding to pre-tRNA. The FP-based HTS assay can be applied to screen large scale compound libraries to identify novel RNase P inhibitors and tRNA binders. The principle and framework in this report could also be adopted to develop FP assays for RNase P from other organisms, including the novel protein-only enzymes from human mitochondria and plants, and other tRNA processing enzymes. Important factors in the assay development include careful design of substrate constructs, assay conditions and orthogonal assays to confirm whether the polarization is accurately reflecting the enzymatic activity. Furthermore, the FP binding assay using end-labeled pre-tRNA provides a direct method to study binding and stabilizing of pre-tRNA by small molecules, which could be applied to study other large RNAs with similar size and mobility.

## 2.5 Materials and Methods

### 2.5.1 Chemicals and Reagents

Nucleotide triphosphates, spermidine and other chemicals were obtained from Sigma at the highest purity unless otherwise indicated. SDS and $tRNA^{mix}$ from baker's yeast were purchased from Fisher Scientific. Inorganic pyrophosphatase was purchased from Roche Applied Science. 5-Iodoacetamido-fluorescein (5-IAF) was obtained from Invitrogen (now Life Technologies). Iriginol hexaacetate was purchased from MicroSource Discovery Systems, Inc. Guanosine 5'-monothiophosphate (GMPS) was synthesized from 2', 3' isopropylidene-guanosine and thiophosphoryl chloride as described in [82]. $His_6$-T7 RNA polymerase was purified by Ni-NTA chromatography as described previously [83]. Buffer solutions were prepared by Milli-Q treated deionized water (Millipore Corporation) and autoclaved or filtered by Stericup filter units (Millipore Corporation).

### 2.5.2 Assay Buffers

The following buffers were made fresh before use in the cleavage and/or binding assays: Buffer A (50 mM Tris/Mes pH = 5.5, 10 mM $MgCl_2$, 200 mM KCl, 20 mM DTT); Buffer B (50 mM Tris-HCl pH = 7.2, 10 mM $MgCl_2$, 100 mM KCl, 20 mM DTT); Buffer C (similar to buffer B except for pH = 8); HTS buffer (similar to buffer B with 12 mg/ml yeast $tRNA^{Mix}$, 10 mM spermidine, and 0.01% (v/v) NP-40).

### 2.5.3 Preparation of RNA and P Protein

P protein and P RNA were prepared as previously described [84, 85]. Fl-pre-$tRNA^{Asp}$ containing a 5-nucleotide leader sequence (Fl-pre-tRNA, Scheme 2-1) was

prepared from procedures adapted from previous reports [41, 43]. Pre-tRNA$^{Asp}$ with a 5′ monothiophosphate terminus was transcribed in the presence of 4 mM ATP, CTP, UTP, 4-5 mM GMPS, and 0.8-1 mM GTP, 0.1 μg/μL T7 RNA polymerase, 0.8-1 μg/μL linearized DNA template, 1 mM spermidine, 5 mM DTT, 2 μg/mL pyrophosphatase, 50 mM Tris–HCl (pH 8.0) and 20-28 mM $MgCl_2$, incubated at 37 °C for overnight (20 mM $MgCl_2$) or for 4-6 hours with addition of 20 μM NTPs every 30 min (28 mM $MgCl_2$). The transcribed 5'-GMPS-pre-tRNA was buffer exchanged and concentrated into a degassed labeling buffer (10 mM Tris-HCl, pH7.2 and 1 mM EDTA) by at least three iterations of centrifugal filtration (Amicon Ultra, 10,000 MWCO, Millipore Corporation) at 4°C and then incubated with 20- to 40- fold excess of 5-IAF at 37 °C overnight to obtain Fl-pre-tRNA followed by purification using denaturing PAGE. The radiolabeled pre-tRNA substrate was prepared by incubating with calf intestinal alkaline phosphatase (NEB) followed by 5′ end-labeling using T4 polynucleotide kinase (NEB) and [γ-$^{32}$P] ATP and purified as described in [46]. All RNAs were purified by electrophoresis on a 6% (P RNA) or 10% (pre-tRNA) polyacrylamide/bis (39:1) denaturing gel containing 7 M urea. Excised RNA bands were soaked into a TES buffer (10 mM Tris, pH 8, 1 mM EDTA, 0.1% SDS, and 500 mM NaCl) at 4°C overnight. Filtered solutions with eluted RNA were concentrated and exchanged into buffer containing 10 mM Tris, 1 mM EDTA and 500 mM NaCl by Amicon as described above and ethanol precipitated for storage at -80°C.

### 2.5.4 Single- and Multiple-turnover Experiments

Before use, P RNA and pre-tRNA were denatured by heating for 3 min at 95°C in autoclaved Milli-Q water and then refolded for kinetic and thermodynamic assays

by first incubating for 10-15 min at 37°C followed by addition of according buffers and incubation for at least 30 min. Then P protein was added to the P RNA for a 30 min incubation at 37°C to form the holoenzyme.

For gel assays, time points for the cleavage reaction catalyzed by RNase P were taken by diluting aliquots of reaction mix into an equal volume of EDTA quenching solution [10 M urea, 200 mM EDTA (pH 8.0), 0.05% bromophenol blue, and 0.05% xylene cyanol], as described in [46]. Cleavage of pre-tRNA substrate was analyzed by a 10% denaturing gel and visualized by Typhoon phosphorimager using phosphor ($^{32}$P-label) or fluorescence (fluorescein label) scan. The percentage of cleavage was quantified by ImageQuant 5.2 or ImageJ software.

Real-time fluorescence polarization cleavage assays were performed in a black 96-well microplate (Corning Incorporation, #3915 or #3686) by monitoring the polarization signal of fluorescein ($\lambda_{ex}$ = 485 nm and $\lambda_{em}$ = 535 nm) using a TECAN plate-reader (Genois, G factor=0.95, or Infinite F500, G factor=0.94). The reactions were initiated by addition of the enzyme or substrate using single- or multi-channel pipettes. Experiments measuring single-turnover reactions were carried out using excess enzyme concentrations ([E] = 360 to 500 nM, [S] = 10 to 25 nM) in buffer A at 37 °C. The single-turnover cleavage rate constant ($k_{obs}$) was calculated by fitting Equation 2-1 to a percentage cleaved progress curves calculated by Equation 2-2:

$$Y = Y_{\infty}\left(1 - e^{-k_{obs}t}\right) \qquad \textbf{Equation 2-1}$$

Where

$$Y = \frac{(3 - P_B)(P - P_F)}{(3 - P)(P_B - P_F) + (g - 1)(3 - P_F)(P_B - P)} \qquad \textbf{Equation 2-2}$$

The total fluorescence change during single-turnover reaction is adjusted by the enhancement factor, $g = F^B/F^F$, and $P_B$ and $P_F$ are the polarization values of the RNase P holoenzyme-bound substrate and cleaved product, respectively [86].

When the Fl-pre-tRNA was measured at 37˚C, a non-linear decrease in polarization for the first few minutes was observed after initiating reactions by first moving out the plates from the temperature controlled plate-reader chamber. This was not detected when experiments were performed at room temperature, which indicates that the initial drop in FP is due to temperature difference between ambient and instrument during operations. Therefore, substrate-alone controls were presented in the experiments to adjust for this effect. The multiple-turnover measurements of RNase P activity were performed under excess substrate ([S]=0.01 to 1 μM, [E]=0.15 to 1 nM) in buffer B, buffer C, or HTS buffer. The substrate-only controls were included on each plate and the FP trace of the substrate-only control was subtracted from reaction traces to adjust for temperature variation. The linear initial rates (mP/sec) from the time courses were obtained and converted to reaction velocity (nM/sec) by Equation 2-3 as describe in [87].

$$v_0 = \frac{\left(\frac{\Delta P_t}{\Delta t}\right)}{\Delta P_c}[\mathrm{S}] \qquad \textbf{Equation 2-3}$$

$\Delta P_c/\Delta t$ is the slope of the linear initial rate for multiple turnover reaction time courses. $\Delta P_c$ is the polarization signal change upon complete conversion of substrate to product. The Michaelis-Menten equation [88] was fit to the dependence of the initial reaction velocity on the concentration of pre-$tRNA^{Asp}$ to obtain steady-

state kinetic parameters, $k_{cat}$, $K_M$, and $k_{cat}/K_M$ (Figure 2-2). All data analyses were performed using Prism 5.03 (GraphPad Software).

The dose-response curves of multiple-turnover activity of RNase P on inhibitors were measured as described in figure and table legends (Figure 2-3 and Table 2-2) using 96-well microplate FP assays. The enzyme and substrate concentrations were kept constant with varying inhibitor concentrations. For NeoB and KanB reactions were performed in the absence of DMSO because aminoglycosides are highly soluble in aqueous solution. The Ir6Ac inhibitor was dissolved freshly in DMSO and 1% DMSO was included in the reaction for all inhibitor concentrations. The initial rates in the DMSO blank (MIN inhibition and 100% activity) and in the presence of 80 mM $CaCl_2$ or without enzyme (MAX inhibition and 0% activity) were used as negative and positive controls for inhibition respectively to calculate percent activity using Equation 2-4, where *Inh* is the initial rate at given inhibitor concentration:

$$\%Activity = \frac{Inh - MAX}{MIN - MAX} \qquad \textbf{Equation 2-4}$$

The concentration of an inhibitor that results in 50% loss of the enzyme activity ($IC_{50}$) was calculated using Equation 2-5 where *N* is the Hill coefficient:

$$\%Activity = \frac{100}{1 + \left(\frac{[\mathrm{I}]}{\mathrm{IC}_{50}}\right)^{N}} \qquad \textbf{Equation 2-5}$$

### 2.5.5 Dissociation Constant Determined by Fluorescence Polarization

The affinity of aminoglycosides (neomycin B or kanamycin B) for Fl-pre-tRNA was measured using FP (Figure 2-4). The compounds were incubated with Fl-pre-

tRNA at 37°C for 15 min in the plate-reader before collecting data. The titration curve was fit to Equation 2-6 to obtain the dissociation constant, $K_d$:

$$Y = P_f + \left(P_b - P_f\right) \times \frac{([\mathrm{I}] + [\mathrm{S}] + K_d) - \sqrt{([\mathrm{I}] + [\mathrm{S}] + K_d)^2 - 4[\mathrm{I}][\mathrm{S}]}}{2[\mathrm{S}]} \qquad \textbf{Equation 2-6}$$

In the equation, $P_f$ is the polarization of unbound Fl-pre-tRNA and $P_b$ is signal from fully bound Fl-pre-tRNA·compound complex.

### 2.5.6 Calculation of Fluorescence Polarization in Relation to Molecular Weight

A theoretical dependence of polarization on the molecular weight of the 5' end fluorescein-labeled RNA (Figure 2-5) was calculated according to Stoke's (Equation 2-7) and Perrin's equation (Equation 2-8) ([45] and reference therein).

$$\theta = \frac{\eta V}{RT} = \frac{\eta M}{RT}(\bar{\nu} + h) \qquad \textbf{Equation 2-7}$$

$$\left(\frac{1}{P} - \frac{1}{3}\right) = \left(\frac{1}{P_0} - \frac{1}{3}\right)\left(1 + \frac{\tau}{\theta}\right) = \left(\frac{1}{P_0} - \frac{1}{3}\right)\left(1 + \frac{\tau RT}{V}\right) \qquad \textbf{Equation 2-8}$$

$P_0$ is the limiting polarization in the absence of depolarization factors, $\tau$ is the fluorescence lifetime, $\theta$ is rotational correlation time, $\eta$ is viscosity, $M$ is molecular weight, R is gas constant =8.31 x $10^7$ erg/K/mol. $\bar{\nu}$ is theoretical volume for globular protein, and $h$ is the degree of hydration. The data (solid line) in Figure 2-5 was generated by applying $P_0$ = 300 mP, $\tau$ = 4 ns, $\eta$ = 0.0069 P, R = 8.31 x $10^7$erg/K/mol, T =310 K, $\bar{\nu}$ = 0.75 ml/g and $h$ = 0.2 [89].

### 2.5.7 High-throughput Screening

To determine the optimum conditions for the end-point HTS assay, RNase P cleavage reactions were carried out at 30 ˚C in a black 384-well microplate (Corning Corporation, Catalog # 3676) by quenched by the addition of 80 mM $CaCl_2$ at various time points (Figure 2-4). The enzyme was pre-incubated with 2% DMSO for 30 min before the reaction was initiated by addition of equal volume of substrate. The FP signal was measured using a PheraStar plate reader (BMG Labtech) with a FP filter module ($\lambda_{ex}$ = 485 nm and $\lambda_{em}$ = 520 nm).

The HTS library was provided by the Center for Chemical Genomics at University of Michigan. For the primary compound screen of ~2880 compounds (n=1), reactions were carried out using final concentrations of 10 μM compound, 1% DMSO, 0.15 nM RNase P and 20 nM Fl-pre-tRNA at 30 ˚C in HTS buffer condition. First, enzyme was added by a Multidrop Combi reagent dispenser with a micro-multidrop cassette (Thermo Fisher) before each compound (in DMSO) or DMSO (negative controls, column 1 and 2) was pinpointed (Biomek FX Pintool, Beckman Coulter) into the solution. Then 80 mM $CaCl_2$ was added to the positive control wells (column 23 and 24). RNase P was incubated with compounds at 30 ˚C for 30 min before reactions were initiated by addition of Fl-pre-tRNA substrate. The plates were incubated for another 35 min at 30 ˚C before addition of $CaCl_2$ to stop the reactions. The microplates were read once by the PheraStar plate reader and plate-stackers using well H23 of each plate to adjust the gain and beam position.

Compounds with percent inhibition values of greater than or equal to three times standard deviation (3SD) of the negative controls were defined as active and

samples with fluorescence intensity (perpendicular channel) of greater or less than 3SD of negative controls were considered false positives. Promiscuous compounds as identified by previous HTS in the MScreen database (appears as hits in ≥21% of screens recorded in CCG) were also excluded from further study.

A confirmation screen of compounds and NPEs chosen from the primary screen was carried out under HTS conditions with modifications. Briefly, the compound samples in triplicate were incubated with Fl-pre-tRNA substrate first and the plates were read before addition of RNase P to identify compounds that bind to Fl-pre-tRNA substrate. The triage criteria of the confirmation screens were to take samples showed repeatable 30% or more inhibition activity as actives. False positives were identified from florescence intensity (perpendicular channel) of greater or less than 3SD of negative control reads. Active compounds identified from the confirmation screens were picked by a Mosquito X1 robot (BMG Labtech) for dose-response assays using the same conditions. Samples showed concentration dependent inhibition activity were identified as actives. Hits selected from the dose-response assay were further tested by 5' end labeled $^{32}$P-pre-tRNA substrate in a gel assay. The $^{32}$P assay was carried out at room temperature using 100 nM unlabeled pre-tRNA substrate mixed with < 4 nM $^{32}$P labeled substrate with 0.5 nM RNase P and two different concentrations of samples. Samples that inhibit RNase P at both concetrations from radioactivity assay are determined as final hits.

The robustness of the HTS assay was evaluated by calculating the Z'-factor according to Equation 2-9, where $\sigma_{c+}$ and $\sigma_{c-}$ stand for standard deviation for

positive and negative controls respectively and $\mu_{c+}$ and $\mu_{c-}$ are the average values from positive and negative controls.

$$Z' = 1 - \frac{(3\sigma_{c+} + 3\sigma_{c-})}{|\mu_{c+} - \mu_{c-}|} \qquad \textbf{Equation 2-9}$$

As seen from the Equation 2-8, the Z'-factor is a screening window coefficient and is defined as the ratio of the separation band to the signal dynamic range of the assay. A Z'-factor higher than 0.5 indicates a robust assay [52].

## 2.6 Appendix A

This appendix contains figures of supporting data for the development of the fluorescence polarization (FP) assay. The experiments are briefly described in the figure legend. No discussion is included.

### 2.6.1 Cation Concentrations Affect FP of Fl-pre-tRNA

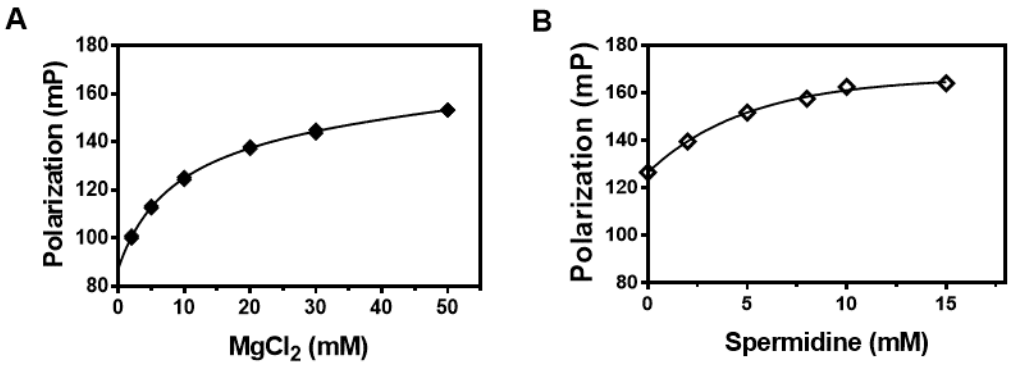


**Figure A-1:** Fluorescence polarization of Fl-pre-tRNA in response to cation concentrations. **(A)** FP of Fl-pre-tRNA increased with increasing [Mg2+]. Measured in 50 mM Tris-HCl (pH 7.2), varying MgCl2, 100 mM KCl, 20 mM DTT with 20 nM Fl-pre-tRNA, 0.4 nM B. subtilis RNase P holoenzyme with 4 nM P protein. Samples in duplicates were incubated in the plate (Corning #3915) for at least 15 min before reading at room temperature, G factor=0.99. **(B)** FP of Fl-pre-tRNA increased with increasing [Spermidine]. Measured in identical buffer conditions as A with 10 mM MgCl2.

### 2.6.2 Spermidine Enhances Cleavage Activity of *B. subtilis* RNase P

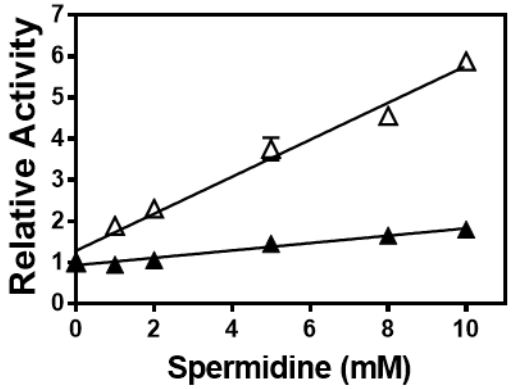

**Figure A-2:** Spermidine enhances multiple-turnover activity of B. subtilis RNase P holoenzyme (▲) and P RNA (△). Measured in 50 mM Tris-HCl (pH 7.2), 10 mM $MgCl_2$, 100 mM KCl, 12 mg/ml yeast $tRNA^{Mix}$, 20 mM DTT with 20 nM Fl-pre-tRNA and 0.5 nM holoenzyme (5 nM P protein) or P RNA at room temperature in duplicates. Relative activity was calculated with respect to the cleavage rate in the absence of spermidine.

### 2.6.3 $Mg^{2+}$ and Spermidine Are Competitive with Neomycin B Inhibition of *B. subtilis* RNase P

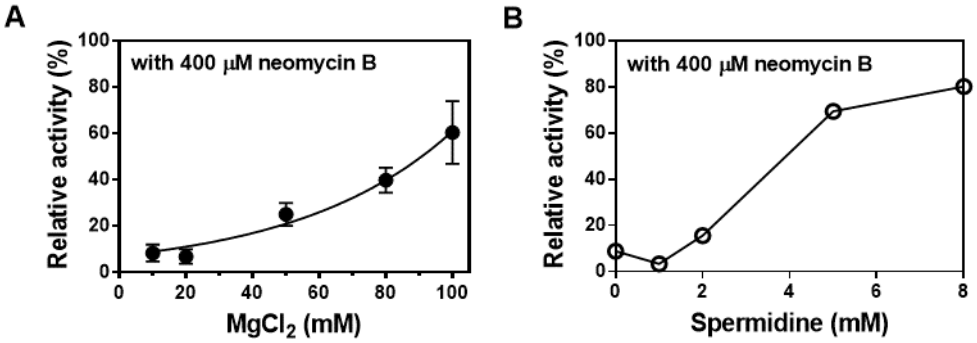


**Figure A-3:** $Mg^{2+}$ and spermidine are competitive with inhibition of *B. subtilis* RNase P by neomycin B. **(A)** [$Mg^{2+}$] dependence (●) of relative activity of RNase P cleavage in 400 μM neomycin B. Relative activity is a ratio of the cleavage rate in presence of neomycin B compared to the rate in the absence of neomycin B at specified [$Mg^{2+}$]. Measured in 50 mM Tris-HCl (pH 7.2), 100 mM KCl, 20 mM DTT with 50 nM Fl-pre-tRNA, 0.4 nM *B. subtilis* RNase P holoenzyme with 4 nM P protein at 37˚C in duplicates. **(B)** [Spermidine] dependence (○) of relative activity of RNase P cleavage in 400 μM neomycin B. Similar conditions in (A) except that 10 mM $MgCl_2$ was included in the buffer.

### 2.6.4 Optimization for High-throughput Screen: Test of $Mg^{2+}$, DMSO and NP-40

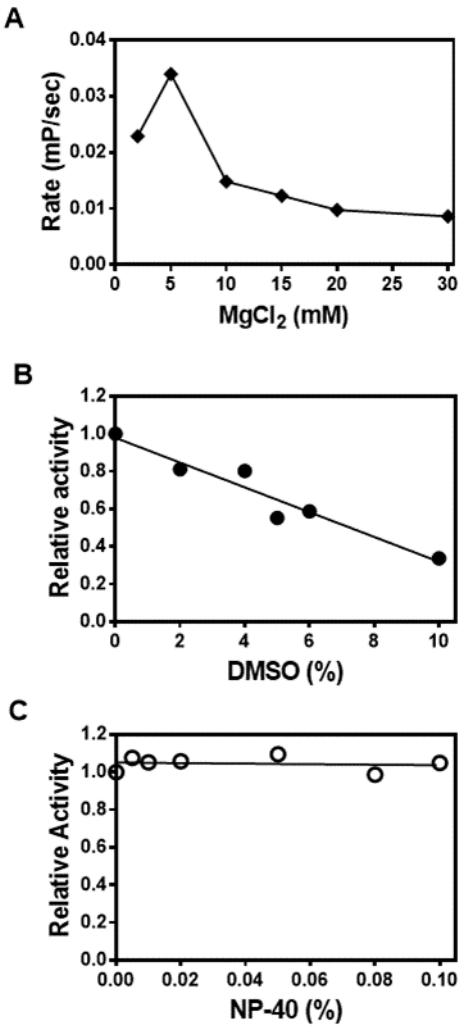


**Figure A-4:** Test of RNase P cleavage activity in response to [$Mg^{2+}$], [DMSO] and [NP-40]. **(A)** Measured in 50 mM Tris-HCl (pH 7.2), varying $MgCl_2$, 100 mM KCl, 20 mM DTT, 10 mM spermidine with 20 nM Fl-pre-tRNA, 0.4 nM *B. subtilis* RNase P holoenzyme with 10-fold access of P protein at room temperature and in duplicates. **(B)** Measured in 50 mM Tris-HCl (pH 7.2), 10 mM $MgCl_2$, 100 mM KCl, 20 mM DTT and varying DMSO (v/v) with 50 nM Fl-pre-tRNA and 4 nM RNase P holoenzyme (6 nM P protein) at room temperature. **(C)** Same buffer condition as in (B) except for using 1 nM RNase P holoenzyme.

### 2.6.5 Follow-up on the Hits from the Natural Product Library[4]

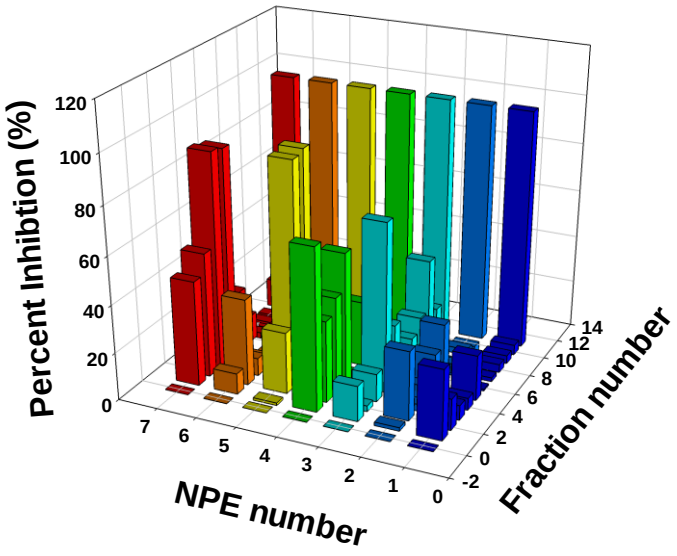


**Figure A-5:** Test of inhibition of B. subtilis RNase P cleavage activity by regrowth extracts and extract fractions of hits from the NPE library. Graph is showing preliminary results for 7 strains. Fraction No. 0 is the negative control (DMSO blank) while No. 11 is the positive control (80 mM $CaCl_2$). Fraction No. 1 is the crude extract and No. 2-10 are fractions from a reverse-phase HPLC purification (from high to low hydrophilic fractions). Samples were dissolved in DMSO to 15 mg/ml and measured at a final concentration of 0.15 mg/ml (1%) in 50 mM Tris-HCl (pH 7.2), 5 mM $MgCl_2$, 100 mM KCl, 20 mM DTT, 12 mg/ml yeast $tRNA^{Mix}$, 10 mM spermidine, 0.01% (v/v) NP-40 with 20 nM Fl-pre-tRNA and 0.15 nM RNase P holoenzyme (1.5 nM P protein) at 30˚C. Initial rate was calculated from the linear region of the reaction progress curve observed by FP and the percent inhibition was calculated using Equation 2-3.

[4] Regrowth of microbes and HPLC fractionation of extracts was carried out by Dr. Avi Raveh from Prof. David Sherman's laboratory.

### 2.6.6 A 96-well Plate Bacterial Growth Assay for Evaluation of Antibacterial Activity[5]

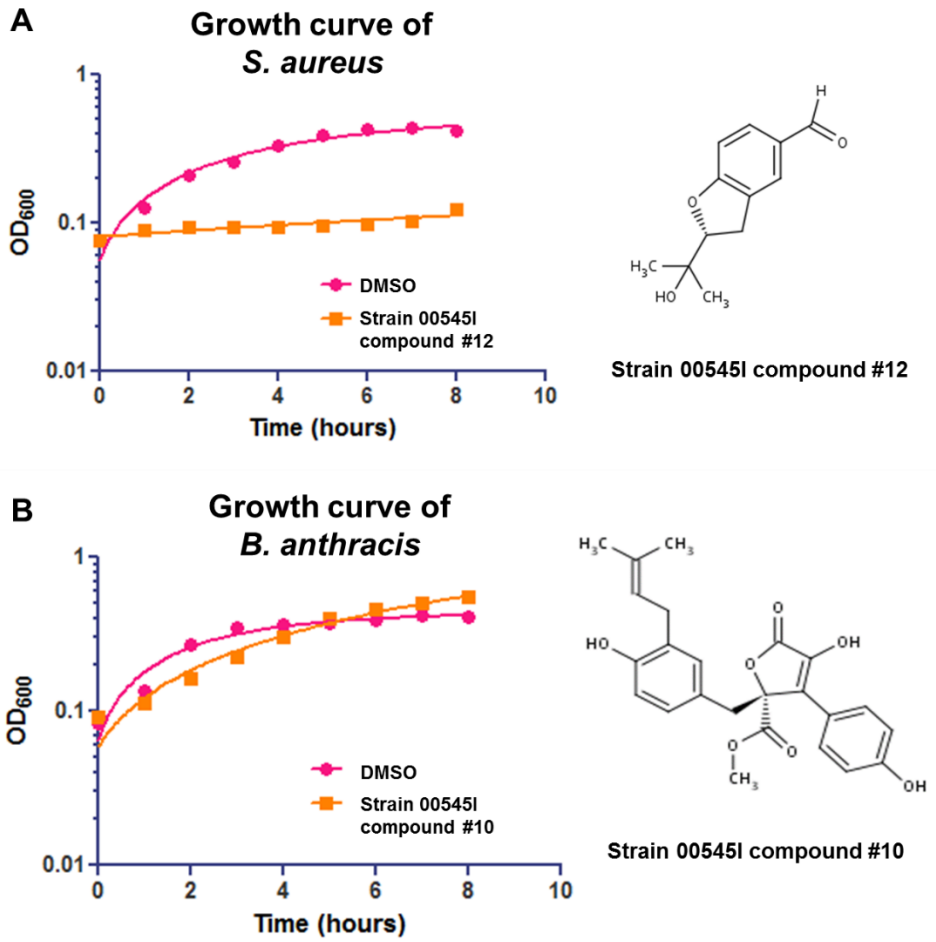


**Figure A-6:** Test of antibacterial growth activity by two natural products extracted from NPE hits using a 96-well plate assay. Compound concentration is 0.15 mg/mL. Cells were grown in LB media at 37 ˚C.

[5] Michael Schillaci-Schofield in Professor David Sherman's laboratory provided bacteria strains and assay reagents. Xin Liu and Michael Schillaci-Schofield performed experiments.

## 2.7 References


1. Wilson, W.D. and K. Li, *Targeting RNA with small molecules.* Curr Med Chem, 2000. **7**(1): p. 73-98.
2. Tor, Y., *Targeting RNA with small molecules.* Chembiochem, 2003. **4**(10): p. 998-1007.
3. Thomas, J.R. and P.J. Hergenrother, *Targeting RNA with small molecules.* Chem Rev, 2008. **108**(4): p. 1171-224.
4. Cooper, T.A., L. Wan, and G. Dreyfuss, *RNA and disease.* Cell, 2009. **136**(4): p. 777-93.
5. Kazantsev, A.V. and N.R. Pace, *Bacterial RNase P: a new view of an ancient enzyme.* Nat Rev Microbiol, 2006. **4**(10): p. 729-40.
6. Kirsebom, L.A., *RNase P RNA mediated cleavage: substrate recognition and catalysis.* Biochimie, 2007. **89**(10): p. 1183-94.
7. Walker, S.C. and D.R. Engelke, *Ribonuclease P: the evolution of an ancient RNA enzyme.* Crit Rev Biochem Mol Biol, 2006. **41**(2): p. 77-102.
8. Hernandez-Cid, A., et al., *Ribonucleases P/MRP and the expanding ribonucleoprotein world.* IUBMB Life, 2012. **64**(6): p. 521-528.
9. Peck-Miller, K.A. and S. Altman, *Kinetics of the processing of the precursor to 4.5 S RNA, a naturally occurring substrate for RNase P from Escherichia coli.* J Mol Biol, 1991. **221**(1): p. 1-5.
10. Komine, Y., et al., *A tRNA-like structure is present in 10Sa RNA, a small stable RNA from Escherichia coli.* Proc Natl Acad Sci U S A, 1994. **91**(20): p. 9223-7.
11. Alifano, P., et al., *Ribonuclease E provides substrates for ribonuclease P-dependent processing of a polycistronic mRNA.* Genes Dev, 1994. **8**(24): p. 3021-31.
12. Li, Y. and S. Altman, *A specific endoribonuclease, RNase P, affects gene expression of polycistronic operon mRNAs.* Proc Natl Acad Sci U S A, 2003. **100**(23): p. 13213-8.
13. Marvin, M.C., et al., *Accumulation of noncoding RNA due to an RNase P defect in Saccharomyces cerevisiae.* RNA, 2011. **17**(8): p. 1441-50.
14. Altman, S., et al., *RNase P cleaves transient structures in some riboswitches.* Proc Natl Acad Sci U S A, 2005. **102**(32): p. 11284-9.
15. Seif, E. and S. Altman, *RNase P cleaves the adenine riboswitch and stabilizes pbuE mRNA in Bacillus subtilis.* RNA (New York, N.Y.), 2008. **14**(6): p. 1237-1243.
16. Hsieh, J., A. Andrews, and C. Fierke, *Roles of protein subunits in RNA-protein complexes: lessons from ribonuclease P.* Biopolymers, 2004. **73**(1): p. 79-89.
17. Walker, S. and D. Engelke, *Ribonuclease P: the evolution of an ancient RNA enzyme.* Critical reviews in biochemistry and molecular biology, 2006. **41**(2): p. 77-102.
18. Smith, J., J. Hsieh, and C. Fierke, *Importance of RNA-protein interactions in bacterial ribonuclease P structure and catalysis.* Biopolymers, 2007. **87**(5-6): p. 329-338.
19. Lai, L.B., et al., *Unexpected diversity of RNase P, an ancient tRNA processing enzyme: challenges and prospects.* Febs Letters, 2010. **584**(2): p. 287-296.
20. Holzmann, J., et al., *RNase P without RNA: identification and functional reconstitution of the human mitochondrial tRNA processing enzyme.* Cell, 2008. **135**(3): p. 462-474.
21. Gobert, A., et al., *A single Arabidopsis organellar protein has RNase P activity.* Nature structural & molecular biology, 2010. **17**(6): p. 740-744.
22. Gutmann, B., A. Gobert, and P. Giegé, *PRORP proteins support RNase P activity in both organelles and the nucleus in Arabidopsis.* Genes & development, 2012. **26**(10): p. 1022-1027.
23. Lai, L., et al., *A functional RNase P protein subunit of bacterial origin in some eukaryotes.* Molecular genetics and genomics : MGG, 2011. **286**(5-6): p. 359-369.
24. Taschner, A., et al., *Nuclear RNase P of Trypanosoma brucei: a single protein in place of the multicomponent RNA-protein complex.* Cell reports, 2012. **2**(1): p. 19-25.
25. Eder, P.S., et al., *Bacterial RNase P as a potential target for novel anti-infectives.* Curr Opin Investig Drugs, 2003. **4**(8): p. 937-43.
26. Willkomm, D., et al., *RNase P as a Drug Target*, in *Ribonuclease P*, F. Liu and S. Altman, Editors. 2010, Springer New York. p. 235-256.

27. Vioque, A., *Protein-Synthesis Inhibitors and Catalytic Rna - Effect of Puromycin on Transfer-Rna Precursor Processing by the Rna Component of Escherichia-Coli Rnase P.* Febs Letters, 1989. **246**(1-2): p. 137-139.
28. Mikkelsen, N.E., et al., *Inhibition of RNase P RNA cleavage by aminoglycosides.* Proc Natl Acad Sci U S A, 1999. **96**(11): p. 6155-60.
29. Eubank, T.D., et al., *Inhibition of bacterial RNase P by aminoglycoside-arginine conjugates.* FEBS Lett, 2002. **511**(1-3): p. 107-12.
30. Kawamoto, S.A., et al., *Studies on the mechanism of inhibition of bacterial ribonuclease P by aminoglycoside derivatives.* Nucleic Acids Res, 2008. **36**(2): p. 697-704.
31. Bichenkova, E.V., et al., *Strong, specific, reversible binding ligands for transfer RNA: Comparison by fluorescence and NMR spectroscopies with distamycin binding for a new structural class of ligand.* Nucleosides & Nucleotides, 1998. **17**(9-11): p. 1651-1665.
32. Hori, Y., et al., *Synthetic inhibitors of the processing of pretransfer RNA by the ribonuclease P ribozyme: enzyme inhibitors which act by binding to substrate.* Biochemistry, 2001. **40**(3): p. 603-8.
33. Hori, Y., et al., *Porphyrins and porphines bind strongly and specifically to tRNA, precursor tRNA and to M1 RNA and inhibit the ribonuclease P ribozyme reaction.* Biochim Biophys Acta, 2005. **1730**(1): p. 47-55.
34. Toumpeki, C., et al., *Activation of bacterial ribonuclease P by macrolides.* Biochemistry, 2008. **47**(13): p. 4112-8.
35. Olson, P., et al., *Small molecule inhibitors of Staphylococcus aureus RnpA alter cellular mRNA turnover, exhibit antimicrobial activity, and attenuate pathogenesis.* PLoS pathogens, 2011. **7**(2).
36. Willkomm, D., et al., *Evaluation of bacterial RNase P RNA as a drug target.* Chembiochem : a European journal of chemical biology, 2003. **4**(10): p. 1041-1048.
37. Childs, J.L., A.W. Poole, and D.H. Turner, *Inhibition of Escherichia coli RNase P by oligonucleotide directed misfolding of RNA.* RNA, 2003. **9**(12): p. 1437-45.
38. Gruegelsiepe, H., et al., *Antisense inhibition of Escherichia coli RNase P RNA: mechanistic aspects.* Chembiochem, 2003. **4**(10): p. 1049-56.
39. Gruegelsiepe, H., O. Brandt, and R.K. Hartmann, *Antisense inhibition of RNase P: mechanistic aspects and application to live bacteria.* J Biol Chem, 2006. **281**(41): p. 30613-20.
40. Irwin, J. and B. Shoichet, *ZINC--a free database of commercially available compounds for virtual screening.* Journal of chemical information and modeling, 2005. **45**(1): p. 177-182.
41. Rueda, D., et al., *The 5' leader of precursor tRNAAsp bound to the Bacillus subtilis RNase P holoenzyme has an extended conformation.* Biochemistry, 2005. **44**(49): p. 16130-9.
42. Hsieh, J. and C.A. Fierke, *Conformational change in the Bacillus subtilis RNase P holoenzyme--pre-tRNA complex enhances substrate affinity and limits cleavage rate.* RNA, 2009. **15**(8): p. 1565-77.
43. Hsieh, J., et al., *A divalent cation stabilizes the active conformation of the B. subtilis RNase P x pre-tRNA complex: a role for an inner-sphere metal ion in RNase P.* J Mol Biol, 2010. **400**(1): p. 38-51.
44. Lea, W.A. and A. Simeonov, *Fluorescence polarization assays in small molecule screening.* Expert Opin Drug Discov, 2011. **6**(1): p. 17-32.
45. Jameson, D.M. and J.A. Ross, *Fluorescence polarization/anisotropy in diagnostics and imaging.* Chem Rev, 2010. **110**(5): p. 2685-708.
46. Kurz, J.C., S. Niranjanakumari, and C.A. Fierke, *Protein component of Bacillus subtilis RNase P specifically enhances the affinity for precursor-tRNAAsp.* Biochemistry, 1998. **37**(8): p. 2393-400.
47. Owicki, J.C., *Fluorescence polarization and anisotropy in high throughput screening: perspectives and primer.* J Biomol Screen, 2000. **5**(5): p. 297-306.
48. Jameson, D.M. and G. Mocz, *Fluorescence polarization/anisotropy approaches to study protein-ligand interactions: effects of errors and uncertainties.* Methods Mol Biol, 2005. **305**: p. 301-22.
49. Weber, G., *Polarization of the fluorescence of macromolecules. I. Theory and experimental method.* Biochem J, 1952. **51**(2): p. 145-55.

50. Kirk, S.R. and Y. Tor, *tRNA(Phe) binds aminoglycoside antibiotics.* Bioorg Med Chem, 1999. **7**(9): p. 1979-91.
51. Guerrier-Takada, C., et al., *Metal ion requirements and other aspects of the reaction catalyzed by M1 RNA, the RNA subunit of ribonuclease P from Escherichia coli.* Biochemistry, 1986. **25**(7): p. 1509-15.
52. Zhang, J.H., T.D. Chung, and K.R. Oldenburg, *A Simple Statistical Parameter for Use in Evaluation and Validation of High Throughput Screening Assays.* J Biomol Screen, 1999. **4**(2): p. 67-73.
53. Quentin, V., *RNA's coming of age as a drug target.* Journal of Inclusion Phenomena and Macrocyclic Chemistry, 2009. **65**.
54. Guan, L. and M.D. Disney, *Recent advances in developing small molecules targeting RNA.* ACS Chem Biol, 2012. **7**(1): p. 73-86.
55. Blakeley, B.D., et al., *Methods for identifying and characterizing interactions involving RNA.* Tetrahedron, 2012. **68**(43): p. 8837-8855.
56. Rossi, A.M. and C.W. Taylor, *Analysis of protein-ligand interactions by fluorescence polarization.* Nat Protoc, 2011. **6**(3): p. 365-87.
57. Shi, X. and D. Herschlag, *Fluorescence polarization anisotropy to measure RNA dynamics.* Methods Enzymol, 2009. **469**: p. 287-302.
58. Singh, K.K., et al., *Fluorescence polarization for monitoring ribozyme reactions in real time.* Biotechniques, 2000. **29**(2): p. 344-8, 350-1.
59. Bonin, P.D. and L.A. Erickson, *Development of a fluorescence polarization assay for peptidyl-tRNA hydrolase.* Anal Biochem, 2002. **306**(1): p. 8-16.
60. Wang, Y., et al., *RNA molecules that specifically and stoichiometrically bind aminoglycoside antibiotics with high affinities.* Biochemistry, 1996. **35**(38): p. 12338-46.
61. Luedtke, N.W. and Y. Tor, *Fluorescence-based methods for evaluating the RNA affinity and specificity of HIV-1 Rev-RRE inhibitors.* Biopolymers, 2003. **70**(1): p. 103-19.
62. Eubank, T.D., et al., *Inhibition of bacterial RNase P by aminoglycoside-arginine conjugates.* FEBS Letters, 2002. **511**(1-3): p. 107-12.
63. Berchanski, A. and A. Lapidot, *Bacterial RNase P RNA is a drug target for aminoglycoside-arginine conjugates.* Bioconjug Chem, 2008. **19**(9): p. 1896-906.
64. Mikkelsen, N.E., et al., *Aminoglycoside binding displaces a divalent metal ion in a tRNA-neomycin B complex.* Nat Struct Biol, 2001. **8**(6): p. 510-4.
65. Igarashi, K. and K. Kashiwagi, *Modulation of cellular function by polyamines.* Int J Biochem Cell Biol, 2010. **42**(1): p. 39-51.
66. McMahon, M.E. and V.A. Erdmann, *Binding of spermidine to transfer ribonucleic acid.* Biochemistry, 1982. **21**(21): p. 5280-5288.
67. Quigley, G.J., M.M. Teeter, and A. Rich, *Structural analysis of spermine and magnesium ion binding to yeast phenylalanine transfer RNA.* Proc Natl Acad Sci U S A, 1978. **75**(1): p. 64-8.
68. Sakai, T.T., et al., *The binding of polyamines and of ethidium bromide to tRNA.* Nucleic acids research, 1975. **2**(7): p. 1005-1022.
69. Ouameur, A.A., P. Bourassa, and H.A. Tajmir-Riahi, *Probing tRNA interaction with biogenic polyamines.* RNA, 2010. **16**(10): p. 1968-79.
70. Brannvall, M., N.E. Mikkelsen, and L.A. Kirsebom, *Monitoring the structure of Escherichia coli RNase P RNA in the presence of various divalent metal ions.* Nucleic Acids Res, 2001. **29**(7): p. 1426-32.
71. Tabor, C.W. and H. Tabor, *1,4-Diaminobutane (putrescine), spermidine, and spermine.* Annu Rev Biochem, 1976. **45**: p. 285-306.
72. Ferguson, B.Q. and D.C. Yang, *Methionyl-tRNA synthetase induced 3'-terminal and delocalized conformational transition in tRNAfMet: steady-state fluorescence of tRNA with a single fluorophore.* Biochemistry, 1986. **25**(3): p. 529-39.
73. Suzuki, T., A. Nagao, and T. Suzuki, *Human mitochondrial tRNAs: biogenesis, function, structural aspects, and diseases.* Annu Rev Genet, 2011. **45**: p. 299-329.
74. Payne, D.J., et al., *Drugs for bad bugs: confronting the challenges of antibacterial discovery.* Nat Rev Drug Discov, 2007. **6**(1): p. 29-40.
75. Andrews, J.M., *Determination of minimum inhibitory concentrations.* J Antimicrob Chemother, 2001. **48 Suppl 1**: p. 5-16.

76. Dixon, R.A., *Phytoestrogens.* Annu Rev Plant Biol, 2004. **55**: p. 225-61.
77. Khan, S.A., et al., *Soy Isoflavone Supplementation for Breast Cancer Risk Reduction: A Randomized Phase II Trial.* Cancer Prevention Research, 2012. **5**(2): p. 309-319.
78. Nechuta, S.J., et al., *Soy food intake after diagnosis of breast cancer and survival: an in-depth analysis of combined evidence from cohort studies of US and Chinese women.* The American Journal of Clinical Nutrition, 2012. **96**(1): p. 123-132.
79. Torres-Larios, A., et al., *Crystal structure of the RNA component of bacterial ribonuclease P.* Nature, 2005. **437**(7058): p. 584-7.
80. Kazantsev, A.V., et al., *Crystal structure of a bacterial ribonuclease P RNA.* Proc Natl Acad Sci U S A, 2005. **102**(38): p. 13392-7.
81. Reiter, N.J., et al., *Structure of a bacterial ribonuclease P holoenzyme in complex with tRNA.* Nature, 2010. **468**(7325): p. 784-9.
82. Behrman, E.J., *An improved synthesis of guanosine 5'-monothiophosphate.* Journal of Chemical Research (Synopses), 2000. **2000**(9): p. 446-447.
83. He, B., et al., *Rapid mutagenesis and purification of phage RNA polymerases.* Protein Expr Purif, 1997. **9**(1): p. 142-51.
84. Niranjanakumari, S., et al., *Protein component of the ribozyme ribonuclease P alters substrate recognition by directly contacting precursor tRNA.* Proc Natl Acad Sci U S A, 1998. **95**(26): p. 15212-7.
85. Niranjanakumari, S., J.C. Kurz, and C.A. Fierke, *Expression, purification and characterization of the recombinant ribonuclease P protein component from Bacillus subtilis.* Nucleic Acids Res, 1998. **26**(13): p. 3090-6.
86. Mocz, G., et al., *Probing the nucleotide binding sites of axonemal dynein with the fluorescent nucleotide analogue 2'(3')-O-(-N-Methylanthraniloyl)-adenosine 5'-triphosphate.* Biochemistry, 1998. **37**(27): p. 9862-9.
87. Sem, D.S. and P.A. McNeeley, *Application of fluorescence polarization to the steady-state enzyme kinetic analysis of calpain II.* FEBS Lett, 1999. **443**(1): p. 17-9.
88. Michaelis, L., et al., *The original Michaelis constant: translation of the 1913 Michaelis-Menten paper.* Biochemistry, 2011. **50**(39): p. 8264-9.
89. Lakowicz, J.R., *Principles of Fluorescence Spectroscopy*. 2006: Principles of Fluorescence Spectroscopy, by J.R.~Lakowicz.~ISBN 0-387-31278-1.~ Berlin: Springer, 2006.

# CHAPTER 3

# PROBING METAL ION BINDING SITES NEAR A CONSERVED URIDINE IN THE P4 HELIX OF *B. SUBTILIS* RNASE P BY ATOMIC MODIFICATIONS[1]

## 3.1 Abstract

Ribonuclease P (RNase P) is a ribonucleoprotein enzyme that catalyzes the essential step of 5' end maturation of tRNA. Bacterial RNase P is composed of one catalytic RNA subunit and one protein subunit important for molecular recognition. As in many other large ribozymes, divalent metal ions stabilize the folded structure and enhance substrate binding and the catalytic activity of RNase P. Identification of the RNA moieties involved in metal-binding and discerning the function of these interactions is an important remaining question in the RNA catalysis field. The recently solved crystal structure of bacterial RNase P proposed that a catalytic metal ion directly coordinates the carbonyl oxygen of the bulged uracil in the conserved helix P4 of the RNA subunit. To date, there is little biochemical evidence for this direct interaction. To examine this proposal and to further investigate the functional importance of the functional importance of the bulged U, I substituted this conserved uracil in the P4 helix of circularly permuted *Bacillus subtilis* RNase P with 4-thiouridine, 4-deoxyuridine, 3-methyluridine and rSpacer (abasic modification). The

[1] Data in Chapter 3 is in preparation for a manuscript entitled "The universally conserved uridine in helix P4 of bacterial RNase P is an outer-sphere metal ligand for metal-dependent substrate binding, catalysis, and conformational change" by Xin Liu, Yu Chen, and Carol A. Fierke.

4-thiouridine substitution decreases substrate affinity in sub-saturating $Ca^{2+}$. Additionally, all functional group modifications, including 4-thiouridine, 4-deoxyuridine, and 3-methyluridine, decrease the single-turnover cleavage rate of the holoenzyme by 16- to 23-fold at pH 5.2 where phosphodiester bond cleavage is rate limiting. This effects disappears at high pH where a conformational change step is rate limiting. Furthermore, the activity of the 4-thiouridine modified holoenzyme is only marginally rescued by the addition of manganese ions, arguing against an inner-sphere metal interaction. In contrast, the abasic modification, which removes the uracil base while retaining the ribose and backbone, does not affect the cleavage rate at low pH but decreases the pH-independent isomerization rate by at least 6-fold. These data suggest that this universally conserved bulge uridine is important for metal-dependent pre-tRNA binding and catalysis by RNase P, likely by coordinating at least one metal ion through an outer-sphere interaction and stabilization of an active conformation.

## 3.2 Background

Metal ions have important structural, catalytic, and co-catalytic roles in ribozyme-catalyzed reactions [1]. Most metal ions interact electrostatically with the negatively charged phosphate backbone to stabilize the complex three-dimensional structure of the RNA [2]. However, a small number of specifically bound metal ions can coordinate functional groups in the ribozyme to stabilize substrate binding and/or transition states during catalysis [3-5]. Metal ions also participate in conformational change steps during ribozyme catalytic pathways [6, 7]. Dissecting

the exact positions and roles of important metal ions for ribozyme catalysis has been a major challenge in the RNA field.

To identify functionally important metal ion ligands in RNA, various strategies, including nucleotide analog-interference mapping, atomic mutagenesis, metal ion rescue, lanthanide cleavage, and X-ray crystallography with heavy metal soaks, have been developed over the past two decades (for a review of these methods see [8]). Important mono- and divalent metal ions and their ligands have been identified in several ribozymes, such as the hepatitis delta virus (HDV) enzyme [9, 10], hammerhead ribozyme [11, 12], and group I and II introns [5, 6, 13-15], by biochemical and X-ray analysis. However, crystallization of large ribozymes remains challenging, and discrepancies about the sites of metal ions have been observed in various structures and between structures and biochemical models [16]. Therefore, both crystallographic and biochemical data are important for identifying functional metal sites and their involvement in the catalytic mechanism of large ribozymes [8].

Ribonuclease P (RNase P) is a divalent metal ion dependent ribonucleoprotein endonuclease that catalyzes hydrolysis of a specific phosphodiester bond in precursor tRNAs (pre-tRNA) to remove the 5' leader sequence [17-19]. RNase P in most organisms contain one catalytic RNA subunit (P RNA) and different numbers of protein subunits [20-24]. In bacterial RNase P, the single protein subunit (P protein) is essential *in vivo* and enhances substrate binding, metal affinity and cleavage rate at physiological salt conditions [25-28]. The bacterial P RNA subunit is a ribozyme that is catalytically active under high ionic strength conditions *in vitro* [29]. RNase P catalytic activity requires divalent metal ions such as magnesium ions [30-32].

Measurements of isotopic effects using $^{18}$O-water suggest that a magnesium-bound hydroxide is the nucleophile for a RNase P catalyzed phosphodiester bond hydrolysis reaction [33]. RNase P is also activated by the addition of manganese and to a lesser extent by calcium and zinc, *in vitro* [34-36]. A large number of (>150) $Mg^{2+}$ ions associate with RNase P [30-32] but only a handful of these magnesium ions form specific contacts with functional groups in RNase P [32, 37]. The interaction of these metals can be either direct coordination of functional groups (inner-sphere coordination), or water-mediated (outer-sphere coordination) [2]. Kinetic studies of magnesium activation of the RNase P•pre-tRNA (ES) complex suggest that at least two types of inner-sphere metal ions activate *B. subtilis* RNase P catalysis (Scheme 3-1). One class of high affinity metal ion stabilizes an active ES* conformation and another class of lower affinity metal ion activates cleavage [38]. However, the binding sites for these essential metal ions and their explicit contributions to RNase P structure and function are just coming into focus in ribozyme catalysis.

Several metal binding sites in both the pre-tRNA substrate and RNase P RNA have been implicated based on biochemical and crystallographic evidence (Figure 3-1). In pre-tRNA, potential inner-sphere metal ligands include: the *pro*-$R_P$ nonbridging oxygen, as demonstrated by phosphorothioate substitution and metal rescue experiments [39-41]; the *pro*-$S_P$ oxygen and the 3' bridging oxygen, as indicated by enhanced miscleavage when sulfur is substituted [42]. Atomic mutagenesis studies also suggested that the 2' OH of the cleavage site coordinates a metal ion through a bound water molecule [43].

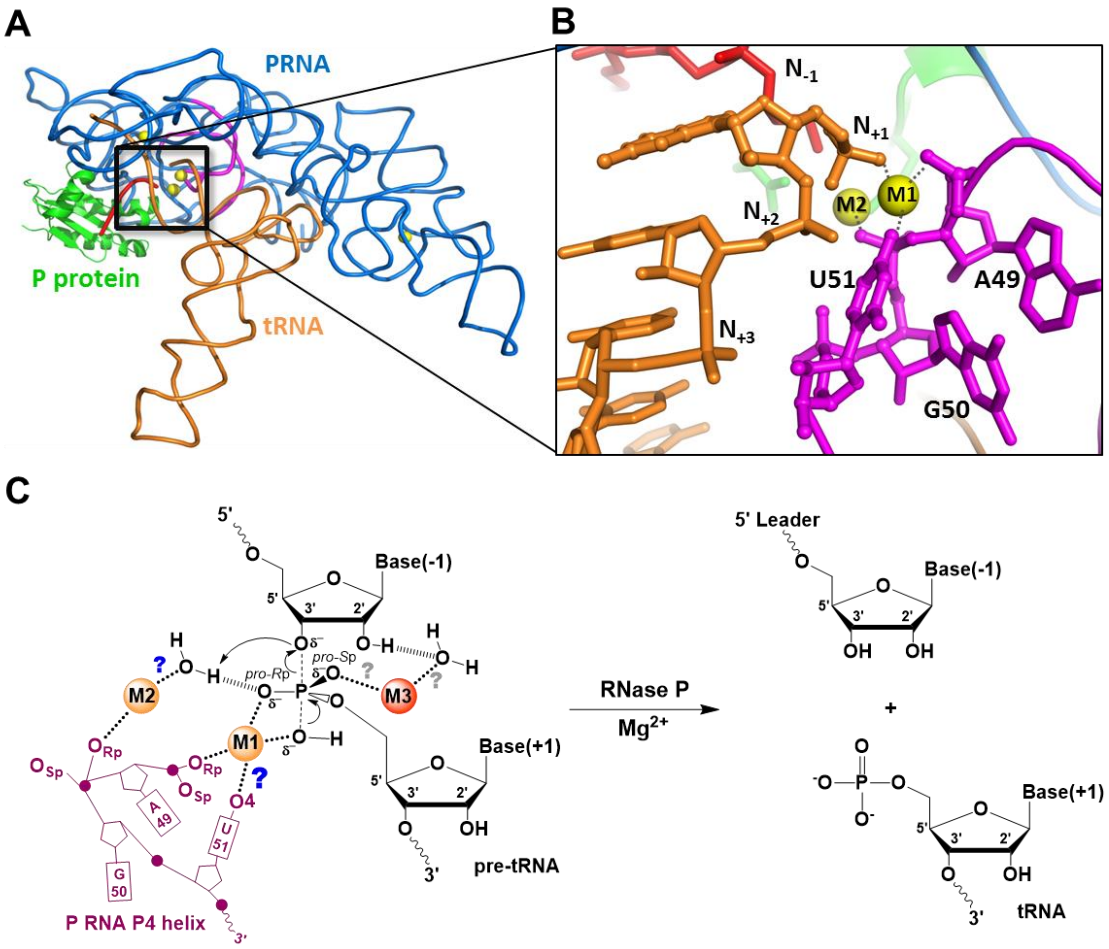


**Figure 3-1:** Structure of bacterial RNase P and proposed metal ion binding sites in the reaction mechanism. **(A)** A cartoon representation of the crystal structure of *T. maritima* RNase P holoenzyme in complex with tRNA and an oligonucleotide leader (4.2 Å resolution, PDB code: 3Q1R) [44], showing the P RNA (blue), the P4 helix (magenta) of P RNA, P protein (green), tRNA (orange), leader (red), and metal ions (yellow spheres). **(B)** An expanded view of the boxed region in (A), displaying the putative active site near P4 helix and the 5' end of tRNA [44]. Residue numbers were adjusted to match the numbering in *B. subtilis* RNase P. Two metal ions are proposed to contact conserved nucleotides (A49-U51) in helix P4 and the 5' phosphate of tRNA (gray dashed lines). One metal (M1, $Eu^{3+}$ soak) is located within 2.1 Å of three oxygen atoms: the *pro-R*p nonbridging oxygen in N+1 position of tRNA, the *pro-S*p nonbridging oxygen in A49, and the O4 of the U51 base. The second metal (M2, $Sm^{3+}$ soak) is clearly visible only when the leader was soaked into the crystal [44], and is located within 2.2 Å of the *pro-R*p nonbridging oxygen of G50. **(C)** The RNase P catalyzed reaction showing possible metal ion coordinations [8, 17, 44]. The purple diagram is showing a part of the P4 helix (pentagons: ribose rings; solid circles: backbone phosphate). A proposal [44] combining the metals observed in the crystal structure (above) with previous biochemical studies [45-47] suggested that the M1 metal (orange sphere) directly coordinates ligands in the P4 helix and the scissile bond and activates a hydroxyl nucleophile [33], while the M2 metal (orange) could stabilize product formation. Another metal ion (M3, red sphere) is proposed by biochemical data probing moieties in pre-tRNA [39-42]. Question marks designate proposed metal ion-ligand interactions that lack either direct biochemical (blue) or crystallographic (gray) evidence.

In the P RNA, helix P4 is the most highly conserved region and is critical for binding metals important to catalysis [48, 49]. Phosphorothioate substitution in both *E. coli* and *B. subtilis* RNase P RNA suggested that the non-bridging oxygen atoms in the backbone phosphate of A49 and G50 (*B. subtilis* numbering) are inner-sphere metal ligands [45-47]. X-ray absorption and NMR spectroscopic studies on a P4 helix stem-loop model for *B. subtilis* RNase P suggest that an inner-sphere $Mg^{2+}$ ion interacts with G378 and G379 [50, 51] (Figure 1-9, Chapter 1). A number of possible metal ion binding sites near residues A48, A49, G50, G378 and G379 (*B. subtilis* numbering) have also been identified by anomalous scattering in diffraction analysis of heavy metal ions soaked into *B. stearothermophilus* catalytic domain crystals (3.5 Å resolution) [52] (Figure 1-5, Chapter 1). Metal soaks of a recently solved crystal structure of the *T. maritima* RNase P•tRNA ternary complex led to the proposal that two catalytic metal ions bind near A49, G50 and U51 in helix P4 as part of the active site [44] (Figure 3-1).

In the two-metal-ion mechanism proposed using data from the recent RNase P crystal structure, the carbonyl oxygen-4 (O4) of the conserved bulge uridine in the helix P4 is proposed to directly coordinate the catalytic metal ion [44] (Figure 3-1). This bulged uridine is universally conserved among all RNase P RNA [49]. In *E. coli* RNase P RNA, site-directed mutations that delete or alter the position of the bulged uridine in the helix P4 affect the cleavage rate and pre-tRNA affinity of P RNA. Furthermore, these mutations decrease the cooperativity and affinity for rescue of the *pro-*$R_P$ phosphorothioate modified pre-tRNA by $Cd^{2+}$ [53]. However, when the bulged U is substituted with 4-thiouridine modification, this nucleotide cross-links to

+5 position in pre-tRNA, suggesting that this base is not located near the cleavage site under these conditions [54]. Mutation of this uridine in the *T. maritima* RNase P to cytosine decrease the catalytic efficiency ($k_{cat}/K_M$) of the holoenzyme by 10-fold and 200- to 1700-fold [55] when coupled with P protein mutants that affect substrate affinity [56]. These biochemical studies suggest that the P4 helix positions the catalytic metal ions and the pre-tRNA substrate, but do not provide direct evidence for an inner-sphere interaction of the bulged uridine with a catalytic metal ion.

Therefore, I combined atomic mutagenesis and mechanistic studies to directly examine whether this conserved uridine coordinates a catalytic metal ion and to probe the biochemical role of the bulged U in the RNase P catalytic pathway. To this end, the conserved uridine (U51) in the P4 helix of *B. subtilis* RNase P was replaced with a series of atomic mutations, including 4-thiouridine (4SU), 4-deoxyuridine (4deOU), 3-methyluridine (3MU) and an abasic/rSpacer modification (abU), which deletes the base and keeps the ribose and backbone (Figure 3-2). Substrate affinity, single-turnover cleavage activity, and metal ion rescue have been measured to evaluate the effects of these mutations on the divalent metal ion-dependent RNase P activity. These data indicate that the carbonyl oxygen of the bulged uridine in the helix P4 of RNase P RNA is not an inner-sphere ligand for a catalytic metal. However, these data are most consistent with a model of which the universally conserved uridine coordinates a metal ion through water-mediated interactions. This outer-sphere metal interaction of the bulged uridine is involved in stabilizing substrate affinity and catalysis of pre-tRNA cleavage as well as contributing to stabilization of an active conformation that formed in the RNase P kinetic pathway.

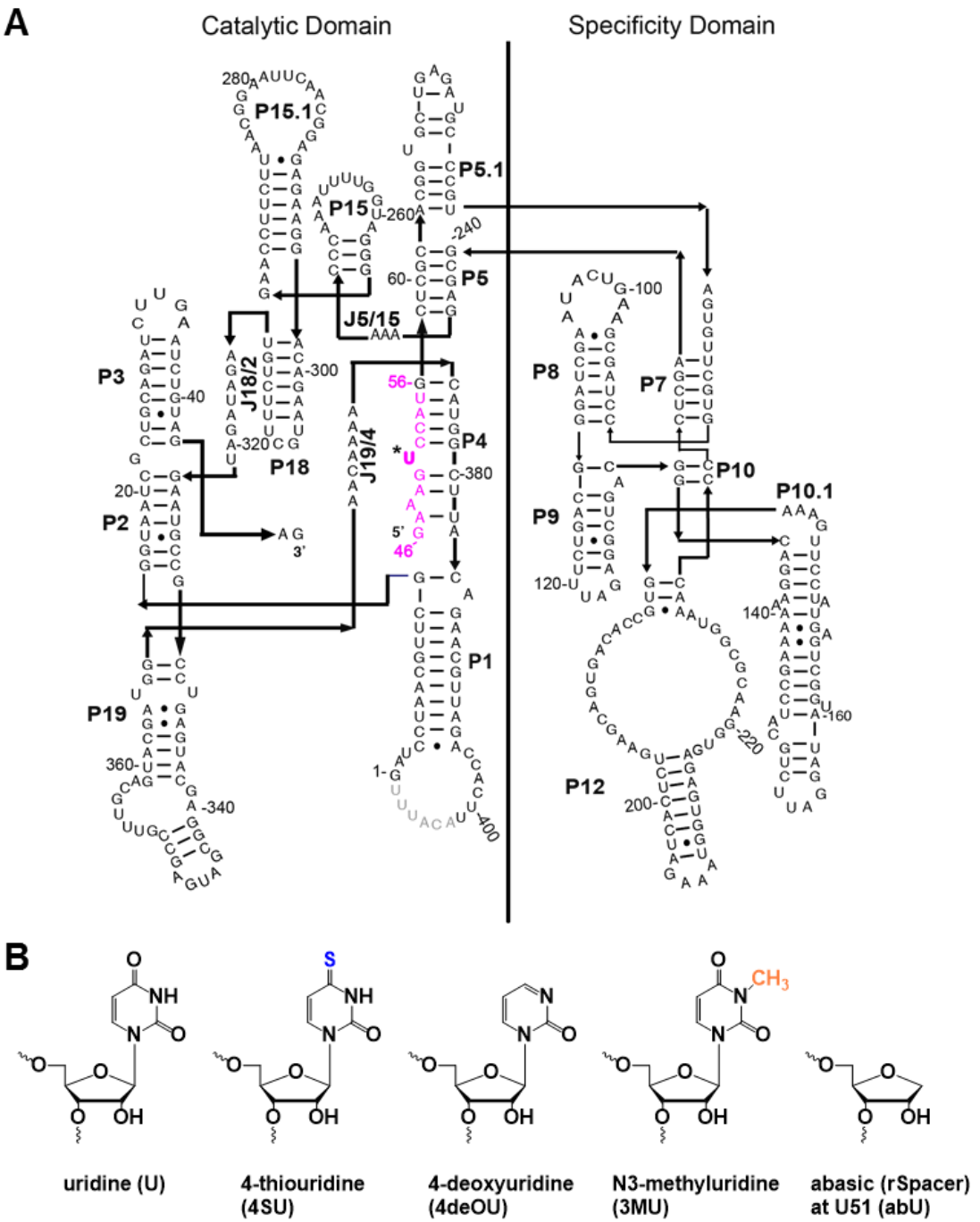


**Figure 3-2:** Probing metal-ligand interactions in the P4 helix of B. subtilis RNase P by circular permutation and atomic mutagenesis. **(A)** Secondary structure of the circular permuted *B. subtilis* P RNA (cpPRNA) [46] highlighting one strand of the P4 helix (magenta) and U51 (*). The usual 5' and 3' termini of P RNA are joined by a six-nucleotide loop. The secondary structure was drawn based on the *B. stearothermophilus* P RNA crystal structure [57]. The cpPRNA used in this study contains sequences either from G46 to G45 (46P, wild-type like) or from G56 to G45 (56P, truncated). **(B)** Chemical structures of the wild type uridine and analogs. The modified nucleotides were incorporated into P RNA by ligating the corresponding 10-mer ribooligonucleotide to the 5' end of GMP-transcribed 56P RNA.

## 3.3 Results

### 3.3.1 Preparation of P RNA Mutant with Modified Bulged Uridine (U51) in the P4 Helix

To examine the biochemical role of the conserved U51 in metal binding and catalysis by *B. subtilis* RNase P, four different modifications of the bulged uridine (Figure 3-2) were incorporated into P RNA by ligation of a 10-mer ribooligonucleotide to a circular permuted P RNA (56P, Figure 3-2). The 10-mer ribooligonucleotide has a sequence identical to the 5' strand of the P4 helix (G46-U55) except for modifications of the uracil base of U51. The carbonyl oxygen at position 4 (O4), a proposed inner-sphere metal ligand, was substituted by a sulfur atom in 4-thiouridine (4SU) or deleted in the 4-deoxyuridine (4deOU) substitution. The 3-methyluridine (3MU) modification installs a bulky methyl group on the base and the abasic/rSpacer modification (abU) completely removes the uracil base but maintains the ribose sugar and the backbone. These substitutions were chosen to probe the metal binding sites near this bulged uridine at a single-atom level with minimum disruption of the base-paring geometry, in contrast to previous site-directed mutagenesis studies [54, 55].

Using an optimized ligation method (see Materials and Methods) [46] with T4 DNA ligase and a DNA splint, a 10-mer ribooligonucleotide with either the 4SU or 4deOU modification was ligated onto the 5' end of 56P RNA with a 40-80% efficiency, as determined by primer extension analysis (Figure B-1, Appendix B). The ligation efficiency of ribooligonucleotides containing the 3MU or abU modification was lower, despite increasing reaction times and longer DNA-splint

sequences (3MU, 10-20% and abU 20-30%). To compare the functional effects of these atomic modifications, an *in vitro* transcribed 46P RNA and a ligation control (10nt) prepared by ligation of a wild type 10-mer ribooligonucleotide (50-80% ligation efficiency) to 56P were both used to control for the effects of circular permutation and ligation. Both the 46P and 10nt holoenzymes have single-turnover activities comparable to wild type P RNA. The truncated 56P RNA is inactive and does not interfere with RNase P activity or substrate binding [46].

### 3.3.2 4-thiouridine Substitution at U51 Affects Metal Dependent Pre-tRNA Affinity for RNase P[2]

Divalent metal ions enhance the affinity of RNase P for pre-tRNA [37]. To evaluate whether the substitution of the O4 oxygen of U51 with sulfur alters the metal dependent pre-tRNA affinity, I measured the binding affinity of a 5' $^{32}$P-labeled pre-tRNA$^{Asp}$ to wild type and mutant RNase P holoenzymes under sub-saturating (5mM) to saturating (10 mM) $Ca^{2+}$ concentrations at pH 6 (Figure 3-3 and Table 3-1). Under these conditions, the cleavage of substrate catalyzed by RNase P is very slow (~$10^{-5}$ $s^{-1}$) [58], therefore the dissociation constant can be measured using a spin column assay to separate free and bound pre-tRNA [59].

The affinity of the 4SU mutant and 46P RNase P holoenzyme is similar (within 2 fold) to that of wild type at a saturating concentration (10 mM) of $Ca^{2+}$ (Table 3-1 and Figure 3-3). These data indicate that the circular permutation in the 5' half of the P4 helix and the sulfur substitution of O4 do not significantly perturb the overall structure and interaction with pre-tRNA at saturating $Ca^{2+}$ (10 mM).

[2] The $K_{d, app}$ data for the wild type holoenzyme were collected by Yu Chen and Xin Liu.

However, at 5 mM $Ca^{2+}$, the circular permutation of P RNA decreases the substrate affinity by 10-fold (Table 3-1). The 4SU mutant further decreases the substrate affinity by 3-fold compared to the circular-permuted 46P control (Table 3-1 and Figure 3-3). The 10-fold decrease in substrate affinity caused by circular permutation of this region is likely due to a modest perturbation of P RNA structure. The sulfur substitution of the O4 in U51 further reduced the substrate affinity, indicating that O4 might be involved in the metal dependent substrate binding.

**Table 3-1 :** Circular permutation of helix P4 and 4SU modification alter metal-dependent substrate affinity of RNase P holoenzyme.

| | 5 mM $CaCl_2$[a] | | 10 mM $CaCl_2$[a] | |
|---|---|---|---|---|
| Holoenzyme[a] | $K_{d,\,app}$(nM)[a] | $K^{variant}_{d,app}/K^{wt}_{d,app}$ | $K_{d,\,app}$ (nM)[a] | $K^{variant}_{d,app}/K^{wt}_{d,app}$ |
| WT | 2.4 ± 0.2 | 1 | 2 ± 0.5[b] | 1 |
| 46P | 27 ± 2 | 10 | 4.7 ± 0.9 | 2 |
| 4SU | 72 ± 4 | 30 | 3.5 ± 0.3 | 2 |

[a] The apparent dissociation constant, $K_{d,app}$, was measured in 50 mM Tris/Mes (pH 6), ~380 mM KCl, and varying $CaCl_2$ (5 to10 mM) by a spin column assay at 37˚C and calculated by Equation 3-1.
[b] Value taken from [60] measured in the same conditions as in [a].

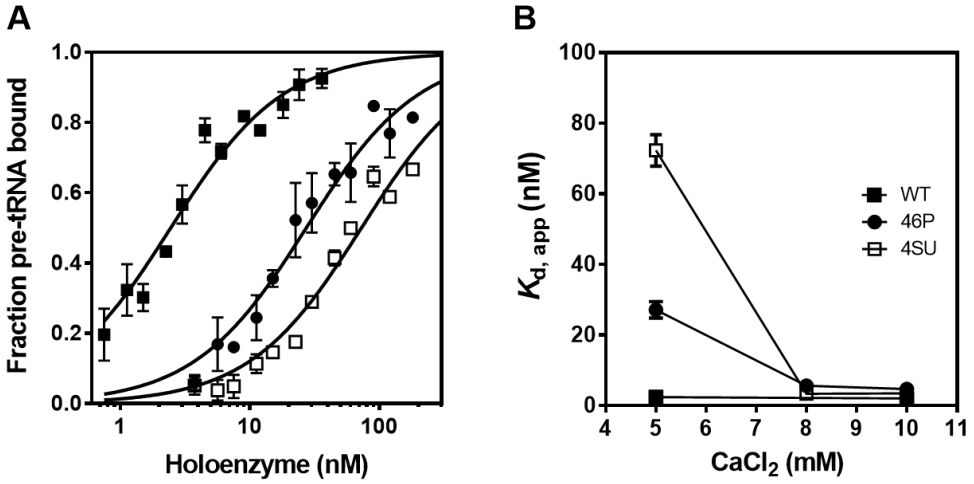

**Figure 3-3:** The 4-thiouridine (4SU) modification affects the metal dependent substrate affinity. **(A)** Binding of $^{32}$P-pre-tRNA substrate in 5 mM $CaCl_2$ by wild type (■), 46P (●) and 4SU (□) RNase P. Reaction conditions are described in Table 3-1. The fraction bound values were obtained from two to four independent experiments. The dissociation constants, $K_{d,\,app}$, were determined from the fix of a simple binding isotherm to the data (solid lines). $K_d$ values are listed in Table 3-1. **(B)** The dissociation constants, $K_{d,\,app}$ were measured at varying $CaCl_2$ concentrations.

### 3.3.3 Atomic Modifications 4SU, 4deOU and 3MU Decrease Cleavage Catalyzed by RNase P Holoenzyme at Low pH

Therefore, to further investigate the effects of these modifications on catalysis, single-turnover reactions were carried out in saturating divalent metal ion conditions, such as 10-20 mM $Ca^{2+}$ or $Mg^{2+}$, where the substrate affinity of the mutant is comparable to the wild type. Single-turnover cleavage of a 5' fluorescein labeled pre-tRNA$^{Asp}$ (Fl-pre-tRNA$^{Asp}$) catalyzed by wild-type and mutant RNase Ps were measured. The observed rate constants are not dependent on the RNase P concentrations (360 nM and 500 nM at pH 6), indicating that the enzyme is saturating in these experiments. These single turnover cleavage reactions are well described by a single exponential function (Equation 3-3, Figure 3-4).

For wild type RNase P, the observed single-turnover rate constant ($k_{obs}$) is log-linearly dependent on pH from pH 4.5 to 6. Previous data indicate this linear pH dependence means that phosphodiester bond cleavage is the rate limiting step under these conditions [61]. At high pH, the observed cleavage rate of RNase P is no longer dependent on pH as indicated by a plateau in the pH profile, suggesting that the rate-limiting step switches to a conformational change step prior to substrate cleavage (transition from ES to ES* in Scheme 3-1) [61, 62].

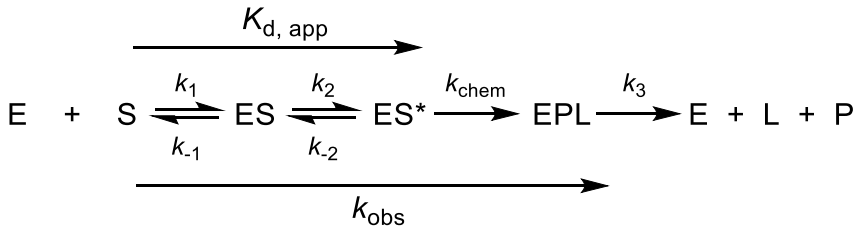


**Scheme 3-1:** A minimum kinetic mechanism for bacterial RNase P including substrate binding ($k_1$), conformational change ($k_2$), substrate cleavage ($k_{chem}$) and product dissociation ($k_3$) [61]. (E) RNase P holoenzyme; (S) pre-tRNA; (ES) RNase P•pre-tRNA complex; (ES*) RNase P•pre-tRNA complex after conformational change; (EPL) RNase P•tRNA•5' leader complex; (L) 5' leader; (P) tRNA product. The apparent dissociation constant for pre-tRNA binding to RNase P is: $K_{d, app}$= [E][S]/([ES]+[ES*])=$K_1$/(1+$K_2$). The overall observed rate constants under single-turnover condition is $k_{obs}=k_2k_{chem}/(k_{chem}+k_2+k_{-2})$ [59].

To test if the U51 modifications affect catalysis by RNase P, single-turnover cleavage rates were measured at pH 5.2 (Table 3-2). Modification of the functional group in the base at U51, including the sulfur substitution of O4 (4SU), deletion of the O4 (4SU), and insertion of a methyl group at position 3 (3MU), decrease the single turnover cleavage rate constant by 17- to 23-fold at pH 5.2 (Table 3-2). The cleavage of the Fl-pre-tRNA$^{Asp}$ substrate by these mutants is at the correct site as indicated by PAGE analysis (Figure B-2, Appendix B). These data demonstrate that the structure of the uracil base is important for efficient cleavage. However, even though sulfur substitution of the O4 in the U51 decreases the cleavage activity about 20-fold, this effect is smaller than the activity decrease (300- to $10^4$-fold) observed by phosphorothioate modification of the proposed inner-sphere sites in the backbone phosphate of the P4 helix [45-47] and pre-tRNA substrate [39-41].

Remarkably, removing the entire uracil base of U51 (abU) does not alter the single-turnover cleavage rate at this pH (Table 3-2) and no mis-cleavage is observed (Figure B-2, Appendix B), suggesting that the uracil base of this universally conserved residue is not absolutely required for accurate and efficient RNase P

catalysis at this pH.

**Table 3-2**: Single-turnover cleavage rate constants for the cleavage of Fl-pre-tRNA$^{Asp}$ substrate by wild type and mutant RNase P holoenzyme

| Holoenzyme[a] | $k_{obs}^{holo}$ ($sec^{-1}$), pH 5.2[a] | $k_{obs}^{holo,wt} / k_{obs}^{holo,variant}$ |
|---|---|---|
| WT | 0.035 ± 0.002 | 1 |
| 46P | 0.034 ± 0.001 | 1 |
| abU | 0.033 ± 0.001 | 1 |
| 4SU | 0.00179 ± 0.00001 | 20 |
| 4deOU | 0.0015 ± 0.0001 | 23 |
| 3MU | 0.00205 ± 0.00002 | 17 |

[a] Single-turnover cleavage was observed by a decrease in anisotropy of a fluorescein labeled pre-tRNA substrate (as decribed in Figure 3-4) measured in a saturating concentration of RNase P (360 nM), 10 nM Fl-pre-tRNA$^{Asp}$ substrate, 50 mM Tris/Mes, ~200 mM KCl, 20 mM $MgCl_2$, and 20 mM DTT.

### 3.3.4 The Deletion of Uracil Base at U51 Decreases Cleavage Rate at High pH

To further investigate the effects of the substitutions at U51 on the RNase P cleavage mechanism, the pH dependence of the observed single-turnover rate constant was measured for each of the U51 substitutions (Figure 3-4 and Table 3-3). Although the complete deletion of the uracil base (abU) does not affect the cleavage rate constant at low pH, the cleavage rate constant is only log-linearly dependent on pH within a small range (pH 4.5-5.2, Table 3-3). In contrast, the cleavage rate constants catalyzed by RNase P with modifications on the uracil base (4SU, 4deOU and 3MU) show a log-linear dependence from pH 4.5 to 7.2. The activity of RNase P with the deleted uracil base thus behaves differently than both wild type RNase P and atomic modifications of U51 base.

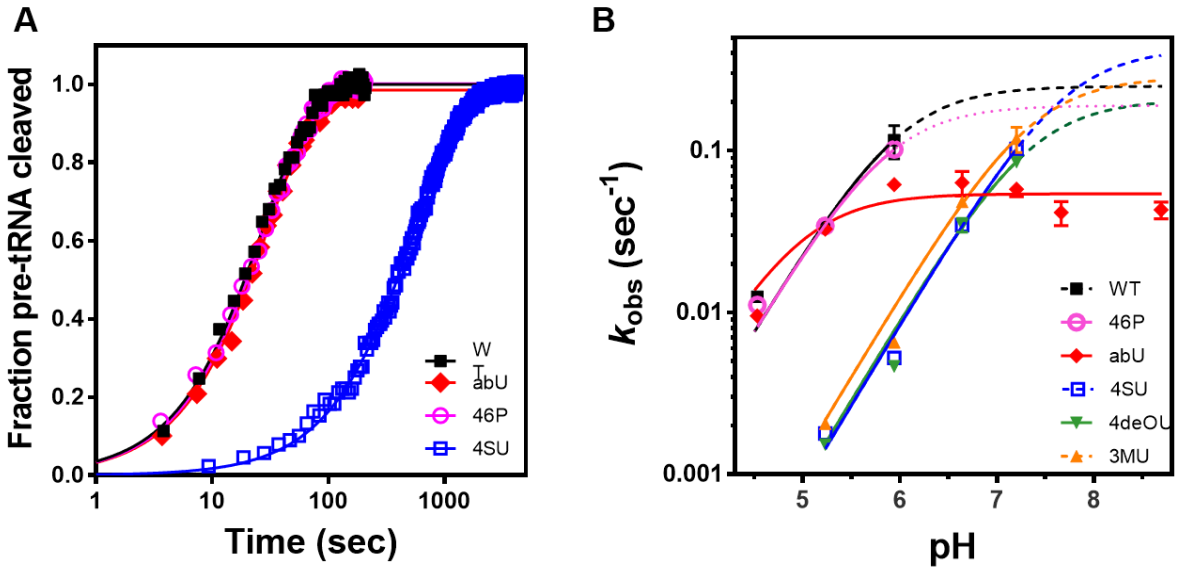


**Figure 3-4:** Atomic modifications of U51 alter the pH dependent activity of RNase P. **(A)** Typical time courses for the single-turnover cleavage of Fl-pre-tRNA catalyzed by RNase P (360 nM RNase P holoenzyme and 10 nM Fl-pre-tRNA$^{Asp}$) measured in 50 mM Tris/Mes, pH 5.2 (37˚C), 200 mM KCl, 20 mM DTT with 20 mM $MgCl_2$ by fluorescence polarization/anisotropy. Percent cleavage was calculated from the decrease in anisotropy of the Fl-pre- tRNA$^{Asp}$ substrate by Equation 3-2 to adjust for total fluorescence change. A single exponential (Equation 3-3) is fit to the data and the single-turnover cleavage rate ($k_{obs}$) was listed in Table 3-3. **(B)** The pH dependence of the observed single-turnover rate constants for wild-type and mutant RNase P measured in the same buffer conditions as in (A) with KCl concentrations adjusted to maintain constant ionic strength. Each point contains 2 to 5 independent measurements (error bars are showing standard deviations). A single ionization equation (Equation 3-4) was fit to these data to calculate the apparent p$K_a$ and pH-independent rate constants listed in Table 3-3.

**Table 3-3:** The pH-independent rate constants ($k_{max}$) and apparent p$K_a$ values of wild type and U51 mutant RNase P holoenzyme-catalyzed single-turnover reactions.

| Holoenzyme[a] | $k_{max}^{holo}$ (sec$^{-1}$)[b] | p$K_{a,\,app}$[b] | $k_{max}^{holo,wt}/k_{max}^{holo,variant}$ |
|---|---|---|---|
| WT | 0.3 ± 0.1[c] | 6.0 ± 0.3[c] | 1 |
| 46P | 0.19 ± 0.01[c] | 5.9 ± 0.1[c] | 1.5 |
| abU | 0.054 ± 0.003 | 5.0 ± 0.2 | 6 |
| 4SU | 0.4 ± 0.1[c] | 7.7 ± 0.2[c] | 0.8 |
| 4deOU | 0.21 ± 0.03[c] | 7.4 ± 0.1[c] | 1.5 |
| 3MU | 0.3 ± 0.1[c] | 7.3 ± 0.2[c] | 1 |

[a] Single-turnover activity of RNase P was measured in 20 mM $MgCl_2$ (pH 4.5-8.7 at 37˚C) as described in Figure 3-4.
[b] The $k_{max}$ and p$K_a$ were calculated from fitting the data in Figure 3-3 to a single ionization model by Equation 3-4.
[c] These values are extrapolated from fitting Equation 3-4 to the current data which best estimate the lowest possible values of apparent $k_{max}$ and p$K_a$ for WT, 46P, 4SU, 4deOU and 3MU RNase P.

By fitting a single ionization model (Equation 3-4) to the pH profile, the apparent p$K_a$ and a pH-independent rate constant ($k_{max}$) can be calculated. For wild-type RNase P, the apparent ionization in pH profile reflects a change in rate-limiting steps from the pH-dependent cleavage ($k_{chem}$) to a pH-independent conformational change ($k_2$) at pH > 7 (Scheme 3-1) [61]. The uracil base modifications, 4SU, 4deOU and 3MU, increase the apparent p$K_a$ value by up to 1.7 units while decrease the pH-independent rate constant, $k_{max}$, modestly (< 1.5-fold). In contrast, the base deletion by the abU mutant lowers the apparent pKa by at least 1 pH unit and reduces the $k_{max}$ by at least 6-fold. At $k_{max}$, the conformational change is the rate-limiting step [61]. Therefore, these data indicate that the abasic modification of the U51 affects a conformational change step during the RNase P-catalyzed reaction, while the alteration of uracil base functional groups (4SU, 4deOU, 3MU) affects the hydrolytic cleavage step (Scheme 3-1). A more accurate value of the conformational change rate constant, $k_{max}$, and p$K_a$ for wild type, 46P, and base-modified (4SU, 4deOU and 3MU) RNase P can be calculated by measuring the cleavage rate at higher pH (> 8) by rapid-quench or stopped-flow methods that require significantly higher quantities of enzymes [62]. Nevertheless, the current pH profiles clearly demonstrate that the two classes of mutants, base deletion (abU) and the base modifications (4SU, 4deOU and 3MU) affect different steps in the RNase P catalytic pathway.

### 3.3.5 U51 Modifications Alter the Cooperativity and the Apparent Affinity of Magnesium to P RNA

To examine whether the modifications affect the metal dependence of P RNA differently than the RNase P holoenzyme, the magnesium dependence of the single-turnover cleavage rate constant catalyzed by P RNA was measured at pH 6 where the cleavage step is rate-limiting (Figure 3-5). Similar to the holoenzyme, the abasic mutant catalyzes the single-turnover cleavage of Fl-pre-tRNA$^{Asp}$ at a rate constant that is similar to the reaction catalyzed by wild type and 46P RNA. Furthermore, the base modification mutants, 4SU, 4deOU and 3MU, catalyze cleavage 5 to 9 times slower than wild type and 46P RNA at saturating magnesium concentration (Table 3-4 and Figure 3-5).

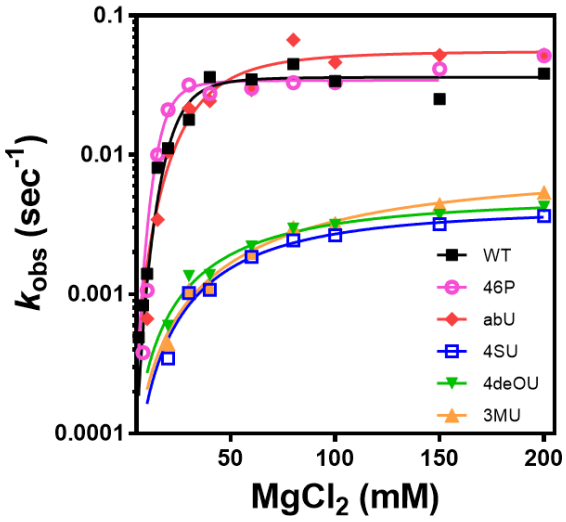


**Figure 3-5:** $Mg^{2+}$ dependence of wild type and U51 mutant P RNA-catalyzed single-turnover cleavage rate. Single-turnover cleavage of the Fl-pre-tRNA$^{Asp}$ (10 nM) by saturating P RNA (360 nM) was measured in 50 mM Tris/Mes, pH 6 (37˚C) with 6 - 200 mM $MgCl_2$, 20 mM DTT and varying KCl concentrations (from 4 to 40 mM $MgCl_2$ the KCl concentration varied from 112 to 5 mM; at higher $Mg^{2+}$ concentration KCl was maintained at 5 mM) using a fluorescence polarization/anisotropy assay. A single exponetnal function (Equation 3-5) was fit to the decrease in anisotropy of Fl-pre-tRNA$^{Asp}$ to calculate the single turnover cleavage rate constants ($k_{obs}$) by P RNA. The $Mg^{2+}$ dependce of $k_{obs}$ was fit to Equation 3-6 to calculate the apparent affinity and the Hill coefficient ($n_H$) for the $Mg^{2+}$ activation ($K_{1/2, Mg}$) of the P RNA cleavage activity and these values are listed in Table 3-4.

**Table 3-4:** $Mg^{2+}$ dependence of P RNA catalyzed single-turnover cleavage rate

| P RNA[a] | $k_{max}^{P\ RNA}$ ($sec^{-1}$)[b] | $K_{1/2,Mg^{2+}}^{Cleavage}$ (mM)[b] | $n_H$[b] | $k_{max}^{P\ RNA,wt}/k_{max}^{P\ RNA,variant}$ |
|---|---|---|---|---|
| WT | 0.036 ± 0.003 | 25 ± 3 | 4 ± 1 | 1 |
| 46P | 0.034 ± 0.002 | 19 ± 2 | 4 ± 1 | 1 |
| abU | 0.056 ± 0.008 | 40 ± 9 | 3 ± 1 | 0.6 |
| 4SU | 0.0042 ± 0.0004 | 70 ± 10 | 1.7 ± 0.2 | 9 |
| 4deOU | 0.0050 ± 0.0006 | 70 ± 13 | 1.5 ± 0.2 | 7 |
| 3MU | 0.008 ± 0.002 | 130 ± 40 | 1.4 ± 0.2 | 5 |

**a** P RNA catalyzed single-turnover cleavage of Fl-pre-$tRNA^{Asp}$ was measured as described in the legend of Figure 3-5.
**b** Equation 3-6 was fit to the data shown in Figure 3-4 to calculate the maximum cleavage rate, an apparent magnesium affinity ($K_{1/2,\ Mg}$) and the Hill coefficient ($n_H$).

The activity of wild-type and 46P RNA are enhanced by magnesium with an apparent $Mg^{2+}$ affinity ($K_{1/2,Mg}$) of 25 and 19 mM, respectively, and a Hill coefficient ($n_H$) of 4 (Table 3-4) . The base modification mutants (4SU, 4deOU and 3MU) and the abasic mutant (abU) differentially affect both the Hill coefficient ($n_H$) and the apparent $Mg^{2+}$ affinity ($K_{1/2,\ Mg}$) (Table 3-4). The 4SU and 4deOU modifications decrease the apparent $Mg^{2+}$ affinity by > 3-fold and decrease the cooperativity to $n_H$ ~ 1.4 to 1.7 (Table 3-4). The 3MU substitution has the largest effect on the apparent $Mg^{2+}$ affinity (7-fold decrease in $K_{1/2,\ Mg}$) although the maximum cleavage rate is comparable to or slightly better than the other two base modification mutants. Conversely, the Hill coefficient ($n_H$ = 3 ± 1) of the abU P RNA is within error of the wild type value and the apparent magnesium affinity is decreased marginally (2-fold). These data indicate that alterations in uracil base affect metal binding but complete removal of the base has little effect on catalytic activity or metal affinity.

One explanation of these data is that the uracil base forms hydrogen bonds with a metal-water ligand and alterations of the functional groups in the base affect the affinity and reactivity of this metal ion. However, the deleted base is replaced with water molecules, which then are able to realign to adequately stabilize and position the active metal ion.

### 3.3.6 Manganese Does Not Rescue 4SU Holoenzyme Activity

Although the sulfur substitution of the proposed inner-sphere ligand, O4 of U51, decreases cleavage activity of both *B. subtilis* RNase P holoenzyme and P RNA, the effects are much smaller than previously observed deleterious effects on catalysis for sulfur substitution of a $Mg^{2+}$ ligand in both phosphorothioate experiments [45-47] and model systems [63]. To further investigate the possibility that the O4 atom directly coordinates a magnesium ion, manganese ions were added to reactions catalyzed by 4SU holoenzyme to determine whether the cleavage activity can be rescued [8]. Increasing concentrations of $Mn^{2+}$ in the presence of 10 and 20 mM $Mg^{2+}$ decrease the single-turnover rate constant for both the 10nt control (ligation of a wild type ribooligonucleotide to 56P RNA) and 4SU to different extents (Figure 3-6). Low concentrations of $Mn^{2+}$ (<10 mM, with 20 mM $Mg^{2+}$) did not rescue the 4SU activity (data not shown). However, in higher concentrations of $Mn^{2+}$ (50-100 mM, with 10 mM $Mg^{2+}$), the 4SU RNase P activity is inhibited to a smaller degree leading to a modest $Mn^{2+}$ rescue with $k_{rel}$ = $(k_{Mn}/k_{Mg})^{4SU}/(k_{Mn}/k_{Mg})^{10nt}$ of ≤ 2-fold (Figure 3-6) [8]. Other metal ions frequently used for rescue experiments, such as $Zn^{2+}$ or $Cd^{2+}$, were not tested because of their significant inhibitory effect on *B. subtilis* RNase P cleavage activity [46].

The modest rescue effect does not provide direct evidence for an inner-sphere coordination of the O4 site. However, direct coordination cannot be ruled out solely by an absence of rescue activity [8]. However, the high activity of the abasic mutant indicates that the uracil base is not essential for efficient cleavage of pre-tRNA (Table 3-1 and Figure 3-3), arguing against an inner-sphere coordination of the uracil base for catalysis during the transition state.

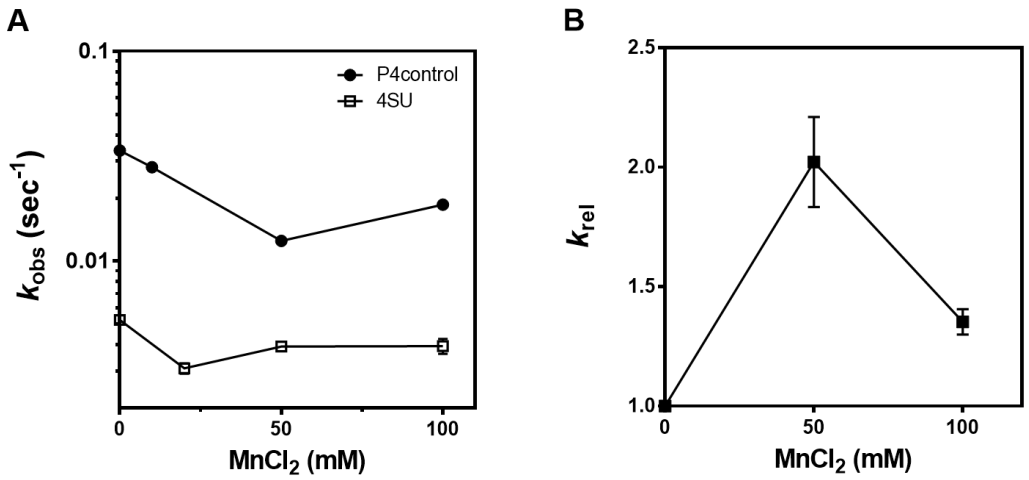


**Figure 3-6:** Manganese ions modestly rescue 4-thiouridine holoenzyme activity. **(A)** The single turnover rate constant ($k_{obs}$) for cleavage of pre-tRNA by control RNase P (ligation of a wild type 10-mer riboologonulcetide to 56 P RNA, 10nt in short, ●) and 4SU mutant (□) with varying concentrations of $MnCl_2$ (0-100 mM) with 200 mM KCl, 10 mM $MgCl_2$, 50 mM Tris/Mes pH 6 at 37˚C, 360 nM holoenzyme and 10 nM Fl-pre-tRNA$^{Asp}$) was measured by fluorescence polarization. **(B)** The differential effect of $Mn^{2+}$ ions on the 10nt and 4SU RNase P activity is illustrated by the value of $k_{rel} = (k_{Mn}/k_{Mg})^{4SU}/(k_{Mn}/k_{Mg})^{10nt}$.

### 3.3.7 4SU Does Not Affect Cleavage in $Ca^{2+}$

In addition, the single-turnover rate constant catalyzed by the 4SU holoenzyme was measured in saturating concentrations of $Ca^{2+}$ (10 mM) (Figure 3-7). In $Ca^{2+}$, the cleavage rate constant is much slower and the cleavage step is rate limiting at all pH values [60]. Under these conditions the single-turnover rate constant of the 4SU mutant is comparable to that of the wild type and all control holoenzymes (Figure

3-7). These data suggest that the O4 in U51 is not important for positioning a catalytic $Ca^{2+}$ for RNase P catalyzed cleavage reactions. This loss of O4 interaction could indicate that $Ca^{2+}$ localizes to an alternative position, which is consistent with the less efficient catalysis.

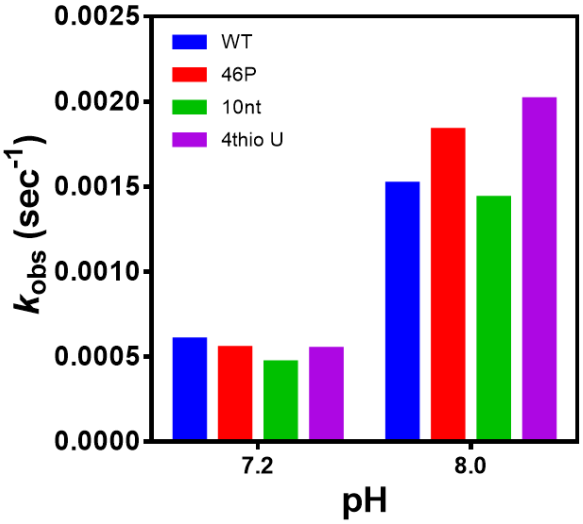


**Figure 3-7:** The 4-thiouridine modification does not alter RNase P holoenzyme-catalyzed single-turnover cleavage rate constant in $Ca^{2+}$. Single-turnover cleavage of 10 nM Fl-pre-$tRNA^{Asp}$ substrate catalyzed by 360 nM RNase P holoenzyme was measured in 50 mM Tris/Mes, varying pH with ~189 mM KCl to maintain ionic strength, 20 mM DTT, and 10 mM $CaCl_2$ by the fluorescence polarization assay. The rate constant, $k_{obs}$, was calculated from Equation 3-3 as described in Materials and Methods.

### 3.4 Discussion

Helix P4 contains 6 of the 13 universally conserved nucleotides in P RNA [64] and is proposed to be part of the active site of RNase P, as illustrated by the recently solved crystal structure of *T. maritima* RNase P ternary complex [44]. This structure revealed two metal ions ($Eu^{3+}$ and $Sm^{3+}$ soak) that bind near A49, G50 and the 5' end of tRNA (Figure 3-1), leading to a proposal that a carbonyl oxygen at position 4 (O4) of the uracil base of a conserved uridine (U51) is an inner-sphere metal ligand for one of the metal ions that stabilize the transition state of the RNase P-catalyzed

hydrolysis (Figure 3-1). To test this hypothesis, I examined the biochemical role of this universally conserved uridine (U51) in *B. subtilis* RNase P by combining atomic mutagenesis and detailed kinetic analysis. The functional effects of these modifications can be grouped into two classes. First, modifications of the base in U51 alter metal-dependent pre-tRNA affinity and decrease RNase P catalyzed cleavage rate constant and cooperativity at low pH, but affect the cleavage activity of RNase P modestly at high pH. Second, the deletion of the uracil base at U51 retains the wild-type level single-turnover cleavage rate at low pH, but substantially lowers the apparent p$K_a$ and decreases the conformational change rate constant. These data argue against an inner-sphere coordination of the O4 to a catalytic metal ion, but suggest that this conserved uracil base plays a role in stabilizing an active conformation of the RNase P•pre-tRNA (ES) complex prior to cleavage.

### 3.4.1 Helix P4 Is Important for Metal Ion Stabilized Substrate Binding

A previous study showed that circular permutation of the P4 helix and phosphorothioate substitutions minimally affect the substrate affinity at saturating divalent metal ion concentrations [46]. In this work, I also observed comparable affinity of the pre-tRNA$^{Asp}$ substrate for both circular permuted 46P RNase P and the 4SU mutant at saturating (8 mM and 10 mM) $Ca^{2+}$ (Table 3-1 and Figure 3-3). However, at sub-saturating $Ca^{2+}$ (5 mM), the circular permutation (46P) destabilizes the substrate affinity by 1.5 kcal/mol[3]. Addition of the sulfur substitution of O4 in the uracil destabilizes substrate affinity by an additional 0.5 kcal/mol in comparison to wild type holoenzyme. Previous site-directed mutagenesis data also indicated that

[3] $\Delta\Delta G = -RT\ln(K_{d,app}^{variant} / K_{d,app}^{wt})$

deletion of the bulge and a movement of the bulged uridine up- or down-stream in the helix can result in up to a 200-fold decrease in substrate affinity to P RNA (1 M NaCl and 25 mM $MgCl_2$) [65], suggesting the importance of the structure of the helix for substrate binding.

Under low divalent metal conditions, circular permutation and sulfur substitution could affect substrate affinity through either incorrect folding of P RNA and/or perturbation of metal coordination that enhances substrate binding. Nonetheless, higher divalent metal ion concentrations can compensate for the substrate affinity defect caused by these perturbations, demonstrating the coupling between metal ion binding and substrate affinity and suggesting that P4 helix contains metal binding sites that are associated with substrate binding. Future experiments that monitor the $Mg^{2+}$ dependence of P RNA folding by circular dichroism could test the effects of these modifications on P RNA stability [66].

### 3.4.2 U51 Coordinates a Co-catalytic Metal Ion through Outer-sphere Coordination

In previous phosphorothioate experiments in RNase P [45-47], disruption of an inner-sphere contact of a catalytic metal frequently resulted in an enormous decrease in catalytic activity (300- to $10^4$-fold). Some of the catalytic defects caused by substitution of oxygen with sulfur can be rescued by addition of thiophilic metal ions, such as manganese [45-47]. In this study, at low pH where cleavage is the rate limiting step [67], both sulfur substitution (4SU) and removal of O4 in U51 produced a relatively modest decrease in the single-turnover cleavage rate constant (~20-fold for holoenzyme and ~9-fold for P RNA). The cleavage rate catalyzed by RNase P

holoenzyme with these two single-atom modifications increased linearly with pH. A fit of a single ionization to this pH dependence suggests that the apparent p$K_a$ increases but the $k_{max}$ is comparable to that of wild type holoenzyme. Additionally, manganese only marginally rescues the activity of 4SU holoenzyme ($k_{rel}$<2) at low pH. The small rescue effect cannot completely rule out an inner-sphere metal ion interaction because the different sizes among sulfur, oxygen, manganese and magnesium could disturb the active site structure, and differential solution conditions may also complicate the interpretation [8, 68]. In addition, differential manganese rescue effects have been observed with phosphorothioate substitution of the *pro*-$S_p$ oxygen of A49 for *B. subtilis* holoenzyme and P RNA [46]. To examine this possibility, manganese rescue of the P RNA catalyzed cleavage activity of the 4SU mutant will be measured in the near future.

Strikingly, the abU modification that completely deletes this conserved uracil base but retains the ribose and backbone moieties had no effect on the chemistry step (pH 4.5 - 5). These data indicate that the O4 ligand does not form an essential inner-sphere interaction with a metal ion to stabilize the transition state for catalysis.

Multiple magnesium ions (≥ 3) are required for RNase P function, as demonstrated by the Hill coefficients ($n_H$ ~4) for the magnesium dependence of cleavage [30, 32]. The analysis of the magnesium dependence of the cleavage rate catalyzed by P RNA shows that modifications on the uracil base, including sulfur substitution (4SU) or deletion of O4 (4deOU) and insertion of a methyl group (3MU), decreases cleavage rate constant and possibly the number of metal ions from 4 to 2 (Table 3-4). The sterically largest modification, addition of the methyl group (3MU)

has the largest effect on the apparent $Mg^{2+}$ affinity (5-fold decrease in $K_{1/2, Mg}$) and cooperativity ($n_H$ ~1.4). In contrast, removal of the uracil base by the abasic modification (abU) only decreases the apparent $Mg^{2+}$ affinity by < 2-fold and decreases the metal cooperativity by 1, indicating that the uracil base is not essential for directly stabilizing the chemical step, although the decrease in cooperativity could suggest the loss of an active site metal ion. Moreover, the reduced apparent $Mg^{2+}$ affinity and cooperativity of the atomic modifications on the uracil base (4SU, 4deOU and 3MU) suggest that this site is involved in correctly positioning at least one co-catalytic metal ion, likely through outer-sphere coordination mediated by water molecules.

Outer-sphere metal ions have previously been suggested to enhance RNase P reactivity [34, 37]. Data presented here suggest that the carbonyl oxygen of the conserved uracil likely position at least one co-catalytic metal ion by a water-mediated outer-sphere interaction (Figure 3-8). We postulate that the wild type O4 oxygen in this conserved uridine forms a hydrogen bond with a water molecule to coordinate a co-catalytic metal ion in the optimal position for activity. Therefore, substitution of O4 with a larger sulfur atom (4SU), deletion of the O4 (4deOU) or insertion of a methyl group (3MU) on the base creates steric hindrance or alter hydrogen-bonding interactions to skew the position of the metal ion. Conversely, removal of the uracil base could generate space for additional water molecules at the active site that allow the co-catalytic metal ion to be positioned correctly (Figure 3-8).

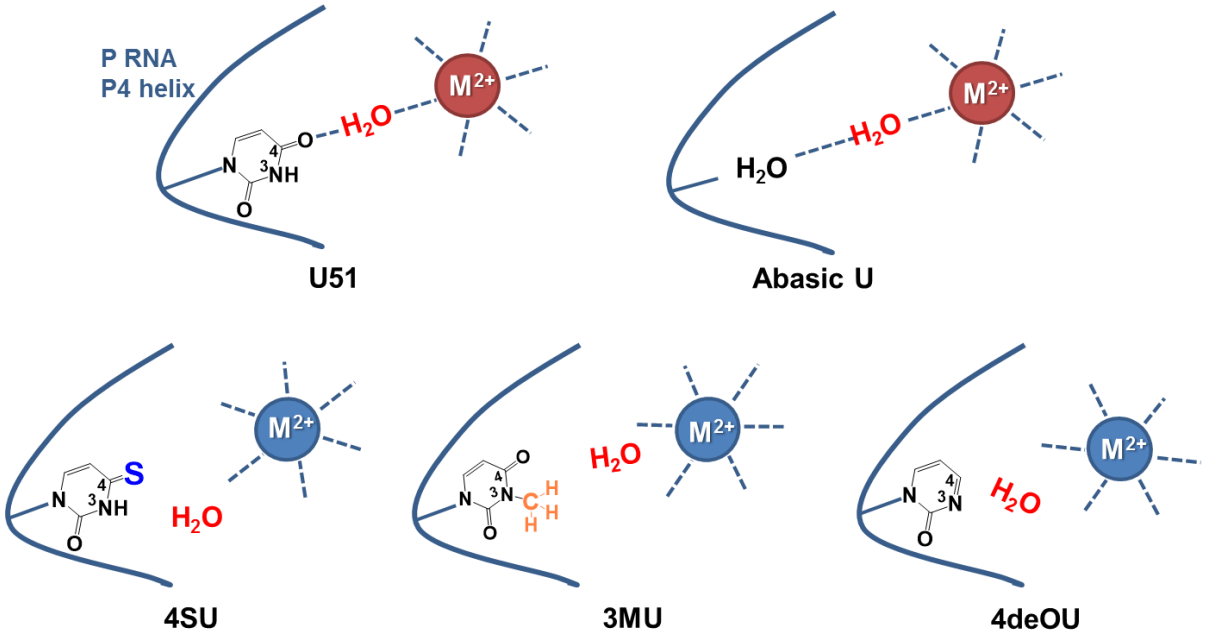


**Figure 3-8:** A cartoon diagram showing a model of U51 coordinating a co-catalytic metal ion through an outer-sphere interaction. The atomic modifications on the uracil base, 4-thiouridine (4SU), 4-deoxyuridine (4deOU) and 3-methyluridine (3MU), interrupt the water-mediated interaction with a metal ion, but the abasic modification may provide more space for one or more additional water molecules to stabilize the outer-sphere interaction.

These experimental data suggest that the proposed direct interaction of the O4 to M1 metal in the crystal structure of the RNase P ternary complex [44] is not important for stabilizing the catalytic transition state. The low resolution (4.2 Å) of the crystal structure combined with the larger volume of the soaked metal ions ($Sm^{3+}$ and $Eu^{3+}$) might have limited identification of an intervening water molecule. In addition, because the crystal structure is of a complex with products (E·tRNA·Leader) rather than with substrate (E·pre-tRNA), it is possible that the metal coordination is altered in this complex. This possibility is exemplified by distinct conformational states observed in crystal structures of the hepatitis delta virus (HDV) ribozyme, which displays different arrangements of the active site including ejection of catalytic metal ions from pre- to post-cleavage states [69-71].

### 3.4.3 U51 Enhances Conformational Kinetics

Conformational changes also occur in RNase P during the catalytic cycle [67]. After formation of an initial encounter complex between RNase P (E) and pre-tRNA (S), the ES complex undergoes a conformational change to form an active conformer (ES*) prior to the chemical cleavage step [67] (Scheme 3-1). The apparent rate of this conformational change step is independent of pH and becomes rate-limiting at high pH (>7) for wild type RNase P [67]. The removal of the uracil base to form an abasic site (abU) substantially reduces this conformational change rate constant without affecting the cleavage rate constant, thereby lowers the apparent p$K_a$ by at least 1-2 pH units (Figure 3-4, Table 3-3). Similar abasic modifications have previously been shown to dramatically reduce activity of a hammerhead ribozyme by up to $10^6$-fold [72]. In some cases, the reduced activity caused by the abasic modifications could be partially rescued (20- to 300-fold activation) by addition of specific exogenous bases that restore hydrogen bonding and base stacking interactions [72]. The abasic modification in RNase P, however, does not alter the cleavage rate constant (Table 3-2 and Figure 3-4). Instead, the abasic modification of this conserved uridine decreases the conformational change rate constant by at least 6-fold. These data indicate that in RNase P the uracil base affects the conformational change step prior to cleavage.

P RNA has two independent folding domains, the specificity domain (S-domain) and the catalytic domain (C-domain) [73]. (Figure 3-2). The conformational change coupled to pre-tRNA binding is observed for the C-domain alone albeit with a reduced rate, as measured by fluorescence stopped-flow and time-resolved

fluorescence resonance energy transfer (trFRET) experiments (Hsieh and Fierke, manuscript in preparation). Since helix P4 is the most conserved region in the C-domain P RNA [48, 49], it is highly likely that alterations in the structure of this helix, possibly including the bulged U51, are involved in the conformational change for substrate recognition by the C-domain [54, 65]. The conformational change step is proposed to be a proofreading step to recognize a cognate substrate for RNase P [62]. The alteration in the conformational changes step caused by the abasic U51 futher implicates the role of this region of P4 in this step (Figure 3-4).

Furthermore, structural data suggest that the conserved uridine is able to adopt different conformations (Figure 3-9). In contrast to the ternary complex, a previous free P RNA structure shows the uridine is in a different “flipped out” conformer [57] (Figure 3-9). The differences between secondary structures of the A-type (*T. maritima*) and B-type P RNA (*B. stearothermophilus)* could be a possible reason for this difference. However, solution structural studies of both A-type and B-type P RNAs using 2'-hydroxyl acylation analyzed by primer extension (SHAPE) and small angle X-ray scattering (SAXS) indicate that the conserved uridine bulge in free P RNA is largely solvent exposed under these experimental conditions [74], which is consistent with the “flipped out” conformation observed the free P RNA crystal structures [57, 75].

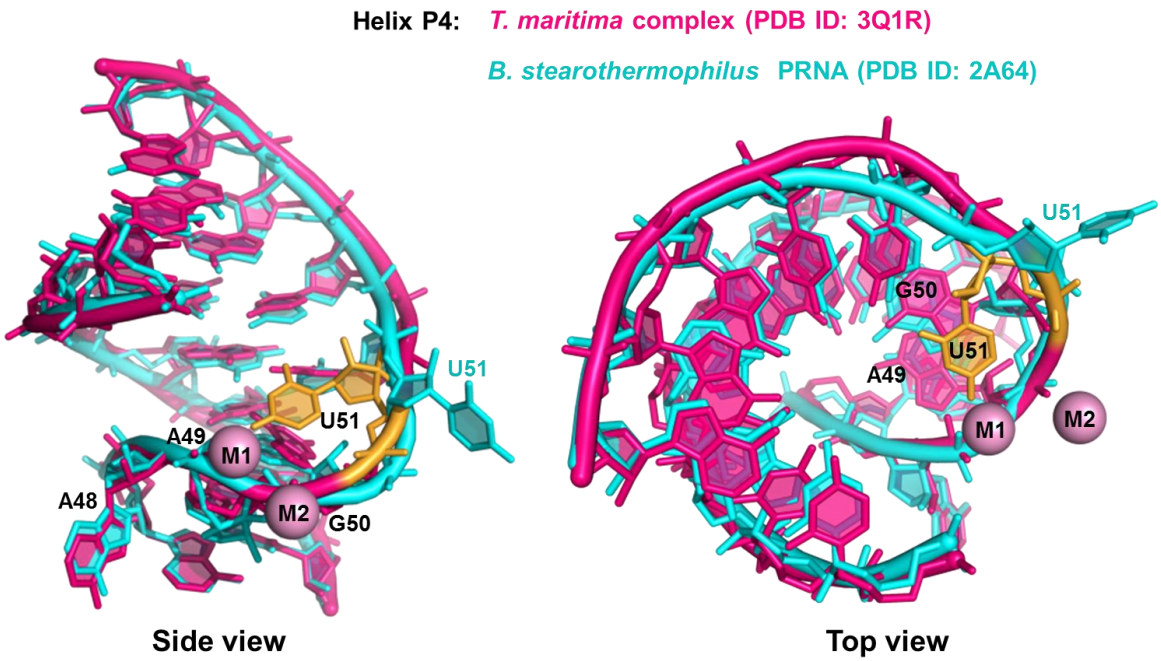


**Figure 3-9:** The universally conserved uridine in P4 helix is in different conformations between free P RNA and holoenzyme-substrate bound crystal structures. Two different views (side view in left and top view in right) are shown for an overlay of the P4 helix region in crystal structures of the *B. stearothermophilus* P RNA (PDB ID: 2A64, in cyan) [57] and the *T. maritima* RNase P ternary complex (PDB ID: 3Q1R, in dark pink) [44]. The universally conserved uridine (U51, *B. subtilis* numbering) in the RNase P·tRNA complex [44] is in an inward position (orange), while the U51 in the free P RNA is bulged out (cyan) [57]. The two metal ions observed in the RNase P·tRNA complex [44] are pink. The RMSD is 1.1 by superimposing the helix backbone using PyMOL software.

Bulged nucleotides are common motifs in folded RNA molecules and have been shown to associate with RNA-ligand binding [76, 77] and conformational transitions [78, 79]. In a highly conserved domain in the spliceosome, the U6 RNA internal stem-loop, a uracil base flips from a bulged position into a stacked and base-paired position upon deprotonation of an adjacent adenine [78, 79]. This uracil flipping at high pH is coupled with the disruption of the A-C wobble pair adjacent to the U bulge and allows binding of an important metal ion to the *pro*-$S_p$ non-bridging oxygen of the backbone phosphate in this conserved uridine [80, 81]. The different conformer of U51 observed in different crystal structures may reflect the

conformational transitions in RNase P (Figure 3-9). The uridine bulge in the P4 helix of RNase P could potentially undertake a movement from a bulged position to an inward location after the initial substrate binding to stabilize the active ES* conformer prior to catalysis (Figure 3-10). Further mechanistic studies are necessary to test this hypothesis.

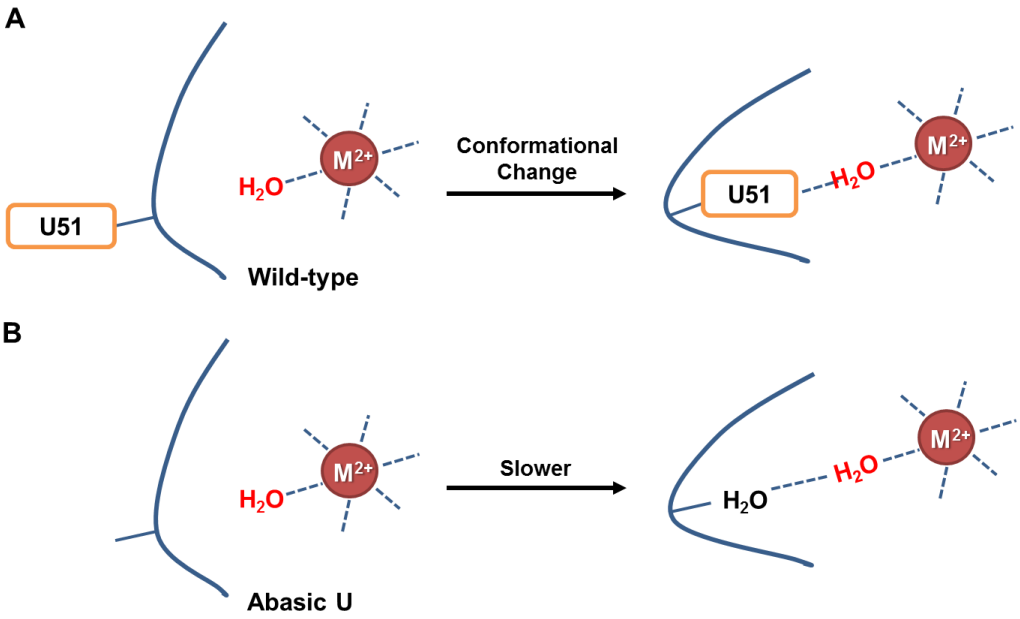


**Figure 3-10:** A diagram showing a model in which the universally conserved uridine changes conformations. **(A)** The conserved bulge uridine (51) in P4 helix may flips from the solvent exposed conformation to an inward position to contact an outer-sphere metal ion that stabilizes the ES* conformation prior to RNase P catalyzed cleavage reaction. **(B)** The abasic modification of U51 allows positioning of the outer-sphere metal ion through additional water molecule but the conformational change rate constant is slower due to the deletion of the uracil base.

In the RNase P kinetic pathway, the ES* conformer is suggested to be stabilized by a high affinity inner-sphere magnesium ion as indicated by the stabilization of this complex with $Ca^{2+}$ or $Mg^{2+}$ but not $Co(NH_3)_6^{3+}$ [62]. The 6-fold rate reduction by abasic modification is inconsistent with a specific inner-sphere metal interaction. However, at least one outer-sphere metal ion is associated with this nucleotide for conformational change, as indicated by a Hill coefficient reduction

from 4 to 3 in the $Mg^{2+}$ dependence of the P RNA cleavage rate (Table 3-4), suggesting that at least one metal ion is associated with this conformational change with possibily an outer-sphere interaction. Two conserved arginine residues in the P protein subunit have also been previously shown to stabilize the active ES* conformer [60]. The leader sequence in the pre-tRNA substrate is also proposed to rearrange to adopt an extended conformation upon binding to RNase P [82] as observed in the crystal structure [44]. It is expected that other residues contribute synergistically to stabilize the conformational transitions. However, the ligands that bind a proposed inner-sphere metal ion that stabilize the conformational change [62] have not yet been identified.

### 3.4.4 Conclusions and Implications

In this chapter, a combination of atomic mutagenesis and kinetic studies demonstrate that a universally conserved uridine (U51) in RNase P RNA interacts with and positions a metal ion, likely via interactions with a water-metal ligand important for substrate binding and catalysis. Notably, the uracil base of this conserved nucleotide is not essential for catalysis but contributes to stabilization of an active conformer of RNase P. These results suggest that the O4 of U51 does not form an inner-sphere interaction with a metal ion impoartant for stabilization of the transition state (Figure 3-1). However, inner-sphere coordination could occur in other complexes that formed during the catalytic cycles, such as E·tRNA·Leader product complex as observed in the recent crystal structure. A completely clear picture of coordination of metal ions that stabilizes the transition state of RNase P requires further efforts. Higher resolution crystal structures of RNase P in complex with metal

ions in different conformational states could provide valuable insights. Similarly, solution structures and metal probing studies could also provide further insights. Detailed mechanistic studies, such as the one described in this chapter, examining both cleavage and conformational change steps provide a framework to probe functionally important metal ion sites in the RNase P kinetic pathway.

The conserved uridine in the P4 helix reported here is the first nucleotide identified in the P RNA that is important for stabilizing the active ES* conformation. The ability of RNA to dynamically switch between conformations is frequently crucial for ribozyme function [83, 84]. The global conformational change coupled to substrate binding in RNase P has been demonstrated by mechanistic studies [62, 67], but the temporal, spatial and molecular details of important conformational change steps during the RNase P kinetic pathway are still not clear. Recently, advanced NMR techniques have been developed that can detect transient movement of single nucleotides in RNA that are potentially important for function [85]. It will be intriguing to investigate whether similar types of micro-movements also contribute to the function of RNase P.

In addition, The abasic modification demonstrated in this study provides a potential strategy to probe functions of conserved bases in conformational changes and activity in both RNase P and other RNA systems [72], analogous to the alanine scanning mutagenesis strategy used to study proteins [86]. Further mechanistic and structural studies, such as stopped-flow fluorescence assays and FRET experiments [62], will provide more insights into the effects of the abasic modification on the conformational change step in RNase P.

## 3.5 Materials and Methods

### 3.5.1 Materials and Reagents

All nucleotide triphosphates and other chemicals were purchased from Sigma at the highest purity (RNase and DNase free grade) unless otherwise specified. Sodium dodecyl sulfate (SDS) was purchased from Fisher Scientific. Inorganic pyrophosphatase was purchased from Roche Applied Science. Ultra-pure urea was from MP Biomedicals. 5-Iodoacetamido-fluorescein (5-IAF) was obtained from Invitrogen (now Life Technologies) and dissolved in anhydrous DMSO (Sigma). Guanosine 5'-monothiophosphate (GMPS) was synthesized from 2', 3' isopropylidene-guanosine and thiophosphoryl chloride as described in [87]. $His_6$-T7 RNA polymerase was purified by Ni-NTA chromatography as described previously [88]. Buffer solutions were prepared by Milli-Q (Millipore Corporation) treated deionized water and sterilized either by autoclave (inorganic buffers such as $MgCl_2$, $CaCl_2$ and KCl) or filtration (EDTA stock solution and solutions containing Mes) using Stericup filter units (Millipore Corporation). Tris/Mes stock solutions at various pH values were made at room temperature and the pH was re-measured at 37˚C.

All DNA oligonucleotides were purchased from Integrated DNA Technologies (IDT). Ribooligonuctcoties containing atomic modifications of the uridine were purchased from different vendors and deporotected according to manufacturing procedure before use. The 10-mer ribooligonucleotides containing wild type (10nt) or 4-thiouridine (4SU) were from Dharmacon (now Thermo Scientific). The 10-mer ribooligonulceotides with 4-deoxyuridine (4deOU), 3-methyluridine (3MU), and rSpacer (abasic, abU) modifications were synthesized by the Keck Oligo Synthesis

Resource (Yale School of Medicine).

### 3.5.2 Preparation of P Protein, Substrate and Unmodified P RNA

*B. subtilis* RNase P protein was expressed in BL21(DE3)pLysS cells and purified as previously described [89, 90]. The *B. subtilis* Fl-pre-tRNA$^{Asp}$ substrate containing a 5-nucleotide leader sequence was prepared as described previously [62, 82] by 5′ monothiophosphate guanosine (5’ GMPS) primed *in vitro* run-off transcription (4 mM ATP, GMPS, CTP, UTP, and 0.8 mM GTP in 50 mM Tris-HCl pH 8, 1 mM spermidine, 5 mM DTT and 20 mM $MgCl_2$ for 6-12 hrs at 37˚C) using T7 RNA polymerase from a DNA template linearized by BstNI restriction enzyme (New England Biolabs, NEB). The transcribed 5’-GMPS-pre-tRNA was buffer exchanged and concentrated into a degassed labeling buffer (10 mM Tris-HCl, pH 7.2 and 1 mM EDTA) for labeling by 5-IAF at 37 °C overnight. The $^{32}$P 5’ end labeled pre-tRNA substrate was prepared by incubating regularly transcribed (4 mM rNTPs and same conditions as above) pre-tRNA with calf intestinal alkaline phosphatase (NEB) followed by 5′ end-labeling using T4 polynucleotide kinase (NEB) and [γ-$^{32}$P] ATP according to manufacturing instructions and purified by denaturing PAGE followed by phenol/chloroform extraction and ethanol precipitation [58]. The wild-type, circular permuted 46P and 56P RNAs were transcribed *in vitro* as previously reported [46] by T7 polymerase using DNA templates linearized by DraI, KpnI or BasI restriction enzymes (NEB), respectively. All RNAs were purified by electrophoresis on a 6% (P RNA) or 10-12% (pre-tRNA) polyacrylamide/bis denaturing gel containing 7 M urea.

### 3.5.3 Preparation of Mutants by Ligation[4]

The 10-mer ribooligonulceotide containing the same sequence as the 5' end strand of the P4 helix (5' GAA AGU* CCA U 3') with either the wild type uridine or modifications (indicated by the asterisk sign, Figure 3-2) was ligated to the 5' end of guanosine monophosphate (GMP) transcribed 56P RNA in the presence of a DNA splint that is complementary to all 10-nt of the RNA oligo and the first 23 or 41 nt of 56P RNA (5'-GGG CAT CTC AGC ACC GTG CGA GCATGG ACT TTC A-3' [46] or 5'-GCT AGG CAC GAA CACTAC GGG CAT CTC AGC ACC GTG CGA GCATGG ACT TTC-3') catalyzed by T4 DNA ligase. The previously reported ligation method [46] was used to ligate the 4-thiouridine ribooligonucleotide to GMP-56P RNA and the yield was 30-70%. A modified ligation protocol was developed to increase the ligation yield [91-93]. Specifically, 4 μM GMP-56P RNA, 28 μM 10-mer ribooligonucleotide and 28 μM DNA splint were annealed in 66 mM Tris-HCl (pH 7.6), 6.6 mM $MgCl_2$ and 10 mM DTT by denaturing at 75°C for 5 min and cooled down at room temperature for 35 min before addition of a final concentration of 200 μM ATP, 4 μM T4 DNA ligase and 0.2 unit/μL of Sperase·In™ RNase inhibitor (Ambion, now Life Technology). To monitor the ligation reactions, a small amount of the ligation reaction mix was folded by incubation at 37 °C in 50 mM Tris-HCl (pH 8), 40 mM $MgCl_2$, 980 mM KCl and 20 mM DTT for a measurement of multiple turnover cleavage activity (10 nM P RNA, 50 nM Fl-pre-$tRNA^{Asp}$). The ligation reactions progressed for 3-9 hours before being quenched by EDTA dye (10 M urea, 200 mM EDTA (pH 8.0), 0.05% bromophenol blue, and 0.05% xylene cyanol), and the ligated P RNA was purified by 6% PAGE. The ligation efficiency was determined by primer

[4] The modified ligation method was adapted from a protocol developed by Yu Chen.

extension analysis using a 6FAM labeled primer that anneals to nucleotide 114 to 95 (Figure 3-2) [46] (5'-6FAM-GCC CTA GCT TAT GAC TTC GC-3'). The 6FAM-primer (9 pmol) was annealed to P RNA (27 pmol) in 50 mM Tris-HCl (pH 8.3), 75 mM NaCl and 10 mM DTT by denaturing for 3 min at 95˚C followed by a 15 min incubation at 37˚C. A subsequent extension step took place at 42˚C for 30 min by the addition of 10 mM $MgCl_2$, 0.8 mM dNTPs, and 2.5 unit/µL reverse transcriptase (Promega). Reactions were visualized by a 6% denaturing gel, scanned using a Typhoon Phosphorimager (detection limit was determined to be 5 fmol of fluorescein) and quantified by ImageQuant or ImageJ software (Figure B-1, Appendix B).

### 3.5.4 Determination of Pre-tRNA Dissociation Constant by Spin Column

The affinity of $^{32}$P 5' end labeled pre-tRNA$^{Asp}$ with a 5-nt leader to RNase P holoenzyme was measured as described previously (Figure 2-4A). The recombinant P protein was dialyzed against binding buffers containing 50 mM Tris/Mes, pH 6, ~380 mM KCl, and 5-10 mM $CaCl_2$ at 4˚C. P RNA was folded by denaturation in water at 95˚C for 3 min followed by a 30 min incubation at 37˚C before addition of desired binding buffers. The P RNA were then buffer exchanged with the same binding buffer by Amicon centrifugation filters (MWCO 10,000, Millipore) by at least three iterations. RNase P holoenzyme was reconstituted by mixing P RNA and P protein at a 1:1 ratio. RNase P holoenzyme (0-400 nM) was incubated with $^{32}$P 5' end labeled pre-tRNA$^{Asp}$ (<< 1 nM) for 5 min at 37˚C. The holoenzyme-substratemixture was loaded onto a pre-packed G-75 Sephadex (GE health) spin column (Corning Life Sciences). The unbound substrate was separated from the mixture by centrifugation for 15 seconds at 6000 rpm. The amount of bound and

unbound substrate was measured by scintillation counting. A single binding isotherm (Equation 3-1) was fit to the data to obtain the dissociation constant, $K_{d,\,app}$ (Scheme 3-1):

$$\text{Fraction bound} = \frac{[ES] + [ES^*]}{[S_{\text{total}}]} = \frac{[E_{\text{total}}]}{K_{\text{d,app}} + [E_{\text{total}}]} \qquad \textbf{Equation 3-1}$$

### 3.5.5 Single-turnover Experiments

Single-turnover experiments were performed at saturating concentrations of divalent metal ions (10 or 20 mM $Mg^{2+}$ or $Ca^{2+}$) and saturating RNase P (360 - 500 nM), as indicated in the figure and table legend, to investigate the catalytic activity of the mutants. The RNase P holoenzyme were prepared similar to described above except for that the P protein and P RNA were not dialyzed or buffer exchanged because of the high metal ion concentrations used in the single-turnover cleavage experiments. Folded enzymes and substrates were kept at 37˚C until use.

The single-turnover cleavage of FI-pre-$tRNA^{Asp}$ was carried out in a black 96-well microplate with non-binding surface (Corning Incorporation, #3686) by monitoring the anisotropy change of fluorescein ($\lambda_{ex}$ = 485 nm and $\lambda_{em}$ = 535 nm) using the fluorescence polarization function of a TECAN plate-reader (Infinite F500, G factor = 0.93). The substrate was pre-incubated in the plates to perform the gain and Z-position adjustments of the plate-reader and the reactions were initiated by addition of RNase P. Experiments measuring single-turnover reactions were carried out using excess holoenzyme or P RNA ([E] = 360 – 500 nM and [S] = 10 nM) at 37 °C.

For the RNase P holoenzyme catalyzed single-turnover reactions, the total

fluorescence intensity decreased from the initial substrate-RNase P complex ($F^0$) to cleaved product ($F^\infty$), and the extent of this decrease varies with pH. Therefore, an enhancement factor g, defined as described previously [94], was used to correct for the total fluorescence change when calculating the fraction cleaved (Y) from the anisotropy time trace using Equation 3-2. The enhancement factor is defined by $g = F^0/F^\infty$. The $r_0$ and $r_\infty$ are the anisotropy values of the RNase P holoenzyme-bound substrate and cleaved product, respectively, measured for each experiment.

$$Y = 1 - \frac{r - r_\infty}{r_0 - r_\infty + (g-1)(r_0 - r)} \qquad \textbf{Equation 3-2}$$

The single-turnover cleavage rate constant ($k_{obs}$) was then calculated by fitting a single exponential model (Equation 3-3) to the fraction cleavage as a function of time.

$$Y = Y_\infty\left(1 - e^{-k_{obs}t}\right) \qquad \textbf{Equation 3-3}$$

The p$K_a$ values and pH-independent rate constants for reactions catalyzed by RNase P holoenzyme were calculated by fitting a single ionization model (Equation 3-5) to the pH profile:

$$pH = \frac{k_{max}^{holo}}{1 + 10^{(pK_a - pH)}} \qquad \textbf{Equation 3-4}$$

For the P RNA catalyzed single-turnover reactions, the total fluorescence intensity remains constant during the reaction and the anisotropy time course data are well described by a one phase exponential decay model. Therefore, Equation 3-5 was fit to the anisotropy time course to calculate the single-turnover rate constant ($k_{obs}$). All data analyses were performed using Prism 5.03 or 6.0 (GraphPad

Software).

$$r = (r_0 - r_\infty)e^{-k_{obs}t} + r_\infty \quad \textbf{Equation 3-5}$$

Equation 3-6 was fit to the magnesium dependence of the P RNA catalyzed single-turnover cleavage rate data to calculate the apparent magnesium affinity ($K_{1/2,Mg^{2+}}^{Cleavage}$) and Hill coefficient ($n_H$):

$$k_{obs} = \frac{k_{max}^{P\ RNA}\,[Mg^{2+}]^{n_H}}{\left(K_{1/2,Mg^{2+}}^{Cleavage}\right)^{n_H} + [Mg^{2+}]^{n_H}} \quad \textbf{Equation 3-6}$$

## 3.6 Appendix B

### 3.6.1 Ligation Efficiency of Different Atomic Modifications

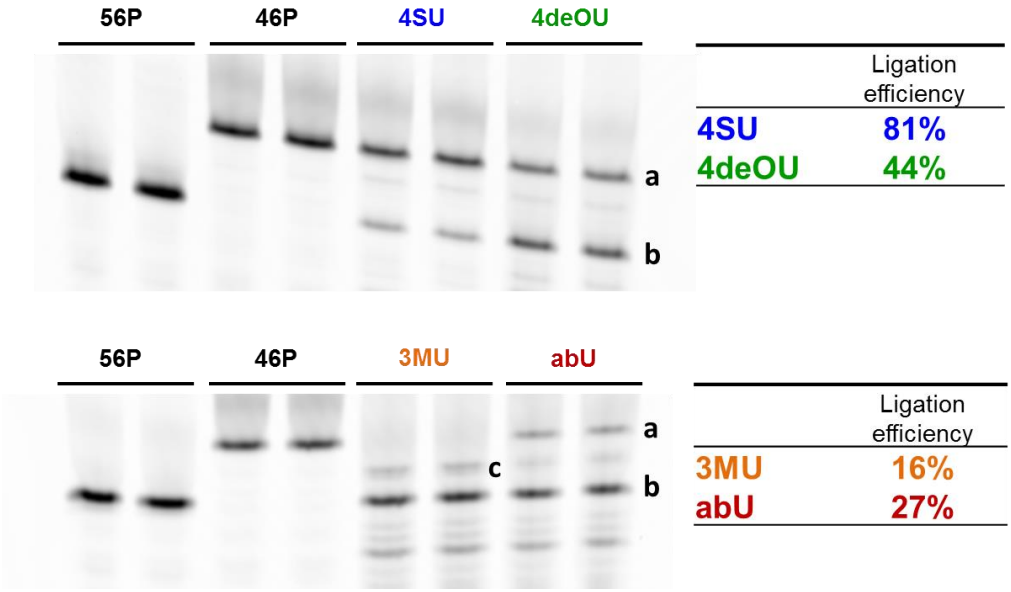


**Figure B-1:** Ligation efficiency of 10-mer ribooligonucleotides containing single atom modifications of U51 are determined by primer extension analysis. Experiment procedure is described in Materials and Methods. The primer extension reaction by 6FAM labeled primer was visualized by a 6% denaturing polyacrylamide gel scanned by Typhoon Phosphorimager. The ligation efficiency is calculated by the ratio of the intensity (I) of the bands corresponding to primer extension products of 46P and 56P RNA controls: $\%=I_a/(I_a+I_b)$. For 3MU, band a is not observed likely due to the blockage of extension by the methyl group, so the band c was used to calculate ligation efficiency: $\%=I_c/(I_c+I_b)$.

### 3.6.2 RNase P with Atomic Modifications in U51 Accurately Catalyze Cleavage of Fl-pre-tRNA$^{Asp}$

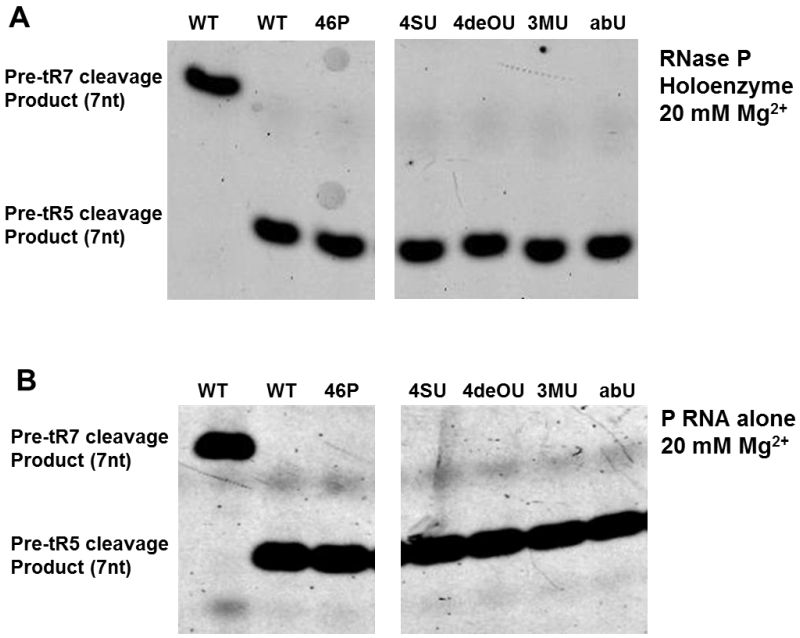


**Figure B-2:** RNase P containing single atom modifications catalyze cleavage of pre-tRNA substrate at correct site. Reaction conditions are: 50 mM Tris/MES pH 6, 20 mM $MgCl_2$, 200 mM KCl and 20 mM DTT, with fluorescently labeled pre-tRNA$^{Asp}$ with 10 nM either a 7-nt 5' leader (pre-tR7) or 5-nt 5' leader (pre-tR5) and 360 nM RNase P. Reaction time is 10 min for holoenzyme in **(A)** and 2 hours for P RNA alone in **(B)**. Products are resolved by a 22% PAGE.

## 3.7 References


1. Sigel, R.K. and A.M. Pyle, *Alternative roles for metal ions in enzyme catalysis and the implications for ribozyme chemistry.* Chem Rev, 2007. **107**(1): p. 97-113.
2. Misra, V.K. and D.E. Draper, *On the role of magnesium ions in RNA stability.* Biopolymers, 1998. **48**(2-3): p. 113-35.
3. DeRose, V.J., *Metal ion binding to catalytic RNA molecules.* Curr Opin Struct Biol, 2003. **13**(3): p. 317-24.
4. Hougland, J.L., et al., *Functional identification of catalytic metal ion binding sites within RNA.* PLoS Biol, 2005. **3**(9): p. e277.
5. Forconi, M., et al., *Functional identification of ligands for a catalytic metal ion in group I introns.* Biochemistry, 2008. **47**(26): p. 6883-94.
6. Shan, S.O. and D. Herschlag, *Dissection of a metal-ion-mediated conformational change in Tetrahymena ribozyme catalysis.* RNA, 2002. **8**(7): p. 861-72.
7. Woodson, S.A., *Metal ions and RNA folding: a highly charged topic with a dynamic future.* Curr Opin Chem Biol, 2005. **9**(2): p. 104-9.
8. Frederiksen, J.K. and J.A. Piccirilli, *Identification of catalytic metal ion ligands in ribozymes.* Methods, 2009. **49**(2): p. 148-66.
9. Chen, J.-H., et al., *A Catalytic Metal Ion Interacts with the Cleavage Site G·U Wobble in the HDV Ribozyme†.* Biochemistry, 2009. **48**(7): p. 1498-1507.
10. Veeraraghavan, N., et al., *Metal Binding Motif in the Active Site of the HDV Ribozyme Binds Divalent and Monovalent Ions.* Biochemistry, 2011. **50**(13): p. 2672-2682.
11. Maderia, M., L.M. Hunsicker, and V.J. DeRose, *Metal−Phosphate Interactions in the Hammerhead Ribozyme Observed by 31P NMR and Phosphorothioate Substitutions†.* Biochemistry, 2000. **39**(40): p. 12113-12120.
12. Osborne, E.M., et al., *The Identity of the Nucleophile Substitution May Influence Metal Interactions with the Cleavage Site of the Minimal Hammerhead Ribozyme.* Biochemistry, 2009. **48**(44): p. 10654-10664.
13. Sigel, R.K., A. Vaidya, and A.M. Pyle, *Metal ion binding sites in a group II intron core.* Nat Struct Biol, 2000. **7**(12): p. 1111-6.
14. Marcia, M. and Anna M. Pyle, *Visualizing Group II Intron Catalysis through the Stages of Splicing.* Cell, 2012. **151**(3): p. 497-507.
15. Gordon, P.M., R. Fong, and J.A. Piccirilli, *A Second Divalent Metal Ion in the Group II Intron Reaction Center.* Chemistry & biology, 2007. **14**(6): p. 607-612.
16. Nelson, J.A. and O.C. Uhlenbeck, *When to believe what you see.* Mol Cell, 2006. **23**(4): p. 447-50.
17. Kazantsev, A.V. and N.R. Pace, *Bacterial RNase P: a new view of an ancient enzyme.* Nat Rev Microbiol, 2006. **4**(10): p. 729-40.
18. Smith, J.K., J. Hsieh, and C.A. Fierke, *Importance of RNA-protein interactions in bacterial ribonuclease P structure and catalysis.* Biopolymers, 2007. **87**(5-6): p. 329-38.
19. Kirsebom, L.A., *RNase P RNA mediated cleavage: substrate recognition and catalysis.* Biochimie, 2007. **89**(10): p. 1183-94.
20. Hall, T.A. and J.W. Brown, *The ribonuclease P family.* Methods Enzymol, 2001. **341**: p. 56-77.
21. Evans, D., S.M. Marquez, and N.R. Pace, *RNase P: interface of the RNA and protein worlds.* Trends Biochem Sci, 2006. **31**(6): p. 333-41.
22. Walker, S.C. and D.R. Engelke, *Ribonuclease P: the evolution of an ancient RNA enzyme.* Crit Rev Biochem Mol Biol, 2006. **41**(2): p. 77-102.
23. Hartmann, E. and R.K. Hartmann, *The enigma of ribonuclease P evolution.* Trends Genet, 2003. **19**(10): p. 561-9.
24. Torres-Larios, A., et al., *Structure of ribonuclease P--a universal ribozyme.* Curr Opin Struct Biol, 2006. **16**(3): p. 327-35.
25. Crary, S., S. Niranjanakumari, and C. Fierke, *The protein component of Bacillus subtilis ribonuclease P increases catalytic efficiency by enhancing interactions with the 5' leader sequence of pre-tRNAAsp.* Biochemistry, 1998. **37**(26): p. 9409-9416.

26. Kurz, J. and C. Fierke, *The affinity of magnesium binding sites in the Bacillus subtilis RNase P x pre-tRNA complex is enhanced by the protein subunit.* Biochemistry, 2002. **41**(30): p. 9545-9558.
27. Kurz, J., S. Niranjanakumari, and C. Fierke, *Protein component of Bacillus subtilis RNase P specifically enhances the affinity for precursor-tRNAAsp.* Biochemistry, 1998. **37**(8): p. 2393-2400.
28. Sun, L., et al., *Evidence that substrate-specific effects of C5 protein lead to uniformity in binding and catalysis by RNase P.* The EMBO journal, 2006. **25**(17): p. 3998-4007.
29. Guerrier-Takada, C., et al., *The RNA moiety of ribonuclease P is the catalytic subunit of the enzyme.* Cell, 1983. **35**(3 Pt 2): p. 849-857.
30. Smith, D. and N.R. Pace, *Multiple magnesium ions in the ribonuclease P reaction mechanism.* Biochemistry, 1993. **32**(20): p. 5273-81.
31. Perreault, J.P. and S. Altman, *Pathway of activation by magnesium ions of substrates for the catalytic subunit of RNase P from Escherichia coli.* J Mol Biol, 1993. **230**(3): p. 750-6.
32. Beebe, J.A., J.C. Kurz, and C.A. Fierke, *Magnesium ions are required by Bacillus subtilis ribonuclease P RNA for both binding and cleaving precursor tRNAAsp.* Biochemistry, 1996. **35**(32): p. 10493-505.
33. Cassano, A.G., V.E. Anderson, and M.E. Harris, *Analysis of Solvent Nucleophile Isotope Effects: Evidence for Concerted Mechanisms and Nucleophilic Activation by Metal Coordination in Nonenzymatic and Ribozyme-Catalyzed Phosphodiester Hydrolysis†.* Biochemistry, 2004. **43**(32): p. 10547-10559.
34. Cuzic, S. and R.K. Hartmann, *Studies on Escherichia coli RNase P RNA with Zn2+ as the catalytic cofactor.* Nucleic Acids Res, 2005. **33**(8): p. 2464-74.
35. Brannvall, M. and L.A. Kirsebom, *Manganese ions induce miscleavage in the Escherichia coli RNase P RNA-catalyzed reaction.* J Mol Biol, 1999. **292**(1): p. 53-63.
36. Smith, D., et al., *Influence of metal ions on the ribonuclease P reaction. Distinguishing substrate binding from catalysis.* J Biol Chem, 1992. **267**(4): p. 2429-36.
37. Kurz, J.C. and C.A. Fierke, *The affinity of magnesium binding sites in the Bacillus subtilis RNase P x pre-tRNA complex is enhanced by the protein subunit.* Biochemistry, 2002. **41**(30): p. 9545-58.
38. Hsieh, J., et al., *A divalent cation stabilizes the active conformation of the B. subtilis RNase P•pre-tRNA complex: a role for an inner-sphere metal ion in RNase P* submitted, 2010.
39. Warnecke, J.M., et al., *Ribonuclease P (RNase P) RNA is converted to a Cd(2+)-ribozyme by a single Rp-phosphorothioate modification in the precursor tRNA at the RNase P cleavage site.* Proceedings of the National Academy of Sciences, 1996. **93**(17): p. 8924-8928.
40. Li, X. and P. Gegenheimer, *Ribonuclease P Catalysis Requires Mg2+ Coordinated to the pro-RP Oxygen of the Scissile Bond†.* Biochemistry, 1997. **36**(9): p. 2425-2438.
41. Pfeiffer, T., et al., *Effects of phosphorothioate modifications on precursor tRNA processing by eukaryotic RNase P enzymes.* Journal of Molecular Biology, 2000. **298**(4): p. 559-565.
42. Warnecke, J.M., et al., *Active site constraints in the hydrolysis reaction catalyzed by bacterial RNase P: analysis of precursor tRNAs with a single 3'-S-phosphorothiolate internucleotide linkage.* Nucleic Acids Research, 2000. **28**(3): p. 720-727.
43. Persson, T., S. Cuzic, and R.K. Hartmann, *Catalysis by RNase P RNA: UNIQUE FEATURES AND UNPRECEDENTED ACTIVE SITE PLASTICITY.* Journal of Biological Chemistry, 2003. **278**(44): p. 43394-43401.
44. Reiter, N.J., et al., *Structure of a bacterial ribonuclease P holoenzyme in complex with tRNA.* Nature, 2010. **468**(7325): p. 784-9.
45. Christian, E.L., N.M. Kaye, and M.E. Harris, *Helix P4 is a divalent metal ion binding site in the conserved core of the ribonuclease P ribozyme.* RNA, 2000. **6**(4): p. 511-519.
46. Crary, S.M., J.C. Kurz, and C.A. Fierke, *Specific phosphorothioate substitutions probe the active site of Bacillus subtilis ribonuclease P.* RNA, 2002. **8**(7): p. 933-47.
47. Christian, E.L., N.M. Kaye, and M.E. Harris, *Evidence for a polynuclear metal ion binding site in the catalytic domain of ribonuclease P RNA.* EMBO J, 2002. **21**(9): p. 2253-62.
48. Frank, D.N. and N.R. Pace, *In vitro selection for altered divalent metal specificity in the RNase P RNA.* Proc Natl Acad Sci U S A, 1997. **94**(26): p. 14355-60.

49. Frank, D.N. and N.R. Pace, *Ribonuclease P: unity and diversity in a tRNA processing ribozyme.* Annu Rev Biochem, 1998. **67**: p. 153-80.
50. Getz, M.M., et al., *Structural plasticity and Mg2+ binding properties of RNase P P4 from combined analysis of NMR residual dipolar couplings and motionally decoupled spin relaxation.* RNA, 2007. **13**(2): p. 251-66.
51. Koutmou, K.S., et al., *NMR and XAS reveal an inner-sphere metal binding site in the P4 helix of the metallo-ribozyme ribonuclease P.* Proc Natl Acad Sci U S A, 2010. **107**(6): p. 2479-84.
52. Kazantsev, A.V., A.A. Krivenko, and N.R. Pace, *Mapping metal-binding sites in the catalytic domain of bacterial RNase P RNA.* RNA, 2009. **15**(2): p. 266-276.
53. Kaye, N.M., et al., *Conservation of Helical Structure Contributes to Functional Metal Ion Interactions in the Catalytic Domain of Ribonuclease P RNA.* Journal of Molecular Biology, 2002. **324**(3): p. 429-442.
54. Christian, E.L., et al., *The P4 metal binding site in RNase P RNA affects active site metal affinity through substrate positioning.* RNA, 2006. **12**(8): p. 1463-1467.
55. Reiter, N.J., A.K. Osterman, and A. Mondragón, *The bacterial ribonuclease P holoenzyme requires specific, conserved residues for efficient catalysis and substrate positioning.* Nucleic Acids Research, 2012. **40**(20): p. 10384-10393.
56. Koutmou, K.S., et al., *Protein–Precursor tRNA Contact Leads to Sequence-Specific Recognition of 5′ Leaders by Bacterial Ribonuclease P.* Journal of Molecular Biology, 2010. **396**(1): p. 195-208.
57. Kazantsev, A.V., et al., *Crystal structure of a bacterial ribonuclease P RNA.* Proceedings of the National Academy of Sciences of the United States of America, 2005. **102**(38): p. 13392-13397.
58. Kurz, J.C., S. Niranjanakumari, and C.A. Fierke, *Protein component of Bacillus subtilis RNase P specifically enhances the affinity for precursor-tRNAAsp.* Biochemistry, 1998. **37**(8): p. 2393-400.
59. Koutmou, K.S., J.J. Day-Storms, and C.A. Fierke, *The RNR motif of B. subtilis RNase P protein interacts with both PRNA and pre-tRNA to stabilize an active conformer.* RNA, 2011. **17**(7): p. 1225-1235.
60. Koutmou, K.S., J.J. Day-Storms, and C.A. Fierke, *The RNR motif of B. subtilis RNase P protein interacts with both PRNA and pre-tRNA to stabilize an active conformer.* RNA, 2011. **17**(7): p. 1225-35.
61. Hsieh, J. and C.A. Fierke, *Conformational change in the Bacillus subtilis RNase P holoenzyme–pre-tRNA complex enhances substrate affinity and limits cleavage rate.* RNA, 2009. **15**(8): p. 1565-1577.
62. Hsieh, J., et al., *A divalent cation stabilizes the active conformation of the B. subtilis RNase P x pre-tRNA complex: a role for an inner-sphere metal ion in RNase P.* J Mol Biol, 2010. **400**(1): p. 38-51.
63. Pecoraro, V.L., J.D. Hermes, and W.W. Cleland, *Stability constants of Mg2+ and Cd2+ complexes of adenine nucleotides and thionucleotides and rate constants for formation and dissociation of MgATP and MgADP.* Biochemistry, 1984. **23**(22): p. 5262-71.
64. Frank, D.N. and N.R. Pace, *RIBONUCLEASE P: Unity and Diversity in a tRNA Processing Ribozyme.* Annual Review of Biochemistry, 1998. **67**(1): p. 153-180.
65. Kaye, N.M., et al., *Conservation of helical structure contributes to functional metal ion interactions in the catalytic domain of ribonuclease P RNA.* J Mol Biol, 2002. **324**(3): p. 429-42.
66. Pan, T. and T.R. Sosnick, *Intermediates and kinetic traps in the folding of a large ribozyme revealed by circular dichroism and UV absorbance spectroscopies and catalytic activity.* Nat Struct Biol, 1997. **4**(11): p. 931-8.
67. Hsieh, J. and C.A. Fierke, *Conformational change in the Bacillus subtilis RNase P holoenzyme--pre-tRNA complex enhances substrate affinity and limits cleavage rate.* RNA, 2009. **15**(8): p. 1565-77.
68. Frederiksen, J.K., et al., *Metal-ion rescue revisited: Biochemical detection of site-bound metal ions important for RNA folding.* RNA, 2012. **18**(6): p. 1123-1141.
69. Ferre-D'Amare, A.R., K. Zhou, and J.A. Doudna, *Crystal structure of a hepatitis delta virus ribozyme.* Nature, 1998. **395**(6702): p. 567-74.

70. Harris, D.A., D. Rueda, and N.G. Walter, *Local Conformational Changes in the Catalytic Core of the Trans-Acting Hepatitis Delta Virus Ribozyme Accompany Catalysis†.* Biochemistry, 2002. **41**(40): p. 12051-12061.
71. Ke, A., et al., *A conformational switch controls hepatitis delta virus ribozyme catalysis.* Nature, 2004. **429**(6988): p. 201-5.
72. Peracchi, A., et al., *Rescue of abasic hammerhead ribozymes by exogenous addition of specific bases.* Proc Natl Acad Sci U S A, 1996. **93**(21): p. 11522-7.
73. Loria, A. and T. Pan, *Domain structure of the ribozyme from eubacterial ribonuclease P.* RNA, 1996. **2**(6): p. 551-63.
74. Kazantsev, A.V., et al., *Solution structure of RNase P RNA.* RNA, 2011. **17**(6): p. 1159-1171.
75. Torres-Larios, A., et al., *Crystal structure of the RNA component of bacterial ribonuclease P.* Nature, 2005. **437**(7058): p. 584-7.
76. Wu, H.N. and O.C. Uhlenbeck, *Role of a bulged A residue in a specific RNA-protein interaction.* Biochemistry, 1987. **26**(25): p. 8221-7.
77. Ippolito, J.A. and T.A. Steitz, *A 1.3-A resolution crystal structure of the HIV-1 trans-activation response region RNA stem reveals a metal ion-dependent bulge conformation.* Proc Natl Acad Sci U S A, 1998. **95**(17): p. 9819-24.
78. Reiter, N.J., et al., *Dynamics in the U6 RNA intramolecular stem-loop: a base flipping conformational change.* Biochemistry, 2004. **43**(43): p. 13739-47.
79. Blad, H., et al., *Dynamics and metal ion binding in the U6 RNA intramolecular stem-loop as analyzed by NMR.* J Mol Biol, 2005. **353**(3): p. 540-55.
80. Yean, S.L., et al., *Metal-ion coordination by U6 small nuclear RNA contributes to catalysis in the spliceosome.* Nature, 2000. **408**(6814): p. 881-4.
81. Huppler, A., et al., *Metal binding and base ionization in the U6 RNA intramolecular stem-loop structure.* Nat Struct Biol, 2002. **9**(6): p. 431-5.
82. Rueda, D., et al., *The 5' leader of precursor tRNAAsp bound to the Bacillus subtilis RNase P holoenzyme has an extended conformation.* Biochemistry, 2005. **44**(49): p. 16130-9.
83. Walter, N.G., *The blessing and curse of RNA dynamics: past, present, and future.* Methods, 2009. **49**(2): p. 85-6.
84. Dethoff, E.A., et al., *Functional complexity and regulation through RNA dynamics.* Nature, 2012. **482**(7385): p. 322-30.
85. Dethoff, E.A., et al., *Visualizing transient low-populated structures of RNA.* Nature, 2012. **491**(7426): p. 724-8.
86. Morrison, K.L. and G.A. Weiss, *Combinatorial alanine-scanning.* Current Opinion in Chemical Biology, 2001. **5**(3): p. 302-307.
87. Behrman, E.J., *An improved synthesis of guanosine 5'-monothiophosphate.* Journal of Chemical Research (Synopses), 2000. **2000**(9): p. 446-447.
88. He, B., et al., *Rapid mutagenesis and purification of phage RNA polymerases.* Protein Expr Purif, 1997. **9**(1): p. 142-51.
89. Niranjanakumari, S., et al., *Protein component of the ribozyme ribonuclease P alters substrate recognition by directly contacting precursor tRNA.* Proc Natl Acad Sci U S A, 1998. **95**(26): p. 15212-7.
90. Niranjanakumari, S., J.C. Kurz, and C.A. Fierke, *Expression, purification and characterization of the recombinant ribonuclease P protein component from Bacillus subtilis.* Nucleic Acids Res, 1998. **26**(13): p. 3090-6.
91. Moore, M.J. and C.C. Query, *Joining of RNAs by splinted ligation.* Methods Enzymol, 2000. **317**: p. 109-23.
92. Kurschat, W.C., et al., *Optimizing splinted ligation of highly structured small RNAs.* RNA, 2005. **11**(12): p. 1909-14.
93. Ke, A. and J.A. Doudna, *Crystallization of RNA and RNA-protein complexes.* Methods, 2004. **34**(3): p. 408-14.
94. Mocz, G., et al., *Probing the nucleotide binding sites of axonemal dynein with the fluorescent nucleotide analogue 2'(3')-O-(-N-Methylanthraniloyl)-adenosine 5'-triphosphate.* Biochemistry, 1998. **37**(27): p. 9862-9.

# CHAPTER 4

# SUBSTRATE RECOGNITION OF HUMAN MITOCHONDRIAL RNASE P: PROTEIN PURIFICATION AND PRE-TRNA CLONING

## 4.1 Abstract

The essential step of removing extraneous sequences at the 5' end of precursor tRNA (pre-tRNA) is catalyzed by ribonuclease P (RNase P), a ribonucleoprotein complex in most organisms. However, recently discovered human mitochondrial RNase P (mtRNase P) is composed solely of three protein subunits (MRPP1, MRPP1 and MRPP3). Mutations in mtRNase P subunits and mitochondrial transfer RNAs (mt-tRNAs) have been implicated in a number of human diseases. Moreover, the majority of mt-tRNAs lack consensus sequences conserved for secondary and tertiary structures in classic tRNA. Both human mtRNase P and mt-tRNAs are poorly characterized. To study the catalytic mechanism and substrate recognition of human mtRNase P, I have optimized purification of mtRNase P and subcloned a series of human mitochondrial precursor tRNA (mt-pre-tRNA) genes that include all four types of human mt-tRNA. The reconstituted human mtRNase P complex as well as MRPP3 subunit alone are catalytically active under single-turnover conditions. This work lays the foundation to investigate the catalytic mechanism and mt-pre-tRNA recognition by human mtRNase P.

## 4.2 Background

Mitochondrial dysfunction is increasingly implicated in human aging, neurodegenerative diseases, cancer, diabetes and various rare diseases [1, 2]. Dysfuntion of mitochondria often originates from damages and mutations in the mitochondrial genomic DNA (mtDNA) [3-7]. Recent advances in RNA sequencing technology and identification of mitochondrial RNA processing and modification enzymes provided new ground for investigation of RNA biogenesis in human mitochondria [8-10]. In addition, nearly half of the disease-related mtDNA point mutations are mapped to mt-tRNA genes [11, 12]. Unraveling the mechanism of human mt-tRNA processing may provide valuable insights into understanding mitochondria-related diseases.

### 4.2.1 RNA Processing in Human Mitochondria

The compact human mitochondrial genome is maternally inherited with a circular mitochondrial DNA (mtDNA) 16,569 bp in length and encodes genes for all 13 proteins of respiratory chain complexes, 2 rRNAs (12S and 16S), and 22 tRNAs [13] (Figure 4-1). Human mtDNA is transcribed into three long polycistronic precursor RNAs from both strands (termed “heavy” and “light”) with tRNAs intermingled with rRNAs and mRNAs [14]. These precursor RNAs are processed according to the “tRNA punctuation model” in which recognition and excision of tRNA genes by endonucleases are the first steps for mitochondrial mRNA biogenesis [15, 16]. Recently, comprehensive analysis of the mitochondrial transcriptome identified small RNA transcripts derived mostly from mt-tRNAs genes [9]. Deep sequencing also identified long noncoding RNAs (lncRNAs) that are

generated from 5' end processing of light strand transcripts [17]. Biological functions and biogenesis pathways of these mitochondrial sRNAs and lncRNAs are unclear.

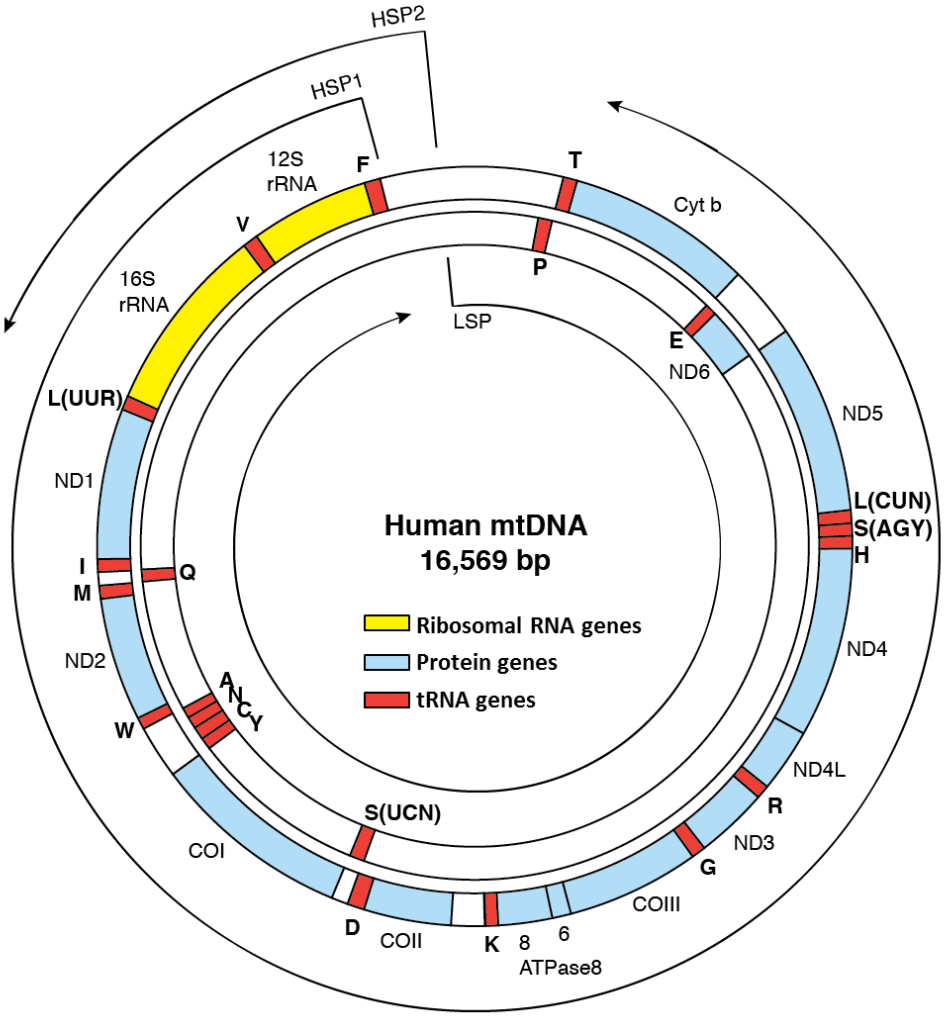


**Figure 4-1:** Distribution of tRNA genes in human mitochondrial genome. The mt-tRNA genes (red) are interspersed in the genome [13]. Human mt-tRNA genes are located in both the heavy and light DNA strands. The black arrows indicate the transcription direction from two heavy-strand promoter (HSP) sites and one light-strand promoter (LSP) site [18].

### 4.2.2 Mitochondrial tRNA Mutations and Diseases

A growing number of mtDNA mutations are implicated in human diseases (see summary in MITOMAP database [19]). With approximately 500 disease-related point mutations reported to date, more than 230 are located in all 22 mt-tRNA genes

(Figure 4-2). Clinical phenotypes of these mutations are diverse, including MELAS (mitochondrial myopathy, encephalopathy, lactic acidosis and stroke-like symptoms), LHON (Leber's hereditary optic neuropathy), opthalmoplegia, deafness, hypotension and diabetes [3, 7].

Understanding how mt-tRNA mutations link to human diseases remains challenging due to the heterogeneity and polymorphic nature of mtDNA, complex combinations between genotype and phenotype, and lack of animal models [20-22]. Solution structure probing showed that pathogenic mutations can affect secondary structure of *in vitro* transcribed mt-tRNAs [12] by destabilizing tertiary contacts [23, 24], causing dimerization of mt-tRNA [24], and weakening structural elements [24, 25]. Biochemical studies also showed that pathogenic mutations in mt-tRNA lead to functional defects in 5' and 3' processing [26-28], posttranscriptional modification [23, 29, 30], aminoacylation [25, 31, 32], and protein synthesis [32-34]. The molecular mechanism of how these pathogenic mutations affect mt-tRNA processing has yet to be investigated by detailed kinetic and structural approaches.

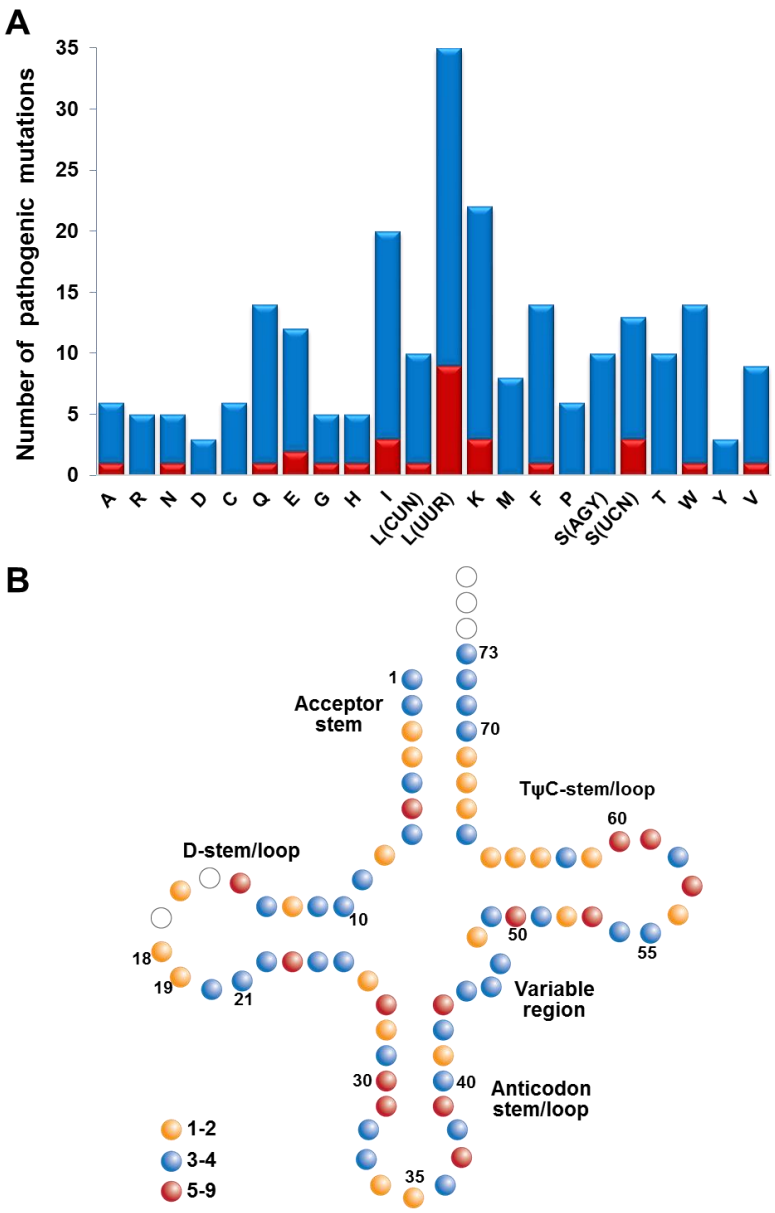


**Figure 4-2:** Distribution and location of disease-associated mutations in human mitochondrial tRNA genes. Data for this graph were generated from analysis of a summary on disease-associated mutations as of March 5, 2013 (see MITOMAP database: http://mitomap.org [19] and Mamit-tRNA database http://mamit-trna.u-strasbg.fr/ [35]). **(A)** A bar graph showing distribution of pathogenic mutations among 22 human mt-tRNA species. Total bar height is equal to the total number of disease-related mutations published in literature while red bars indicate numbers of confirmed pathogenic mutations (definition of "confirmed" in MITOMAP database means reported by at least two independent laboratories). **(B)** Distribution of pathogenic mutations in human mt-tRNA in the context of canonical tRNA secondary structure. Numbers are calculated from total reported mutations. The nucleotide is color-coded according to the number of mt-tRNA species affected by mutations at each nucleotide position. Nucleotide numbering is in accordance to consensus numbering by tRNAdb system (http://trnadb.bioinf.uni-leipzig.de/) [36].

### 4.2.3 The "Bizarre" Human Mitochondrial tRNA

In addition to high mutation rates, mammalian mitochondrial tRNAs are often referred as "bizarre tRNAs" because the majority of mt-tRNAs deviate significantly from the canonical tRNA with secondary cloverleaf structure and tertiary L-shaped structure [18, 35-38]. Although numerous X-ray and NMR structures of canonical tRNAs have been solved either in free form or in complex with proteins [39], only a few NMR studies have been reported on stem-loop elements [40] and full length [41] mammalian mt-tRNAs.

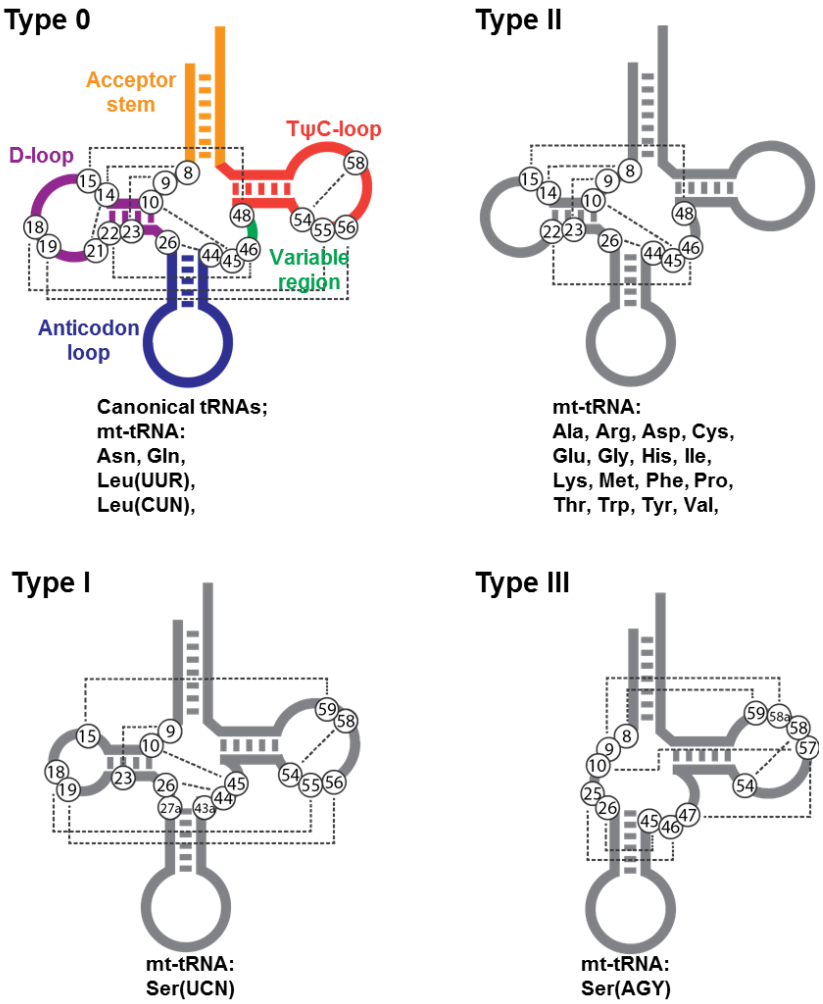


**Figure 4-3:** Four types of human mitochondrial tRNA based on prediction in secondary structure and tertiary interactions with reference to canonical tRNA. Predicted tertiary interactions are indicated by dotted line and conserved nucleotides are circled [18, 37].

Based on sequence conservation and tertiary interactions, mammalian mt-tRNAs can be categorized into four types (Figure 4-3) [18, 37]. The first type (termed Type 0) preserves of the majority of nucleotides involved in canonical tertiary interactions between D-loop/TψC-loop and D-stem-loop/V-loop [42]. The second type (Type I) is comprised only of mt-tRNA$^{Ser(UCN)}$ where the D-loop/TψC-loop interaction is conserved (G18 and G19 in the D-loop, and U55 and C66 in the TψC-loop), alhough D-loop is shortened [43]. In addition, mt-tRNA$^{Ser(UCN)}$ has only one nucleotide (N9), instead of two, linking the acceptor- and D-stem and a 6-bp anticodon-stem instead of 5-bp. The majority of human mt-tRNAs are grouped to the third type (type II). Type II mt-tRNAs lack a strong D-loop/TψC-loop interaction but utilize conserved nucleotides in the D-stem and V-loop to form tertiary contacts [44]. The mt-tRNA$^{Ser(AGY)}$ is the sole member of type III mt-tRNA, which completely lacks the D-stem-loop and forms a non-L-shaped structure in solution [45, 46].

Mitochondrial proteins and mt-tRNAs have been observed to co-evolved. For example, in nematode mitochondria, the elongation factor Tu that has an extended domain to compensate the shortened D-arm or T-armless mt-tRNAs with [47, 48]. It is possible that RNA processing enzymes have specifically evolved to recognize non-canonical mt-tRNAs in human mitochondria.

### 4.2.4 Human Mitochondrial RNase P

RNase P is responsible for 5’ end processing of tRNA by catalyzing hydrolysis of a phosphodiester bond between N(-1) and N1 nucleotides of pre-tRNA [49]. In human mitochondria, RNase P is composed of three protein subunits (Mitochondrial

RNase P proteins, MRPP1, MRPP2, and MRPP3) [50]. This is the first example of a protein-only RNase P. All of the previous identified isoforms of RNase P are ribonucleoprotein (RNP) complexes composed of one catalytic RNA subunit and variable numbers of protein subunits (1 in Bacteria, 4-5 in Archaea and 9-10 in Eukarya) [51-53] (Figure 4-4). Proteinaceous RNase P (PRORP) has also been identified in *Arabidopsis thaliana* where PRORP1 is localized in mitochondria and chloroplast [54], and PRORP2 and PRORP3 are localized in the nucleus [55]. *A. thaliana* PRORPs are orthologs of MRPP3 but function as a single protein for RNase P activity. None of the protein-only RNase P shares significant sequence homology with previous identified protein subunits in RNA-based RNase P. Such a dramatic variety in subunit composition makes RNase P one of the most diverse enzymes and provides an exciting model system to directly compare RNA and protein based catalysis [56].

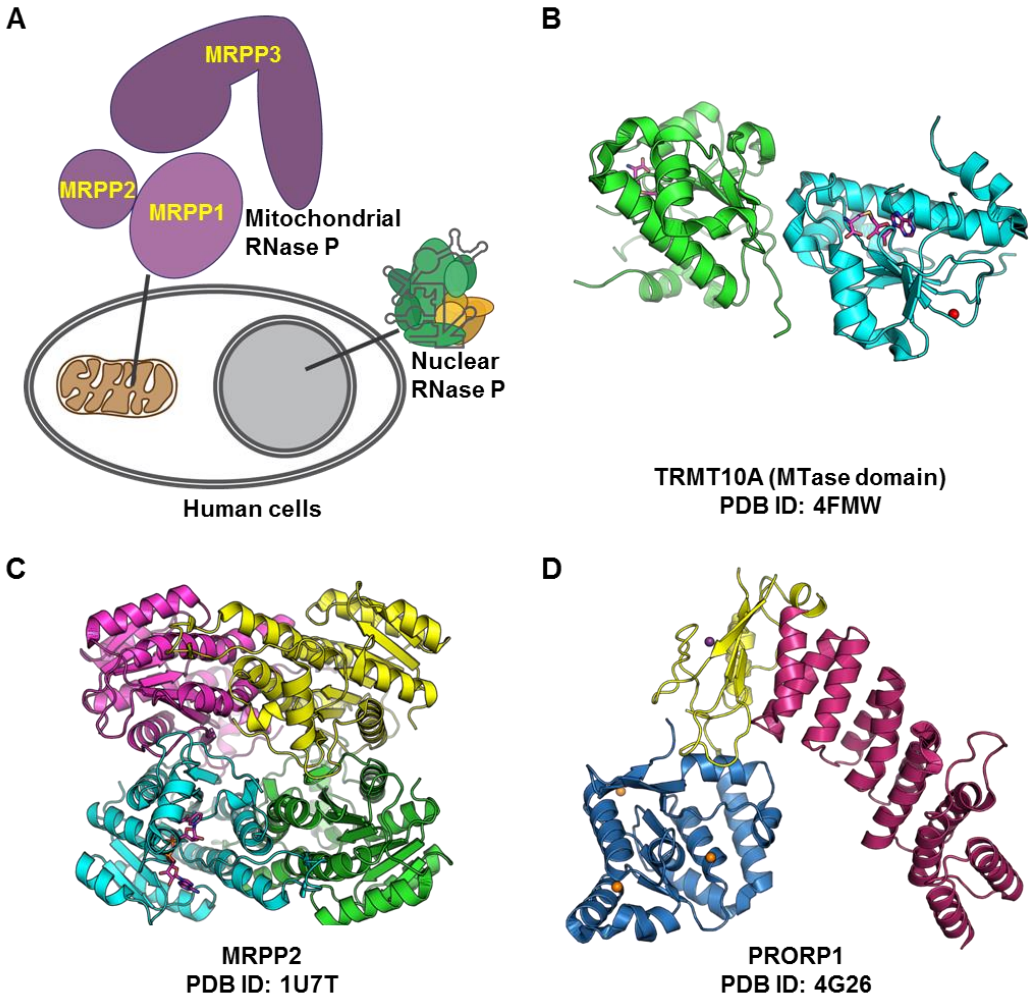


**Figure 4-4:** Human mitochondrial RNase P is composed of three protein subunits. **(A)** Diagram showing different composition of RNase P in human. A ribonucleoprotein RNase P is located in the nucleus and a protein-only RNase P that is formed by three subunits functions in the mitochondria. **(B)** Crystal structure of the methyltransferase domain (MTase domain, C-terminal) of TRMT10A, a MRPP1 analog (PDB ID: 4FMW [57]), showing a homodimer of the MT domain bound with *S*-adenosyl-L-homocysteine (SAH, magenta molecules) and a potassium ion (red sphere). **(C)** MRPP2 crystal structure (PDB ID: 1U7T [58]) as a homotetramer and in complex with nicotinamide adenine dinucleotide (NAD, magenta). **(D)** Crystal structure for PRORP1, an ortholog of MRPP3 in plant *A. thaliana* (PDB ID: 4G26 [59]), showing the metallonuclease domain (blue) with calcium ions (orange spheres), central domain (yellow) with a zinc ion (purple sphere) and the PPR domain (dark pink).

All three subunits of human mtRNase are nuclear encoded and imported into the mitochondria [50]. The first subunit, MRPP1 (gene symbol RG9MTD1, or official name TRMT10C) is an *S*-adenosyl-methionine (SAM) dependent tRNA $m^1G$

methyltransferase [60] that belongs to the TRMT10 family [61]. MRPP1 requires activation by MRPP2 to catalyze the $N^1$ methylation of both G9 and A9 ($m^1R9$) in mt-tRNA *in vitro* and *in vivo* [60]. MRPP1·MRPP2 complex also methylates a nuclear $tRNA^{Arg}$ efficiently [60]. In contrast, MRPP1 paralogs, TRMT10A and TRMT10B, function as a single protein to catalyze $m^1G$ methylation of the nuclear $tRNA^{Arg}$ *in vitro* [60]. Interestingly, a 20-fold higher concentration of MRRP1 alone can also catalyze $m^1G$ methylation of the nuclear $tRNA^{Arg}$ albeit with an at least 20-fold lower efficiency. However, MRPP1 alone cannot catalyze $m^1A$ of mt-$tRNA^{Ile}$. These data indicate that MRPP1 has innate methyltransferase activity but requires MRPP2 for efficiency and specificity toward mt-tRNA [60]. A crystal structure of the MTase domain (C-terminal) of TMRT10A in complex with *S*-adenosyl-homocysteine (SAH) is deposited in PDB (Figure 4-4, PDB ID: 4FMW [57]). This unpublished work shows the first crystal structure of the MTase domain of the TRMT10 family. The C-terminal MTase domain (amino acids 190 to 380) of MRPP1 likely adopts a fold similar to that observed in this structure according to homology structure modeling (Figure C-1, Appendix C). However, the structures of the N-terminal region (amino acids 40-190) of MRPP1 and other TRMT10 family MTase remain to be solved.

The second human mtRNase P subunit, MRRP2 (HSD17B10, or SDR5C1), is a short-chain dehydrogenase/reductase that catalyzes β-oxidation of steroid and fatty acid substrates using $NAD^+$ as a co-substrate [62, 63] (Figure 4-4 and Figure 1-4, Chapter 1). Dysfunction of MRPP2 is also implicated in neurodegenerative diseases such as Alzheimer's disease [64, 65]. MRPP2 has a Rossman-fold motif which binds nicotinamide adenine dinucleotide ($NAD^+$) [63]. In solution and in crystal

structures, MRPP2 forms a homotetramer as shown in complex with $NAD^+$ and an inhibitor (PDB ID: 1U7Z [58], Figure 4-4), or has a deformed active site upon β-amyloid (Aβ) binding (PDB ID 1SO8 [64]).

The third subunit of human mtRNase P, MRPP3 (KIAA0391, or PRORP), is an ortholog of *A. thaliana* PRORP1 [50, 59]. The recently solved crystal structure of PRORP1 reveals that this new class of metallonuclease combines three functional domains to replace the RNA-based RNase P catalyst: a metallonuclease domain (NYN/PIN-domain) containing the active site, a central zinc-binding structural domain, and pentatricopeptide repeats (a PPR domain) important for activity and substrate binding [59] (Figure 4-4). PRORP1 is activated by magnesium and manganese ions *in vitro* and is proposed to use a two-metal-ion general acid/base catalysis mechanism [59]. In contrast to PRORP1, MRPP3 requires both MRPP1 and MRPP2 to catalyzedcleavage of mt-pre-tRNAs [50]. But catalytic activity of MRPP1 and MRPP2 are not required for mtRNase P cleavage activity [60]. Furthermore, the MRPP1·MRPP2 subcomplex does not tighly bind to MRPP3 [50]. The molecular details of exact roles of MRPP1, MRPP2 and MRPP3 in mtRNase P catalysis and substrate recognition remain to be elucidated.

Knockdown of each mtRNase P subunits by siRNA in HeLa cells lead to a deficiency in processing of two mtRNA species [50]. Further, deep sequencing results showed that siRNA knockdown of either MRPP1 or MRPP3 genes leads to accumulation of most mitochondrial precursor RNAs and consequently impaired protein synthesis [8]. MRPP1 and MRPP3 knockdown also affect processing of long noncoding RNAs transcribed from the light strand of mtDNA and likely recognize

structures in the light strand transcript that mirror the sequence of tRNAs in the opposite (heavy) strand [17]. Interestingly, MRPP1 and 2 have been recently showed to co-localize and interact with a newly identified RNA-binding protein, G-rich sequence factor 1 (GRSF1), in conjunction with nascent RNA transcripts to form so called “mitochondrial RNA granules” [66]. GRSF1 contains a RNA recognition motif (RRM) and siRNA knockdown of this protein leads to accumulations of certain mt-tRNA and ncRNA precursors [66] and subsequent defects in mitochondrial protein synthesis [67]. These findings suggest that mtRNase P may function as a catalytic subunit in a larger complex that processes a variety of mitochondrial RNAs.

In recognition of pre-tRNA substrates, both commonality and specificity exist among protein-only and RNA-based RNase P enzymes. It is not unexpected that *A. thaliana* PRORPs (1, 2 and 3) can catalyze cleavage a bacterial substrate (*T. thermophilus* pre-tRNA$^{Gly}$) [68] since plant nuclear and organellar tRNAs are mostly canonical [39, 69]. In a structural model proposed from footprinting and small angle X-ray scattering (SAXS) data, PRORP2 is proposed to interact with *A. thaliana* mt-tRNA$^{Cys}$ in a topology that is similar to the bacterial RNase P ternary complex [70, 71]. In this model, the cleavage site of tRNA is recognized by the metallonuclease domain of PRORP2 whereas the D-TψC-loop interacts with the PPR-domain [70]. Human nuclear RNase P (nRNase P) does not detectably catalyize cleavage a mt-pre-tRNA$^{Tyr}$, but both human mtRNase P and nRNase P can catalyze cleavage of a mt-pre-tRNA$^{Leu(UUR)}$ [72]. The non-canonical features of human mt-tRNAs may explain why human mtRNase P require two additional subunits to recognize the substrates. However, systematic identification of structural determinants and

molecular interactions involved in substrate recognition and catalysis by human mtRNase P has yet to be carried out.

To investigate substrate recognition of human mtRNase P, I purified all three human mtRNase P proteins using recombinant expression from *E. coli* cells. A co-purification strategy for MRRP1 and MRPP2 was developed to produce a MRPP1·MRPP2 complex with optimum purity. A series of human mitochondrial precursor tRNA (mt-pre-tRNA) genes covering all four types of mt-tRNA species have also been subcloned into high-copy number plasmids. Single-turnover cleavage results demonstrate that the recombinant mtRNase P is active *in vitro*. Furthermore, activity measurements demonstrate that the metallonuclease subunit, MRPP3, has vestigial nuclease activity that is activiated by MRPP1·MRPP2 for efficient and accurate RNase P activity.

## 4.3 Results

### 4.3.1 Co-expression and Co-purification of the MRPP1·MRPP2 Complex

Protein co-overexpression facilitates expression and purification of protein complexes in *E. coli* cells [73, 74]. Among the three subunits of human mtRNase P, MRPP1 and MRPP2 form a stable subcomplex [50, 60]. To enhance expression and purification of MRPP1, the gene sequences encoding MRPP1 and MRPP2 were subcloned into a co-expression vector (pCDFDuet-1) for recombinant expression and purification of the MRPP1·MRPP2 complex (Figure 4-5). The MRPP1 gene corresponding to amino acid 40 to 403 (Δ39MRPP1, MRPP1 in short, 42 kDa) was amplified from a plasmid containing MRPP1 encoding sequences and subcloned

between the NcoI and BamHI restriction sites downstream of the T7 promoter-1 (see Materials and Methods). This construct adds as an N-terminal hexa-histidine-tag followed by a TEV-protease cleavage site (HisTevMRPP1, Figure 4-5). The first 39 amino acids sequence removed from the N-terminal of MRPP1 genes are mitochondrial localization sequences. The DNA sequence encoding the entire MRPP2 was inserted between the NdeI and XhoI restriction sites downstream of T7 promoter-2 (MRPP2, 26 kDa, Figure 4-5). Plasmids containing alternative combinations of MRPP1 and MRPP2 genes with different types and locations of His-tags have also been prepared and screened for optimum co-overexpression and co-purification conditions (Table C-1, Appendix C).

**A**

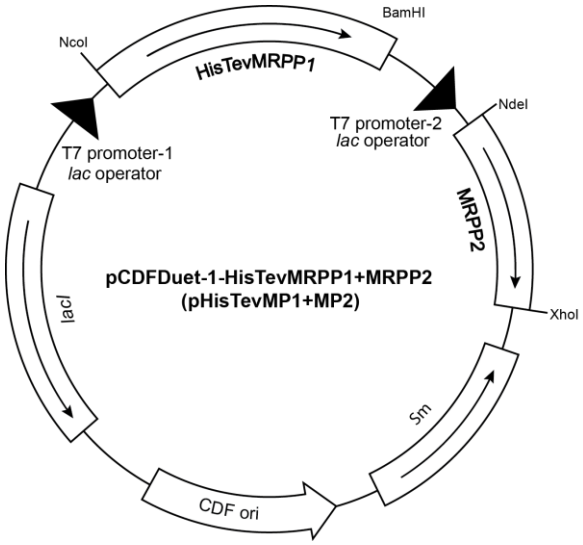


**B**

MKHHHHHHPMSDYDIPTTENLYFQG/HMSSKIPAVTYPKNESTPPSEELELDKWKTTMKSSVQEECVSTISSSKDE
DPLAATREFIEMWRLLGREVPEHITEEELKTLMECVSNTAKKKYLKYLYTKEKVKKARQIKKEMKAAAREEAKNIK
LLETTEEDKQKNFLFLRLWDRNMDIAMGWKGAQAMQFGQPLVFDMAYENYMKRKELQNTVSQLLESEGWNRRNVDP
FHIYFCNLKIDGALHRELVKRYQEKWDKLLLTSTEKSHVDLFPKDSIIYLTADSPNVMTTFRHDKVYVIGSFVDKS
MQPGTSLAKAKRLNLATECLPLDKYLQWEIGNKNLTLDQMIRILLCLKNNGNWQEALQFVPKRKHTGFLEISQHSQ
EFINRLKKAKT

**C**

MAAACRSVKGLVAVITGGASGLGLATAERLVGQGASAVLLDLPNSGGEAQAKKLGNNCVFAPADVTSEKDVQTALA
LAKGKFGRVDVAVNCAGIAVASKTYNLKKGQTHTLEDFQRVLDVNLMGTFNVIRLVAGEMGQNEPDQGGQRGVIIN
TASVAAFEGQVGQAAYSASKGGIVGMTLPIARDLAPIGIRVMTIAPGLFGTPLLTSLPEKVCNFLASQVPFPSRLG
DPAEYAHLVQAIIENPFLNGEVIRLDGAIRMQP

**Figure 4-5:** Co-expression plasmid and protein sequences for MRPP1 and MRPP2. **(A)** A pCDFDuet-1-His6TevMRPP1+MRPP2 (pHisTevMP1+MP2) co-expression vector encoding HisTevMRPP1 and MRPP2 behind two independent T7 promoters. **(B)** Amino acid sequences of MRPP1 protein encoded by pCDFHisTevMP1MP2 plasmid with a His-tag highlighted in yellow, TEV protease cleavage sequence in cyan (cleavage site indicated) and MRPP1 protein sequence (amino acid 40 to 403) underlined. **(C)** Full length MRPP2 protein (amino acids 1 to 261) encoded by pHisTevMP1+MP2 plasmid.

To optimize recombinant overexpression and co-purification of HisTevMRPP1 and MRPP2 in *E. coli* cells, a matrix of conditions varying cell lines, growth media and temperature, IPTG concentrations and expression time was tested, as described in Materials and Methods (results summarized in Table C-1, Appendix C). Expression of soluble MRPP1 is optimal when the co-expression plasmid containing HisTevMRPP1 and native MRPP2 (Figure 4-5) was transformed into RosettaDE3

cells and expressed using auto-induction media at 25˚C overnight. MRPP2 generally expresses at a higher level than MRPP1 under all conditions tested. The HisTev-tag on MRPP1 allows for purification of the MRPP1·MRPP2 complex.

MRPP1 and MRPP2 co-expressed by RossttaDE3 cells and auto-induction was purified by two rounds of immobilized-metal affinity chromatography (IMAC) with chelating sepharose resins charged with $NiSO_4$ (Figure 4-6). On the first Ni(II)-column, HisTev-tagged MRPP1 co-eluted with native non-tagged MRPP2 at 120 mM imidazole after extensive washing of the loaded Ni(II)-column with 55 mM and 120 mM imidazole sequentially to separate protein impurities followed by 1 M NaCl (15 mM imidazole) wash to remove nucleic acids (Figure 4-6). The HisTev-tag in MRPP1 was removed by TEV protease digestion and the MRPP1·MRPP2 complex was further purified by a second Ni(II)-column (Figure 4-5). An MRPP1·MRPP2 complex of high purity were obtained from the second Ni(II) column. Previously observed proteolysis with MRPP1 purified alone was not detected in the purified MRPP1·MRPP2 complex and the proteins are stable. Although theoretical isoelectric points of MRPP1 (pI=9.0) and MRPP2 (pI=7.8) are different, the purified MRPP1·MRPP2 complex remains intact on a cation-exchange column (SP-column) in which the two proteins co-elute at 400 mM NaCl (data not shown). The final yield of MRPP1·MRPP2 complex is about 0.5 mg protein/L cell culture.

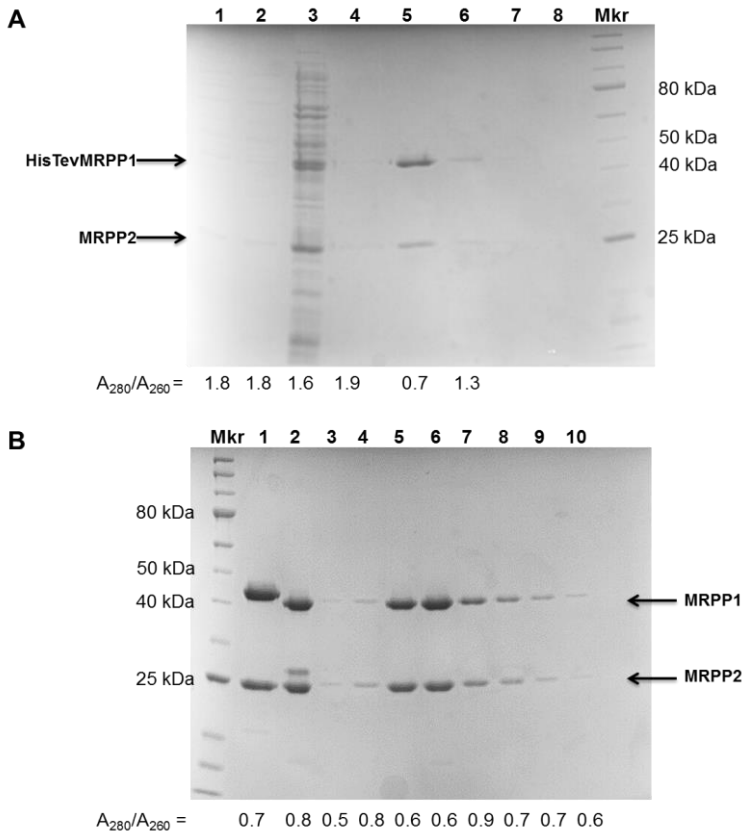


**Figure 4-6:** Co-purification of MRPP1 and MRPP2 as a complex. **(A)** SDS-PAGE analysis (coomassie blue stain) of purification by 1st Ni(II)-chelating sepharose column. Lane 1: 200-fold dilution of lysate from 1 L RosettaDE3 cells containing pHisTevMP1+MP2 vector induced using auto-induction media at 25 ºC overnight; Lane 2: 200-fold dilution of flow-through; Lane 3: wash by 120 mM imidazole; Lane 4: wash by 1 M NaCl (15 mM imidazole); Lanes 5-8: elution by 120 mM imidazole. **(B)** SDS-PAGE analysis of 2nd Ni column (coomassie blue stain): Lane 1: concentrated His6TevMRPP1·MRPP2 purified from the 1st Ni(II)-column as described in (A); Lane 2: overnight cleavage of HisTevMRPP1·MRPP2 complex by TEV protease; Lane 3: flow-through; Lanes 4-10: 50 mM imidazole wash. Purity of the protein samples is also indicated by the ratio of absorbance at 260 nm and 280 nm ($A_{260}/A_{280}$). Detailed buffer conditions are decribed in Materials and Methods.

The concentrations and molar ratio of MRPP1 and MRPP2 in the purified protein complex were estimated by analysis of SDS-PAGE gel (Figure 4-7). Band intensity from a coomassie-blue stained gel image does not directly reflect the relative concentrations of MRPP1 and MRPP2 because dye staining is protein-dependent [75, 76]. Therefore, MRPP2 alone was used as a concentration standard

to calculate concentration of MRPP2 in the complex [75] (Figure 4-7). MRPP1 was difficult to purify in the absence of MRPP2. Therefore, the concentration of MRPP1 in the MRPP1·MRPP2 complex was calculated from the absorbance at 280 nm by subtracting the concentration due to MRPP2 in the complex using calculated extinction coefficient. The molar ratio of MRPP1:MRPP2 varies from 1:2 or 1:4 for fractions collected from the second Ni(II)-column (Figure 4-7).

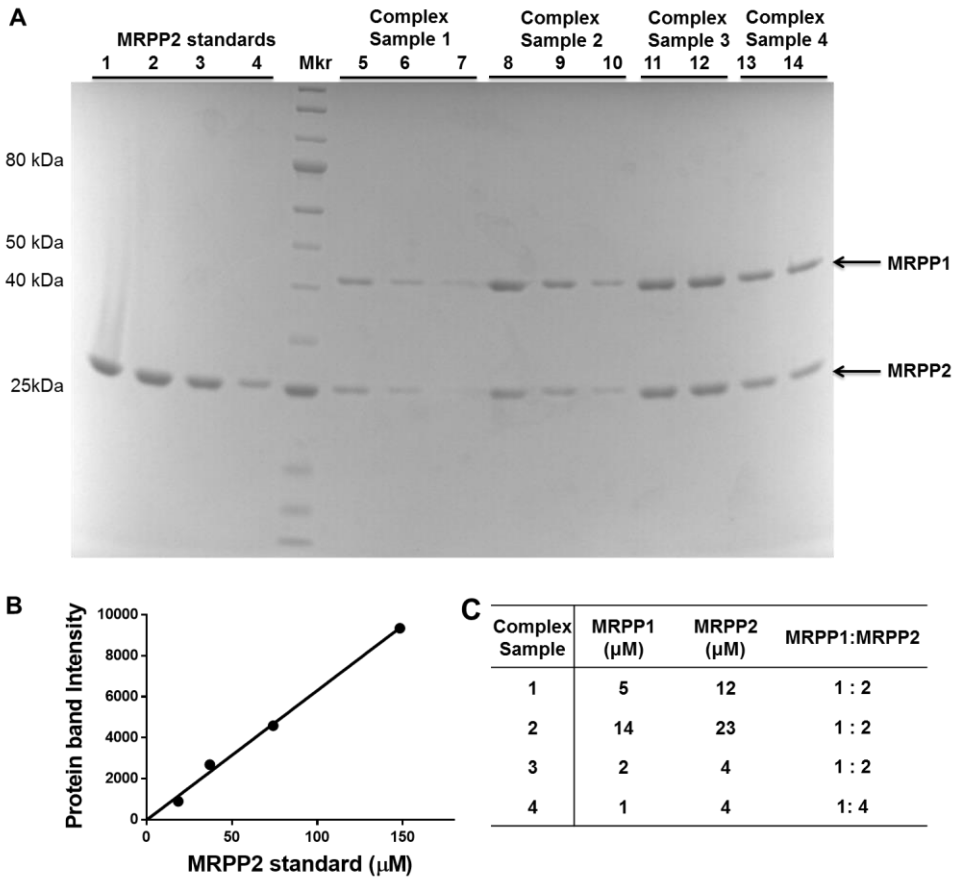


C

| Complex Sample | MRPP1 (μM) | MRPP2 (μM) | MRPP1:MRPP2 |
|---|---|---|---|
| 1 | 5 | 12 | 1 : 2 |
| 2 | 14 | 23 | 1 : 2 |
| 3 | 2 | 4 | 1 : 2 |
| 4 | 1 | 4 | 1: 4 |

**Figure 4-7:** Determination of protein concentrations in the co-purified MRPP1·MRPP2 complex. **(A)** A coomassie blue stained denaturing polyacrylamide gel containing MRPP1·MRPP2 complex samples and MRPP2 standards: Lanes 1-4, serial dilutions of known concentration of MRPP2 protein as standards. Lanes 5-7 and Lane 8-10: serial dilutions of complex sample 1 and sample 2 respectively; Lanes 11-12 and Lanes 13-14: duplicates of complex sample 3 and 4, respectively. Complex samples corresponds to concentrated fractions shown in Figure 4-6: 1: Lanes 3+4; 2: Lanes 5+6; 3: Lanes 7+8; 4: Lanes 9+10. **(B)** A standard curve of the protein band intensity (calculated by ImageJ software) that is linearly dependent on MRPP2 protein concentration. **(C)** Table of calculated concentrations and molar ratio of MRPP1 and MRPP2.

### 4.3.2 Optimization for Purification of MRPP3

Purification of MRPP3 followed the procedure developed by Dr. Wan Lim [77] with additional optimizations to increase yield and purity. The N-terminal HisTev-tagged MRPP3, with the N-terminal 45 amino acid mitochondrial localization sequence deleted (HisTevΔ45MRPP3), was expressed in RosettaDE3 cells by induction with IPTG at 18 ˚C. HisTevΔ45MRPP3 was first purified using a Ni(II)-column followed by TEV protease cleavage preceding a second Ni(II)-column. The Δ45MRPP3 fractions eluted from the second Ni(II)-column retained a considerable amount of nucleic acid contaminant ($A_{260}/A_{280}>1$). Further purification using either an anion-exchange column (DEAE-column) or a cation-exchange column (SP-column) can reduce the $A_{260}/A_{280}$ ratio to ~0.8 but a large fraction of Δ45MRPP3 (pI=8.7) does not bind to the cation-exchange column [77]. These observations indicate that Δ45MRPP3 (pI=8.7) binds strongly to nucleic acid.

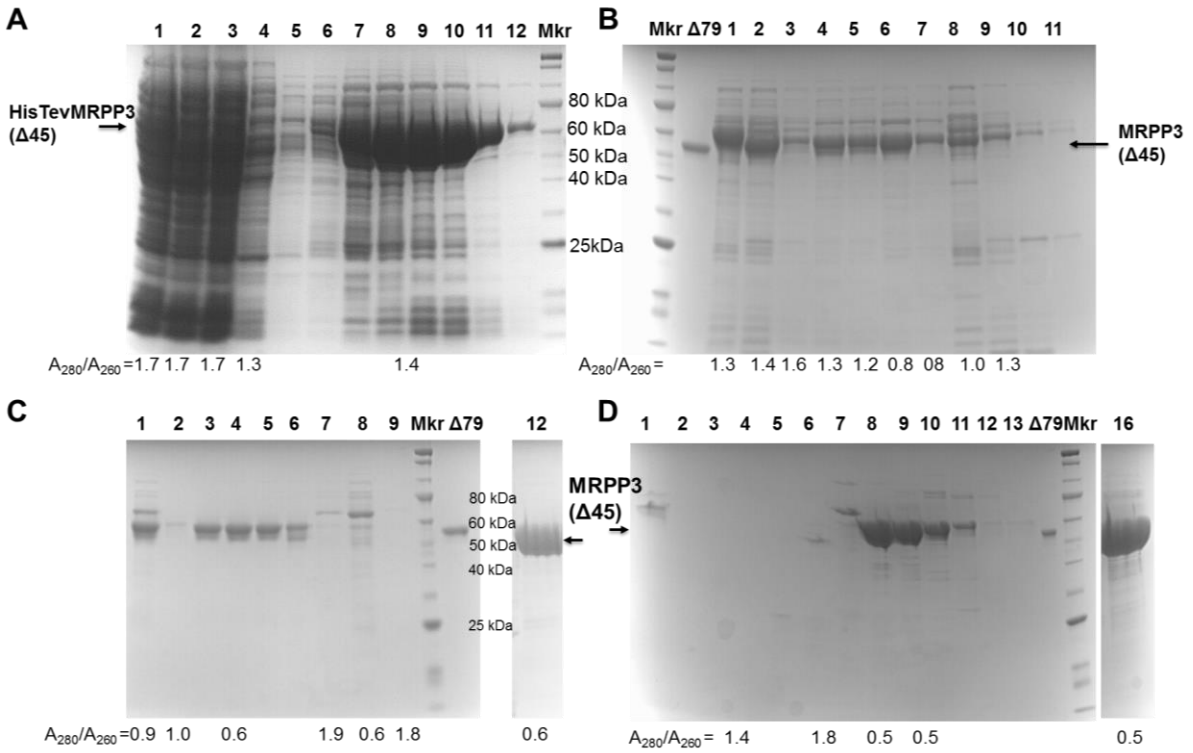


**Figure 4-8:** SDS-PAGE analysis of Δ45MRPP3 purification. **(A)** Purification of HisTevΔ45MRPP3 by a 1st Ni(II)-column. Mkr: protein size marker; Lane 1: crude lysate; Lane 2: flow-through; Lane 3: 50 mM imidazole wash; Lane 4: 50 mM imidazole wash; Lanes 5-12: elution profile using a linear imidazole gradient (50 to 500 mM imidazole). **(B)** 2nd Ni(II)-column after TEV protease cleavage of HisTevΔ45MRPP3 (showing purification of ~1/2 amount of protein from 1st Ni(II)-column). Lane Δ79: a purified Δ79MRPP3 as a size reference; Lane 1: before TEV protease treatment; Lane 2: after overnight digestion with TEV protease. Lane 3: flow-through; Lanes 4-6, 50 mM imidazole wash; Lane 7: 200 mM imidazole, Lanes 8-11: 300-500 mM imidazole. **(C)** Purification of Δ45MRPP3 (~1/2 from the 2nd Ni(II)-column) by a Q-column. Lane 1: flow-through; Lane 3, dialyzed and concentrated into pH 8.6 Tris-HCl buffer; Lane 2: flow-through from the Q-column; Lane 3-6: 150 mM NaCl wash; Lane 7-9: 400 mM to 1 M NaCl; Lane 12: pooled fractions of Δ45MRPP3 (Lane 2-6) concentrated and dialyzed into storage buffer (pH 7.5); **(D)** Purification of Δ45MRPP3 (~1/2 from the 2nd Ni(II)-column) by a phenyl-sepharose column. Lane 1: purified Δ45MRPP3, flow-through sample from (B) Lane 3, dialyzed into 1.8 M $(NH_4)_2SO_4$ buffer; Lane 2: flow-through from the phenyl-column; Lane 3-7: linear gradient from 1.8 M to 0 M $(NH_4)_2SO_4$; Lane 8-13: elution of Δ45MRPP3 protein at 0 M $(NH_4)_2SO_4$; Lane 16: pooled fractions of protein (Lane 8-11) concentrated and dialyzed into storage buffer (pH 7.5). Purify of the protein samples is also indicated by the ratio of $A_{260}/A_{280}$ ratio. Detailed buffer conditions are described in Materials and Methods.

After two Ni(II)-IMAC columns, I applied two different strategies to optimize Δ45MRPP3 purification to increase yield and separate nucleic acid contaminants.

First, Δ45MRPP3 was fractionated using an anion-exchange column (Q-column) at a pH value (Tris-HCl, pH 9.2 at 4˚C) that is 0.5 pH units higher than the pI value of Δ45MRPP3 (Figure 4-8). Δ45MRPP2 elutes at low salt fractions (150 mM NaCl) while nucleic acids as well as protein impurities elute at higher NaCl concentration (Figure 4-8). Alternatively, a hydrophobic interaction column (phenyl-column) also efficiently removes nucleic acids from Δ45MRPP3 but the protein is less pure (Figure 4-8). Final $A_{260}$ to $A_{280}$ ratio of purified Δ45MRPP3 from these two columns is 0.5 to 0.6 and the yield is 3-5 mg protein/L cell culture.

### 4.3.3 Subcloning of Human mt-pre-tRNA Genes[1]

It remains unclear whether all mt-tRNAs are processed with equal efficiency by mtRNase P and whether mtRNase P recognize alternative substrates. In the clustered mt-tRNA region, such as the mt-tRNA$^{Ala}$ to mt-tRNA$^{Asn}$ loci, RNA sequencing identified stable conjoined tRNA transcripts, suggesting the existence of partially processed transcripts [9]. Mature nuclear tRNA, such as tRNA$^{Gln(UUG)}$ [78], tRNA$^{Leu(UAA)}$ and tRNA$^{Lys(UUU)}$ [9], has also been suggested to be imported into mitochondria. The mitochondrial counterparts of these three tRNA species are among the top four mt-tRNAs mapped with the most number of pathogenic mutations (Figure 4-2). The driving force and biological importance of the importation of nuclear tRNA into human mitochondria is unclear. In addition, deep sequencing data suggest that long non-coding RNAs generated in HeLa cell mitochondria are also processed by mtRNase P by recognizing tRNA-like structures that mirrors the

[1] Paul Lin and Xin Liu performed the design and cloning of the mt-pre-tRNA plasmids. Paul Lin performed molecular cloning experiments for 8 constructs reported in Table 4-1.

mt-tRNA genes from the other strand [17]. These observations may indicate that mtRNase P recognizes substrates beyond tRNAs and may have altered processing efficiency towards different substrates.

To study the molecular mechanism and specificity of substrate recognition by human mtRNase P, a library of human mitochondrial precursor tRNA (mt-pre-tRNA) DNA templates was prepared by subcloning mt-pre-tRNA genes into high copy number plasmids (Table 4-1). This mt-pre-tRNA library includes 16 constructs containing 14 species of the 22 mt-tRNA genes and represents all four types of mt-tRNA species. This library includes known mtRNase P substrates, such as mt-pre-tRNA$^{Leu(UUR)}$ [72], mt-pre-tRNA$^{Lys}$ [60], mt-pre-tRNA$^{Ile}$ [60], and mt-pre-tRNA$^{Ser(UCN)}$ [28] (Figures C-3 and C-4, Appendix C). A non-substrate of mtRNase P, mt-pre-tRNA$^{Ser(AGY)}$ [79], is also subcloned in a mt-tRNA cluster (Figure C-4, Appendix C). 5' processing of mt-pre-tRNA$^{Ser(AGY)}$ is achieved by 3' processing of the flanking pre-tRNA$^{His}$ and is therefore independent of mtRNase P. In the 22 human mt-tRNAs, 20 have a purine (G or A) at the N9 position, except for mt-tRNAA$^{Met}$ and mt-tRNA$^{Ser(UCN)}$.

**Table 4-1:** Summary of plasmids containing human mitochondrial pre-tRNA genes.

| Human mt-pre-tRNA Plasmid | | 5' Leader Length (nt) | 33' Trailer Length (nt) | Linearization Site | Vector |
|---|---|---|---|---|---|
| tRNA Species | Pre-tRNA Constructs | | | | |
| **Type 0** | | | | | |
| Leu(UUR) | Leu(UUR)42-39 | 42 | 39 | XbaI | pUC18 |
| Leu(CUN) | Leu(CUN)28-32 | 28 | 32 | XbaI | pUC18 |
| Gln | Gln13-16 | 13 | 16 | XbaI | pUC18 |
| **Type II** | | | | | |
| Arg | Arg19-14 | 19 | 14 | XbaI | pUC18 |
| Asp | Asp19-40 | 19 | 40 | XbaI | pUC18 |
| Glu | Glu12-35 | 12 | 35 | XbaI | pUC18 |
| Gly | Gly26-54 | 26 | 54 | XbaI | pUC18 |
| His | See Ser(AGY) | | | | |
| Lys | Lys10-34 | 10 | 34 | XbaI | pUC18 |
| Ile | Ile42-24 | 42 | 24 | XbaI | pGEM-3Z |
| | Ile11-5 | 11 | 5 | BamHI | pUC19 |
| Met | Met10-40 | 10 | 40 | XbaI | pUC18 |
| Tyr | Tyr55-39[a] | 55 | 39 | BamHI | pGEM-1 |
| | Tyr55-0[b] | 55 | 0 | BstNI | pGEM-1 |
| | Tyr5-0 | 5 | 0 | BstNI | pUC19 |
| **Type I** | | | | | |
| Ser(UCN) | Ser(UCN)36-5 | 36 | 5 | XbaI | pUC18 |
| **Type III** | | | | | |
| Ser(AGY) | His-Ser(AGY)-Leu(UCN)35-35 | 35 | 35 | XbaI | pUC18 |

[a] A gift from Dr. Walter Rossmanith (Medical University of Vienna, Austria).
[b] Plasmid prepared by Dr. Wan Lim

The human mitochondrial genomic DNA is extracted from human tissue culture cells (HEK293) and the subcloning is streamlined to a rapid process of PCR amplification, blunt-end ligation with pUC18 vector and blue-white selection of transformed cells. Using this method, various sequences of potential mitochondrial substrates, such as long stretches of tRNA clusters (e.g. the His-Ser(AGY)-Leu(UCN), Table 4-1), can be subcloned quickly. This mt-pre-tRNA library will be

useful for exploring sequence and structural determinants in mt-pre-tRNA for both 5' processing catalyzed by mtRNase P and specificity of $m^1G9$ or $m^1A9$ methylation catalyzed by MRPP1.

### 4.3.4 Sequence Analysis of the 5' Leader and 3' Trailer Gene Sequences of mt-pre-tRNA Genes

Biochemical studies identified sequence-specific contacts between the the pre-tRNA substrate and bacterial RNase P, including interaction of uridine at N(-1) [80, 81] and adenosine at N(-2) [77] with RNase P RNA (P RNA), purine at N(-4) with conserved residues (F20 an Y34) in RNase P protein [82], and 3' RCCA with a conserved GGU-motif in the P15-loop in P RNA [83]. These sequence-specific interactions correlate well with sequence preference observed in the bacterial pre-tRNA genome [82]. Potential sequence preference at the 5' and 3' regions of human mt-pre-tRNA genes may provide clues to sequence-specific recognition by human mtRNase P. Therefore, I performed sequence analysis [82] for both the 5' leader and the 3' trailer region of human mt-pre-tRNA genes to evaluate potential sequence preferences in the regions flanking the mt-tRNA genes.

Sequence logo plots were generated by analyzing the nucleotide content of the 5' leader (N(-15) through N(-1)) and 3' trailer (N(+1) to N(+15)) of all 22 the human mt-tRNA genes (Figure 4-9). In these sequence logo plots, the the relative height of the letters correlates to nucleotide composition at this position, and the total bar height reflects the degree of information content enrichment with respect to background [82]. The background nucleotide content was calculated either from all 22 mt-pre-tRNA gene sequences from N(-15) through N(-1) for 5' leader or from

N(+1) through N(+15) for 3’ trailer. Nucleotide enrichment is observed at various positions in both the 5’ leader and 3’ trailer sequences (Figure 4-9).


**Figure 4-9:** Sequence preferences in the 5’ leader and 3’ trailer of human mitochondrial precursor-tRNAs. Nucleotide logo size is showing the nucleotide composition in the 5’ leader **(A)** and 3’ trailer **(B).**

To determine if the observed nucleotide enrichment is statistically significant, chi-square analysis was performed against the background information content from either the 15-nt sequences or the entire human mitochondrial genome. When tested against the background content of the 15-nt sequences proximal to tRNA genes

(26% A, 18% G, 28% C, 29% U for 5' leader analysis and 31% A, 19% G, 22% C, 28% U for 3' trailer analysis), nucleotide enrichment is statistically insignificant ($p > 0.05$) for most positions except for N(+7), N(+9) and N(+10) positions in 3' trailer genes. However, when tested against background nucleotide content of the entire human mitochondrial genome (heavy strand mtDNA sequence, 31% A, 13% G, 31% C, 25%U), enrichments are significant ($p \leq 0.05$) at N(-1), and N(-4) through N(-7) in the 5' leader and N(+1), N(+3), N(+7), N(+9) and N(+10) in the 3' trailer. The overall sequence enrichment in the 5' leader is modest (bit < 0.3) but a high frequency of uridine is observed at N(-1). A preference for for uridine at N(-1) in the 5' leader of mt-tRNA may be biological relevant since a pathogenic mutation of U to C has been reported at this position in mt-tRNA$^{Gln}$ [84]. An enrichment of U at position N(-1) has also been observed in pre-tRNA genes from diverse bacteria, archaea and eukarya [85] and has been demonstrated to form a specific interaction with nucleotide A248 in *E. coli* RNase P RNA [80]. In the 3' trailer, a strong enrichment of A followed by G and U is indicated at position N(+1). Biological relevance of these observed sequence enrichment to mtRNase P activity awaits experimental investigation.

### 4.3.5 Reconstitution of Human mtRNase P Activity

The metallonuclease subunit of mtRNase P, MRPP3, is an ortholog of *A. thaliana* PRORP1 [59]. PRORP1 contains three distinct domains (Figure 4-4): a metallonuclease domain, a structural zinc domain and a pentatricopetide repeat (PPR domain) (Figure 4-4) [59]. MRPP3 contains all of the active site residues conserved in PRORPs [59] and has a 20% sequence identity and 29 % sequence similarity to PRORP1, indicating high structural homology (for a homology model of

MRPP3, see Figure C-2, Appendix C). It is intriguing to investigate why MRPP3 requires two other proteins [50, 60] while PRORP1 alone functions efficiently for RNase P activity [54, 59, 86].

I measured single-turnover cleavage activity catalyzed by both MRPP3 and the mtRNase P complex using a mt-pre-tRNA$^{Ile42-24}$ substrate labeled with fluoresscein at the 5' end (Fl-pre-tRNA$^{Ile42-24}$, 20 nM, sequence see Table C-2, Appendix C). At 37 ˚C, all three proteins (MRPP1:2:3=1 µM:2 µM:500 nM)[2] are required to catalyze cleavage of the 42-nt 5' leader from Fl-pre-tRNA$^{Ile}$ in 4.5 mM $MgCl_2$ and 260 mM NaCl (Figure 4-10). Interestingly, a 5' end product of less than 39-nt in length is observed in the reactions with either MRRP3 alone or MRRP3 with one other subunit. This shorter length (< 39-nt) 5' product is likely miscleavage catalyzed by MRRP3, considering the high purity of the protein, the broad range RNase inhibitor (SUPERase·IN$^{TM}$) included in the reaction buffer.

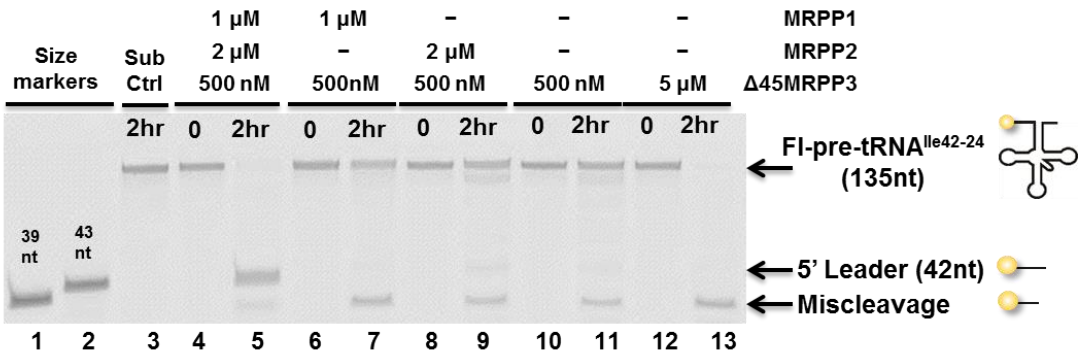


**Figure 4-10:** Single-turnover cleavage catalyzed by recombinant human mtRNase P proteins at 37 ºC. The 5' end fluorescently labeled substrate Fl-mt-pre-tRNA$^{Ile42-24}$ has a 42-nt 5' leader and a 24-nt 3' trailer. Reactions were performed at 37˚C in 30 mM Tris-HCl pH 8, 4.5 mM $MgCl_2$, 2 mM TCEP, 0.02 mM BSA, 0.1 unit/uL SUPERase·IN$^{TM}$ RNase inhibitor. The reactions were mixing enzyme with substrate and quenched by EDTA quench buffer. The reaction products were resolved on a 12 % denaturing PAGE and scanned by a Typhoon phosphorimager for fluorescence (see materials and methods). The 42-nt leader (correct size) product of is observed most prominently in reactions catalyzed by all three subunits (Lane 5). In the absence of all three subunits, the leader product is shorter (< 39-nt),

[2] Dr. Wan Lim purified the individual MRRP1 and MRPP2 proteins used in this assay.

reflecting miscleavage (Lanes 7, 9, 11, 13). Complete cleavage after 2 hour is observed in reactions catalyzed by both MRPP1+2+3 (500 nM MRPP3, Lane 5) and MRPP3 alone (5 µM, Lane 13).

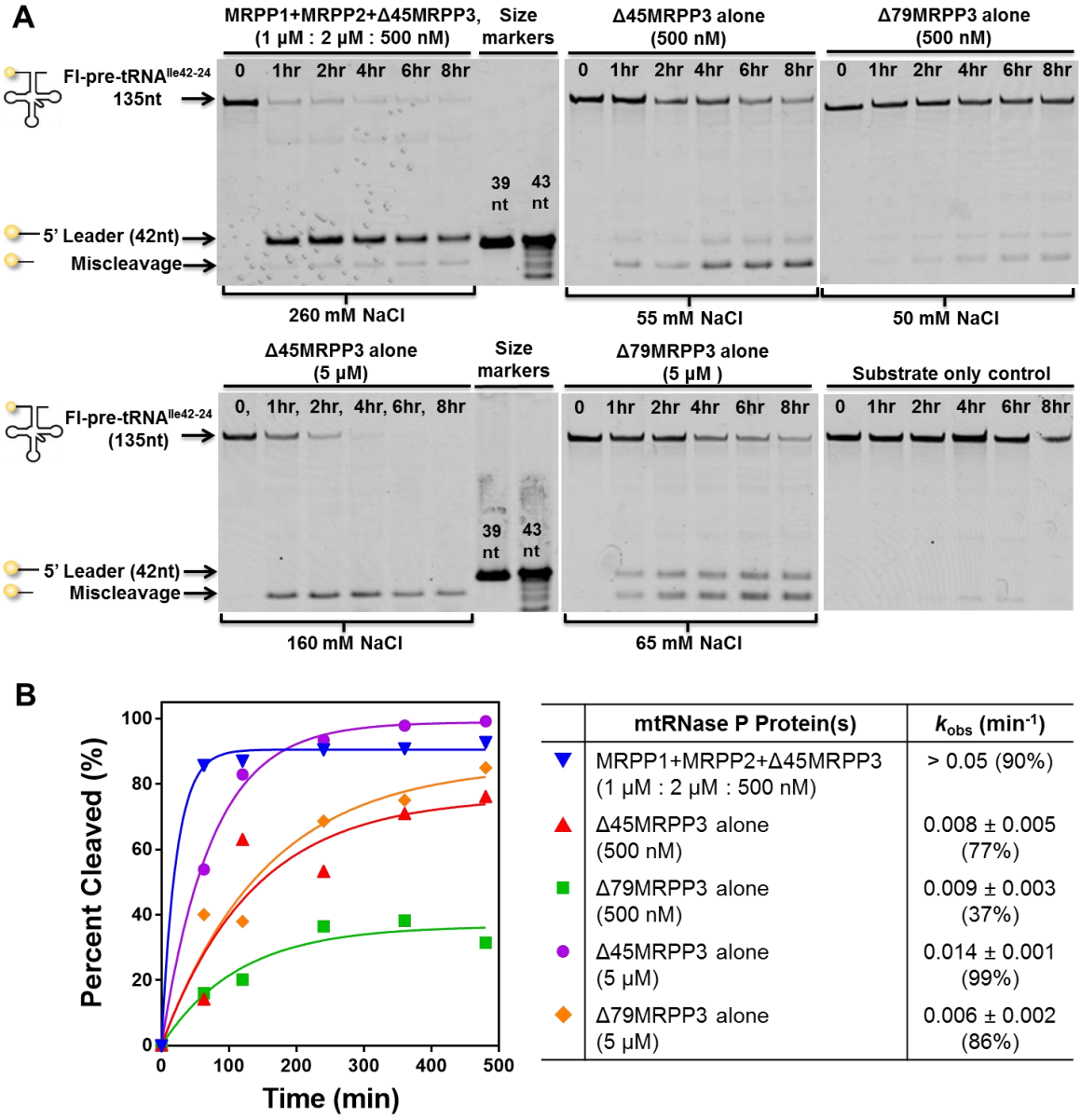


**Figure 4-11:** Single-turnover cleavage activity of recombinant human mtRNase P proteins at 21 ˚C. **(A)** Cleavage of 20 nM 5' end fluorescently labeled Fl-mt-pre-tRNA$^{Ile42-24}$ (Fl-pre-tRNA$^{Ile42-24}$) substrate catalyzed by recombinant human mtRNase P proteins (500 nM or 5 µM, MRPP1+2+3 or MRPP3 alone) measured at 21 ˚C in 30 mM Tris-HCl pH 8, 4.5 mM $MgCl_2$, 50 to 260 mM NaCl, 2 mM TCEP, 0.02 mM BSA and 0.1 unit/µL SUPERase·IN$^{TM}$ RNase inhibitor. Reactions were quenched by addition of EDTA quench buffer and resolved by 10% denaturing PAGE. The 5' end cleavage product by RNase P is 42nt in length and a miscleavage product (< 39-nt) is also observed. **(B)** Calculation of single-turnover cleavage rate constant ($k_{obs}$) from quantification of the percent substrate cleaved based on images shown in (A). The percent substrate cleavage was determined by quantifying the decrease

in intensity of the substrate band. A single exponential equation (Equation 4-4) was fit to the time-dependence of cleavage to obtain $k_{obs}$ (summarized in the table). The percentage values in parenthesis in the table indicate the percent cleavage at the end point of each reaction.

Similarly, when measured at 21 ˚C, a condition similar to a previous report [50], the mtRNase P complex combing all 3 proteins (MRPP1:2:3=1 μM:2 μM:500 nM) catalyzes single-turnover cleavage of Fl-mt-pre-tRNA$^{Ile42-24}$ substrate efficiently ($k_{obs}$> 0.05 min$^{-1}$, 90% completion), generating a 42-nt 5' leader and a small amount (<10%) of miscleaved product (Figure 4-11). Both miscleaved and correct size product were observed for reactions containing MRPP3 alone. But different cleavage activity and cleavage-site selection occurred in reactions with N-terminal truncations (Δ45 and Δ79[3]) and in two different concentrations (500 nM and 5 μM). With 500 nM MRPP3, both the correct size and miscleaved products are observed and Δ45MRRP3 ($k_{obs}$ = 0.008 ± 0.005 min$^{-1}$, 77% completion) and Δ79MRPP3 ($k_{obs}$ = 0.006 ± 0.002 min$^{-1}$ 37% completion). Although the $k_{obs}$ of 500 nM Δ45MRRP3 and Δ79MRPP3 catalyzed cleavage rate are comparable, Δ45MRRP3 is more active because the reaction catalyzed by Δ45MRRP3 has a higher completion at the end point (77% Δ45MRRP3 by vs 37% Δ79MRRP3). Interestingly, at higher concentration (5 μM), the miscleaved product (< 39-nt) is the main product from Δ45MRPP3 ($k_{obs}$ = 0.014 ± 0.001 min$^{-1}$, 99% completion) while equal amount of the correct size and miscleaved products were observed from Δ79MRRP3 reaction albeit a 2-fold slower cleavage rate ($k_{obs}$ = 0.006 ± 0.002 min$^{-1}$, 86% completion). Since activity of Δ45MRPP3 and Δ79MRPP3 are comparable when in complex with

[3] Michael Howard purified Δ79MRRP3 with two IMAC columns, followed by a cation exchange column and a size exclusion column.

MRPP1 and 2 (data not shown), the different cleavage pattern observed at 5 μM MRPP3 reactions could be due to a 2.5-fold difference in NaCl concentration (160 mM NaCl for 5 μM Δ45 and 65 mM NaCl for Δ79). These data suggest that the MRPP1·MRPP2 complex both activate MRPP3 and provide molecular recognition to cleave at the correct size. It may have mono ion dependent nuclease activity by itself but requires MRRP1 and 2 for precise catalysis.

### 4.4 Discussions

Newly identified protein-only RNase P in human mitochondria and plants sparked great interest in elucidating the mechanism of this new class of endonuclease to compare with that of ancient ribozyme based catalysis [59]. Processing of the 5’ end of mt-pre-tRNA by mtRNase P is likely the first step in mt-tRNA processing [27] and mRNA biogenesis in mitochondria [15]. Mitochondrial tRNA is also a hot spot for pathogenic mutations. To investigate the mechanism of molecular recognition by human mtRNase P, I purified recombinant mtRNase P proteins (Figure 4-6 and Figure 4-8) and prepared a series of mt-pre-tRNA substrates (Table 4-1). In contrast to previous reports, single-turnover kinetic data presented here suggest that although all three mtRNase P proteins are required for precise catalysis, MRRP3 alone also retains metallonuclease activity in the absence of other subunits (Figure 4-10 and Figure 4-11).

### 4.4.1 Purification of Human mtRNase P Proteins

Protein co-expression and co-purification can increase solubility and facilitate purification of eukaryotic protein complexes [73, 74]. MRPP1 and MRPP2 form a stable complex and were previously co-purified using affinity chromatography [50, 60]. Therefore, I chose to purify MRPP1 in complex with MRPP2 by co-overexpressing a HisTev-tagged MRPP1 with native MRPP2 (Figure 4-5). A highly pure MRPP1·MRPP2 complex was obtained by two steps of Ni(II)-affinity chromatography with a relative low yield (0.5 mg protein/L culture). For the first Ni(II)-column, two extensive wash steps after initial wash (55 mM imidazole) are crucial for obtaining pure protiens (Figure 4-6). Washing the column with 120 mM imidazole until the absorbance at 280 nm ($A_{280}$) reaches a flat baseline ensures separation of lower affinity protein impurities and protein complex formed with MRPP1. A lower imidazole concentration (100 mM) wash for this step was not sufficient to clean up these impurities (data not shown). The second wash step with 1 M NaCl (15 mM imidazole) successfully removes nucleic acids, a major issue for purifying proteins with high pI value (pI for MRPP1 is 9.0). In a recent report, a high purity MRPP1·MRRP2 complex was also obtained by co-purification of non-tagged MRPP1 with separately purified His-tagged MRPP2 [60]. Compare to this strategy, my method is simpler and has a higher yield for MRPP1 because MRPP1 is tagged and proteins are expressed and purified in a single step. In addition, use of a cleavable tag in this work produces non-tagged proteins and minimizes metal contamination.

To increase the protein yield, the purification could be further optimized. For example, we can optimize procedure for cell lysing, increase column size, reload flow-through for multiple runs of chromatography, or load the proteins with a higher NaCl concentration to reduce nucleic acids binding [87].

### 4.4.2 A Library of Human mt-pre-tRNA Substrates

I cloned a library of mt-pre-tRNA DNA templates for studying the substrate selectivity by human mtRNase P. Earlier literature data indicated that human nuclear (an RNP) and mitochondrial RNase Ps have discrete but overlapping substrate specificity [88]. Partially purified mtRNase P did not detectably cleave a nuclear substrate, n-pre-tRNA$^{Ser}$ (polyU sequence at 3' trailer) and catalyzed miscleavage of an *E. coli* pre-tRNA$^{Tyr}su_3^+$ (Figure 1-12, Chapter 1) in 4-nt upstream of cleave site [72]. A human mt-pre-tRNA$^{Tyr}$ (Table C-2 and Figure C-4, Appendix C) could not be detectably cleaved by human nRNase P [72]. However, a mt-pre-tRNA$^{Leu(UUR)}$ (Table C-2 and Figure 1-12 and C-3) was cleaved by both nRNase P and mtRNase P [72]. In plants, both nuclear and organellar tRNAs are mostly canonical, resembling eubacterial tRNAs in both primary sequence and secondary structure [69]. *A. thaliana* PRORP enzymes also catalyze cleavage of *T. thermophilus* pre-tRNA$^{Gly}$ likely by coordination of a different non-bridging oxygen (*pro*-$S_p$) than that of bacterial RNase P (*pro*-$R_p$) [68] (Figure 1-8, Chapter 1). Model substrates of RNP RNase P enzymes include tRNA mimics with a 5' leader, coaxially stacked acceptor-stem and TψC-stem/loop connected by a 0-1 nt linker and containing a 3' RCCA [89, 90]. A minimum substrate with a 3-bp-stem, tetraloop and 3' RCCA has also been used [91, 92]. RNA-dependent RNase P also cleaves other substrates, including

pre-mRNA and unstructured RNAs [93, 94]. In human mitochondria, the need for recognizing non-canonical mt-tRNA substrates may explain why mtRNase P requires multiple subunits. However, substrate determinants for human mtRNase P activity remain to be investigated.

In the mt-tRNA genes, a purine (G or A) is conserved at position 9 (R9) in all but two species, mt-tRNA$^{Ser(UCN)}$ and mt-tRNA$^{Met}$. Several mt-tRNA are methylated at the R9 position *in vivo* [8, 18], including mt-tRNA$^{Asp}$, mt-tRNA$^{Ile}$, mt-tRNA$^{Leu(UUR)}$, mt-tRNA$^{Leu(CUN)}$, mt-tRNA$^{Lys}$, and mt-tRNA$^{Trp}$. Biochemical experiments demonstrated that *in vitro* MRPP1·MRPP2 complex catalyzes R9 methylation of mt-tRNA$^{His}$, mt-tRNA$^{Ile}$, mt-tRNA$^{Leu(UUR)}$, mt-tRNA$^{Lys}$, mt-tRNA$^{Tyr}$ and a nuclear tRNA$^{Arg}$ [60]. Unmodified primary transcripts of certain mt-tRNAs are poorly structured in solution [95, 96] but may be stabilized by posttranscriptional modification. For example, a single m$^1$A methylation at A9 switches the mt-tRNA$^{Lys}$ transcript from an extended hairpin (9-nt acceptor-stem and distrupted TψC-stem) to a canonical cloverleaf structure (7-nt acceptor-stem) as demonstrated by solution structure probing and single molecule FRET experiments [97-99]. Furthermore, although mt-tRNA$^{Leu(UUR)}$ preserves the majority of canonical tertiary contacts, the D-stem-loop and anticodon-stem-loop of the *in vitro* transcripts are primarily unstructured in solution as indicated by solution structure probing [100]. Mutations that increase base paring in the D- and anticodon-stem stabilize mt-tRNA$^{Leu(UUR)}$ structure and increase aminoacylation by its cognate synthetase [100]. It is intriguing to investigate whether mt-pre-tRNA methylated at position 9 could alter cleavage efficiency and/or specificity by mtRNase P proteins.

The 5’ leader and 3’ sequences flanking the tRNA genes in bacteria have also been proposed to be co-evolved with specific regions of RNase P [77, 80-83]. In bacterial tRNA, the 3’ RCCA motif interacts with RNase P RNA by base pairing with a conserved GGU-motif in the L15 loop [83]. Biochemical studies identified a sequence preference of uridine at position N(-1) in 5’ leader and suggest a U(-1)-A248 base pairing in J5/15 of *E. coli* RNase P RNA [81]. These interactions have also been observed in the recent crystal structure of bacterial RNase P ternary complex [71]. In addition, it has been shown that identity of base-pairing between N(-1) and the determinant nucleotide N73 affect cleavage-site selection by *E. coli* and *P. furiosus* RNase P in model substrates [101]. Preference for adenine at N(-4) in *B. subtilis* results from an interaction with conserved residues in the P protein (F20 an Y34) that enhances binding affinity [82]. These specific sequence preferences correlate well with observed enrichment of these nucleotides in the genome [82].

Sequence enrichment in positions flanking the 5’ and 3’ end of human mt-tRNA is also observed, as illustrated in the sequence logo plots (Figure 4-9). These sequence enrichments may be biological relevant. For example, a sequence preference of U>A>G>>C is statistically significant at the N(-1) position in the 5’ leader (Figure 4-9). A novel pathogenic mutation linked to a type of maternally inherited hypertension has been identified at this position, which affects two flanking mt-tRNAs in the opposite strands (U to C in mt-tRNA$^{Gln}$ and A to G in mt-tRNA$^{Met}$) [84]. However, these sequence enrichments may also reflect sequence conservation in the flanking genes [27]. Further experiments measuring 5’ and 3’ sequence-

dependent substrate affinity and cleavage rates will likely reveal if these sequence preferences are related to mtRNase P activity.

### 4.4.3 Activity of Human mtRNase P Proteins

Protein subunits play a role in cleavage-site selection by RNA-based RNase P complex [101]. For example, cleavage of pATSerC$_{GAAA}$ and pMini3bpCG model substrates catalyzed by *Pyrococcus furiosus* (*Pfu*) RNase P RNA complexed with 2 of the 4 protein subunits (RPP21·RPP29) results in either miscleaved products or no product at 30 mM $MgCl_2$ [101]. Interestingly, correct cleavage can be achieved by addition of all four proteins (RPP21·RPP29 and POP5·RPP30) or higher $MgCl_2$ concentration (300 mM) [101]. This study demonstrated an intricate interaction network between substrate and RNase P subunits.

In human mtRNase P, the metallonuclease, MRPP3, requires two other subunits to function [50, 59, 60] despite predicted structural homology to the fully functional ortholog PRORP1 (see a homology model in Figure C-2, Appendix C). Consistent with previous reports [50, 60], data presented in this chapter demonstrated that all three subunits, MRPP1, 2 and 3, are required to accurately and efficiently catalyze cleavage at correct site of Fl-mt-pre-tRNA$^{Ile42\text{-}24}$ (Figure 4-10 and Figure **4-11**). Interestingly, MRPP3 alone catalyzes 5' end cleavage more slowly and at the incorrect stie, producing significant quantities of a miscleaved product (Figure 4-10). Addition of either MRPP1 or MRPP2, with MRPP3 has similar activity to MRPP3 alone (4.5 mM $MgCl_2$). This vestigial metallonuclease activity by MRPP3 is consistently observed with two independently purified truncations (Δ45 and Δ79) suggesting that it is not due to a contaminating nuclease. MRPP3 has also been

shown to cleave another non-canonical mt-tRNA substrate, mt-pre-tRNA$^{Tyr55\text{-}39}$, but the product identity is unclear [77]. Concentrations of monovalent ions may play an important role in the nuclease activity or site of cleavage of MRPP3 (Figure 4-11) possible by affecting mt-pre-tRNA secondary structures. The role of mono and divalent metal ion concentrations in enhancing cleavage activity and cleavage site-selection should be explored in detail in the future.

Additional experiments can be done to verify whether the observed miscleavage activity is catalyzed by MRRP3. For example, pre-treatment of MRRP3 with micrococcal nuclease could rule out contaminating bacterial RNase P. MRPP3 activity can be reduce by protease treatment or mutategensis of active site residues to compare with intact or wild type MRPP3 in catalyzing cleavage of mt-pre-tRNA substrates [59]. In addition, a 5’ monophosphate group (5’ $PO_4$) in the tRNA body product and a 3’ hydroxyl (3’ OH) group in the leader product is a signature of the endonuclease activity of RNase P [49]. Therefore, two-dimensional thin layer chromatography (2D-TLC) analysis can be performed to identify the 5’ monophosphate group at 5’ end of the tRNA-body product using specific α-$^{32}$P-NTP labeled pre-tRNA. In addition, the 5’ $PO_4$ group in the tRNA body product can be captured by RNA ligase and then the full product sequence could be identified by a procedure similar to the next generation sequencing for small RNAs (small RNA-seq) [102-104].

### 4.4.4 Speculation on the Roles of mtRNase P Proteins in Substrate Recognition of mt-pre-tRNA

It is striking that a single protein catalyst has evolved that can replace the function of a large ribonucleoprotein complex, as demonstrated by the ability of *T. brucei* PRORP1 to replace yeast nuclear RNase P *in vivo* [105]. *A. thaliana* PRORPs also catalyze cleavage of a *T. thermophilus* pre-tRNA substrate (pre-tRNA$^{Gly}$, Figure 1-12, Chapter 1) [68]. Substrate specificity therefore seems unlikely to be the driving force for evolving a protein-only RNase P in plants [56]. However, the non-canonical features of human mt-tRNAs may explain why two additional subunits, a tRNA methyltransferase (MRPP1) and a dehydrogenase (MRPP2), are required for RNase P functionality in human mitochondria.

MRPP1 alone is a methyltransferase that can methylate G9 of a nuclear tRNA$^{Arg}$ with low efficiency but does not methylate mt-tRNAs [60]. MRPP1 is activated by MRPP2 for efficient catalysis to catalyze both G9 and G9 methylation in mt-tRNA substrates [60]. MRPP1 belongs to the TrmD methyltransferase superfamily [61]. TrmD methyltransferases identified to date function as homodimers [106]. The cystal structure of methyltransferase domain of TRMT10A, a MRPP1 analog, also shows a homodimer , but this structure is in the absecen of the N-terminal region of the protein (Figure 4-4 and C-1) [57]. Although MRPP1 and MRPP2 forms a tightly bound complex (Figure 4-6), gel shift affinity data suggest that MRPP1 binds tightly to tRNA ($K_D$ ~100 nM) but MRPP2 does not ($K_D$ >> 1 µM) [60]. In addition, neither MRPP1 nor MRPR2 tightly associates with MRPP3 [50]. Furthermore, the catalytic activity of neither MRPP1 nor MRPP2 is required to

activate MRPP3 activity [60]. Given this functional hierarchy and large non-canonical mt-tRNA pool, substrate recognition and catalysis by mtRNase P could involve an orchestra of complex events such as conformational and/or structural changes in mt-pre-tRNA substrates and in protein subunits.

Secondary and/or tertiary structure features of mt-tRNA may be a factor for observed specificities of RNA-dependent RNase P, mtRNase P, and PRORP1. For RNP RNase P that the a coaxially stacked acceptor-stem/TψC-stem/loop of tRNA is sufficient for RNase P recognition and catalysis [107]. The acceptor-stem of tRNA is usually a 7-nt helix but bacterial RNase P can correctly catalyze cleavage of a 9-nt helix (Figure 1-12, Chapter 1) while the human nuclear RNase P miscleave this substrate at -2 position [90]. These data suggest that protein-rich RNase P have a more strick “measuring mechasim” in recognizing pre-tRNA structure. However, in primery mt-tRNA transcripts, extended hairpins are formed with a 9-nt acceptor-stem are observed in mt-tRNA$^{Lys}$ and mt-tRNA$^{Asp}$ by solution structure probing [97, 108]. $N^1$ methylation of A9 is sufficient to switch this hairpin to a cloverleaf structure by disrupting an A9-U64 base pairing [97-99]. In type 0 mt-tRNAs, such as mt-tRNA$^{Leu(UUR)}$ and mt-tRNA$^{Ser(UCN)}$, both canonical tertiary interactions between the D-loop/TψC-loop and the canonical coaxial acceptor-stem-loop structure are preserved [32, 100]. But the anticodon domain and D-stem remain largely unstructured in mt-tRNA$^{Leu(UUR)}$, as indicated by high accessibility to modifying chemicals and nucleases [100]. These observations suggest that structure of primary mt-tRNA transcripts are poorly folded in solution compare to that of canonical tRNA.

One possible function for the MRPP1·MRPP2 subcomplex is to stabilize a productive conformation of mt-tRNA that facilitates recognition and catalysis by MRPP3. Structural studies have previously demonstrated a remarkable ability of tRNA modification enzymes to alter tRNA structure upon binding. For example, a tRNA ψ55 pseudouridine synthase binds a TψC-stem-loop model substrate of which three nucleotides, including the modification site (G55),flipped out in the crystal structure [109]. Furthermore, in a cocrystal structure of archaeosine tRNA–guanine transglycosylase (ArcTGT), the bound $tRNA^{Val}$ assumes a "λ-form" with a protruded D-stem-loop to expose the modification site (G15) [110]. In canonical L-shaped form of tRNA, the N9 nucleotide is buried within the folded structure of tRNA making tertiary contacts with N23 in D-stem (Figure 4-12) [111]. However, a detectable population of A9 base pairs with nucleotides in the TψC-stem was observed for mt-$tRNA^{Lys}$ and mt-$tRNA^{Asp}$ by solution structure probing [97, 108]. Therefore, recognition of the G9 or A9 nucleotide by the MRPP1·MRPP2 complex may require significant rearrangement of mt-tRNA conformation to expose the R9 nucleotide [112]. Consequently, binding of MRPP1·MRPP2 to mt-tRNA may alter the mt-tRNA structure, defining productive mt-tRNA structure that is recognized by mt-RNase P (Figure 4-12). This hypothesis can be tested by biochemical studies such as solution structure probing of free and mtRNase P-bound mt-pre-tRNA, comparison of cleavage activity by various types of primary and R9 methylated mt-pre-tRNA, as well as mutagenesis of mtRNase P proteins and mt-pre-tRNA substrates. Structural studies by co-crystallization and solution NMR would be challenging but will provide clear pictures of how this mtRNase P complex recognizes substrates.

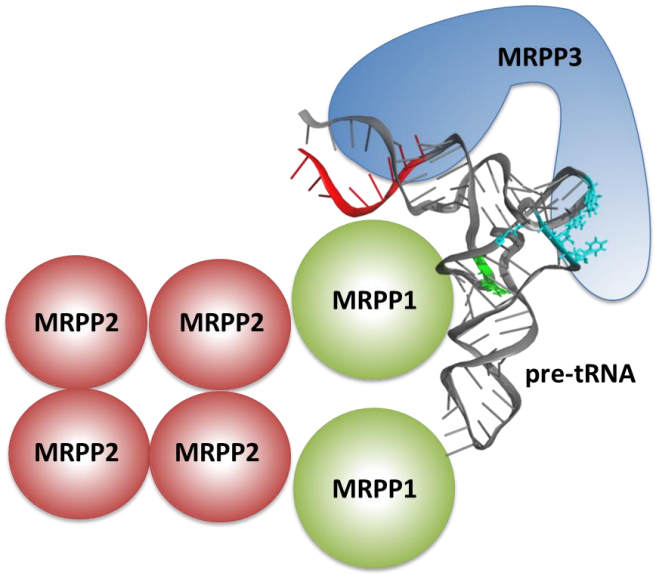


**Figure 4-12:** A model illustrating a propoased interaction of human mitochondrial RNase P with pre-tRNA substrate. In the cartoon presentation of a pre-tRNA, the 5' leader (red) is positioned close to the metallonoclease domain of MRPP3 while the nucleotides in the the D-TψC region (cyan), which were proposed to interact with the PPR domain by footprinting experiments [70], are positioned near the PPR domain. The methylation site (purine at N9) of tRNA recognized by MRPP1 is highlighted in green [113]. The model of one pre-tRNA per MRPP1 is based on proposal that two tRNA bind to one homodimer of TrmD methyltransferases [106].

MRPP2 does not tightly associate with meither mt-tRNA or MRPP3 [50, 60]. Its role in activating MRPP1 methylation and mtRNase P cleavage likely comes from protein-protein interactions. Consistent with this, MRPP2 has been shown to interact with β-amyloid (Aβ) peptides [64]. Furthermore, MRPP1·MRPP2 co-localizes with a newly identified mitochondrial RNA-binding protein, GRSF1 [66]. The C-terminal domain of MRPP1 likely has a similar structure to the recently solved MTase domain of TMRT10A (Figure C-1, Appendix C) but the N-terminal region (amino acids 39 to 190) of MRPP1 has little sequence homology to known structural motifs and has a predicted coiled coil region (amino acids 138 to169). The function of the N-terminal region of MRPP1 awaits exploration. Dissecting MRPP1-MRPP2 interactions important for catalysis of tRNA methylation and activation of mtRNase P will

advance our knowledge of the function and mechanism of this essential RNA processing complex.

### 4.4.5 Conclusion

This work developed materials and methods for further systematic investigation of substrate recognition and catalytic function of the poorly characterized protein-only human mtRNase P complex. Single-turnover cleavage results indicate that MRPP3 alone can cleavages of the 5' leader of an mt-pre-tRNA$^{Ile}$ substrate in the absence of two other protein subunits, although with significant miscleavage and lower rate constant. Analysis of the molecular mechanism of human mtRNase P in processing wild-type and pathogenic mt-pre-tRNA substrates will shed light on understanding the role of mt-tRNA processing in mitochondria biogenesis and pathogenesis.

## 4.5 Materials and methods

### 4.5.1 Subcloning of MRPP1 and MRPP2 Subunits for Co-expression

Genes encoding MRPP1 and MRPP2 proteins were subcloned into a pCDFDuet-1 (Novogen) co-expression vector by three rounds of molecular cloning (Figure 4-5). First, a DNA insert containing the full coding sequence of MRPP2 (261 amino acids) and a stop codon was obtained from double digestion of an engineered pETM11-based vector that contain the MRPP2 encoding sequence (pMR2-TEV-His[4]) [77] by NdeI and XhoI restriction enzymes (New England BioLabs, NEB)

[4] The pMR2-TEV-His plasmid was made by Dr. Wan Lim.

according to the manufacture's specifications. This insert was then ligated (Quick Ligation™ Kit, NEB) into the second multiple cloning site (MCS2) of the pCDFDuet-1 vector to generate a plasmid encoding native MRPP2 sequence (pCDFMP2).

Second, coding sequences corresponding to amino acids 39 to 403 of MRPP1 (deletion of the N-terminal mitochondrial localization sequence) and a stop codon were amplified using polymerase chain reaction (PCR) from a plasmid template (pJEJ449) provided by Dr. Jane Jackman (Ohio State University). The PCR reaction was carried out in standard PCR buffer (Strategene) with 0.04 unit/µL *PfuTurbo*® DNA polymerase (Stratagene), 0.2 mM dNTP (Invitrogen), 1 ng/µL plasmid template and 0.5 µM of the following primers: forward primer (FRP), '5-CAG TCT CAT ATG TCT TCC AAA ATA CCA GCT-3'; reverse primer, (RVP), 5'- GGA AGT CTC GAG TTA AGT CTT TGC CTT CTT TAG TC -3' (Integrated DNA Technologies). The PCR cycles are: (1) denaturation at 95 ˚C for 2 min; (2) a sequence of denaturation at 95 ˚C for 2 min followed by annealing at 55 ˚C for 1 min and elongation at 72 ˚C for 2 min that was repeated by 30 times; (3) a final elongation step at 72 ˚C for 5 min. The PCR product and a pETM11-based vector (kanamycin resistant, engineered HisTev tag) were double digested with NdeI and XhoI restriction enzymes (NEB). The double digested PCR insert was ligated to the pETM11 vector to produce a plasmid encoding an N-terminal hexa-histidine-tag followed by a cleavage sequence for TEV protease and the Δ39MRPP1 gene (pETM11HisTevMP1).

Next, the MRPP1 sequence, including the N-terminal TEV-cleavage tag, was amplified using the same PCR amplification conditions described above and with the following primers: forward primer (FRP), '5- CGA TCA CCA TGG GTA TGA AAC

ATC ACC ATC ACC AT -3'; reverse primer, (RVP), 5'- CCA AGT GGA TCC TTA AGT CTT TGC CTT CTT TAG TC -3' (Integrated DNA Technologies). The PCR product was double digested by NcoI-HF and BamHI-HF restriction enzymes (NEB) and ligated into the first multiple cloning site (MCS1) of the pCDFMP2 vector between NcoI and BamHI sites. This generated a plasmid encoding an N-terminal TEV-cleavable his-tagged Δ39MRPP1 and native MRPP2 controlled by two separate T7 promoters (pHisTevMP1+MP2). Plasmid constructs containing alternative combinations of the two proteins were also subcloned into pCDFDuet-1 vector (Table C-1, Appendix C). Sequence are confirmed using two pairs of sequenceing primers as manuafarcture recommended for MCS1 and MCS2 for pCDFDuet-1 vector at University of Michgian DNA Sequencing Core (Novogen).

### 4.5.2 Overexpression and Purification of Recombinant Human mtRNase P Subunits

Optimum conditions for expression of MRPP1 and MRPP2 from the co-expression plasmid were determined by analysis of the expression level in cell lysates and for Ni(II)-sepharose column affinity. The conditions tested included: *E. coli* cell strain (BL21(DE3), BL21(DE3)pLysS, Rosetta(DE3)), expression media (LB-media, Overnight Express™ Instant TB Medium by Novogen), growth temperature (16 to 25 ˚C) and concentration of isopropylthio-β-D-galactopyranoside (IPTG, 0 to 1 mM). The expression level and solubility of MRPP1 and MRPP2 in cell extracts were analyzed using the B-PER Protein Extraction Reagents (Thermo Scientifc) with procedures similar to manufacture specified protocol with addition of lysozyme and DNase I treatment for cell lysis. The soluble and insoluble fractions of cell extracts

were analyzed by SDA-PAGE. Small scale immobilized-metal affinity chromatography (IMAC) column was utilized to test the nickel affinity of the His-tagged proteins to the Ni(II)-column.

For co-overexpression and co-purification of HisTev-tagged MRPP1 and native MRPP2, the pHisTevMP1+MP2 plasmid was transformed into RosettaDE3 *E. coli* cells and the proteins were expressed by growing cells in Overnight Express™ Instant TB Medium with 50 mg/L streptomycin and 34 mg/L chloramphenicol at 25 ˚C for 16 to 24 hours. Cells were harvested and resuspended in buffer A (20 mM Tris-HCl pH7.5, 10% glycerol, 150 mM NaCl, 1 mM $MgCl_2$, 1 mM TCEP, 30 mL buffer/L cell culture) with 15 mM imidazole and kept frozen at -80 ˚C until purification. Prior to lysing the cells, one tablet of protease inhibitor (Complete EDTA free) and final concentrations of 30 unit/µL RNase-free DNase I (Promega or Qiagen) and 5 mM $MgCl_2$ were added to the cell suspension and the mixture was incubated at 37 ˚C for 30 min to 1 hour. Cells were lysed by sonication on ice with the addition of 1 mg/mL lysozyme followed by centrifugation at 16, 000 rpm for 1 hour at 4˚C.

The cleared cell lysate was purified by immobilized-metal affinity chromatography column with $NiSO_4$-charged chelating sepharose fast-flow resin (GE Healthcare) using an Econo Gradient Pump system (BioRad) at room temperature. Specifically, the Ni(II)-column (2 mL) was loaded with ~40 mL lysate and washed extensively by three steps: buffer A with 55 mM imidazole, followed by 120 mM imidazole and 1 M NaCl (15 mM imidazole). Each wash step was performed until the absorption at 260 nm ($A_{260}$) and 280 nm ($A_{280}$) of the fractions reaches a flat

baseline. A protein complex of HisTev-tagged MRPP1 and native MRPP2 was then eluted upon addition of 120 mM imidazole in buffer A. The fractions containing the purified HisTevMRPP1·MRPP2 complex were concentrated by centrifugal filtration (Amicon MWCO 10K, Millipore Corporation) and dialyzed overnight at 4 ˚C against buffer A with His-tagged TEV protease added in the dialysis cassette (MWCO, 10K). The TEV protease (50 unit per mg of substrate protein) is His-tagged and purified in our lab. The TEV-cleaved proteins were applied to a second Ni(II)-IMAC column to separate the HisTev-tag, His-tagged TEV protease and other impurity from the native MRPP1·MRPP2 complex. The fractions containing the complex were concentrated to 0.1-1 mg/mL and exchanged to buffer B (Amicon MWCO10K) and stored in -20˚C. The final yield for purified MRPP1·MRPP2 complex is about 0.5 mg protein/L cell culture.

To estimate the protein concentration in the MRPP1·MRPP2 complex, a separately purified MRPP2 protein [5] was used as the standard for quantifying MRPP2 concentration in a coomassie blue stained SDS-polyacrylamide gel (Figure 4-7). Absorbance of the protein samples at 280 nm ($A_{280}$) was measured using a NanoDrop 2000 UV-Vis spectrometer (Thermo Scientific). The theoretical extinction coefficient for denatured MRPP1 ($\varepsilon_{280}^{MRPP1}$ = 62,130 $M^{-1}cm^{-1}$) and MRPP2 ($\varepsilon_{280}^{MRPP2}$ = 4,720 $M^{-1}cm^{-1}$) were calculated using the ProtParam server (Expasy Protein Parameter Tool [114]). Serial dilutions of known concentrations of MRPP2 (20-150 μM, with a further 10-fold further dilution when loaded on the gel) and the MRPP1·MRPP2 complex were denatured and resolved on the same SDS-

[5] The MRPP2 protein was purified by Michael Howard using several chromatographic seperations: a Ni(II)-column, TEV-cleavage, a second Ni(II)-column, an SP-column and a blue-sepharose column.

polyacrylamide gel. The gel was stained by coomassie blue and the intensity of each protein band in the image was analyzed using ImageJ software. A standard curve was generated by fitting a linear equation to the dependence of the band intensity on the concentration of MRPP2. Then the concentration of MRPP2 in the complex was calculated from the band intensity using the standard curve. Finally, the concentration of MRPP1 was estimated from the measured $A_{280}$ after subtraction of the $A_{280}$ contribution by MRPP2 using the calculated extinction coefficient.

To purify MRPP3, the plasmid encoding amino acids 46 to 583 of MRPP3 (Δ45MRPP3) with an N-terminal HisTev-tag (pMR3-TEV-His[6]) [77] was transformed into Rosetta(DE3) *E. coli* cells and grown in LB-media at 37 ˚C to an $OD_{600}$ ~ 0.6-0.8 followed by induction of the protein by addition of 660 µM IPTG and incubation for 16 hours at 18˚C. Cells were resuspended in buffer B (20 mM MOPS, pH 7.8, 10% glycerol, 150 mM NaCl, 1 mM $MgCl_2$, 1 mM TCEP; ~30 mL buffer/L cell culture) with 15 mM imidazole and were frozen in -80 ˚C. Cells expressing HisTev-MRPP3 were lysed by 2-3 passes through a chilled micro-fluidizer and purified by a Ni(II)-IMAC column (5 mL) similar to procedures described previously [77]. HisTev-MRPP3 was eluted using a linear gradient from 50 to 500 mM imidazole in buffer C (20 mM Tris-HCl, pH 8.6 in 25 ˚C and pH 9.2 in 4 ˚C, 10% glycerol, 150 mM NaCl, 1 mM $MgCl_2$, 1 mM TCEP) and the pooled fractions (300-500 mM imidazole) were subjected to TEV protease (50 unit per mg of substrate protein) cleavage while dialyzing against buffer B at 4 ˚C overnight. The cleaved Δ45MRPP3 was further purified using a second Ni(II)-IMAC column (Figure 4-8) .

[6] The pMR3-TEV-His plasmid was made by Dr. Wan Lim.

Non-tagged Δ45MRPP3 was further purified by either anion-exchange chromatography (Q Sepharose High Performance, GE Healthcare) or hydrophobic interaction chromatography (Phenyl Sepharose High Performance, GE Healthcare). For the anion-exchange column, MRPP3 was dialyzed into buffer C (20 mM Tris-HCl, pH 8.6 in 25 ˚C and pH 9.2 in 4 ˚C, 10% glycerol, 150 mM NaCl, 1 mM $MgCl_2$, 1 mM TCEP) at 4 ˚C and loaded onto a Q-column (2 mL). Pure MRPP3 are eluted at 150 mM NaCl (Figure 4-5) and protein and nucleic acid elutes at higher salt (400 mM to 1 M NaCl). For the hydrophobic interaction column, MRPP3 was dialyzed into buffer D (50 mM MOPS, pH 7.5, 10% glycerol, 1.8 M $(NH_4)_2SO_4$, 1 mM MgCl2, 1 mM TCEP) and purified on a Pheny-sepharose column (2 mL) using a linear gradient of decreasing concentration of $(NH_4)_2SO_4$ from 1.8 M to 0 M. MRPP3 eluted at the fractions with 0 M $(NH_4)_2SO_4$ (Figure 4-8). MRPP3 samples purified from either a Q-column or a Phenyl-column were collected separately and exchanged into buffer E (50 mM MOPS, pH 7.5, 10% glycerol, 300 mM NaCl, 1 mM TCEP) for storage at -20˚C until use. Final yield for Δ45MRPP3 is about 3-5 mg/L cell culture. Concentration of Δ45MRPP3 is calculated with a theoretical extinction coefficient of 85, 830 $M^{-1}cm^{-1}$.

### 4.5.3 Cloning of Human mt-pre-tRNA Genes

The genomic DNA from human mitochondria was extracted from HEK293 cells using a mitochondrial DNA isolation kit (BioVision). The yield of mitochondrial DNA was 5-12 µg from ~ 5 X $10^7$ HEK293 cells. Target human mt-pre-tRNA genes containing 5' leader, tRNA body and 3' trailer sequences were amplified by PCR with 0.04 unit/µL *PfuTurbo*® DNA polymerase (Stratagene), 0.2 mM dNTP (Invitrogen), 1-

2 ng/µL mitochondrial genomic DNA and 0.4-0.5 µM primers (Table C-3, Appendix C).

The mt-pre-tRNA genes were subcloned into high copy number plasmids to prepare DNA templates for transcription of mt-pre-tRNA catalyzed by T7 RNA polymerase [115]. The PCR primers containing T7 promoter sequences preceding the pre-tRNA genes are designed to start with at least one G following the TATA sequence and a T is avoided as the second nucleotide downstream of TATA based on specificity of T7 RNA polymerase [116]. Primers were also designed with an estimated melting temperature ($T_m$) in the range of 58 to 63 ˚C (accounting 50 mM NaCl and 2.5 mM $MgCl_2$ by Oligo Analzyer, Integrated DNA Technologies) and GC-content of 40-60%. Therefore the leader and trailer lengths were varied (Table 4-1). Typical PCR reaction cycles were: (1) denaturation at 95 ˚C for 2 min, (2) denaturation at 95 ˚C, annealing at 52 to 58 ˚C for 30 sec and elongation at 72 ˚C for 1 min. (3) a final elongation step at 72 ˚C for 5 -10 min.

Several different vectors were used for cloning mt-pre-tRNA genes. PCR products for mt-pre-tRNA$^{Ile42-24}$ (first number indicates length of 5' leader while second number is the length of 3' trailer) were ligated into a high-copy number plasmid vector (pGEM-3Z, Promega) by double digestion of both the PCR product and the vector with EcoRI and XbaI restriction enzymes (NEB) followed by ligation (Quick Ligation™ Kit, NEB). Sequence of mt-pre-tRNA$^{Ile42-24}$ was confirmed by sequencing results by the University of Michigan Sequencing Core using the SP6 primer. A secondary procedure was used for cloning mt-pre-tRNA genes into pUC18 or pUC19 vectors. A plasmid containing an mt-pre-tRNA$^{Tyr}$ gene (Tyr5-0) was

generated by first amplifying the target gene using the mt-pre-tRNA$^{Tyr}$ (Tyr55-0)[7] plasmid as template by *PfuTurbo*® DNA polymerase (Stratagene), followed by a blunt-end ligation of the PCR product into the pUC18 vector digested with the SmaI restriction enzyme (NEB). The ligation reaction was transformed into XL1Blue *E. coli* cells and plated on LB-agar top dressed with IPTG (to enhance production of *lac*Z) and 5-bromo-4-chloro-indolyl-β-D-galactopyranoside (X-gal, Fisher Scientific) for blue-white screening [117]. White colonies were picked for extraction of plasmid DNA and sequencing using the M13-Reverse primer (University of Michigan DNA Sequencing Core). The majority of target genes of mt-pre-tRNA were amplified from human mitochondrial genomic DNA and ligated into SmaI digested pUC18 vector followed by blue white screening. Large quantities of mt-pre-tRNA plasmid (1-5 mg) were prepared using either a Maxi (Sigma, or Qiagen) and/or a Giga plasmid prep kit (Sigma) to serve as DNA templates for subsequent synthesis of mt-pre-tRNAs by *in vitro* run-off transcription by catalyzed T7 polymerase [116].

### 4.5.4 Sequence Analysis of Human mt-pre-tRNA Genes

The complete sequence of the human mitochondrial genome (NC_012920.1) was downloaded from GenBank. The annotated mt-tRNA genes from both the heavy and light strand DNA were analyzed and the first 15 nucleotides upstream [N(-15) to N(-1) for 5' leader] and downstream [N(+1) to N(+15) for 3' trailer] of each tRNA were identified. Background nucleotide compositions for the 5' leader or 3' trailer regions were calculated from all 22 corresponding 15-nt sequences. The information content indicating nucleotide frequencies and enrichment at each position (shown as

[7] Dr. Wan Lim generated the Tyr55-0 plasmid.

sequence logo in Figure 4-9) were calculated relative to background information content from all 15-nt sequences [82, 118] to generate a sequence logo plot [119, 120] (Figure 4-9). The total bar height (in bits) in the sequence logo plot equals the information content at position N(i), $R_{N(i)}$, calculated by Equation 4-1:

$$R_{N(i)} = H_{bkgd} - H_{N(i)} - e_n \qquad \textbf{Equation 4-1}$$

Where $H_{bkgd}$ is the background information entropy from positions N(-1) to N(-15) (for 5' leader calculation) or positions N(+1) to N(+15) (for 3' trailer calculation), $H_{N(i)}$ is the entropy of position i, and $e_n$ is a correction factor by sample size (n = 22 sequences in this analysis, Equation 4-2).

$$e_n = \frac{3}{2n\ln(2)} \qquad \textbf{Equation 4-2}$$

$H_{bkgd}$ and $H_{N(i)}$ were calculated using Equation 4-3, in which $f_b$ is the observed frequency of a given nucleotide position (for $H_{N(i)}$) or in the total sequence combining all 15 positions in the 22 sequences for ($H_{bkgd}$).

$$H_{bkgd\ or\ N(i)} = -\sum_{b\in(A,G,C,U)} f_b log_2(f_b) \qquad \textbf{Equation 4-3}$$

To evaluate the probability ($p$) that the observed nucleotide content is due to random fluctuations in the background nucleotide composition, chi-square analysis was performed by comparing the nucleotide content at each position to both the 15-nt region proximal to tRNA genes and the overall genomic background content calculated from the heavy strand of mtDNA [82].

### 4.5.5 Single-turnover Cleavage Measurements

Fluorescently labeled mt-pre-tRNA$^{Ile42-24}$ (Fl-pre-tRNA$^{Ile42-24}$) was prepared by conjugating 5-iodoacetamidofluorescein (5-IAF, Invitrogen, now Life Technologies) to pre-tRNA$^{Ile42-24}$ transcribed using T7 polymerase *in vitro* with a 5' monothiophosphate guanosine (5' GMPS), as described previously [121]. To measure cleavage activity of mtRNase P, Fl-pre-tRNA$^{Ile42-24}$ was denatured by heating for 3 min at 95°C in water and refolded by first incubating for 10-15 min at 37°C followed by addition of the desired buffer and incubation for another 30 min at 37 ˚C or 21 ˚C.

Single-turnover activity of the recombinant human mtRNase P was measured at conditions similar to previous reports [50] with 30 mM Tris-HCl pH 8, 40-260 mM NaCl, 4.5 mM $MgCl_2$, 2 mM TCEP, 0.02 mM BSA, 0.1 unit/µL RNase inhibitor (SUPERase·IN$^{TM}$, Ambion, now Life Technologies) at 37˚C (Figure 4-10) or 21˚C (Figure 4-11). MRPP1 and MRPP2 proteins used in this experiment were purified separately[8] as described in [77]. The Δ45MRPP3 was purified using two rounds of Ni(II)-IMAC column and one Q-column and Δ79MRPP3 was purified using two rounds of Ni(II)-column followed by a SP-column (GE Healthcare) and a size-exclusion column (Sephacryl S-200 GE Healthcare)[9]. Single turnover kinetics were measured by reacting 20 nM Fl-pre-tRNA$^{Ile42-24}$ with either MRPP3 alone (500 nM or 5 µM) or with addition of other subunits (MRPP1:MRPP2:MRPP3 = 1 µM:2 µM:500 nM, MRPP1:MRPP3=1 µM:500 nM, MRPP2:MRPP3=2 µM:500 nM). Time points were taken by quenching the reaction with an equal volume of quenching solution

[8] Dr. Wan Lim purified the MRPP1 and MRPP2 used in this experiment.
[9] Michael Howard purified Δ79MRPP3.

(10 M urea, 200 mM EDTA pH 8, 0.05% bromophenol blue, and 0.05% xylene cyanol). The extent of substrate cleavage was visualized by applying quenched solutions to a 12% or 10% denaturing polyacrylamide/bis gel containing 7 M urea followed by fluorescence scanning by a Typhon Phosphorimager ($\lambda_{ex}$ = 480 nm, $\lambda_{em}$ = 535 nm). The scanned images were analyzed using ImageJ software and the percent cleavage of the substrate was determined from the disappearance of the substrate band (Figure 4-10). A single exponential equation (Equation 4-4) was fit to the percent cleavage time course to calculate the single-turnover cleavage rate constant ($k_{obs}$).

$$Y = Y_{\infty}\left(1 - e^{-k_{obs}t}\right) \qquad \textbf{Equation 4-4}$$

## 4.6 Appendix C

I have compiled detailed figures and tables related to Chapter 4 in this appendix so that future members can have easy access to this plethora of basic information related to human mtRNase P and mt-tRNA. The main contents of the following supporting figures and tables are:

- Homology modeling and sequence alignment analysis for MRPP1 (Figure C-1) and MRPP3 (Figure C-2)
- Summary of molecular biology and purification of recombinant human mtRNase P proteins (Table C-1).
- Molecular biology and sequence summary of mt-pre-tRNA genes presented in this chapter (Tables C-2 and C-3, and Figures C-3 and C-4)
- Sequence alignment (Figure C-5) and flanking sequences (5’ leader and 3’ trailer) of all 22 human mt-tRNA genes (Table C-4).

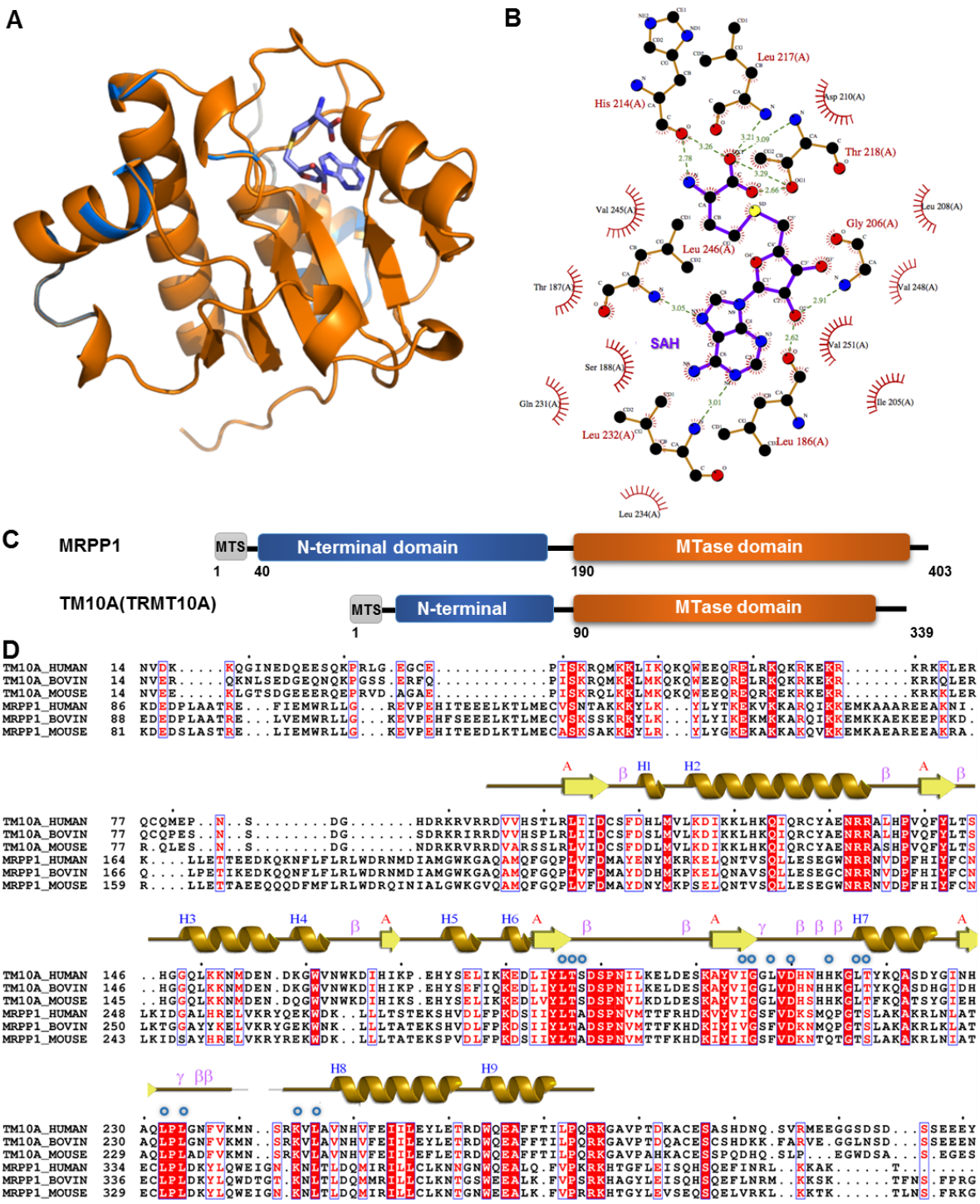


**Figure C-1:** Structure modeling and multiple sequence alignment of MRRP1 with TRMT10 (TM10) family methyltransferases. **(A)** A superposition of TM10A MTase domain (chain A, in orange, PDB ID: 4FMW [57]) with a homolog structure model of C-terminal region of MRPP1 (blue). TM10A bound SAH is shown (light blue). Homology modeling was performed on Phyre2 server [122] by structure based alignment of full MRPP1 sequence to possible remotely related candidate structures. Amino acids 196 to 379 in MRPP1 were predicted to

adopt an identical fold to this TM10A MTase domain (confidence score: 100%). No significant hit for the N-terminal region of MRPP1 was identified. **(B)** Two-dimensional projection of contacting and second shell residues for SAH, generated from 4FMW pdb file by LigPlot$^{+}$ [123]. **(C)** Diagram illustrating size and domain composition of human MRPP1 and TM10A. MTS: mitochondrial localization sequence. MTase domain: methyltransferase domain. Structure of N-terminal domain(s) of TM10 family MTase has not been determined to date. **(D)** Multiple sequence alignment of 15 TM10 family MTase sequences (showing 6). Protein sequences of eukaryotic TM10, TM10A, TM10B and MRPP1 analogs were identified from PSI-BLAST search (http://www.ebi.ac.uk/Tools/sss/psiblast/) [124] and aligned by Clustal Omega [125]. Color-shading indication of sequence conservation were generated by ESPript 2.2 [126]. Boxed regions indicate both complete (red highlight) and partial conservations (red letter). Secondary structure diagram corresponds to PDBsum [127] annotation of TM10A chain A. Putative SAH ligands are marked by blue circles. Overall sequence identity and similarity between MRPP1 and TM10A are 22% and 29%, respectively.

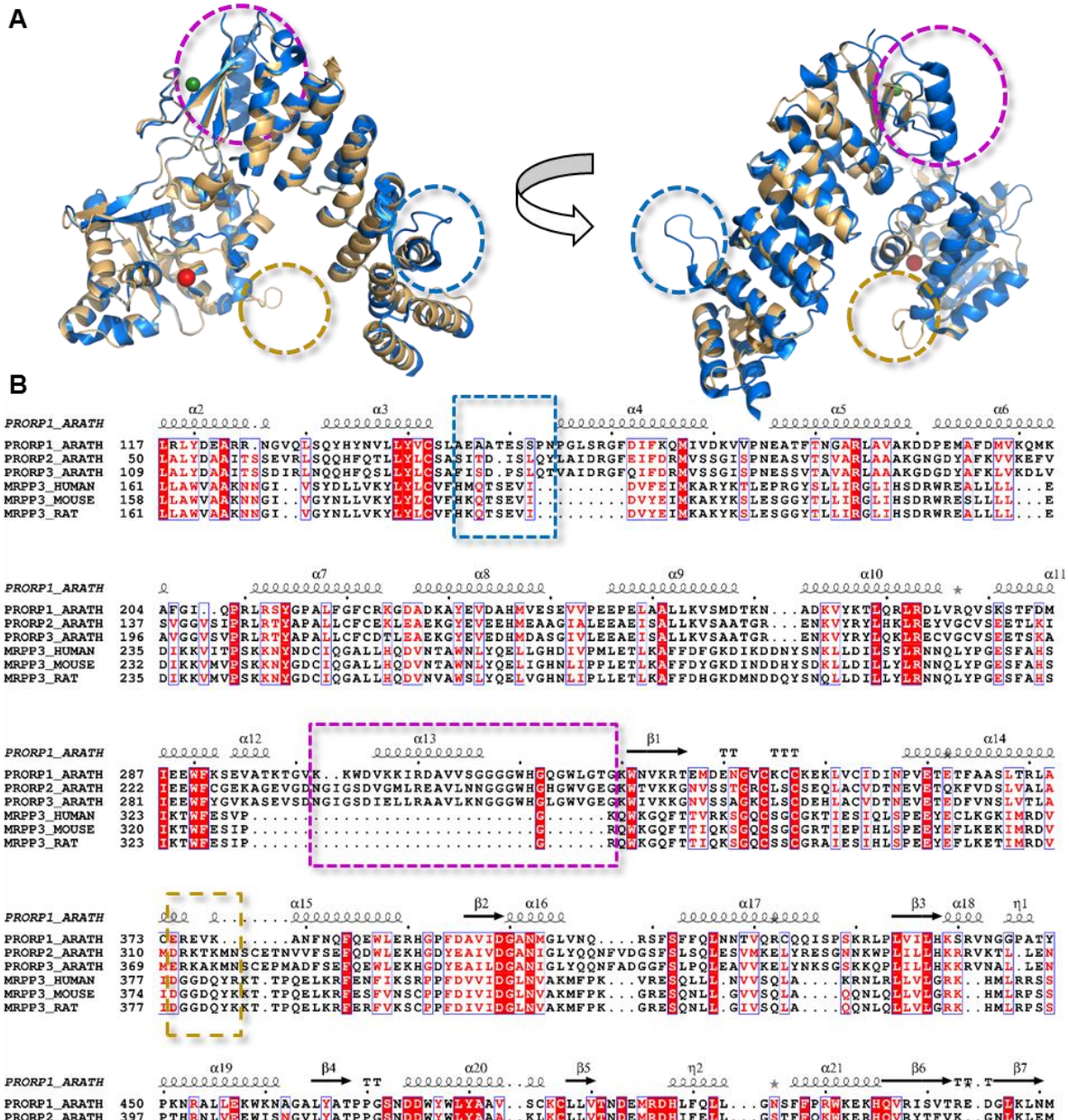


**Figure C-2:** Homology model of MRPP3 and multiple sequence alignments of PRORP proteins. **(A)** Alignment of PRORP1 (Blue) crystal structure (PDB ID: 4G26 [59]) with a homology model structure of MRPP3 (yellow, amino acids 141 to 582). Calcium ion (red sphere) in the active site and the zinc ion (green sphere) in the central domain of PRORP1 are shown. Homology modeling of MRPP3 structure was performed on Phyre2 server [122]

and the returning model has a 100% confidence score. Three regions showing discrepancies between the MRPP3 model and PRORP1 structure are boxed in both the structure cartoon and in the sequence alignment in (B). **(B)** Multiple sequence alignment of 20 PRORP protein sequences showing *A. thaliana* PRORP1, 2, and 3 and three mammalian MRPP3 proteins. Secondary structure is annotated based on PRORP1 structure using ESPript 2.2 [126]. Sequences in dash-line boxes correspond to structure elements that differ between MRPP3 model and PRORP1 structure. Full sequence identity and similarity between MRPP3 and PRORP1 are 20% and 29%, respectively.

**Table C-1:** Molecular biology for subcloning MRPP1 and MRPP1·MRPP2 complex.

| | Protein Construct [a] | Primer Sequences | Parent Vector | Restriction Enzyme | Plasmid Name [b] | Notes to Results [c] |
|---|---|---|---|---|---|---|
| **1** | His3CMRPP1+MRPP2 | | | | | |
| **1-1** | Round 1: | Double digestion of pETM11HisTevMRPP2 [d] | pCDFDuet-1 | NdeI XhoI | pCDFMP2 (pXL001) | N/D |
| **1-2** | Round 2: | Double digestion of pJEJ494 [e] | pXL001 | NcoI-HF BamHI-HF | pHis3CMP 1+MP2 (pXL002) | Weak Ni(II)-column affinity or low expression level |
| **2** | MRPP1TevHis+MRPP2 | | | | | |
| **2-1** | Round 1: | For: 5'- CTG GTT CCA TGG GTA TGT CTT CCA AAA TAC CAG CTG -3' Rev: 5'- GGA CGT CTC GAG AGT CTT TGC CTT CTT TAGTCT GTT G -3' | pETM11-NcoI- -XhoI-TevHis [f] | NcoI-HF XhoI | pMP1TevHi s (pXL003) | Low expression and insoluble MRPP1TevHis |
| **2-2** | Round 2: | For: 5'- CTG GTT CCA TGG GTA TGT CTT CCA AAA TAC CAG CTG -3' Rev: 5'- CGCTAA GGATCC ATC TCA GTG GTG GTG GTG -3' | pXL001 | NcoI-HF BamHI-HF | pMP1TevHi s (pXL004) | Low expression or insoluble MRPP1TevHis |
| **3** | HisTevMRPP1+MRPP2 | | | | | |
| **3-1** | Round 1: | See: 4. 5 Materials and Methods: | pETM11HisT evMP2 | NdeI XhoI | pETM11His TevMP1 (pXL005) | Good expression in BL21DE3pLys cells and affinity to Ni(II) column [g] |
| **3-2** | Round 2: | See: 4. 4 Materials and Methods: | pXL001 | NcoI-HF BamHI-HF | pHisTevMP 1+MP2 (pXL006) | See: 4.2 Results |
| **4** | HisTevMRPP2+MRPP1 | | | | | |
| **4-1** | Round 1: | Same as in row 3-1 | pCDFDuet-1 (Novagen) | Same as in row 8 | pCDFMP1 (pXL007) | N/D |
| **4-2** | Round 2: | For: 5'- CGA TCA CCA TGG GTA TGA AAC ATC ACC ATC ACC AT -3' Rev: 5'- GGA TTG GAT CCT CAA GGC TGC ATA CGA ATG -3' | pXL007 | NcoI-HF BamHI-HF | pHisTevMP 2+MP1 (pXL008) | Low expression of HisTevMRPP1 |
| **5** | HisTevMRPP2+HisTevMPP2 | | | | | |
| **5-1** | Round 1: | Same as in row 3-2 | pCDFDuet-1 (Novagen) | NcoI-HF BamHI-HF | pCDFHisTe vMP1 (pXL009) | N/D |
| **5-2** | Round 2: | For: 5'- GTC AGA GAG ATC GAA ACA TCA CCA TCA CCA TCA -3' Rev: 5'- GTG ATT CTC GAG TCA AGG CTG CA -3' | pXL009 | EcoRV XhoI | pHisTevMP 1+HisTevM P2 (pXL010) | Low expression of HisTevMRPP1 |
| **6** | Non-tagged MRPP1 | | | | | |
| | | Double digestion of pXL005 | pET21-a(+) | NdeI XhoI | pET21-a(+)MP1 (pXL011) | N/D |

[a] MRPP1 corresponds to Δ39 N-terminal truncation and MRPP2 is full length. His3C: hexahistidine (His6) tag followed by a cleavage sequence by 3C protease at N-terminal of protein sequences. HisTev: His6 tag tagged followed by TEV protease cleavage site at N-terminal. TevHis: TEV cleavage site followed by His6 tag and stop codon.
[b] Plasmid name in parenthesis corresponds to Xin Liu's laboratory notebook recording.
[c] See Materials and Methods for experimental conditions used for evaluation of expression and purification.
[d] Cloning of pETM11HisTevMRPP2 was described in Dr. Wan Lim's thesis [77].
[e] pJEJ494 was a gift from Dr. Jane Jackman (Ohio State University).
[f] The pETM11-NcoI-XhoI-TevHis parent vector is engineered by Andrea Stoddard. A stop codon is engineered downstream of the C-terminal TevHis tag.
[g] Expression and purification of HisTevMRPP1 from BL21DE3pLysS cells were carried out by Michael Howard.

**Table C-2:** DNA sequences of 16 plasmids for mt-pre-tRNA. T7 promoter sequence in blue, 5' leader and 3' trailer sequences in lower case and sequence corresponding to transcribed RNA underlined.

| mt-pre-tRNA | Sequence of DNA Template | Linearization site | Vector |
|---|---|---|---|
| **Type 0** | | | |
| Leu(UUR)42-39 | TAATACGACTCACTATAgcaacttagtattatacccacacccacccaaga acagggtttGTTAAGATGGCAGAGCCCGGTAATCGCATAAAACTTAAAAC TTTACAGTCAGAGGTTCAATTCCTCTTCTTAACAacatacccatggccaa cctcctactcctcattgtctaga | XbaI | pUC18 |
| Leu(CUN)28-32 | TAATACGACTCACTATAgcccatgtctaacaacatggctttctcaACTTT TAAAGGATAACAGCTATCCATTGGTCTTAGGCCCCAAAAATTTTGGTGCA ACTCCAAATAAAAGTAaataaccatgcacactactataaccactctaga | XbaI | pUC18 |
| Gln | TAATACGACTCACTATAgctgaccttacttTAGGATGGGGTGTGATAGGT GGCACGGAGAATTTTGGATTCTCAGGGATGGGTTCGATTCTCATAGTCCT AGaaataaggggtctaga | XbaI | pUC18 |
| **Type II** | | | |
| Arg19-14 | TAATACGACTCACTATAggattagactgaaccgaatTGGTATATAGTTTA AACAAAACGAATGATTTCGACTCATTAAATTATGATAATCATATTTACCA Aatgcccctctctaga | XbaI | pUC18 |
| Asp19-40 | TAATACGACTCACTATAgcctccatgacttttttcaaAAGGTATTAGAAAA ACCATTTCATAACTTTGTCAAAGTTAAATTATAGGCTAAATCCTATATAT CTTAatggcacatgcagcgcaagtaggtctacaagacgctctaga | XbaI | pUC18 |
| Glu12-35 | TAATACGACTCACTATAggggtcattggtGTTCTTGTAGTTGAAATACAA CGATGGTTTTTCATATCATTGGTCGTGGTTGTAGTCCGTGCGAGAATAat gatgtatgctttgtttctgttgagtgtgtctaga | XbaI | pUC18 |
| Gly26-54 | TAATACGACTCACTATAggtctccatctattgatgagggtcttACTCTTT TAGTATAAATAGTACCGTTAACTTCCAATTAACTAGTTTTGACAACATTC AAAAAAGAGTAataaacttcgccttaattttaataatcaacaccctccta gccttactactctaga | XbaI | pUC18 |
| Lys10-34 | TAATACGACTCACTATAggctagagccCACTGTAAAGCTAACTTAGCATT AACCTTTTAAGTTAAAGATTAAGAGAACCAACACCTCTTTACAGTGAaat gccccaactaaatactaccgtatggctctaga | XbaI | pUC18 |
| Ile42-24 | TAATACGACTCACTATAgggcgaattcattacaatctccagcattcccccc tcaaacctaAGAAATATGTCTGATAAAAGAGTTACTTTGATAGAGTAAAT AATAGGAGCTTAAACCCCCTTATTTCTAggactatgagaatcgaacctct aga | XbaI | pGEM-3Z |
| Ile11-5 | TAATACGACTCACTATAgctcaaacctaAGAAATATGTCTGATAAAAGAG TTACTTTGATAGAGTAAATAATAGGAGCTTAAACCCCCTTATTTCTAgga tcc | BamHI | pUC19 |
| Met10-40 | TAATACGACTCACTATAgccatcctaaAGTAAGGTCAGCTAAATAAGCTA TCGGGCCCATACCCCGAAAATGTTGGTTATACCCTTCCCGTACTAattaa tcccctggcccaacccgtcatctactctactctaga | XbaI | pUC18 |
| Tyr55-39* | TAATACGACTCACTATAgggagaccggaattctagagaatagtcaacggt cggcgaacatcagtgggggtgaGGTAAAATGGCTGAGTGAAGCATTGGAC TGTAAATCTAAAGACAGGGGTTAGGCCTCTTTTTACCAgctccgaggtga ttttcatattgaattgcaaattggatcc | BamHI | pGEM-1 |
| Tyr55-0 | TAATACGACTCACTATAgggagaccggaattctagagaatagtcaacggt cggcgaacatcagtgggggtgaGGTAAAATGGCTGAGTGAAGCATTGGAC TGTAAATCTAAAGACAGGGGTTAGGCCTCTTTTTACCAgg | BstNI | pGEM-1 |
| Tyr5-0 | TAATACGACTCACTATAggtgaGGTAAAATGGCTGAGTGAAGCATTGGAC TGTAAATCTAAAGACAGGGGTTAGGCCTCTTTTTACCAgg | BstNI | pUC19 |
| **Type I** | | | |
| Ser(UCN) | TAATACGACTCACTATAgacaaagttatgaaatggtttttctaatacctt tttGAAAAAGTCATGGAGGCCATGGGGTTGGCTTGAAACCAGCTTTGGGG GGTTCGATTCCTTCCTTTTTTGtctaga | XbaI | pUC18 |
| **Type III** | | | |
| His-Ser(AGY)-Leu(UCN) | TAATACGACTCACTATAgctcaaccccgacatcattaccgggttttcctc ttGTAAATATAGTTTAACCAAAACATCAGATTGTGAATCTGACAACAGAG GCTTACGACCCCTTATTTACCGAGAAAGCTCACAAGAACTGCTAACTCAT GCCCCCATGTCTAACAACATGGCTTTCTCAACTTTTAAAGGATAACAGCT ATCCATTGGTCTTAGGCCCCAAAAATTTTGGTGCAACTCCAAATAAAAGT aataaccatgcacactactataaccaccctctaga | XbaI | pUC18 |

**Table C-3:** Primers for subcloning mt-pre-tRNA genes by blunt-end ligation.

| Sequence Name | Sequence |
|---|---|
| Arg-For | TAA TAC GAC TCA CTA TAG GAT TAG ACT GAA CCG AAT TG |
| Arg-Rev | GGA AGT CTA GAG AGG GGC ATT TGG TAA ATA TG |
| Asp-For | TAA TAC GAC TCA CTA TAG CCT CCA TGA CTT TTT CAA AA |
| Asp-Rev | GTG AAT CTA GAG CGT CTT GTA GAC CTA CTT G |
| Gly-For | TAA TAC GAC TCA CTA TAG GTC TCC ATC TAT TGA TGA GGG |
| Gly-Rev | GGT AGT CTA GAG TAG TAA GGC TAG GAG GGT G |
| His-For | TAA TAC GAC TCA CTA TAG CAA CCC CGA CAT CAT TAC C |
| His-Rev | GTC CAT CTA GAG AGT TAG CAG TTC TTG TGA GC |
| Met-For | TAA TAC GAC TCA CTA TAG CCA TCC TAA AGT AAG GTC AGC |
| Met-Rev | GTG CTT CTA GAG TAG AGT AGA TGA CGG GTT G |
| Phe-For | TAA TAC GAC TCA CTA TAG CCC ACA GTT TAT GTA GCT TAC C |
| Phe-Rev | GCA ATT CTA GAG AAA GGC TAG GAC CAA ACC |
| Trp-For | TAA TAC GAC TCA CTA TAG CCA CGC TAC TCC TAC CTA TC |
| Trp-Rev | GCA AGT CTA GAG CAG AGT GGG GTT TTG CAG |
| Thr-For | TAA TAC GAC TCA CTA TAG CCA ACT ATC TCC CTA ATT G |
| Thr-Rev | GCT GAT CTA GAG CTA ATG GTG GAG TTA AAG |
| Val-For | TAA TAC GAC TCA CTA TAG ACG AAC CAG AGT GTA GC |
| Val-Rev | GAG GAT CTA GAG TTT AGC TCA GAG CGG TC |
| Ala-For | TAA TAC GAC TCA CTA TAG GTC CCA TTG GTC TAG TAA GG |
| Ala-Rev | GGT GAT CTA GAC TGT AAC AGC TAA GGA CTG C |
| Asn-For | TAA TAC GAC TCA CTA TAG CGG GAG AAG TAG ATT GAA G |
| Asn-Rev | GGA GTT CTA GAG CTA AGC CCT TAC TAG ACC |
| Cys-For | TAA TAC GAC TCA CTA TAG GCT AAA GAC AGG GGT TAG GC |
| Cys-Rev | GAC TCT CTA GAC AAT CTA CTT CTC CCG CC |
| Glu-For | TAA TAC GAC TCA CTA TAG GGG TCA TTG GTG TTC TTG |
| Glu-Rev | GAG ACT CTA GAC ACA CTC AAC AGA AAC AAA GC |
| Gln-For | TAA TAC GAC TCA CTA TAG CTG ACC TTA CTT TAG GAT GG |
| Gln-Rev | GTG AAT CTA GAC CCC TTA TTT CTA GGA CTA TGA G |
| Pro-For | TAA TAC GAC TCA CTA TAG CTT CCC CAT GAA AGA ACA G |
| Pro-Rev | CTG AAT CTA GAC AAG GAC AAA TCA GAG AAA AAG TC |
| I-Q-M-Hvy-For | TAA TAC GAC TCA CTA TAG CAT TAC AAT CTC CAG CAT TCC |
| I-Q-M-Hvy-Rev | GCT CAT CTA GAC CTG CAA AGA TGG TAG AGT AG |
| M-Q-I-Lt-For | TAA TAC GAC TCA CTA TAG CCT GCA AAG ATG GTA GAG TAG |
| M-O-I-Lt-Rev | GCT GAT CTA GAC ATT ACA ATC TCC AGC ATT CC |
| Y-C-N-A-W-Lt-For | TAA TAC GAC TCA CTA TAG AGA ATA GTC AAC GGT CGG |
| Y-C-N-A-W-Lt-Rev | GCT GAT CTA GAC CAC GCT ACT CCT ACC TAT C |
| S-D-Hvy-For | TAA TAC GAC TCA CTA TAG CAC CCT ACC ACA CAT TC |
| S-D-Hvy-Rev | GAC ACT TTA AAC GTC TTG TAG ACC TAC TTG C |
| D-S-Lt-For | TAA TAC GAC TCA CTA TAG CGT CTT GTA GAC CTA CTT GC |
| D-S-Lt-Rev | GAC ACT TTA AAC ACC CTA CCA CAC ATT C |
| L-S-H-Hvy-For | TAA TAC GAC TCA CTA TAG CTC AAC CCC GAC ATC ATT AC |
| L-S-H-Hvy-Rev | GAC GAT CTA GAG GTG GTT ATA GTA GTG TGC ATG |
| T-P-Hvy-For | TAA TAC GAC TCA CTA TAG CCA ACT ATC TCC CTA ATT G |
| T-P-Hvy-Rev | GAC CAT CTA GAC ATA GCG GTT GTT GAT G |
| P-T-Lt-For | TAA TAC GAC TCA CTA TAG CAT AGC GGT TGT TGA TG |
| P-T-Lt-Rev | GAC CAT CTA GAC CAA CTA TCT CCC TAA TTG |

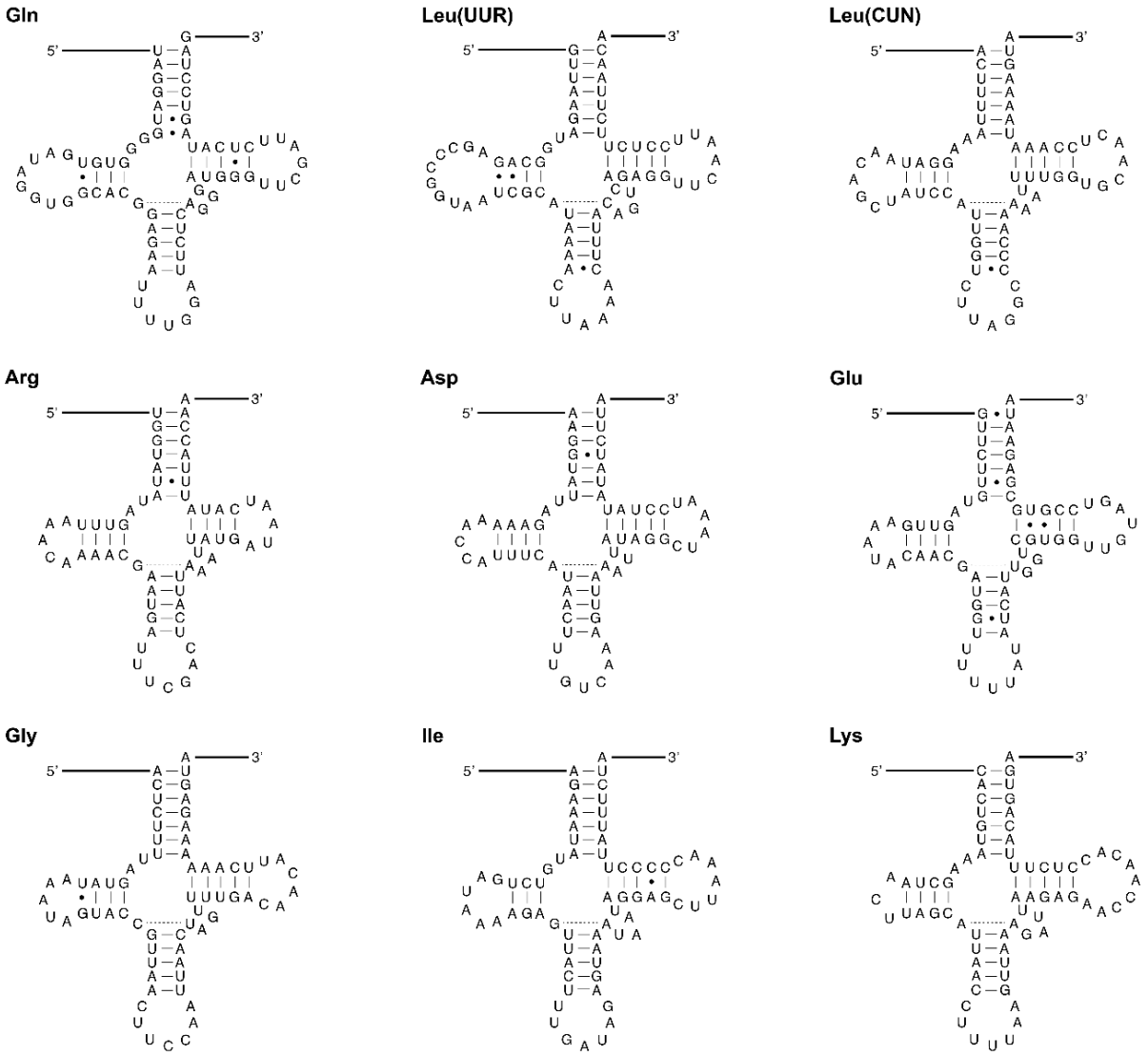


**Figure C-3:** Secondary structures of cloned human mitochondrial pre-tRNA species (part 1) indicated in Table 4-1, showing sequences of the mt-tRNA body (N1 to N73).

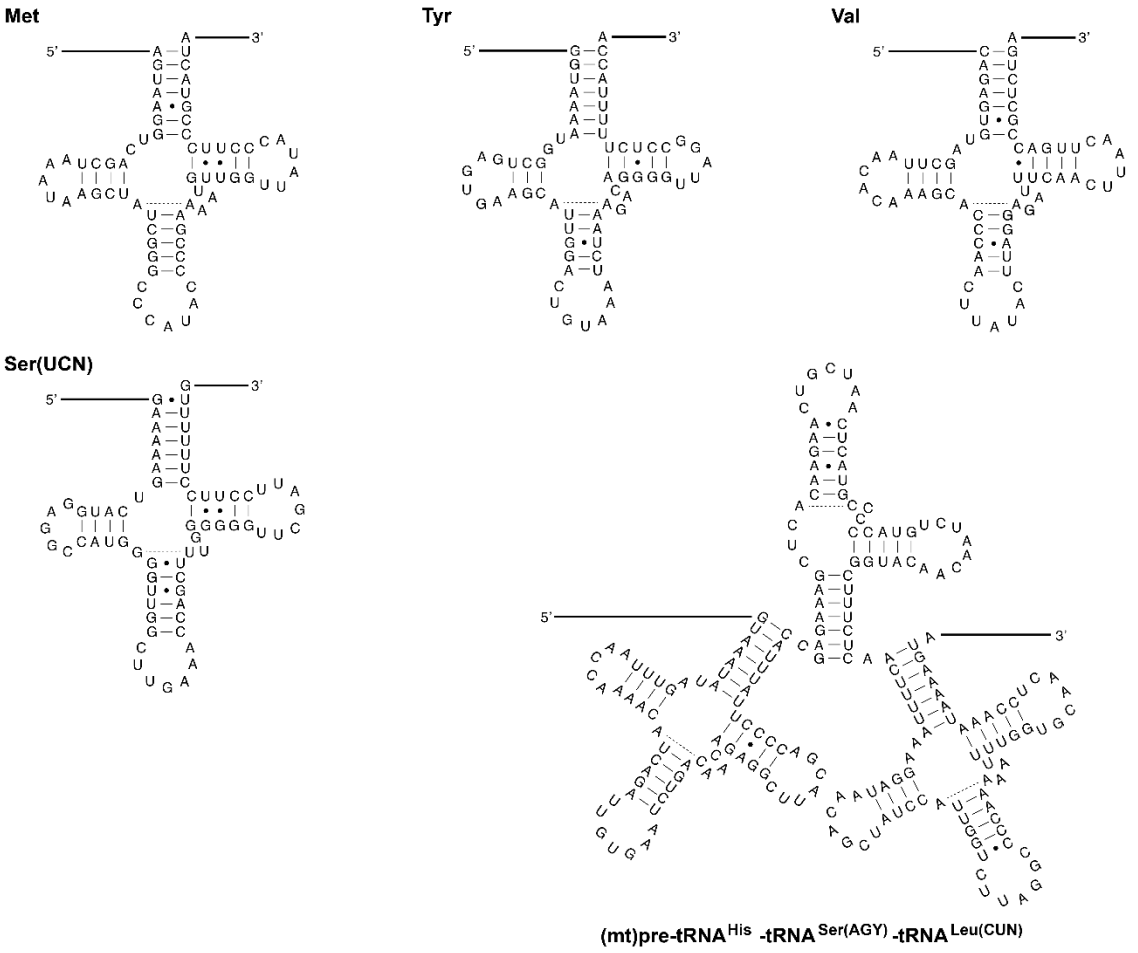


**Figure C-4:** Secondary structures of cloned human mitochondrial pre-tRNA species (part 2) indicated in Table 4-1, showing sequences of the mt-tRNA body (N1 to N73).

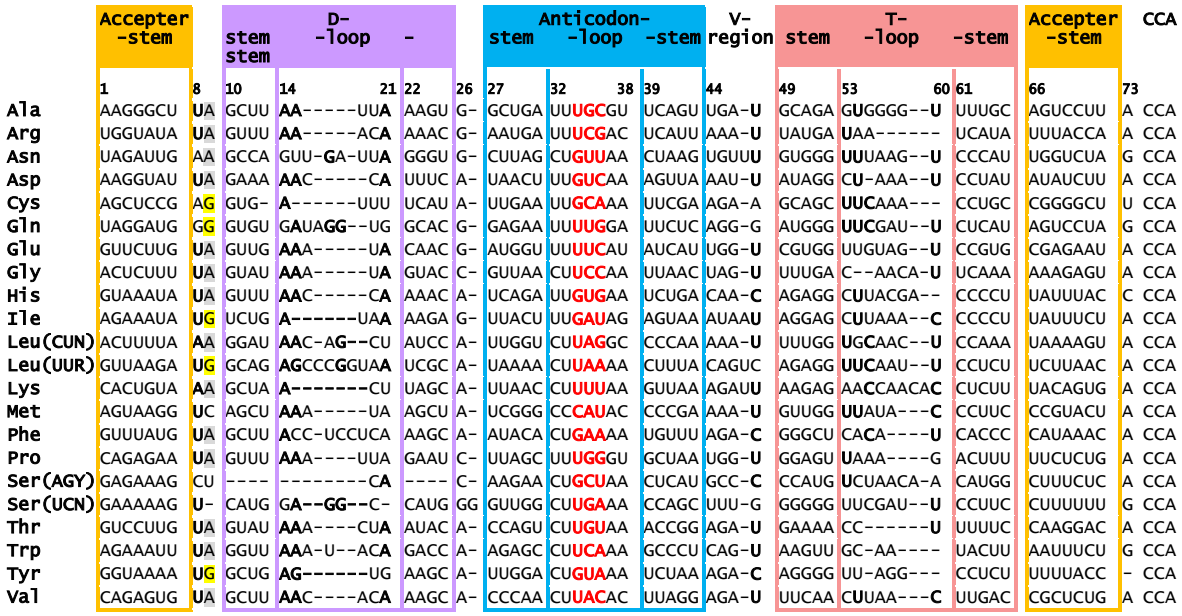


**Figure C-5:** Sequence alignment of all 22 human mitochondrial tRNA sequences. Primary sequence alignment was downloaded from mt-tRNA database [36] and the manually adjusted based on sequence conservation of canonical tRNA. 3' CCA sequence is not encoded in the human mtDNA. The determinant nucleotide of mt-tRNA$^{Tyr}$ (A73) encoded in the genome is discounted in the mt-tRNAdb, which is likely due to the finding that tRNAs with a 3' CCACCA sequence (CCA from N71 to N73) are targeted to a rapid tRNA degradation pathway [128].

**Table C-4:** Human mitochondrial tRNA sequences including 5' leader, tRNA body and 3' trailer genes. Yellow highlight indicates tRNA species transcribed from the light strand of mtDNA.

| | tRNA | 5' Leader | Body | 3' Trailer |
|---|---|---|---|---|
| **1** | Ala | 5' UCC CAU UGG UCU AGU 3' | 5' AAG GGC UUA GCU UAA UUA AAG UGG CUG AUU UGC GUU CAG UUG AUG CAG AGU GGG GUU UUG CAG UCC UUA 3' | 5' GCU GUU ACA GAA AUU 3' |
| **2** | Arg | 5' UAG ACU GAA CCG AAU 3' | 5' UGG UAU AUA GUU UAA ACA AAA CGA AUG AUU UCG ACU CAU UAA AUU AUG AUA AUC AUA UUU ACC AA 3' | 5' AUG CCC CUC AUU UAC 3' |
| **3** | Asn | 5' CGG CGG CGG GAG AAG 3' | 5' UAG AUU GAA GCC AGU UGA UUA GGG UGC UUA GCU GUU AAC UAA GUG UUU GUG GGU UUA AGU CCC AUU GGU CUA G 3' | 5' UAA GGG CUU AGC UUA 3' |
| **4** | Asp | 5' CCA UGA CUU UUU CAA 3' | 5' AAG GUA UUA GAA AAA CCA UUU CAU AAC UUU GUC AAA GUU AAA UUA UAG GCU AAA UCC UAU AUA UCU UA 3' | 5' AUG GCA CAU GCA GCG 3' |
| **5** | Cys | 5' AGG CCU CUU UUU ACC 3' | 5' AGC UCC GAG GUG AUU UUC AUA UUG AAU UGC AAA UUC GAA GAA GCA GCU UCA AAC CUG CCG GGG CUU 3' | 5' CUC CCG CCU UUU UUC 3' |
| **6** | Gln | 5' UAG CUG ACC UUA CUU 3' | 5' UAG GAU GGG GUG UGA UAG GUG GCA CGG AGA AUU UUG GAU UCU CAG GGA UGG GUU CGA UUC UCA UAG UCC UAG 3' | 5' AAA UAA GGG GGU UUA 3' |
| **7** | Glu | 5' AUU GGG GUC AUU GGU 3' | 5' GUU CUU GUA GUU GAA AUA CAA CGA UGG UUU UUC AUA UCA UUG GUC GUG GUU GUA GUC CGU GCG AGA AUA 3' | 5' AUG AUG UAU GCU UUG U 3' |
| **8** | Gly | 5' AUU GAU GAG GGU CUU 3' | 5' ACU CUU UUA GUA UAA AUA GUA CCG UUA ACU UCC AAU UAA CUA GUU UUG ACA ACA UUC AAA AAA GAG UA 3' | 5' AUA AAC UUC GCC UUA 3' |
| **9** | His | 5' CCG GGU UUU CCU CUU 3' | 5' GUA AAU AUA GUU UAA CCA AAA CAU CAG AUU GUG AAU CUG ACA ACA GAG GCU UAC GAC CCC UUA UUU ACC 3' | 5' GAG AAA GCU CAC AAG 3' |
| **10** | Ile | 5' UCC CCC UCA AAC CUA 3' | 5' GAA AUA UGU CUG AUA AAA GAG UUA CUU UGA UAG AGU AAA UAA UAG GAG CUU AAA CCC CCU UAU UUC UA 3' | 5' GGA CUA UGA GAA UCG 3' |
| **11** | Leu (CUN) | 5' AAC AUG GCU UUC UCA 3' | 5' ACU UUU AAA GGA UAA CAG CUA UCC AUU GGU CUU AGG CCC CAA AAA UUU UGG UGC AAC UCC AAA UAA AAG UA 3' | 5' AAU AAC CAU GCA CAC 3' |
| **12** | Leu (UUR) | 5' CCA AGA ACA GGG UUU 3' | 5' GUU AAG AUG GCA GAG CCC GGU AAU CGC AUA AAA CUU AAA ACU UUA CAG UCA GAG GUU CAA UUC CUC UUC UUA ACA 3' | 5' ACA UAC CCA UGG CCA 3' |
| **13** | Lys | 5' ACC CCC UCU AGA GCC 3' | 5' CAC UGU AAA GCU AAC UUA GCA UUA ACC UUU UAA GUU AAA GAU UAA GAG AAC CAA CAC CUC UUU ACA GUG A 3' | 5' AAU GCC CCA ACU AAA 3' |
| **14** | Met | 5' CAC ACC CCA UCC UAA 3' | 5' AGU AAG GUC AGC UAA AUA AGC UAU CGG GCC CAU ACC CCG AAA AUG UUG GUU AUA CCC UUC CCG UAC UA 3' | 5' AUU AAU CCC CUG GCC 3' |
| **15** | Phe | 5' AAG ACA CCC CCC ACA 3' | 5' GUU UAU GUA GCU UAC CUC CUC AAA GCA AUA CAC UGA AAA UGU UUA GAC GGG CUC ACA UCA CCC CAU AAA CA 3' | 5' AAU AGG UUU GGU CCU 3' |
| **16** | Pro | 5' UUC CCC AUG AAAGA A 3' | 5' CAG AGA AUA GUU UAA AUU AGA AUC UUA GCU UUG GGU GCU AAU GGU GGA GUU AAA GAC UUU UUC UCU GA 3' | 5' UUU GUC CUU GGA AAA 3' |
| **17** | Ser (AGY) | 5' GAC CCC UUA UUU ACC 3' | 5' GAG AAA GCU CAC AAG AAC UGC UAA CUC AUG CCC CCA UGU CUA ACA ACA UGG CUU UCU CA 3' | 5' ACU UUU AAA GGA UAA 3' |
| **18** | Ser (UCN) | 5' UUU CUA AUA CCU UUU 3' | 5' GAA AAA GUC AUG GAG GCC AUG GGG UUG GCU UGA AAC CAG CUU UGG GGG GUU CGA UUC CUU CCU UUU UUG 3' | 5' UCU AGA UUU UAU GUA 3' |
| **19** | Thr | 5' UAC UCA AAU GGG CCU 3' | 5' GUC CUU GUA GUA UAA ACU AAU ACA CCA GUC UUG UAA ACC GGA GAU GAA AAC CUU UUU CCA AGG ACA 3' | 5' AAU CAG AGA AAA AGU 3' |
| **20** | Trp | 5' UAC UAA UAA UCU UAU 3' | 5' AGA AAU UUA GGU UAA AUA CAG ACC AAG AGC CUU CAA AGC CCU CAG UAA GUU GCA AUA CUU AAU UUC UG 3' | 5' UAA CAG CUA AGG ACU 3' |
| **21** | Tyr | 5' CAU CAG UGG GGG UGA 3' | 5' GGU AAA AUG GCU GAG UGA AGC AUU GGA CUG UAA AUC UAA AGA CAG GGG UUA GGC CUC UUU UUA CCA 3' | 5' GCU CCG AGG UGA UUU 3' |
| **22** | Val | 5' UGC ACU UGG ACG AAC 3' | 5' CAG AGU GUA GCU UAA CAC AAA GCA CCC AAC UUA CAC UUA GGA GAU UUC AAC UUA ACU UGA CCG CUC UGA 3' | 5' GCU AAA CCU AGC CCC 3' |

## 4.7 References


1. Shutt, T.E. and G.S. Shadel, *A compendium of human mitochondrial gene expression machinery with links to disease.* Environ Mol Mutagen, 2010. **51**(5): p. 360-79.
2. Youle, R.J. and A.M. van der Bliek, *Mitochondrial fission, fusion, and stress.* Science, 2012. **337**(6098): p. 1062-5.
3. Taylor, R.W. and D.M. Turnbull, *Mitochondrial DNA mutations in human disease.* Nat Rev Genet, 2005. **6**(5): p. 389-402.
4. Tuppen, H.A., et al., *Mitochondrial DNA mutations and human disease.* Biochim Biophys Acta, 2010. **1797**(2): p. 113-28.
5. Wallace, D.C., *Mitochondrial DNA mutations in disease and aging.* Environ Mol Mutagen, 2010. **51**(5): p. 440-50.
6. Park, C.B. and N.G. Larsson, *Mitochondrial DNA mutations in disease and aging.* J Cell Biol, 2011. **193**(5): p. 809-18.
7. Schon, E.A., S. DiMauro, and M. Hirano, *Human mitochondrial DNA: roles of inherited and somatic mutations.* Nat Rev Genet, 2012. **13**(12): p. 878-90.
8. Sanchez, M.I., et al., *RNA processing in human mitochondria.* Cell Cycle, 2011. **10**(17): p. 2904-16.
9. Mercer, T.R., et al., *The human mitochondrial transcriptome.* Cell, 2011. **146**(4): p. 645-58.
10. Rackham, O., T.R. Mercer, and A. Filipovska, *The human mitochondrial transcriptome and the RNA-binding proteins that regulate its expression.* Wiley Interdiscip Rev RNA, 2012. **3**(5): p. 675-95.
11. Florentz, C., et al., *Human mitochondrial tRNAs in health and disease.* Cell Mol Life Sci, 2003. **60**(7): p. 1356-75.
12. Wittenhagen, L.M. and S.O. Kelley, *Impact of disease-related mitochondrial mutations on tRNA structure and function.* Trends Biochem Sci, 2003. **28**(11): p. 605-11.
13. Anderson, S., et al., *Sequence and organization of the human mitochondrial genome.* Nature, 1981. **290**(5806): p. 457-65.
14. Montoya, J., G.L. Gaines, and G. Attardi, *The pattern of transcription of the human mitochondrial rRNA genes reveals two overlapping transcription units.* Cell, 1983. **34**(1): p. 151-9.
15. Ojala, D., J. Montoya, and G. Attardi, *tRNA punctuation model of RNA processing in human mitochondria.* Nature, 1981. **290**(5806): p. 470-4.
16. Ojala, D., et al., *The tRNA genes punctuate the reading of genetic information in human mitochondrial DNA.* Cell, 1980. **22**(2 Pt 2): p. 393-403.
17. Rackham, O., et al., *Long noncoding RNAs are generated from the mitochondrial genome and regulated by nuclear-encoded proteins.* RNA, 2011. **17**(12): p. 2085-93.
18. Suzuki, T., A. Nagao, and T. Suzuki, *Human mitochondrial tRNAs: biogenesis, function, structural aspects, and diseases.* Annu Rev Genet, 2011. **45**: p. 299-329.
19. Ruiz-Pesini, E., et al., *An enhanced MITOMAP with a global mtDNA mutational phylogeny.* Nucleic Acids Res, 2007. **35**(Database issue): p. D823-8.
20. Yarham, J.W., et al., *A comparative analysis approach to determining the pathogenicity of mitochondrial tRNA mutations.* Hum Mutat, 2011. **32**(11): p. 1319-25.
21. Yarham, J.W., et al., *Mitochondrial tRNA mutations and disease.* Wiley Interdiscip Rev RNA, 2010. **1**(2): p. 304-24.
22. Zaragoza, M.V., et al., *Mitochondrial cardiomyopathies: how to identify candidate pathogenic mutations by mitochondrial DNA sequencing, MITOMASTER and phylogeny.* Eur J Hum Genet, 2011. **19**(2): p. 200-7.
23. Helm, M., et al., *Search for differences in post-transcriptional modification patterns of mitochondrial DNA-encoded wild-type and mutant human tRNALys and tRNALeu(UUR).* Nucleic Acids Res, 1999. **27**(3): p. 756-63.
24. Wittenhagen, L.M. and S.O. Kelley, *Dimerization of a pathogenic human mitochondrial tRNA.* Nat Struct Biol, 2002. **9**(8): p. 586-90.

25. Kelley, S.O., S.V. Steinberg, and P. Schimmel, *Fragile T-stem in disease-associated human mitochondrial tRNA sensitizes structure to local and distant mutations.* J Biol Chem, 2001. **276**(14): p. 10607-11.
26. Rossmanith, W. and R.M. Karwan, *Impairment of tRNA processing by point mutations in mitochondrial tRNA(Leu)(UUR) associated with mitochondrial diseases.* FEBS Lett, 1998. **433**(3): p. 269-74.
27. Levinger, L., M. Morl, and C. Florentz, *Mitochondrial tRNA 3' end metabolism and human disease.* Nucleic Acids Res, 2004. **32**(18): p. 5430-41.
28. Toompuu, M., et al., *The 7472insC mtDNA mutation impairs 5' and 3' processing of tRNA(Ser(UCN)).* Biochem Biophys Res Commun, 2004. **322**(3): p. 803-13.
29. Yasukawa, T., et al., *A pathogenic point mutation reduces stability of mitochondrial mutant tRNA(Ile).* Nucleic Acids Res, 2000. **28**(19): p. 3779-84.
30. Yasukawa, T., et al., *Wobble modification defect in tRNA disturbs codon-anticodon interaction in a mitochondrial disease.* EMBO J, 2001. **20**(17): p. 4794-802.
31. Tryoen-Toth, P., et al., *Proteomic consequences of a human mitochondrial tRNA mutation beyond the frame of mitochondrial translation.* J Biol Chem, 2003. **278**(27): p. 24314-23.
32. Toompuu, M., et al., *The 7472insC mitochondrial DNA mutation impairs the synthesis and extent of aminoacylation of tRNASer(UCN) but not its structure or rate of turnover.* J Biol Chem, 2002. **277**(25): p. 22240-50.
33. Chomyn, A., et al., *MELAS mutation in mtDNA binding site for transcription termination factor causes defects in protein synthesis and in respiration but no change in levels of upstream and downstream mature transcripts.* Proc Natl Acad Sci U S A, 1992. **89**(10): p. 4221-5.
34. Flierl, A., H. Reichmann, and P. Seibel, *Pathophysiology of the MELAS 3243 transition mutation.* J Biol Chem, 1997. **272**(43): p. 27189-96.
35. Putz, J., et al., *Mamit-tRNA, a database of mammalian mitochondrial tRNA primary and secondary structures.* RNA, 2007. **13**(8): p. 1184-90.
36. Juhling, F., et al., *tRNAdb 2009: compilation of tRNA sequences and tRNA genes.* Nucleic Acids Res, 2009. **37**(Database issue): p. D159-62.
37. Helm, M., et al., *Search for characteristic structural features of mammalian mitochondrial tRNAs.* RNA, 2000. **6**(10): p. 1356-79.
38. Giege, R., et al., *Structure of transfer RNAs: similarity and variability.* Wiley Interdiscip Rev RNA, 2012. **3**(1): p. 37-61.
39. Cognat, V., et al., *PlantRNA, a database for tRNAs of photosynthetic eukaryotes.* Nucleic Acids Res, 2013. **41**(Database issue): p. D273-9.
40. Bilbille, Y., et al., *The human mitochondrial tRNAMet: structure/function relationship of a unique modification in the decoding of unconventional codons.* J Mol Biol, 2011. **406**(2): p. 257-74.
41. Hayashi, I., G. Kawai, and K. Watanabe, *Higher-order structure and thermal instability of bovine mitochondrial tRNASerUGA investigated by proton NMR spectroscopy.* J Mol Biol, 1998. **284**(1): p. 57-69.
42. Bonnefond, L., et al., *Decreased aminoacylation in pathology-related mutants of mitochondrial tRNATyr is associated with structural perturbations in tRNA architecture.* RNA, 2008. **14**(4): p. 641-8.
43. Watanabe, Y., et al., *Higher-order structure of bovine mitochondrial tRNA(SerUGA): chemical modification and computer modeling.* Nucleic Acids Res, 1994. **22**(24): p. 5378-84.
44. Messmer, M., et al., *Pathology-related mutation A7526G (A9G) helps in the understanding of the 3D structural core of human mitochondrial tRNA(Asp).* RNA, 2009. **15**(8): p. 1462-8.
45. Ueda, T., T. Ohta, and K. Watanabe, *Large scale isolation and some properties of AGY-specific serine tRNA from bovine heart mitochondria.* J Biochem, 1985. **98**(5): p. 1275-84.
46. Yokogawa, T., et al., *Purification and characterization of two serine isoacceptor tRNAs from bovine mitochondria by using a hybridization assay method.* Nucleic Acids Res, 1989. **17**(7): p. 2623-38.
47. Arita, M., et al., *An evolutionary 'intermediate state' of mitochondrial translation systems found in Trichinella species of parasitic nematodes: co-evolution of tRNA and EF-Tu.* Nucleic Acids Res, 2006. **34**(18): p. 5291-9.

48. Sakurai, M., et al., *A protein extension to shorten RNA: elongated elongation factor-Tu recognizes the D-arm of T-armless tRNAs in nematode mitochondria.* Biochem J, 2006. **399**(2): p. 249-56.
49. Kazantsev, A.V. and N.R. Pace, *Bacterial RNase P: a new view of an ancient enzyme.* Nat Rev Microbiol, 2006. **4**(10): p. 729-40.
50. Holzmann, J., et al., *RNase P without RNA: identification and functional reconstitution of the human mitochondrial tRNA processing enzyme.* Cell, 2008. **135**(3): p. 462-74.
51. Hernandez-Cid, A., et al., *Ribonucleases P/MRP and the expanding ribonucleoprotein world.* IUBMB Life, 2012. **64**(6): p. 521-8.
52. Goldfarb, K.C., S. Borah, and T.R. Cech, *RNase P branches out from RNP to protein: organelle-triggered diversification?* Genes Dev, 2012. **26**(10): p. 1005-9.
53. Jarrous, N. and V. Gopalan, *Archaeal/eukaryal RNase P: subunits, functions and RNA diversification.* Nucleic Acids Res, 2010. **38**(22): p. 7885-94.
54. Gobert, A., et al., *A single Arabidopsis organellar protein has RNase P activity.* Nat Struct Mol Biol, 2010. **17**(6): p. 740-4.
55. Gutmann, B., A. Gobert, and P. Giege, *PRORP proteins support RNase P activity in both organelles and the nucleus in Arabidopsis.* Genes Dev, 2012. **26**(10): p. 1022-7.
56. Howard, M.J., et al., *RNase P enzymes: Divergent scaffolds for a conserved biological reaction.* RNA Biol, 2013. **10**(6).
57. Zeng, H., Dong, A., Loppnau, P., Tempel, W., Bountra, C., Weigelt, J., Arrowsmith, C.H., Edwards, A.M., Wu, H., *Crystal structure of methyltransferase domain of human RNA (guanine-9-) methyltransferase domain containing protein 2*, 2012: New York Structural GenomiX Research Consortium (NYSGXRC).
58. Kissinger, C.R., et al., *Crystal structure of human ABAD/HSD10 with a bound inhibitor: implications for design of Alzheimer's disease therapeutics.* J Mol Biol, 2004. **342**(3): p. 943-52.
59. Howard, M.J., et al., *Mitochondrial ribonuclease P structure provides insight into the evolution of catalytic strategies for precursor-tRNA 5' processing.* Proc Natl Acad Sci U S A, 2012. **109**(40): p. 16149-54.
60. Vilardo, E., et al., *A subcomplex of human mitochondrial RNase P is a bifunctional methyltransferase--extensive moonlighting in mitochondrial tRNA biogenesis.* Nucleic Acids Res, 2012. **40**(22): p. 11583-93.
61. Jackman, J.E., et al., *Identification of the yeast gene encoding the tRNA m1G methyltransferase responsible for modification at position 9.* RNA, 2003. **9**(5): p. 574-85.
62. Powell, A.J., et al., *Recognition of structurally diverse substrates by type II 3-hydroxyacyl-CoA dehydrogenase (HADH II)/amyloid-beta binding alcohol dehydrogenase (ABAD).* J Mol Biol, 2000. **303**(2): p. 311-27.
63. Lukacik, P., K.L. Kavanagh, and U. Oppermann, *Structure and function of human 17beta-hydroxysteroid dehydrogenases.* Mol Cell Endocrinol, 2006. **248**(1-2): p. 61-71.
64. Lustbader, J.W., et al., *ABAD directly links Abeta to mitochondrial toxicity in Alzheimer's disease.* Science, 2004. **304**(5669): p. 448-52.
65. Yang, S.Y., X.Y. He, and D. Miller, *Hydroxysteroid (17beta) dehydrogenase X in human health and disease.* Mol Cell Endocrinol, 2011. **343**(1-2): p. 1-6.
66. Jourdain, A.A., et al., *GRSF1 regulates RNA processing in mitochondrial RNA granules.* Cell Metab, 2013. **17**(3): p. 399-410.
67. Antonicka, H., et al., *The mitochondrial RNA-binding protein GRSF1 localizes to RNA granules and is required for posttranscriptional mitochondrial gene expression.* Cell Metab, 2013. **17**(3): p. 386-98.
68. Pavlova, L.V., et al., *tRNA processing by protein-only versus RNA-based RNase P: kinetic analysis reveals mechanistic differences.* Chembiochem, 2012. **13**(15): p. 2270-6.
69. Marechal-Drouard, L., J.H. Weil, and A. Dietrich, *Transfer RNAs and Transfer RNA Genes in Plants.* Annual Review of Plant Physiology and Plant Molecular Biology, 1993. **44**(1): p. 13-32.
70. Gobert, A., et al., *Structural insights into protein-only RNase P complexed with tRNA.* Nat Commun, 2013. **4**: p. 1353.

71. Reiter, N.J., et al., *Structure of a bacterial ribonuclease P holoenzyme in complex with tRNA.* Nature, 2010. **468**(7325): p. 784-9.
72. Rossmanith, W., et al., *Human mitochondrial tRNA processing.* J Biol Chem, 1995. **270**(21): p. 12885-91.
73. Nie, Y., et al., *Getting a grip on complexes.* Curr Genomics, 2009. **10**(8): p. 558-72.
74. Tolia, N.H. and L. Joshua-Tor, *Strategies for protein coexpression in Escherichia coli.* Nat Methods, 2006. **3**(1): p. 55-64.
75. Smith, B., *Quantification of Proteins by Staining in Polyacrylamide Gels*, in *The Protein Protocols Handbook*, J. Walker, Editor. 1996, Humana Press. p. 167-172.
76. Weist, S., et al., *Results and reliability of protein quantification for two-dimensional gel electrophoresis strongly depend on the type of protein sample and the method employed.* Proteomics, 2008. **8**(16): p. 3389-96.
77. Lim, W.H., *Importance of substrate recognition and metal ions in the Ribonuclease P catalysis*, 2011, University of Michigan.
78. Rubio, M.A., et al., *Mammalian mitochondria have the innate ability to import tRNAs by a mechanism distinct from protein import.* Proc Natl Acad Sci U S A, 2008. **105**(27): p. 9186-91.
79. Rossmanith, W., *Processing of human mitochondrial tRNA(Ser(AGY))GCU: a novel pathway in tRNA biosynthesis.* J Mol Biol, 1997. **265**(4): p. 365-71.
80. Zahler, N.H., et al., *The pre-tRNA nucleotide base and 2'-hydroxyl at N(-1) contribute to fidelity in tRNA processing by RNase P.* J Mol Biol, 2005. **345**(5): p. 969-85.
81. Zahler, N.H., E.L. Christian, and M.E. Harris, *Recognition of the 5' leader of pre-tRNA substrates by the active site of ribonuclease P.* RNA, 2003. **9**(6): p. 734-45.
82. Koutmou, K.S., et al., *Protein-precursor tRNA contact leads to sequence-specific recognition of 5' leaders by bacterial ribonuclease P.* J Mol Biol, 2010. **396**(1): p. 195-208.
83. Kirsebom, L.A. and S.G. Svard, *Base pairing between Escherichia coli RNase P RNA and its substrate.* EMBO J, 1994. **13**(20): p. 4870-6.
84. Li, R., et al., *Failures in mitochondrial tRNAMet and tRNAGln metabolism caused by the novel 4401A>G mutation are involved in essential hypertension in a Han Chinese Family.* Hypertension, 2009. **54**(2): p. 329-37.
85. Chen, W.Y., et al., *Fidelity of tRNA 5'-maturation: a possible basis for the functional dependence of archaeal and eukaryal RNase P on multiple protein cofactors.* Nucleic Acids Res, 2012. **40**(10): p. 4666-80.
86. Pavlova, L., et al., *tRNA Processing by Protein-Only versus RNA-Based RNase P: Kinetic Analysis Reveals Mechanistic Differences.* Chembiochem : a European journal of chemical biology, 2012. **13**(15): p. 2270-2276.
87. Structural Genomics, C., et al., *Protein production and purification.* Nat Methods, 2008. **5**(2): p. 135-46.
88. Kirsebom, L.A., *RNase P RNA mediated cleavage: substrate recognition and catalysis.* Biochimie, 2007. **89**(10): p. 1183-94.
89. McClain, W.H., C. Guerrier-Takada, and S. Altman, *Model substrates for an RNA enzyme.* Science, 1987. **238**(4826): p. 527-30.
90. Yuan, Y. and S. Altman, *Substrate recognition by human RNase P: identification of small, model substrates for the enzyme.* EMBO J, 1995. **14**(1): p. 159-68.
91. Hansen, A., et al., *Exploring the minimal substrate requirements for trans-cleavage by RNase P holoenzymes from Escherichia coli and Bacillus subtilis.* Mol Microbiol, 2001. **41**(1): p. 131-43.
92. Brannvall, M., et al., *Evidence for induced fit in bacterial RNase P RNA-mediated cleavage.* J Mol Biol, 2007. **372**(5): p. 1149-64.
93. Walker, S.C. and D.R. Engelke, *Ribonuclease P: the evolution of an ancient RNA enzyme.* Crit Rev Biochem Mol Biol, 2006. **41**(2): p. 77-102.
94. Marvin, M.C., et al., *Binding and cleavage of unstructured RNA by nuclear RNase P.* RNA, 2011. **17**(8): p. 1429-40.
95. Helm, M., *Post-transcriptional nucleotide modification and alternative folding of RNA.* Nucleic Acids Res, 2006. **34**(2): p. 721-33.
96. Motorin, Y. and M. Helm, *tRNA stabilization by modified nucleotides.* Biochemistry, 2010. **49**(24): p. 4934-44.

97. Voigts-Hoffmann, F., et al., *A methyl group controls conformational equilibrium in human mitochondrial tRNA(Lys).* J Am Chem Soc, 2007. **129**(44): p. 13382-3.
98. Dammertz, K., et al., *Single-molecule FRET studies of counterion effects on the free energy landscape of human mitochondrial lysine tRNA.* Biochemistry, 2011. **50**(15): p. 3107-15.
99. Kobitski, A.Y., et al., *Single-molecule FRET reveals a cooperative effect of two methyl group modifications in the folding of human mitochondrial tRNA(Lys).* Chem Biol, 2011. **18**(7): p. 928-36.
100. Sohm, B., et al., *Recognition of human mitochondrial tRNALeu(UUR) by its cognate leucyl-tRNA synthetase.* J Mol Biol, 2004. **339**(1): p. 17-29.
101. Sinapah, S., et al., *Cleavage of model substrates by archaeal RNase P: role of protein cofactors in cleavage-site selection.* Nucleic Acids Res, 2011. **39**(3): p. 1105-16.
102. Wang, Z., M. Gerstein, and M. Snyder, *RNA-Seq: a revolutionary tool for transcriptomics.* Nat Rev Genet, 2009. **10**(1): p. 57-63.
103. Ozsolak, F. and P.M. Milos, *RNA sequencing: advances, challenges and opportunities.* Nat Rev Genet, 2011. **12**(2): p. 87-98.
104. Sorefan, K., et al., *Reducing ligation bias of small RNAs in libraries for next generation sequencing.* Silence, 2012. **3**(1): p. 4.
105. Taschner, A., et al., *Nuclear RNase P of Trypanosoma brucei: a single protein in place of the multicomponent RNA-protein complex.* Cell Rep, 2012. **2**(1): p. 19-25.
106. Ahn, H.J., et al., *Crystal structure of tRNA(m1G37)methyltransferase: insights into tRNA recognition.* EMBO J, 2003. **22**(11): p. 2593-603.
107. McClain, W.H., L.B. Lai, and V. Gopalan, *Trials, travails and triumphs: an account of RNA catalysis in RNase P.* J Mol Biol, 2010. **397**(3): p. 627-46.
108. Messmer, M., et al., *Tertiary network in mammalian mitochondrial tRNAAsp revealed by solution probing and phylogeny.* Nucleic Acids Res, 2009. **37**(20): p. 6881-95.
109. Hoang, C. and A.R. Ferre-D'Amare, *Cocrystal structure of a tRNA Psi55 pseudouridine synthase: nucleotide flipping by an RNA-modifying enzyme.* Cell, 2001. **107**(7): p. 929-39.
110. Ishitani, R., et al., *Alternative tertiary structure of tRNA for recognition by a posttranscriptional modification enzyme.* Cell, 2003. **113**(3): p. 383-94.
111. Shi, H. and P.B. Moore, *The crystal structure of yeast phenylalanine tRNA at 1.93 A resolution: a classic structure revisited.* RNA, 2000. **6**(8): p. 1091-105.
112. Holzmann, J. and W. Rossmanith, *tRNA recognition, processing, and disease: hypotheses around an unorthodox type of RNase P in human mitochondria.* Mitochondrion, 2009. **9**(4): p. 284-8.
113. Rossmanith, W. and J. Holzmann, *Processing mitochondrial (t)RNAs: new enzyme, old job.* Cell Cycle, 2009. **8**(11): p. 1650-3.
114. Artimo, P., et al., *ExPASy: SIB bioinformatics resource portal.* Nucleic Acids Res, 2012. **40**(Web Server issue): p. W597-603.
115. Milligan, J.F. and O.C. Uhlenbeck, *Synthesis of small RNAs using T7 RNA polymerase.* Methods Enzymol, 1989. **180**: p. 51-62.
116. Gruegelsiepe, H., et al., *Enzymatic RNA Synthesis using Bacteriophage T7 RNA Polymerase*, in *Handbook of RNA Biochemistry*. 2008, Wiley-VCH Verlag GmbH. p. 3-21.
117. Joseph, *Molecular Cloning: A Laboratory Manual(Third Edition)*. 2001: cold spring harbor laboratory press.
118. Schneider, T.D., et al., *Information content of binding sites on nucleotide sequences.* J Mol Biol, 1986. **188**(3): p. 415-31.
119. Schneider, T.D. and R.M. Stephens, *Sequence logos: a new way to display consensus sequences.* Nucleic Acids Res, 1990. **18**(20): p. 6097-100.
120. Schneider, T.D., *Consensus sequence Zen.* Appl Bioinformatics, 2002. **1**(3): p. 111-9.
121. Rueda, D., et al., *The 5' leader of precursor tRNAAsp bound to the Bacillus subtilis RNase P holoenzyme has an extended conformation.* Biochemistry, 2005. **44**(49): p. 16130-9.
122. Kelley, L.A. and M.J. Sternberg, *Protein structure prediction on the Web: a case study using the Phyre server.* Nat Protoc, 2009. **4**(3): p. 363-71.
123. Laskowski, R.A. and M.B. Swindells, *LigPlot+: multiple ligand-protein interaction diagrams for drug discovery.* J Chem Inf Model, 2011. **51**(10): p. 2778-86.

124. Altschul, S.F., et al., *Gapped BLAST and PSI-BLAST: a new generation of protein database search programs.* Nucleic Acids Res, 1997. **25**(17): p. 3389-402.
125. Sievers, F., et al., *Fast, scalable generation of high-quality protein multiple sequence alignments using Clustal Omega.* Mol Syst Biol, 2011. **7**: p. 539.
126. Gouet, P., X. Robert, and E. Courcelle, *ESPript/ENDscript: Extracting and rendering sequence and 3D information from atomic structures of proteins.* Nucleic Acids Res, 2003. **31**(13): p. 3320-3.
127. Laskowski, R.A., *PDBsum new things.* Nucleic Acids Res, 2009. **37**(Database issue): p. D355-9.
128. Wilusz, J.E., et al., *tRNAs marked with CCACCA are targeted for degradation.* Science, 2011. **334**(6057): p. 817-21.

# CHAPTER 5

# CONCLUSIONS AND FUTURE DIRECTIONS

## 5.1 Conclusions

The goal of this work was to advance our understanding of the molecular basis of how RNase P recognizes ligands and catalyzes an essential biological reaction. First, this work developed a fast, real-time and robust fluorescence polarization (FP) assay to facilitate kinetic analysis and to identify inhibitors of RNase P as chemical probes and potential novel anti-bacterial agents. Second, a combination of atomic modifications and kinetic analyses established that a universally conserved bulged uridine in the P4 helix of P RNA enhances conformational change kinetics and contacts at least one metal ion through an outer-sphere interaction. Third, this work provides the first evidence that MRPP3 alone is active in catalyzing cleavage of mitochondrial pre-tRNA and the other two subunits of mtRNase P, MRPP1 and 2, increase both the cleavage rate and cleavage site fidelity.

### 5.1.1 A New Real-time FP Assay Facilitates Kinetic Analysis of RNase P and Discovery of Inhibitions

Bacterial RNase P is an attractive novel antibacterial target, but no specific and potent inhibitors have been identified to date [1]. My work developed a facile non-radioactive assay utilizing the change in the anisotropy signal of a fluorescence dye

attached to the 5’ end of a pre-tRNA substrate (Figure 2-1, Chapter 2). This assay is amenable to measuring *B. subtilis* RNase P activity both continuously and in an end-point format suitable for high-throughput screening using micro-plate readers. A new inhibitor, iriginol hexaacetate, (Ir6Ac, $IC_{50}$ = 2 μM) against *B. subtilis* RNase P has been identified from high-throughput screening of a compound library. The fluorescence polarization/anisotropy method also reveals that aminoglycosides inhibit *B. subtilis* RNase P non-specifically by binding to the pre-tRNA substrate. This work provides valuable tools for identification of specific inhibitors against bacterial RNase P and for studying ligand recognition of this enzyme. In the future, this assay should be applicable to analyzing the activity and inhibitor of other forms of RNase P and other nucleases. Additionally, this assay can be used to measure ligand binding to tRNA.

### 5.1.2 The Universally Conserved Bulge Uridine in Helix P4 is Important for Conformational Change

Single atom modifications were incorporated into the P4 helix of a circular permuted RNase P RNA to examine the functional role and interaction with metal ions of a universally conserved bulged uridine (U51 in *B. subtilis* RNase P, Figure 3-2, Chapter 3). Alteration in the substrate affinity of the 4-thiouridine mutant suggest that the O4 oxygen atom of U51 is important for stabilizing pre-tRNA affinity in a divalent metal ion-dependent fashion. The kinetic mechanism of RNase P catalyzed cleavage of pre-tRNA includes a conformational change step that is the rate-limiting step at high pH (pH≥ 8) for the wild-type enzyme [2]. Base modifications, such as 4-thiouridine, 4-deoxyuridine and 3-methyluridine, decrease the single-turnover

cleavage rate catalyzed by RNase P holoenzyme by 20-fold and reduce cooperativity for $Mg^{2+}$ ion-activated cleavage catalyzed by P RNA at low pH (pH < 6). In contrast, deletion of the uracil base (abU) does not affect the single turnover cleavage rate constant. At higher pH, the abU modification significantly decreases the pH-independent conformational change rate constant, while base modifications have only minimal effects. These data suggest that the universally conserved bulged U51 enhances cleavage by positioning an $Mg^{2+}$ ion through outer-sphere coordination and enhances the dynamics for forming an active RNase P-substrate conformation. These results pinpoint the first P RNA residue that is important for the conformational dynamics of RNase P and revise the current proposal that O4 directly coordinates a catalytic metal ion, as proposed from recent crystallographic data [3].

### 5.1.3 MRPP3 Is the Catalytic Component of Human mtRNase P Complex

Unlike other RNA-dependent RNase P enzymes, the newly identified human mtRNase P is composed solely of three proteins (MRPP1, 2 and 3) and so far has been poorly characterized [4, 5]. Previous reported results suggest that *in vitro* MRPP3 is catalytically inactive without two other subunits [4, 5]. Single-turnover cleavage data from this work demonstrate that MRPP3 alone is the subunit that catalyzes cleavage of the 5' leader of an mt-pre-tRNA substrate. Moreover, MRPP1·MRPP2 subcomplex enhances the catalytic efficiency and cleavage site fidelity of the human mtRNase P activity (Figure 4-10 and Figure **4-11**, Chapter 4).

## 5.2 Future Directions

RNase P is an essential yet diverse enzyme and a potential drug target. Bacterial and human forms of RNase P enzymes catalyze the same phosphodiester bond hydrolysis utilizing different substrates and subunits. Numerous fundamental questions remain on mechanisms used by bacterial (RNA-based) and human mitochondrial (protein-based) RNase P to recognize diverse ligand molecules and to achieve precise and efficient catalysis. Furthermore, small molecules that specifically target bacterial RNase P have not yet been identified. Below are my brief proposals on how to further investigate these mechanisms. Specifically, I will discuss experiments for further investigation of inhibitors, metal binding sites and the conformational change step of bacterial RNase P, and propose analytical, structural and biochemical strategies to investigate the structure, function and substrate specificity of human mtRNase P.

### 5.2.1 RNase P Inhibitors and tRNA Ligands

The mechanism of inhibition by the newly identified inhibitor, Iriginol hexaacetate (Ir6Ac) is currently unknown and should be elucidated. First, measurement of the time-dependence of inhibition can distinguish slow tight-binding irreversible inhibitors from rapid reversible inhibitors. Second, monitoring the steady-state kinetics catalyzed by RNase P at varying substrate and inhibitor concentrations will allow dissection of the inhibition mechanism of this compounds (competitive, noncompetitive, uncompetitive or mixed [6]). If the inhibitor binds to the enzyme-substrate (ES) complex, measurement of inhibition as a function of pH should provide information about ES conformers in the catalytic cycle that the inhibitor

interacts with. Competition between inhibitors and $Mg^{2+}$ should also be tested for elucidating the mode of inhibition.

In addition, interactions of P RNA with Ir6Ac could be investigated utilizing the fluorescent properties of this compound. Furthermore, a combination of chemical and enzymatic footprinting experiments using Fe (II)-EDTA, and RNases T1, U2 and V1 can be used to map potential interaction sites of the inhibitor in P RNA [7][8]. The cleavage products can be identified using $^{32}$P-labeled P RNA on a sequencing PAGE gel, and compared to cleavage of RNase P alone. Footprinting pattern from hydroxyl and nuclease cleavage will reveal possible sites that interact with inhibitors on P RNA.

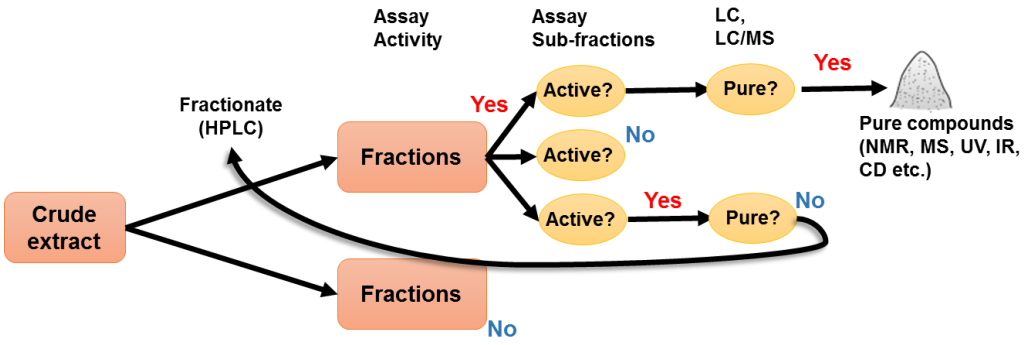


**Figure 5-1:** Scheme for bioactivity-guided fractionation of active compounds from natural product library. Adapted from [9].

HTS screens of small molecules have been previously carried out by GlaxoSmithKline [10] and Message Pharmaceuticals [11], but no high-affinity lead compound with good efficacy has been developed. The crystal structures of *B. stearothermophilus* P RNA [12] and *T. maritima* RNase P with bound tRNA show that the active site of P RNA is large and shallow compare to active sites in proteins [3]. These structural features along with lack of potent and specific small molecule

inhibitors may suggest that the binding pocket of RNase P is less ideal for small molecule inhibitors. Therefore, larger natural products are likely better starting points for discovering inhibitors of bacterial RNase P. In collaboration with the Sherman lab (University of Michigan), the natural product extracts that displayed RNase P inhibition activity have been further fractionated to isolate and identify the natural products responsible for the activity (Figure A-5, Appendix A, Chapter 2). This is an iterative bioactivity-guided process (Figure 5-1). Mixtures of compounds can be extracted and fractionated by high-performance liquid chromatograph (HPLC) from regrowth of microorganisms. Fractions will be tested for inhibition of RNase P activity *in vitro* using the FP assay. To prioritize hits in terms of antibacterial activity, we can use a disk diffusion assay [13] and a 96-well plate bacterial growth assay (Appendix A) for various model strains including *Bacillus anthracis*, *Staphylococcus aureus* and *Escherichia coli* (Figure A-6, Appendix A, Chapter 2). Once a hit is validated from these assays, the active fraction can be further purified until a single active component that inhibits RNase P activity and bacterial growth is determined. It is also possible that several natural product compounds function synergistically and thus a decrease in activity is observed for isolated compounds. In this case, the synergistic effect could be tested by combining compounds isolated from active fractions and measuring inhibition activity. Spectroscopic methods, such as NMR, MS and CD, can be used to determine the chemical structure of the active compounds. Importantly, the metal content of these compounds should be determined by inductively coupled plasma mass spectrometry (ICP-MS) or atomic absorption spectroscopy (AA) to rule out metal contaminants that could inhibit

RNase P activity such as $Cd^{2+}$ [14]. We can also test the antibacterial activity of the isolated inhibitors by determining the minimum inhibitory concentration (MIC) in *E. coli* [15]. Together, these results will broaden our knowledge of RNase P as a drug target and provide more candidate compounds and mechanistic information for developing new antibiotics targeting RNase P in the future.

The 22 human mitochondrial tRNAs (mt-tRNAs) are often called “bizarre tRNAs” because several mt-tRNAs are structurally different from the classic tRNA cloverleaf secondary structure and the L-shaped tertiary structure [16, 17] (Figure 4-3, Chapter 4). Nearly half of the disease-associated human tRNA point mutations are located in human mt-tRNAs (Figure 4-2, Chapter 4). We could optimize the FP assay to perform a high-throughput screen to identify small molecule and natural product ligands that can interact with and potentially stabilize human mt-tRNA. Then the effects of these molecules on processing of wild-type and pathogenic mutant mt-pre-tRNAs by the newly discovered protein-only mtRNase P can be evaluated. These molecules could either function as activators (by stabilizing tRNA structure) or inhibitors of mtRNase P. We could also develop biophysical and computational methodologies, including NMR spectroscopy and *in silico* screening [18] (in collaboration with Professor Hashim Al-Hashimi at University of Michigan), to determine the solution structure of mt-tRNA and to directly measure ligand binding to tRNA. These studies would significantly enhance our understanding of the molecular recognition of bacterial RNase P and the structures and functions of human mt-tRNA and mtRNase P, which will shed light on targeting these molecules to treat human diseases.

### 5.2.2 Metal Ion Binding Site in Helix P4

To further explore the functional role of uracil 51, additional single-atom modifications can be incorporated into circular permuted P RNA (Figure 5-2). For example, sulfur substitution of O2 can test possible metal ion coordination at this position. Currently, a phosphoramidite derivative of 2-thiouridine is not commercially available but the synthesis method is published [19]. IsoCystosine can also be used to probe the O2 position. However, isoC51 could potentially form a wobble base pair with G379 (Figure 5-2). A commercially available 2' deoxy version of 3-methylcytosine (3-methyl-dC) can be used in lieu of U to C mutation to avoid potential base paring of C51 to G379 and evaluate if a bulky methyl group and alteration of the O4 to an amine group have an additive effect on disrupting the outer-sphere coordination. These experiments might provide more details on the interactions between the conserved nucleotide U51, G379 and metal ions.

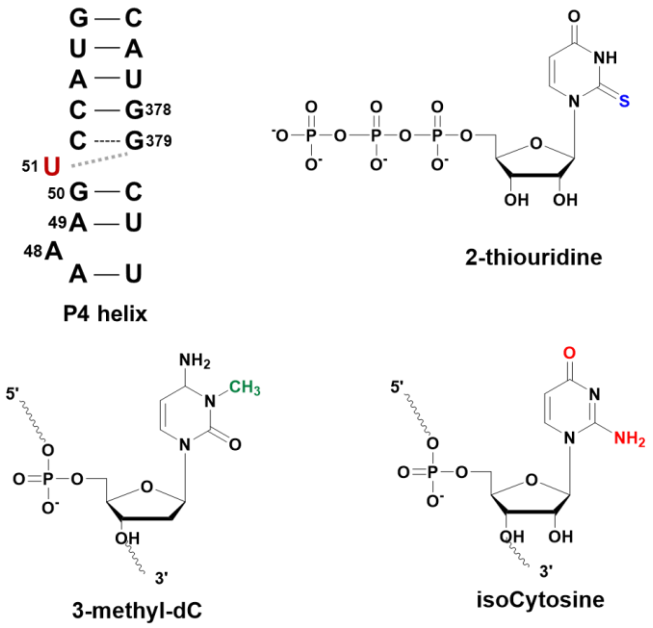


**Figure 5-2:** Additional atomic modifications to probe function and metal ion binding of U51 in helix P4.

Time-resolved fluorescence energy transfer (trFRET) data have indicated that an inner-sphere metal ion-dependent conformational change step occurs upon substrate binding that leads to a ~ 40 Å movement between the C- and S-domain of P RNA (Hsieh and Fierke, unpublished data). This conformational change step can be further investigated by various techniques. First, we can utilize the fluorescence of 4-thiouridine to monitor the conformational change step [20]. Second, small angle X-ray scattering (SAXS) has been applied to measure the solution structure of RNase P [21-23]. SAXS measurements can probe the global conformational change of RNase P by comparing the difference in the structure envelope under various conditions. Third, cryo-electron microscopy (cryo-EM) has revealed the structure of a folding intermediate of the S-domain of P RNA [24]. To further evaluate conformational transitions in RNase P, cryo-EM and single-particle image reconstruction can visualize structures of the wild type RNase P·pre-tRNA complex at varying $Ca^{2+}$ concentrations to reveal changes in the global architectural between the ES and ES* conformations. Additionally, new NMR methods that capture transient structures of RNA could be applied to study the P4 stem-loop RNA model to analyze the conformational change and metal ion binding in *B. subtilis* RNase P RNA at the atomic level [25].

### 5.2.3 Human Mitochondrial RNase P

The structure of the human mtRNase P complex and the stoichiometry of the subunits in the active MRPP 1:2:3 complex have not been established to date. X-ray crystallography trials can be set up to grow crystals of MRPP1·MRPP2 complex, MRPP3 alone, MRPP3·substrate complex as well holoenzyme·substrate ternary

complex by all three proteins and a tightly bound mt-pre-tRNA or model substrate. Purification of MRPP1 protein should be further optimized in addition to purifying MRPP1·MRPP2 as a complex. This will allow variations of the stoichiometry of the three subunits for structure and function studies.

In addition, preliminary data suggest that we can apply ion mobility-mass spectrometry (IM-MS) [26] (Figure 5-3 and Figure 5-4) to measure the stoichiometry and architecture of the mtRNase P complex. In collaboration with Dr. Brandon Ruotolo's laboratory, we used IM-MS to observe both a heterohexamer and heteropentamer of the MRPP1·MRPP2 complex (Figure 5-3) and a PRORP1·pre-tRNA$^{Cys}$ complex (Figure 5-4). Based on these data, a low-resolution topology of the protein and protein·substrate complex can be built. Detailed protein-protein interaction sites could be mapped by protease footprinting and hydrogen/deuterium exchange (HDX) combined with mass spectrometry [27]. Furthermore, in collaboration with Dr. Georgios Skiniotis's laboratory (University of Michigan) we have performed electron microscopy analysis of mtRNase P proteins. EM experiments only require a small amount of materials (~ 10 to 50 ng of protein) and can visualize protein structures at various fixed conditions. Negative staining images of MRPP3 and the MRPP1· MRPP2 complex show relatively good homogeneity in particle size (low level of observed dimerizaitona or aggregation) (Figure 5-5), which suggest possibility for further single particle reconstruction studies [28]. We could optimize the protein sample preparation of mtRNase P to use EM to visualize the architecture of the human mtRNase P holoenzyme, an enzyme-substrate ternary complex (MRPP1 + MRPP2 + MRPP3 + substrate) and a subcomplex (MRPP1 +

MRPP2 + substrate) under various subunit stoichiometries and solution conditions. These medium resolution studies could provide valuable insights into the solution structure of mtRNase P.

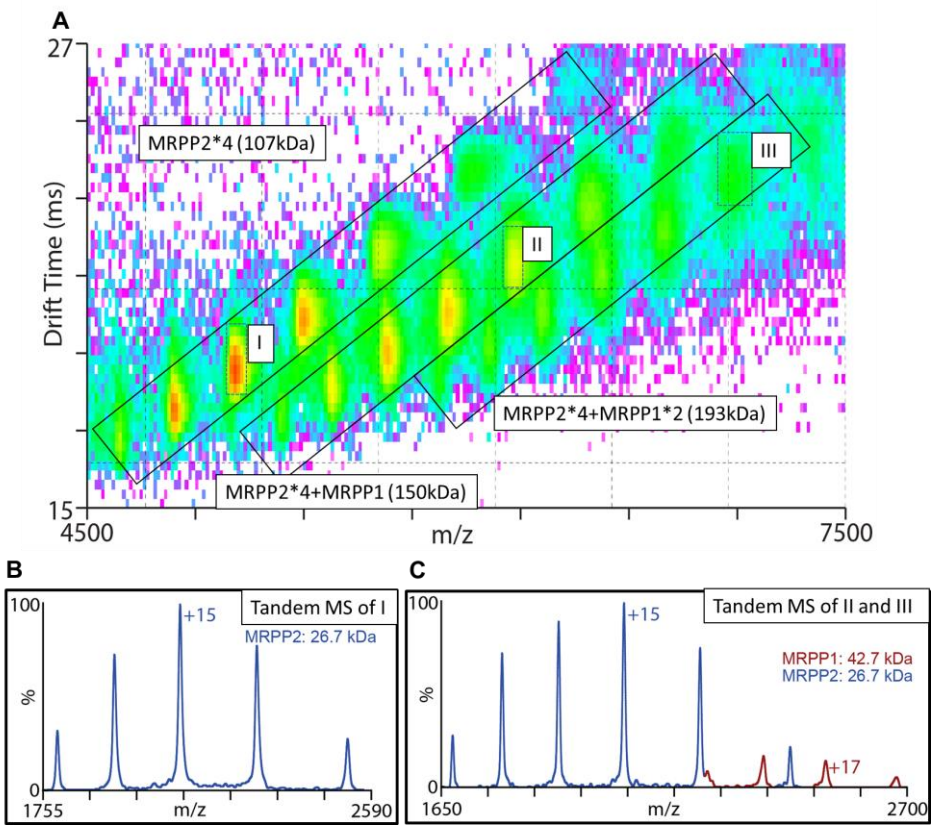


**Figure 5-3:** Ion mobility-mass spectrometry (IM-MS) analysis of the MRPP1·MRPP2 complex. **(A)** Three populations of proteins are observed, I: homotetramer of MRPP2; II: heteropentamer of $(MRPP1)_1(MRPP2)_4$; III: heterohexamer of $(MRPP1)_2(MRPP2)_4$; **(B)** and **(C)** MS/MS analysis of protein molecular weight[1].

[1] IM-MS analyses (Figures 5-3 and 5-4) were performed by Yueyang Zhong in Dr. Ruotolo's laboratory on smaples prepared by Xin Liu (MRPP1·MRPP2 complex) and Michael Howard (PRORP1, pre-tRNA$^{Cys}$, and MRPP2). Figures 5-3 and 5-4 are adapted from figures made by Yueyang Zhong.

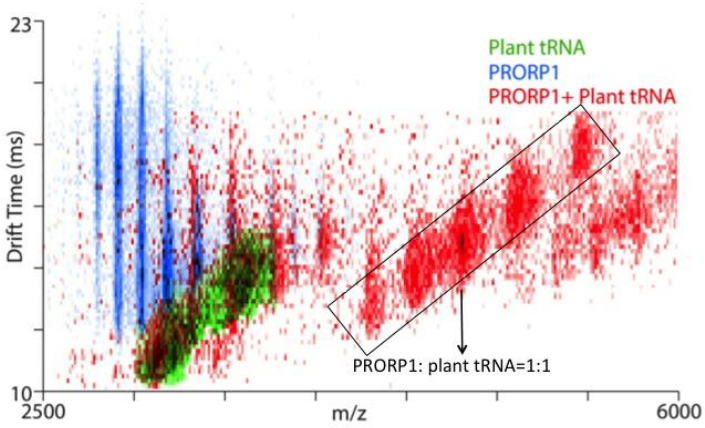


**Figure 5-4:** An overlay of ion mobility-mass spectrometry (IM-MS) analysis of A. thaliana PRORP1 (blue), pre-tRNACys (green) and PRORP1-pre-tRNACys complex (red). PRORP1 alone has broadened drift time which may indicate partial unfolding of the proteins. The PRORP1-pre-tRNA$^{Cys}$ complex has a narrower drift time, which may indicate that substrate enhances folding of PRORP1.

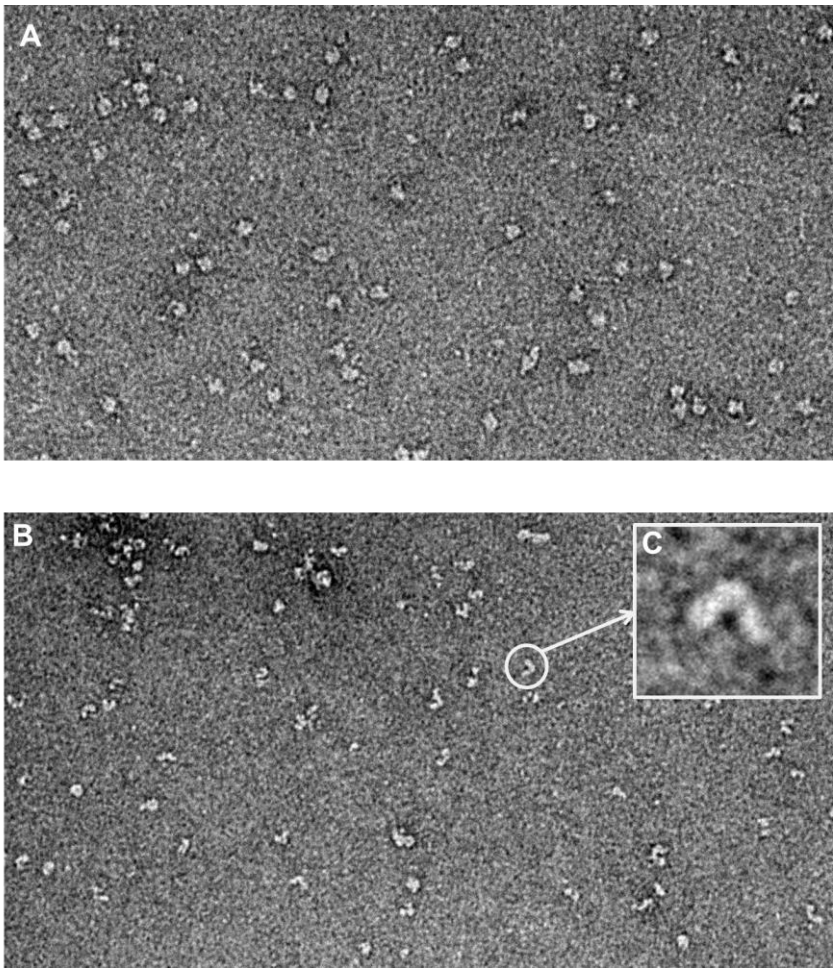

**Figure 5-5:** Negative staining images of human mtRNase P proteins. **(A)** Negative staining image of MRPP1·MRPP2 complex. The resolution of the current image is insufficient to resolve subunit composition but shows protein particles similar in size (low level of dimerization or aggregation). **(B)** MRPP3 and **(C)** A zoom-in view of MRPP3 showing the V-shape of the protein[2].

Catalytic activity and substrate recognition of human mtRNase P can be elucidated using kinetics, substrate affinity and footprinting experiments. Specifically, we can investigate reactivity with substrates representing three types of mt-pre-tRNA structures as well as human nuclear pre-tRNA, including: mt-pre-tRNA$^{Leu(UUR)}$ (type 0, N9=G), mt-pre-tRNA$^{Lys}$ (type II, N9=A), mt-pre-tRNA$^{Ile}$ (type II, N9=G), mt-pre-tRNA$^{Met}$ (type II, N9=C), mt-pre-tRNA$^{Ser(UUR)}$ (type 0) and n-pre-tRNA$^{Ser}$. Substrate affinity could be measured by a fluorescence polarization assay in the presence of different combinations of human mtRNase P subunits and subunit stoichiometries. Catalytic activity can be investigated by measuring the cleavage activity under single- ([E]>>[S], $k_{obs}$, $K_{1/2}$) and multiple-turnover conditions ([E]<<[S], $k_{cat}$, $K_M$, $k_{cat}/K_M$) as a function of subunit stoichiometry, metal ion conditions (such as $Mg^{2+}$ and NaCl concentrations) and co-factors ($NAD^+$ and SAM). We can identify structural features of mt-pre-tRNA that are important for recognition by mtRNase P proteins using hydroxyl radical and enzymatic footprinting (radiochemical or fluorescently labeled substrate), selective 2'-hydroxyl acylation analyzed by primer extension (SHAPE) using fluorescent DNA-primers and automated instrumentation available on campus, and mutagenesis of the substrates. In addition, because mt-pre-tRNA$^{Lys}$ (A9) and mt-pre-tRNA$^{Ile}$ (type II, G9) have been shown to be methylated

[2] Negative-stain imaging was performed by Annie Dosey in Dr. Skiniotis's laboratory on sample prepared by Xin Liu.

by MRPP1 *in vitro* [29], we can compare reactivity with the primary transcript and R9 methylated form of these two substrates.

Several pathogenic point mutations located in the D- and anticodon-domain of mt-tRNA$^{Leu(UUR)}$ decrease the processing rate catalyzed by partially purified human mtRNase P by 2- to 5-fold [30]. The pathogenic insertion mutation (44inC in V-loop) of mt-tRNA$^{Ser(UCN)}$ also affects 5' processing in cells and *in vitro* catalyzed by partially purified mtRNase P [31]. A point mutation at N(+1) (A to G) in mt-pre-tRNA$^{Ile}$ that is linked to a type of maternally inherited hypertension has also been shown to reduce reactivity with human mtRNase P [32]. It is unclear whether these effects are due to global and/or local structure changes of the mt-tRNA substrate and/or loss of sequence specific interaction with mtRNase P. We can investigate both the 5' processing activity and structural effects of pathogenic mutations both in regions of mt-pre-tRNA that bind to mtRNase P proteins and in sites that may disturb mt-tRNA structure using detailed kinetic and solution probing experiments. These studies will advance our understanding of mitochondria-related diseases at a molecular level.

Deep sequencing studies revealed that knockdown of mtRNase P subunits in cells lead to accumulation of precursors for both tRNAs and long noncoding RNAs in mitochondria [4, 33]. In normally growing cells, aberrant partially processed products are also observed in multi-mt-tRNA junctions [34]. To investigate the pre-tRNA processing and other potential substrates by human mtRNase P *in vivo*, it might be possible to probe mitochondrial RNA processing by combining recently developed small RNA-seq [35] and living cell SHAPE [36] techniques to obtain detailed sequence as well as secondary structure information of mitochondrial RNA

transcripts as a function of knockdowns of each human mtRNase P protein in HeLa cells. Together, the studies proposed here would address fundamental questions in the structure and function of human mtRNase P as well as illuminate mitochondrial RNA processing pathway in cells.

## 5.3 References


1. Eder, P.S., et al., *Bacterial RNase P as a potential target for novel anti-infectives.* Curr Opin Investig Drugs, 2003. **4**(8): p. 937-43.
2. Hsieh, J. and C.A. Fierke, *Conformational change in the Bacillus subtilis RNase P holoenzyme--pre-tRNA complex enhances substrate affinity and limits cleavage rate.* RNA, 2009. **15**(8): p. 1565-77.
3. Reiter, N.J., et al., *Structure of a bacterial ribonuclease P holoenzyme in complex with tRNA.* Nature, 2010. **468**(7325): p. 784-9.
4. Holzmann, J., et al., *RNase P without RNA: identification and functional reconstitution of the human mitochondrial tRNA processing enzyme.* Cell, 2008. **135**(3): p. 462-74.
5. Gobert, A., et al., *A single Arabidopsis organellar protein has RNase P activity.* Nat Struct Mol Biol, 2010. **17**(6): p. 740-4.
6. Copeland, R.A., *Enzymes: A Practical Introduction to Structure, Mechanism, and Data Analysis.* Wiley-VCH Inc., 2000.
7. Berchanski, A. and A. Lapidot, *Bacterial RNase P RNA is a drug target for aminoglycoside-arginine conjugates.* Bioconjug Chem, 2008. **19**(9): p. 1896-906.
8. Brenowitz, M., et al., *Probing the structural dynamics of nucleic acids by quantitative time-resolved and equilibrium hydroxyl radical "footprinting".* Curr Opin Struct Biol, 2002. **12**(5): p. 648-53.
9. Koehn, F.E. and G.T. Carter, *The evolving role of natural products in drug discovery.* Nat Rev Drug Discov, 2005. **4**(3): p. 206-20.
10. Payne, D.J., et al., *Drugs for bad bugs: confronting the challenges of antibacterial discovery.* Nat Rev Drug Discov, 2007. **6**(1): p. 29-40.
11. Giordano T., S.M.A., Rao. S. J., *Inhibitors of RNase P proteins as antibacterial compounds*, in *Unites States Patent*2006: US, 7,001,924 B2.
12. Kazantsev, A.V., et al., *Crystal structure of a bacterial ribonuclease P RNA.* Proc Natl Acad Sci U S A, 2005. **102**(38): p. 13392-7.
13. Standards, N.C.f.C.L., *Performance standards for antimicrobial susceptibility testing*, in *ninth informational supplement*1999, NCCLS: Wayne, Pennsyslvania.
14. Crary, S.M., J.C. Kurz, and C.A. Fierke, *Specific phosphorothioate substitutions probe the active site of Bacillus subtilis ribonuclease P.* RNA, 2002. **8**(7): p. 933-47.
15. Andrews, J.M., *Determination of minimum inhibitory concentrations.* J Antimicrob Chemother, 2001. **48 Suppl 1**: p. 5-16.
16. Ueda, T., T. Ohta, and K. Watanabe, *Large scale isolation and some properties of AGY-specific serine tRNA from bovine heart mitochondria.* J Biochem, 1985. **98**(5): p. 1275-84.
17. Yokogawa, T., et al., *Purification and characterization of two serine isoacceptor tRNAs from bovine mitochondria by using a hybridization assay method.* Nucleic Acids Res, 1989. **17**(7): p. 2623-38.
18. Stelzer, A.C., et al., *Discovery of selective bioactive small molecules by targeting an RNA dynamic ensemble.* Nat Chem Biol, 2011. **7**(8): p. 553-9.
19. Nawrot, B. and E. Sochacka, *Preparation of short interfering RNA containing the modified nucleosides 2-thiouridine, pseudouridine, or dihydrouridine.* Curr Protoc Nucleic Acid Chem, 2009. **Chapter 16**: p. Unit 16 2.
20. Favre, A., A.M. Michelson, and M. Yaniv, *Photochemistry of 4-thiouridine in Escherichia coli transfer RNA1Val.* J Mol Biol, 1971. **58**(1): p. 367-79.
21. Fang, X.W., et al., *The Bacillus subtilis RNase P holoenzyme contains two RNase P RNA and two RNase P protein subunits.* RNA, 2001. **7**(2): p. 233-41.
22. Barrera, A., et al., *Dimeric and monomeric Bacillus subtilis RNase P holoenzyme in the absence and presence of pre-tRNA substrates.* Biochemistry, 2002. **41**(43): p. 12986-94.
23. Kazantsev, A.V., et al., *Solution structure of RNase P RNA.* RNA, 2011. **17**(6): p. 1159-1171.
24. Baird, N.J., et al., *Discrete structure of an RNA folding intermediate revealed by cryo-electron microscopy.* J Am Chem Soc, 2010. **132**(46): p. 16352-3.
25. Dethoff, E.A., et al., *Visualizing transient low-populated structures of RNA.* Nature, 2012. **491**(7426): p. 724-8.

26. Zhong, Y., S.J. Hyung, and B.T. Ruotolo, *Ion mobility-mass spectrometry for structural proteomics.* Expert Rev Proteomics, 2012. **9**(1): p. 47-58.
27. Kaltashov, I.A., C.E. Bobst, and R.R. Abzalimov, *H/D exchange and mass spectrometry in the studies of protein conformation and dynamics: is there a need for a top-down approach?* Anal Chem, 2009. **81**(19): p. 7892-9.
28. Cheng, Y. and T. Walz, *The advent of near-atomic resolution in single-particle electron microscopy.* Annu Rev Biochem, 2009. **78**: p. 723-42.
29. Vilardo, E., et al., *A subcomplex of human mitochondrial RNase P is a bifunctional methyltransferase--extensive moonlighting in mitochondrial tRNA biogenesis.* Nucleic Acids Res, 2012. **40**(22): p. 11583-93.
30. Rossmanith, W. and R.M. Karwan, *Impairment of tRNA processing by point mutations in mitochondrial tRNA(Leu)(UUR) associated with mitochondrial diseases.* Febs Letters, 1998. **433**(3): p. 269-74.
31. Toompuu, M., et al., *The 7472insC mtDNA mutation impairs 5' and 3' processing of tRNA(Ser(UCN)).* Biochem Biophys Res Commun, 2004. **322**(3): p. 803-13.
32. Wang, S., et al., *Maternally inherited essential hypertension is associated with the novel 4263A>G mutation in the mitochondrial tRNAIle gene in a large Han Chinese family.* Circ Res, 2011. **108**(7): p. 862-70.
33. Sanchez, M.I., et al., *RNA processing in human mitochondria.* Cell Cycle, 2011. **10**(17): p. 2904-16.
34. Mercer, T.R., et al., *The human mitochondrial transcriptome.* Cell, 2011. **146**(4): p. 645-58.
35. Ozsolak, F. and P.M. Milos, *RNA sequencing: advances, challenges and opportunities.* Nat Rev Genet, 2011. **12**(2): p. 87-98.
36. Spitale, R.C., et al., *RNA SHAPE analysis in living cells.* Nat Chem Biol, 2013. **9**(1): p. 18-20.